بِسْمِ اللهِ الرَّحْمٰنِ الرَّحِيْمِ

IN THE NAME OF ALLAH, THE BENEFICENT, THE MERCIFUL

The University of Aston in Birmingham

ULTRASONIC BONE TOMOGRAPHY IN LIVE PATIENTS

A Thesis submitted for
The Degree of

DOCTOR OF PHILOSOPHY

By

Ali Ismail Ali BASHTER

BSc; Diploma (Cairo); MSc. (London)

Department of Physics

June 1976

ACKNOWLEDGEMENTS

This work would not have been possible without the constant guidance, encouragement and the active assistance of my supervisor, Dr J A Archer-Hall, and my sincere thanks are due to him.

I am also grateful to Dr P E Francois, my advisor, for his valuable advice and encouragement. I should like to express my thanks to Professor S E Hunt for his continuing encouragement.

My grateful thanks are due to the following:-

The staff of the Technical and Electronic workshops for the equipments and constructive help they have given while this work was being carried out.

The Medical Research Council for the financial support of this project.

The Arab Republic of Egypt Atomic Energy Establishment for the grant which made it possible for me to undertake this work.

Last and not least, I should like to express my thanks to my wife and my children for their patience and their continuing push and encouragement.

ABSTRACT

The work described in this thesis involves some of the instrumentation development undertaken for the study of bone mineral loss in the ulna, with a view to being able to quote the actual bone mineral density, with a high resolution. An apparatus for the bone mineral estimation, using x-ray scanning technique has been developed in this Department by J.P. Edwards. The major part of the present project is to develop a means for providing an outline of the cross-section of the ulna, at the level at which the x-ray scanning is performed, by using ultrasonic tomography.

The system involves two matching ceramic bowl transducers (PZT-5 A) attached vertically to the bottom of a rotating drum in which all the electronic circuit elements are mounted. One transducer is used as a reference, with a fixed reflecting metallic rod present at its focus, and the other is used as a scanning transducer. Both transducers are immersed in a water bath, which is designed to accommodate an arm vertically, without discomfort to the patient. The limb is held normal to the axis of symmetry of the scanning transducer, in such a way to allow for a smooth rotation of the latter around the limb. The time for a whole complete rotation of 360° is about 25 seconds.

An electronic switching technique is used to turn on both transducers simultaneously as transmitters in order to transmit a long duration pulses (120μs) of 6.85 MHz ultrasonic waves, and then as receivers for their corresponding returning echoes. Provision has been made for electrical

chopping of the start of the received wave-trains, which removes about 10-15μs worth. The difference in the delay times of the two echoes, which is proportional to the difference in their path lengths, is obtained by comparing the time abrupt cessation of the tail ends of the received signals. Considerable work has been carried out with regard to the construction of backing and matching layers, but the cessation of the wave-trains could not be made abrupt enough to provide sufficiently distinct events. The abrupt event, however, has been achieved by using a shock excitation with sharp onset, at the end of the transmitted pulses. Signals derived from the reflections of these shocks are amplified and fed into a discriminator which determines which of the two pulses returns earlier. The information from the discriminator provides the input for a servomechanism designed to maintain the scanning bowl focus on the bone surface, by appropriate radial movement.

The display system involves a direct mechanical coupling of the servomechanism to a pen, which gives a plot of the outline of the ulna cross-section on a drawing paper attached to the frame of the apparatus with a magnification ratio of 10:1.

In this technique, the outline of the ulna cross-section will be carried out in two separate scans, ech of 270°; one with the arm pronated, and the other in the supinated position. The two scans are combined to give the complete outline of the cross-section of the ulna. The time for each scan is about 18 seconds. This short scan time means that distortions of the observed profile due to movement by the patient are minimized.

It was recognised that the ultimate lateral resolution of the system, depends on the diffraction pattern of the concave bowl transducer. This in turn is dependent on the geometry of the bowl, but as has been shown in Chapter II, is a function of the type of excitation; i.e continuous wave or impulse, and in the case of the latter the bandwidth of the receiving system also.

Consideration has also been given to the limit of axial resolution, which depends on the time discrimination of the two echoes, in Chapter II.

In connection with the trials for construction of matching layers, a new method has been developed (Chapter IV) for determining the velocity of sound in solid materials, by using a thin tapered wedge and a converging beam of high frequency ultrasonic waves.

In addition to this main project, considerable work has been carried out in the development of an artificial bone-like material (Appendix A), in order to be used as a reference for the bone densitometer.

C O N T E N T S

PREFACE

Work has been carried out over the last six years in the Physics Department of Aston University and at Dudley Road Hospital, Birmingham, with the purpose of improving techniques for the study of decalsification in vivo. It is intended that instrumentation be developed in order to determine the actual mineral density at each point of a selected bone, the ulna being chosen in the present case.

Two steps are necessary so that values for bone mineral density may be quoted.

(i) The first step is to determine the total amount and site of bone minerals at each point across the ulna. This has been carried out by using x-ray absorption scan.

(ii) The second step is to determine the path length at each point of the x-ray scan. This could be obtained from an accurate outline of the ulna cross-section at the level at which x-ray beam scanning is performed. This outline cross-section could be obtained by using a transverse tomograph. The term tomography means "writing a cutting" and first came to be used in x-radiology.

The first part of the bone densitometry, i.e. the total bone mineral estimation using x-ray scanning techniques, will be dealt with briefly, since it is related to the bone tomography, which is the major part of the present project.

(i) Bone mineral estimation using x-ray scanning technique

An apparatus for bone mineral estimation in vivo has been developed by J.P.N. Edwards (J.A. Archer-Hall et al, 1973), using a conventional diagnostic x-ray set. Further modifications have been carried out by M.I.Al-Jarallah. This apparatus has been designed so that the beam from the x-ray tube falls on a lead plate with two slots. Beneath one of them there is a detector to sample the x-rays. Through the other slit, an x-ray beam passes down into a water bath which is designed to accommodate the patient's arm firmly in such a manner that the ulna is scanned. The bath with the arm is moved through the beam in a smooth motion by a worm drive at the rate of 1cm/sec. The transmitted beam passes through a defining slit to a second detector. The detectors are small pieces of CsI(Tl) viewed by photo-cells. The light output of the crystals is sufficiently great that a d.c. current, rather than a series of pulses, is obtained.

This apparatus performs an x-ray absorption scan with a spatial resolution of 0.25 mm and negligible positional error, without discomfort to the patient. It also has a number of advantages.

1. It can provide an extremely accurate analysis of the extent and site of bone minerals in the skeleton of the living patient, especially in the ulna.
2. The x-ray dosage to the patient is very low, about one hundredth of that used in taking a radiograph of a whole limb, i.e. about 150 m.rad per scan. Hence repeated scans may be performed at, for example,

monthly intervals in order to determine the response to therapy.

3. The short time scan, which is a few seconds, means that distortions of the observed profile due to movement by the patient, are minimised.

4. This apparatus is made to fit to an unmodified clinical x-ray set, but avoids the difficulties associated with photographic procedures which have been used before.

5. It provides a compensation for the variations in the x-ray intensity and spectral distribution due to fluctuations in the mains supply voltage. This is achieved by the use of the monitor detector and electronic switching techniques, so as to result in an error not exceeding 1.5%.

The principle of operation of this apparatus and its compensation for the variations in the x-ray intensity is summarised as follows:

The photocurrents from the monitor and lower detectors are simultaneously integrated with respect to time, from the start of each half cycle of the mains supply. The integration is carried out for a period of time "t" until the value obtained from the current of the monitor detector reaches a preset value. This value is selected so that the time of integration "t" will be about 1/200 second. If the mains supply voltage, and hence the x-ray output, is high, then the time of integration needed for the preset value will be

shorter, and vice versa, if the supply voltage is lower, then the time of integration will be longer. When the preset value is reached, electronic switching causes the integration of the second current from the lower detector to stop, and the value of the integral is held and fed out to give a y-deflection on an oscilloscope screen. At the end of each half cycle, both integrators are reset to zero and the procedure is repeated.

The voltage for the x-deflection of the oscilloscope is obtained from a tracking potentiometer, whose roller contact moves with the system carrying the limb. The oscilloscope trace of the ulna is made to give a graph in which the increase in ordinate indicates an increase of the bone minerals. The display is photographed for measurements and record purposes.

Calibration of the vertical scale was initially provided by using a reference step wedge made of ivory. This wedge ranges in thickness from 3 mm to 13 mm in 1 mm steps. The wedge is placed in the water bath, beside the limb, so as to be scanned in the same way as the limb. Ivory was chosen as an easily machined material having a composition similar to that of bone. It is realised, however, that ivory is not ideal as a calibration material for the following reasons:

1. It is not homogenous, since it possesses a microstructure which can just be resolved by the apparatus.

2. It has a tendency to absorb water.

3. Also, its elemental composition is not precisely known.

For these reasons, considerable work has been carried out by the writer, under the supervision of Dr. J.A. Archer-Hall, in order to produce an artificial bone-like material to be used as a reference for this apparatus. The intention was to make a material which has a density and an elemental composition, very nearly similar to that of bone, and also precisely known so that it would be possible to indicate the increase of the y-deflection of the oscilloscope, for each x-ray scan, in terms of mgm minerals instead of mm ivory. The physical properties of such a material must fulfil the requirements of being solid, compact, and rigid, so that it can easily be machined to the required shape, i.e. a step wedge. It must also be homogeneous, insoluble in water and has no tendency to absorb water.

The experimental procedures for the preparation of the artificial bone-like material, required for this purpose, will be explained in Appendix "A".

(ii) Bone tomography

After the estimation of the amount and site of bone mineral at each point across the ulna, using the same technique of x-ray absorption scan, it is necessary to determine the corresponding path length, in order to determine the actual bone mineral density. The required path lengths can be obtained from an accurate outline cross-section of the ulna at the level of the x-ray scan, by using a tomograph.

It had initially been proposed by Dr. P. Carpenter, Radiologist at Dudley Road Hospital, that the required ulna cross-section could be provided by x-ray tomography, but it has been shown by experiments on post-mortem ulnas, (in which error due to movement of the patient does not occur) that this technique is not sufficiently accurate for the proposed requirement. The reasons for this have been dealt with in Chapter I.

CHAPTER I

INTRODUCTION

X-RAY TOMOGRAPHS

As explained before, it is required to obtain accurately the outline of the transverse section of the ulna in live patients. Such information of the cross-section profile is to be used in conjunction with the new technique of x-ray bone densitometry which has been successfully developed in this department. This bone densitometer performs a bone absorption scan with high accuracy and spatial resolution, and the tomography information from the profile of the cross-section of the ulna will enable the actual bone density to be determined.

The x-ray tomographs are those in which x-ray beam from a diagnostic x-ray tube, and a film cassette, are used to produce a radiograph of a transverse cross-section (parallel to the cassette) of the required subject. The principle of the x-ray tomograph is based on casting a shadow of each small structure, in the required plane to be tomographed on a separate point upon the film, forming a radiographic picture of the cross-section at that plane. This of course requires the rotation of the film cassette and either the patient or the x-ray tube. Therefore, there are two types of x-ray tomographs:-

(i) One type in which the patient is kept fixed and both the x-ray tube and the film cassette rotate simultaneously in the same direction and in constant ratio, by means of a connecting arm which rotates about an axis, the level of which is adjusted to the selected level of the part to be tomographed.

(ii) The other type of x-ray tomographs, is that one in which the x-ray tube is kept fixed and both the patient and film cassette rotate at the same angular speed. In this type of tomograph, the patient is seated on a saddle, close to a horizontal film cassette, and the x-ray beam is directed at an angle 20-30^{o} to the horizontal.

In both types of x-ray tomographs, the alignment of the x-ray tube is such that, the line FO (Fig. 1.1) between its focal spot F and the centre of rotation of the cassette O, must intersect exactly the vertical axis KL of the patient at the point P, through which the required horizontal plane is to be tomographed. Also, the x-ray tube is energized during one complete rotation of the cassette and the patient (or the x-ray tube itself, in the case of the first type).

1.1. Theory of the x-ray tomographs

The principles underlying x-ray tomographs can be illustrated geometrically. In order to do this, let us consider the second type, in which the x-ray tube is kept

fixed and both the patient and film cassette rotate. Suppose a patient, sitting on a saddle, rotates with a uniform speed about a vertical axis KL (Fig. 1.1) ,and so also does a horizontal film cassette about a vertical axis OM with exactly the same angular velocity.

Let us consider a tiny structure at the point P, on the axis of rotation of the patient (KL), whose shadow falls on the centre of rotation of the film "O". When the patient rotates, this structure rotates and so also does its shadow in space at the point "O". Since the film rotates about its centre O with the same angular speed, the shadow of "P" always remains in the same position on the film "O", forming a sharp image of P. Suppose a point P_1, in the same horizontal level as P, whose shadow falls at the point O_1 on the film. When the patient is rotated, P_1 moves round a horizontal circle of radius PP_1. Accordingly, its shadow at O_1 moves in space and with the same angular velocity, round a horizontal circle of radius OO_1, which is the geometrical projection of PP_1 upon the film. Beneath this moving shadow, there is the film which rotates about O with exactly the same angular velocity. Therefore, the shadow of P_1 always remains stationary on the film, forming a sharply defined image of the point P_1. The same considerations apply to any other point in the same horizontal plane through P. Therefore the resulting tomographic picture represents sharp images of all the structures in that plane. This plane is defined as the plane of cut, which is the horizontal plane through the intersection of the line joining the focal spot of the x-ray

tube to the centre of rotation of the film, and the axis of rotation of the patient.

On the other hand, this is not applicable for any other plane above or below the plane of cut. For example, as the point R (vertically above P) rotates about itself, its shadow at the point Q on the film rotates about itself and does not move in space but remains stationary there, while the film rotates beneath it. Therefore, the shadow of R describes a circular path on the film, whose centre is at the centre of rotation of the film (at O), and its radius is equal to OQ which is the geometrical projection of PR upon the film. Thus the image of R on the film will be blurred. Finally, consider the point R_1, in the same horizontal level as R, whose shadow falls at the point Q_1 on the film. When the patient rotates, R_1 rotates in a circular path around the axis KL, and its shadow moves in space round a horizontal circle but with a different angular velocity from that of the film. Therefore, the shadow of R_1 describes a circular path on the film, and hence its image is blurred. The centre of this circular path is at the point O_1, and its radius is equal to O_1Q_1 which is the geometrical projection of R_1P_1. The same considerations apply to any other point in the same horizontal plane through R.

Therefore, the shadow of any point on other planes above or below the selected plane (the plane of cut) through P, describes a circular path whose centre is at the geometrical projection of the corresponding point on the plane of

cut, and its radius equalsto the geometrical projection upon the film of its vertical separation from the plane of cut.

This result may be expressed analytically as follows: If "y" represents the vertical distance PR, "a" represents the horizontal separation between the focal spot and the axis of rotation of the patient, and "b" represents the horizontal separation between the two axes of rotation of the patient and film cassette, as shown in Fig. 1.1, then

$$c = a + b$$

If "θ" represents the angle made by the central ray FO with the cassette, i.e. with the horizontal, and θ' is the angle made by the ray FQ with the cassette; then

$$OQ = ON \cot \theta'$$

From Fig. 1.1, we have

$$\frac{ON}{PR} = {}^{C}/_{a}$$

or

$$ON = PR\left(\frac{c}{a}\right) = y\,\frac{c}{a}$$

Therefore,

$$OQ = y\left(\frac{c}{a}\right) \cot \theta'$$

This equation gives the radius of the circular path on the film described by the shadow of a structure at a point y(cm) above the plane of cut.

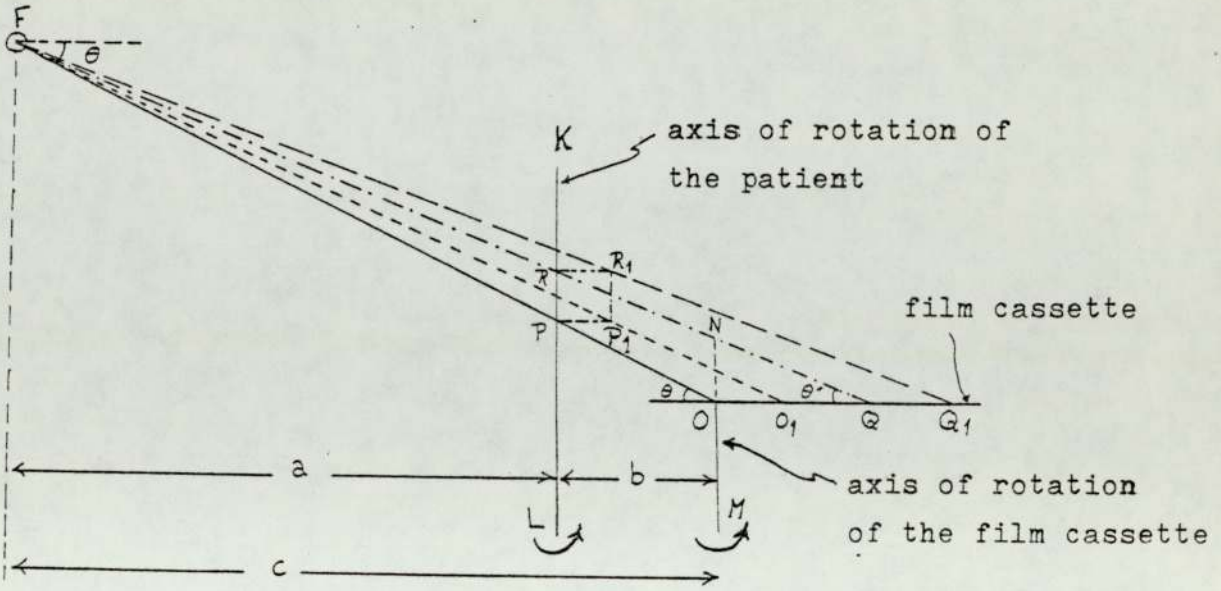

Fig. 1.1 Representation of the transverse axial tomography.

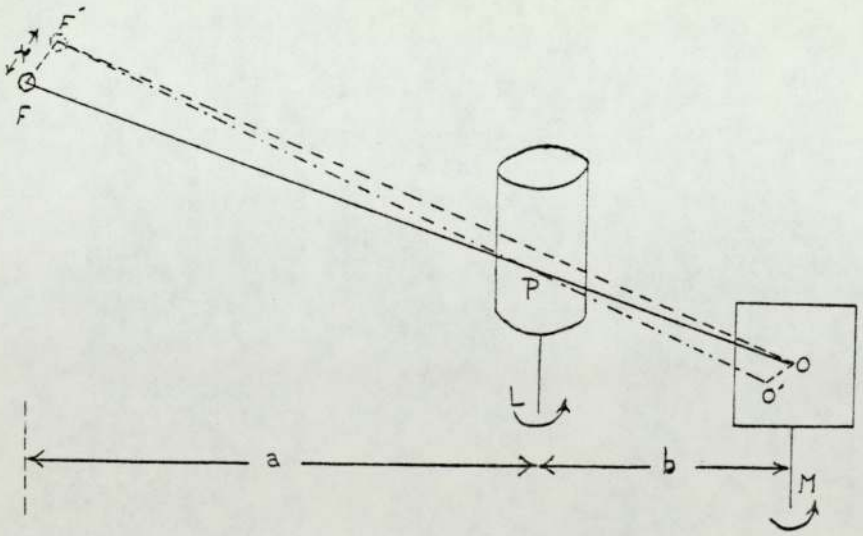

Fig. 1.2 Lateral displacement of the focal spot.

The radiograph, therefore, represents sharp images of points in the selected plane through P (Fig. 1.1), while the representation of the points above or below this plane, is less defined and blurred out on the film. These considerations show that the x-ray tomography produces a tomographic section parallel to the film cassette and perpendicular to the axis of rotation of the patient. It is therefore described as transverse axial tomography (T.A.T.) or horizontal body section, or stratigraphy.

It must be noted that the magnification of the radiograph on the film is in the ratio:

$$\text{The magnification} = \frac{OO_1}{PP_1} = \frac{FO}{FP}$$

By similar triangles (Fig. 1.1) then

$$\text{The magnification} = \frac{c}{a}$$

This means that the magnification of the tomographic picture is equal to the horizontal separation between the focal spot and the axis of rotation of the film (c), divided by that separation between the focal spot and the axis of rotation of the patient (a).

1.2. Errors and disadvantages of x-ray tomographs

Although the principle of x-ray tomography is simple, it is not accurate enough to be suitable for our purpose in order to determine precisely the outline cross-section

of the ulna, where its diameter is about 12-16 mm. and therefore the produced errors will be great. These errors are due to the following reasons:-

1. Geometrical effects
2. Incorrect alignment
3. Mechanical imperfection and lack of synchronism
4. Photographic response
5. Scattered radiation reaching the film

1.2.1 Geometrical effects

The geometrical error arises from the finite size of the x-ray source, which gives rise to an umbra and penumbra. This error is unavoidable and it can be determined by the geometrical projection of the source size upon the film. If the focal spot is d mm. in diameter (or a square i.e. dxd mm) then the geometrical error (Farr, 1964) will be between

$$(b/_a)d, \text{ and } (b/_a)d \operatorname{cosec} \theta$$

Since the dimensions of the x-ray source could be almost 2 mm or more, and since in most of the x-ray tomographs, b= 50 cm, a= 150 cm and $\theta = 30^{\circ}$; then the resulting error due to the finite size of the x-ray source will be about 1.33 mm. This means that in the case of the ulna cross-section profile, an error of about 10% will be produced.

1.2.2. Errors due to incorrect alignment

We have already seen that for an accurate tomograph the x-ray source centre must be in the vertical plane containing the axes of rotation of the patient and film. In such a position the x-ray shadow of P (the section centre) will fall on the film centre O. Now the first trouble is the difficulty of accurately finding the axis and the centre of the internal organ to be tomographed.

If the x-ray tube is raised or lowered, vertically in the plane of figure 1.1, the shadow of the centre P of the selected plane of cut will fall elsewhere. However, the shadow can be brought back to the centre of the film at O, by moving the x-ray tube up or down in the same vertical plane.

On the other hand, if the x-ray beam is shifted horizontally or laterally, i.e. in or out of the plane of the figure, the shadow will fall elsewhere. In this case no movement of the patient up or down, will bring the shadow back to the centre of the film.

Suppose that the focal spot F is displaced laterally by a distance x to the point F′, as shown in Fig. 1.2. The line F′O joining the focal spot to the centre of rotation of the film, does not intersect the axis of rotation of the patient. In this case the shadow of the centre P of the selected plane of cut is displaced laterally on the film to the point O′. Since the film rotates beneath it, the shadow describes a circular path of radius OO′. By similar triangles

we have

$$\frac{OO'}{FF'} = \frac{OP}{FP} = \frac{b}{a}$$

or

$$OO' = x(b/a)$$

Therefore, if the focal spot is moved laterally by a distance x, then the images of all the structures in the required plane of cut will describe a circular path of radius OO' and hence will be blurred on the film by the value of the diameter of this circular path, i.e. 2x(b/a). Suppose that the lateral shift of the x-ray beam is 2 mm., which could easily occur, and substituting for the values of b and a, which are most commonly 50cm and 150 cm respectively; then the resulting error will be about 1.33 mm. This error represents about 10% of the outline of the ulna cross-section.

The lateral shift error may also happen due to a lateral movement of the patient or the film, out of the common vertical plane. It will be serious if the lateral movement of two objects, e.g. the x-ray beam and the patient, occur at the same time and in opposite directions, where the errors will be additive.

1.2.3 Mechanical imperfection and lack of synchronism

Mechanical imperfection such as loose bearings, may result in a lateral shift of any, or both, of the rotating columns. The errors introduced by this effect may be

regarded as that due to a lateral shift of the x-ray beam, which has already been discussed.

Also, the gears in the base of the tomograph which cause the two columns to rotate together may introduce a change of phase. It has been found by Farr (1964) that, during the rotation, a change of phase of 0.1° may introduce a blurring of about 0.33 mm. For a change of phase of 0.5°, which may readily occur, a blurring of about 1.65mm may be introduced. The percentage error due to this effect, in the case of the ulna cross-section could be more than 10%.

1.2.4 Photographic response

The definition (resolution) of the x-ray image on a film depends on the density and contrast, which are affected by many factors. The most important among these factors are:

(i) Variations in the x-ray tube voltage
(ii) Variation in the exposure
(iii) Development of the film
(iv) Screen and film effects.

(i) Blurring due to variations in tube voltage

The x-ray image depends for its formation on differences in absorption by the various parts of the patient. In the energy range where photoelectric absorption is important, bone will absorb much greater amounts of radiation than soft tissue and hence it will cast a sharp shadow. As the energy is increased the differential between bone and soft tissue

will start to disappear and the radiographic picture will show less contrast. Therefore, the contrast on the film decreases as the x-ray tube voltage increases. The density of a film, on the other hand, is proportional to some power "n" of the tube voltage "V" (in kilovolts). It is also proportional to the exposure (It) in milliampere seconds and inversely proportional to the square of the focus to film distance "f" (in cm) as given by the following equation

$$\text{density} = K \frac{V^n It}{f^2}$$

where K is the proportionality constant; I is the tube current in ma; t is the exposure time in seconds; and n is a number which depends on many factors, i.e. the kilovoltage applied, the type of the film or film screen and the thickness of the patient. It has been found (Mattsson, 1955) that for a range of tube voltages up to 100 KVp, n may be placed in the above equation as 3 or 4 for most calculations.

From the discussion, a 5% variation in the tube voltage which may readily occur from half cycle to another of the 50Hz mains supply, may give rise to 20% change in the density of the film. Additional changes in the density may be introduced by variations in the tube current and focus to film distance f. These changes in density will affect the contrast and contribute a blurring in the radiographic picture.

(ii) Blurring due to the variations in exposure

From the above equation it can be seen that for a fixed tube voltage V, and focus to film distance f; the density is

proportional to the exposure (It) in ma.sec. The relation between density and exposure can be plotted as shown in Fig. 1.3. The resulting curve is known as the characteristic curve of the film. At the bottom of the curve there is a curved portion (the toe), followed by a straight portion and then another curved portion (the shoulder) at the beginning of a saturation region. The contrast at any portion of the curve is determined by the slope of the curve at that portion. The curved portions, i.e. the toe and shoulder, are of less use since contrast in these regions is small. At higher densities, beyond the shoulder, the curve becomes flat, yielding a region where density is independent of exposure. It is customary to use films in diagnostic radiology in the density range of the straight portion, where the contrast is high.

In the case of bone tomography, if the density of the tissue image falls in the straight portion of the characteristic curve, the bone image, on the other hand, will be underexposed and falls on the toe region. This will result in a blurred picture of the outline of the ulna cross-section.

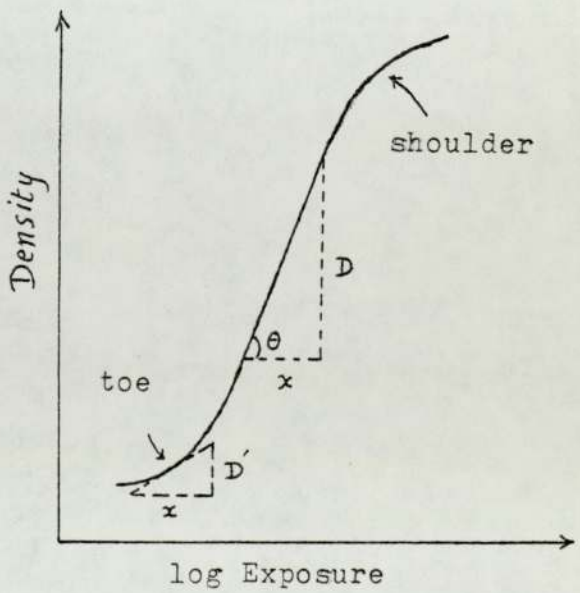

Fig.1.3. hypothetical film characteristic curve.

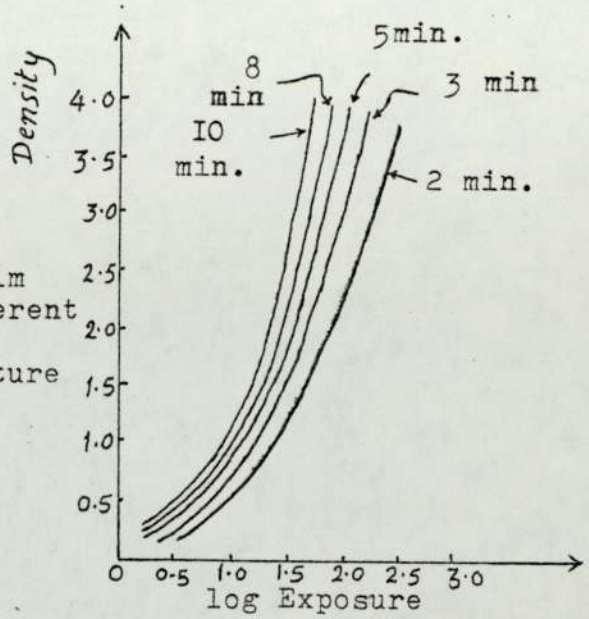

Fig. 1.4. Characteristic curves of x-ray film developed for different periods of time (developer temperature is 20° C)

(iii) Film development

The characteristic curve of a film is dependent on the development time and the developer temperature. For a fixed temperature, if the development time is increased, the characteristic curve becomes steeper and moves progressively to the left, as shown in Fig. 1.4 (Johns, 1961). From these curves it can be seen that for a given exposure the density increases with the development time. Also, fog is caused by the slow development of the silver particles in the absence of previous irradiation. This is known as chemical fog which tends to increase with the development time.

In the same manner, for a given development time, the characteristic curves of a film will be affected by the temperature of the developer. In most types of x-ray films, the effect due to $1^{\circ}C$ rise in temperature is nearly equivalent to that due to 1 minute increase in development time.

Therefore any increase in the temperature and time of development will produce a considerable blurring shrinking of the tomographic picture of the ulna.

(iv) Screen and film blurring

The intensifying screens are two layers of a fluorescent material, which are placed so that the film with its two emulsions is sandwiched between them. The fluorescent material, which is usually calcium tungstate, has a high atomic number so that it absorbs the incident x-rays giving rise to a fluorescent radiation in the region of visible light or near ultraviolet. This light is absorbed by the emulsions of the film giving an image. Since the light is in the visible region it may be stopped by a very thin layer of dirt or grease and hence will produce a region of diffuse image. Also, light rays which have a long path in the screen, more than those which are ejected normal to the screen, will contribute unsharpness of the image. Furthermore, when a poor contact between the screens and the film is achieved, the fluorescent light spreads from its source and causes a diffuse image on the film.

Additional blurring will be introduced by parallax between the two images on a double-emulsion film. Since the x-rays fall on the emulsions of the film, which are about 0.2 mm apart, at a glancing angle θ, then the image of a stationary structure produced on the lower emulsion will be displaced from that on the upper emulsion, in the direction LM (Fig. 1.1) by a distance equal to 0.2 cot θ mm. If θ

is 30°, this displacement amounts to 0.35 mm. The parallax effect may be greater than this value, since the images may be regarded as being generated within the screen coatings, i.e. at a rather greater separation than 0.2 mm. The error introduced by parallax effect, which is unavoidable, may be about 4-5% in the case of the ulna cross-section.

1.2.5 Effect of scattered radiations reaching the film

The scattered radiation reaching the film would tend to mask the shadow cast by the structures in the selected plane of cut and cause unsharpness of the resulting tomographic picture. Also, a regional or overall fog may be produced by scattered radiation depending on its amount and its direction on the film. The effect of scattered radiation is inversely proportional to the square of the patient to film distance.

From the previous discussion it is obvious that the x-ray tomographs will not yield results of sufficient accuracy to be useful in our case of the ulna cross-section profile, where the errors may total 30-40%. Consideration has been given to use an ultrasonic technique as a possible alternative.

CHAPTER II

THEORETICAL STUDIES OF ULTRASONICS AND PROVISIONAL CONCEPTS FOR THE OPERATION OF THE SYSTEM

Introduction

In the first chapter it has been shown that the x-ray tomography is not sufficiently accurate to be useful for our purpose. In this chapter the possibility of using ultrasonics as a means of determining the required cross-section profile of the ulna, will be discussed.

Ultrasonic radiation has been utilised by many workers for the purpose of visualization and localisation of tissue interfaces by using the pulse echo-ranging technique, Wild (1950); Howry (1957); Holmes (1958); Donald and Brown (1961); Kossoff et al (1964, 1965, 1966 & 1968); Robinson et al (1966); Fry et al (1968); and many others.

The principle of pulse echo-ranging technique is that in which a train of short duration pulses of ultrasonic waves, is transmitted from the transducer in a known direction into the patient. When the pulse meets a boundary separating two media of different specific acoustic impedances, part of its energy (depending on the difference in these acoustic impedances) is reflected back. The returning echo is received, usually, by the same transducer which acts as a detector during the period between two successive transmitted pulses. The information obtained from the echo is the direction of the original beam, and the time that it takes to return. The former indicates the direction/...

of the reflecting interface, and the latter gives a measure of the distance of the interface from the transducer surface. This information is usually presented visually, the received signals being amplified and displayed on a cathode-ray screen.

One of the factors which has thought to be of significance to the use of ultrasonics is the marked difference of the acoustic impendances at bone-soft tissue interface. This impedance difference is the greatest of any tissue interface in the body. The mean value of acoustic impedance (ρc) for human tissue is about 1.63×10^6 kg/m^2.sec., and that for bone is about 7×10^6 kg/m^2.sec. Hence, an amplitude reflection of about 62% could be obtained at bone-soft tissue interface. It is expected that an amplitude reflection not exceeding 10% could occur at any other interface.

Most of the previous techniques used in diagnosis involve a broad beam of ultrasonics of large field depth, using plane transducers. Since the resolution of fine details requires looking at one little patch of the scanned bone at each time, the system must imply a small beam width of ultrasonics falling on an area as small as possible. These conditions may be achieved by using a converging beam of ultrasonics with a sharp focus.

Therefore, it has been decided to use a spherical concave transducer in a bath of water surrounding the limb, and a technique maintaining its focus on the bone surface.

The accuracy of any measurements carried out by using ultrasonic waves, will be limited almost entirely by:

(i) the physical conditions relating to diffraction of these waves; and,

(ii) the electronic processing of the signals from transducers.

The former will be discussed in part (A) of this chapter, and the latter will be dealt with in part (B).

PART (A)

STUDY OF ULTRASONIC DIFFRACTION WITH SOME NEW CONCEPTS

An early experimental work was carried out by Willard (1947, 1949), using spherical concave transducers radiating into water, in order to determine the degree of acoustic focusing and the effects of ultrasonic wave diffraction on the sharpness of focus. He found that the ultrasonic diffraction pattern is similar to that of a telescope lens, i.e. a strong core at the central part of the focal plane and successively weaker rings.

O'Neil (1949) has investigated a theory of spherical concave transducers, in which the radius of the circular boundary of the transducer is large compared both with the wavelength and with the depth of the concave surface. This theory is valid only for transducers of a small aperture and a relatively large radius of curvature, i.e. for weakly focusing transducers.

Since it has been shown that the diffraction pattern in the focal plane of a hemispherical bowl, using an analytic integration, is different from that given by classical theory, it has been thought worth while to examine again carefully the effect of diffraction near the centre of curvature for spherical concave transducers of any aperture . This method is based on the following assumptions:

1. The bowl transducer is vibrating in simple harmonic motion normal to its surface.

2. The radius of curvature of the bowl is large compared with the wavelength.
3. The observation points in the focal plane are not far from the centre of curvature.

Having these assumptions in consideration, the Huygen's integral can be applied accurately, by using:

(a) Appropriate geometrical parameters in order to solve mathematically without approximation, one stage of the double integration.
(b) Numerical evaluation of the remaining single integral by the computer.

Following the success of this method it was thought possible that a similar approach to the problem of the flat disc radiator could be made, but using also the full Kirchhoff's integral, which would result in the more exact evaluation of the diffraction pattern than previously obtained.

Further, as it has been decided to use pulse excitation of a bowl transducer, as is used in many other systems, it was thought useful to investigate the effects of this on the diffraction pattern.

Since the Huygen's integral is a special case of the general Kirchhoff's integral, the topics discussed in part (A) of this chapter are presented as follows:-

1. The field distribution of a flat circular transducer, at steady state, using Kirchhoff's integral.

2. Ultrasonic distribution in the focal plane of a spherical bowl transducer, at steady state, using Huygen's integral.

3. Effects of pulse excitation on the diffraction pattern in the focal plane of a bowl transducer, for various conditions of attenuation affecting the bandwidth.

4. The axial ultrasonic distribution around the focus of a concave bowl transducer, at steady state, using the Huygen's integral.

2-A.1 FIELD DISTRIBUTION FOR A FLAT CIRCULAR TRANSDUCER

Using Kirchhoff's Integral

The calculation of the field distribution for a circular piston vibrating in simple harmonic motion has been the subject of numerous investigations; recently Zemanek (1971), and Lockwood and Willette (1973). It may be seen that these apply the Huygen's integral, which is an approximate case of the general Kirchhoff's integral, and in addition other approximations and limitations in some cases.

The purpose of the present work is to develop a method by which the field distribution of a flat disc transducer can be determined more quickly and accurately than by other methods. This method involves:

1. Application of the full Kirchhoff's integral, which has not been done previously.

2. An accurate mathematical analysis using suitable geometrical parameters, in order to obtain an exact single integral which can be evaluated numerically by the computer.

Let us consider an arbitrary surface of area S which vibrates in a simple harmonic motion normal to itself. dS, being an elementary area at a point Q on that surface. P is an observation point in the field at a distance s from Q. Θ being the angle subtended by the outward normal and PQ.

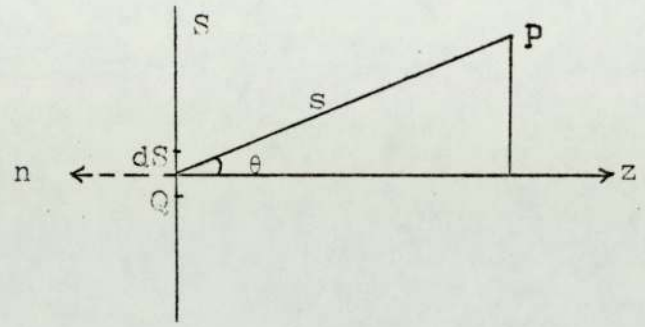

The acoustic potential ϕ_p, at the point P, due to the total contribution from the surface S (Coulson, 1955) is given by:

$$\phi_p = \frac{1}{4\pi} \int_S \left\{ \frac{e^{-jks}}{s} - \frac{\partial \Psi}{\partial n} - \Psi \frac{\partial}{\partial n} \left(\frac{e^{-jks}}{s} \right) \right\} dS$$

where, $k=2\pi/\lambda$; λ denotes the wavelength in the propagating medium.

Ψ, the acoustic potential for an element of area dS, may be given by:

$$\Psi = e^{-jkz}$$

Also, $\frac{\partial z}{\partial n} = -1$; and $\frac{\partial s}{\partial n} = \cos\theta$

Substituting these values into the above equation, then

$$\phi_p = \frac{1}{4\pi} \int_S \left\{ \frac{e^{-jks}}{s} \frac{\partial}{\partial n} \left(e^{-jkz} \right) - e^{-jkz} \frac{\partial}{\partial n} \left(\frac{e^{-jks}}{s} \right) \right\} dS$$

$$= \frac{1}{4\pi} \int_S \left\{ \frac{e^{-jks}}{s} \left[- \frac{\partial}{\partial z} \left(e^{-jkz} \right) \right] - e^{-jkz} \cos\theta \left[\frac{\partial}{\partial s} \left(\frac{e^{-jks}}{s} \right) \right] \right\} dS$$

$$= \frac{1}{4\pi} \int_S \left\{ \frac{e^{-jks}}{s} \left(jke^{-jkz} \right) - e^{-jkz} \cos\theta \left(-\frac{jke^{-jks}}{s} - \frac{e^{-jks}}{s^2} \right) \right\} dS$$

$$= \frac{1}{4\pi} \int_S \left\{ e^{-jkz} \frac{e^{-jks}}{s} \left(jk + jk\cos\theta + \frac{\cos\theta}{s} \right) \right\} dS$$

For a plane disc transducer, at $z = o$, $e^{-jkz} = 1$. Since $\cos\theta = z/s$, the above equation may be written as follows:

$$\phi_P = \frac{1}{4\pi}\int_S \frac{e^{-jks}}{s}\left\{jk\left(1+\frac{z}{s}\right)+\frac{z}{s^2}\right\}dS \qquad \ldots\ldots (2.1)$$

This equation will be used accurately in the following sub-sections for the analysis of the acoustic distribution along the central axis, and the contribution at points inside and outside the cylinder limited by the extension of the disc circumference. From this analysis, the general relation giving the exact field distribution can be determined.

2-A.1.1 The Field Distribution Along the Central Axis

Figure (2.1) shows a plane disc transducer of area S, where P is an observation point at a distance z along the central axis. In order to calculate ϕ_P, due to the total contribution from the surface S, consider a circular elementary band of radius x, width dx, and area dS, where

$$dS = 2\pi x\ dx.$$

This form of element has been chosen as all the points on it are equi-distant (s) from P. From Fig.(2.1) we have

$s^2 = z^2 + x^2$; which by differentiation (where z is constant), gives: $2s\ ds = 2x dx$. Thus,

$$dS = 2\pi\ s\ ds$$

Substituting this value of dS into Eq.(2.1), then

$$\phi_P = \frac{1}{4\pi}\int_{s=z}^{s=s_1} \frac{e^{-jks}}{s}\left\{jk\left(1+\frac{z}{s}\right)+\frac{z}{s^2}\right\}\ 2\pi s\ ds$$

or: $$\phi_P = \frac{1}{2}\int_z^{s_1} e^{-jks}\left\{jk\left(1+\frac{z}{s}\right)+\frac{z}{s^2}\right\}\ ds$$

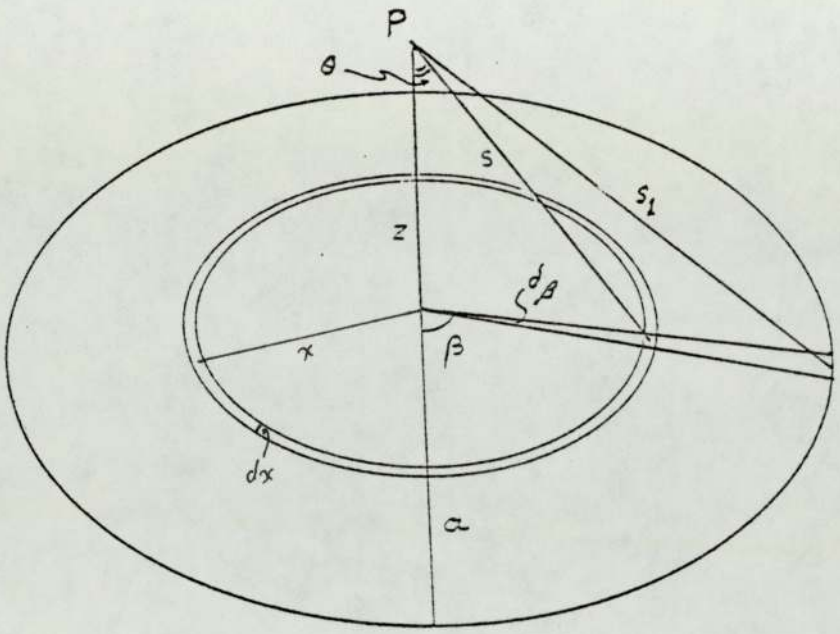

Fig. 2.1 Geometry used in calculating the distribution along the central axis of a flat circular transducer.

Assume that the solution of this integral equals to $e^{-jks} G_{(s)}$, where $G_{(s)}$ is a function of s, i.e.,

$$\phi_p = \frac{1}{2} \int e^{-jks} \left\{ jk\left(1+\frac{z}{s}\right)+\frac{z}{s^2} \right\} ds = \frac{1}{2} \left[e^{-jks} G_{(s)} \right] \quad .... (2.2)$$

Differentiating both sides of Eq.(2.2) with respect to s, then

$$e^{-jks} \left\{ jk\left(1+\frac{z}{s}\right)+\frac{z}{s^2} \right\} = e^{-jks} \frac{dG}{ds} - jk\, G_{(s)}\, e^{-jks}$$

or: $jk\left(1+\frac{z}{s}\right)+\frac{z}{s^2} = \frac{dG}{ds} - jk\, G_{(s)}$

Separating the real and imaginary parts in both sides of the above equation, then

$$G_{(s)} = -\left(1+\frac{z}{s}\right) \text{ ; and } \quad \frac{dG}{ds} = \frac{z}{s^2} \text{ which fits.}$$

Hence, substituting this value of $G_{(s)}$ into Eq.(2.2) gives

$$\phi_p = \frac{1}{2}\int_z^{s_1} e^{-jks}\left\{jk\left(1+\frac{z}{s}\right)+\frac{z}{s^2}\right\}ds = \frac{1}{2}\left[-e^{-jks}\left(1+\frac{z}{s}\right)\right]_z^{s_1} \qquad \ldots\ldots (2.3)$$

$$\text{or: } \phi_p = e^{-jkz} - \frac{1}{2}\left(1+\frac{z}{s_1}\right) e^{-jks_1} \qquad \ldots\ldots (2.4)$$

The real and imaginary parts, L and M, respectively of Eq.(2.4) are given by:

$$L = \text{Cos}(kz) - \tfrac{1}{2}\left(1+\frac{z}{s_1}\right)\text{Cos}(ks_1)$$

$$M = -\text{Sin}(kz) + \tfrac{1}{2}\left(1+\frac{z}{s_1}\right)\text{Sin}(ks_1)$$

The r.m.s. value (R_p) at the point P, is given by:

$$R_p = (L^2 + M^2)^{\frac{1}{2}}$$

Thus,

$$R_p = \left[\left\{\text{Cos}(kz)-\tfrac{1}{2}\left(1+\frac{z}{s_1}\right)\text{Cos}(ks_1)\right\}^2 + \left\{-\text{Sin}(kz)+\tfrac{1}{2}\left(1+\frac{z}{s_1}\right)\text{Sin}(ks_1)\right\}^2\right]^{1/2} \qquad \ldots\ldots\ldots (2.5)$$

Where $s_1 = \sqrt{a^2 + z^2}$; and $k = 2\pi/\lambda$, λ denotes the wavelength in the medium.

Using Eq.(2.5), the axial R_p values, in the near and far-field regions of a plane disc transducer for which $a/\lambda = 5$, have been calculated and plotted in Fig.(2.2). Also this equation was numerically evaluated on an ICL 1904S computer, using program (1) in Appendix (B) which gives the same results and plot (see Fig. 2.5-a).

The same program can also be used to give the plots of the axial distribution of disc transducers for which $a/\lambda = 2.5$ and 1 (see Figs. 2.6-a and 2.7-a).

Fig. 2.2 Near- and farfield axial distribution for a flat circular transducer. $a/\lambda = 5$.

From Fig. (2.2), it can be seen that the axial R_p values have a number of maxima and minima (depending on the ratio of a/λ). The minima have increasing values in the direction towards the transducer, whereas the maxima have smaller values in the same direction. These results are different from those of the previous investigations (recently Zemanek, 1971), where all the axial minima are zero and all the maxima have the same value.

The number, and also the positions of the axial maxima (z_{max}) and minima (z_{min}) from the transducer, were found to agree with the previous results, and hence can be calculated accurately by the following equations (Wells, 1969, pp.55).

$$Z_{min} = \frac{a^2 - n^2\lambda^2}{2n\lambda} \qquad \ldots (2.6)$$

where, $n = 1, 2, 3, 4, \ldots$

$$Z_{max} = \frac{4a^2 - \lambda^2 (2m+1)^2}{4\lambda(2m+1)} \qquad \ldots (2.7)$$

where, $m = o, 1, 2, 3, 4, \ldots$

The position of the last axial maximum $Z'_{max} = \frac{4a^2 - \lambda^2}{4\lambda}$

The calculation of the field of a plane disc transducer may be divided into two regions, one is inside the cylinder limited by the extension of the disc circumference, and the other is outside that limit. In the following sub-sections a mathematical analysis will be carried out in both regions, from which the general relation of the field distribution can be determined.

2-A.1.2 Analysis of the outside field region

The co-ordinate system used in this analysis, is shown in Fig. (2.3-a). The origin of the system is considered to be at the centre C of the disc, whose surface is in the XY-plane, and its central axis is in the Z direction. Hence, the co-ordinate of a radiating point Q on the disc surface is (x,y,o), and that of an observation point P, in the ZY-plane, is (o,b,z), where b is the distance of P from the central axis.

Fig. (2.3-b) shows the geometry involved in the calculation of the outside field region in which b > a, where a is the radius of the disc. The disc surface is considered to be in the plane of the figure, whereas the central axis and the point P are normal to it at the points C and N, respectively.

In order to determine ϕ_p due to the total contribution from the disc surface (S) as given by Eq.(2.1); let us consider the elementary area dS, represented by a circular arc QR of radius ρ and width $d\rho$. This form of element has been chosen as all the points on it are equi-distant (s) from P.

$dS = 2\alpha\rho\ d\rho$, where α is the angle subtended by NQ and NC (Fig. 2.3-b). Since $s^2 = z^2 + \rho^2$; which by differentiation (where z is constant) gives:

$2sds = 2\rho d\rho$. Therefore,

$dS = 2\alpha s\ ds$. Substituting this value into Eq. (2.1), then

$$\phi_p = \frac{1}{2\pi} \int_{s_1}^{s_2} e^{-jks} \left\{ jk\left(1+\frac{z}{s}\right) + \frac{z}{s^2} \right\} \alpha\ ds$$

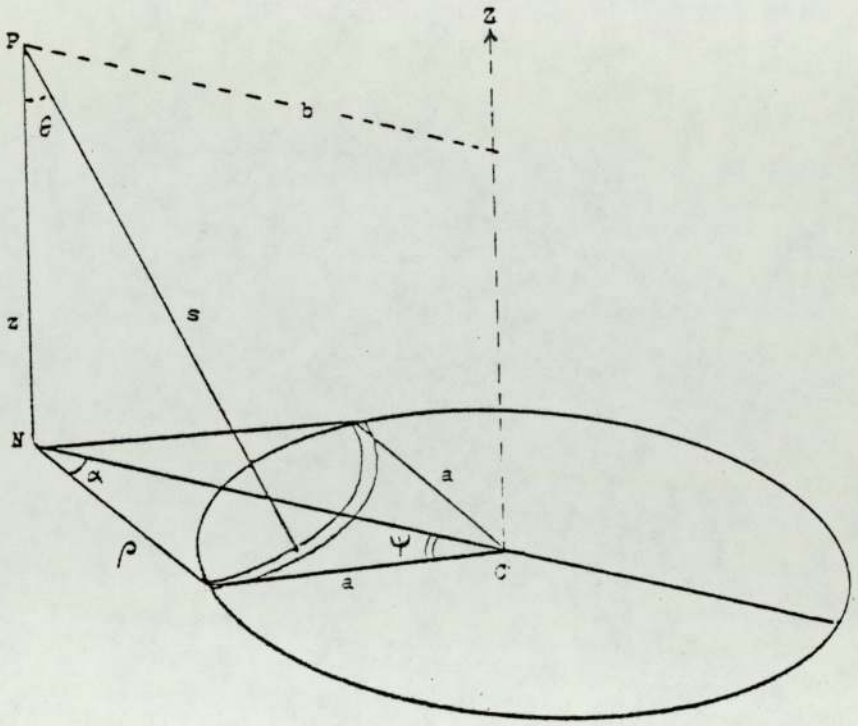

(a)

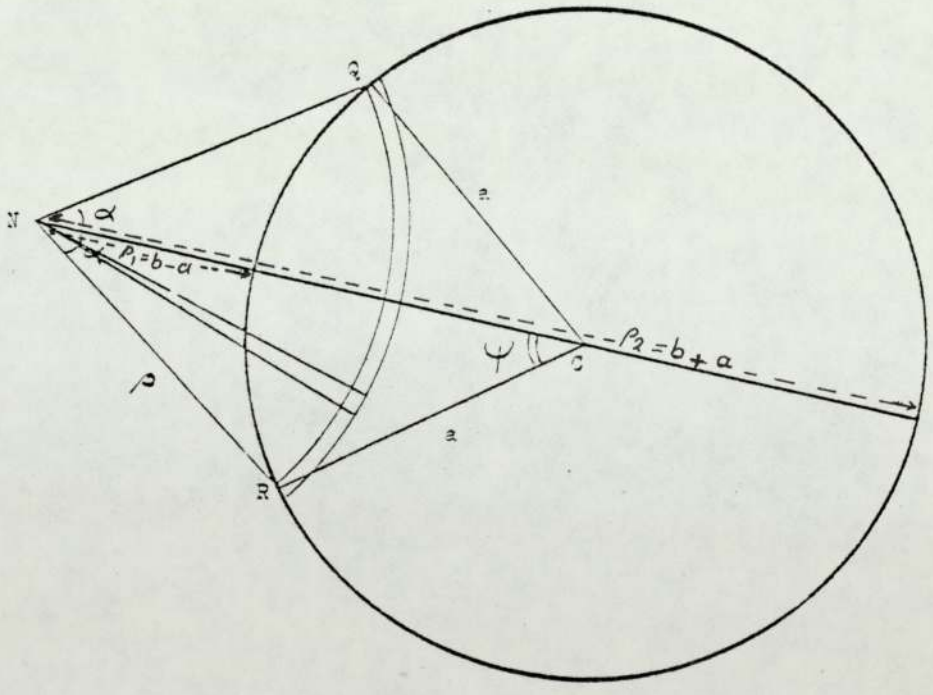

(b)

Fig. 2.3 Geometry used in calculating the distribution in the outside field region (b > a).

where, $s_1 = \sqrt{z^2 + \rho_1^2}$; and $s_2 = \sqrt{z^2 + \rho_2^2}$

Integrating by parts of the above equation, where the variable α is a function of s, and using the solution of the integral given by Eq. (2.3), then

$$\Phi_p = \frac{1}{2\pi}\left[\left\{-e^{-jks}\left(1+\frac{z}{s}\right)\right\}\alpha\right]_{s_1}^{s_2} - \frac{1}{2\pi}\int_{s_1}^{s_2}\left\{-e^{-jks}\left(1+\frac{z}{s}\right)\right\}\frac{d\alpha}{ds}\,ds$$

The first term on the right-hand side of this equation is zero, since α is zero at the limits s_1 and s_2, i.e.

$$\Phi_p = \frac{1}{2\pi}\int_{s_1}^{s_2} e^{-jks}\left(1+\frac{z}{s}\right)\,d\alpha \qquad \ldots\ (2.8)$$

In order to solve this integral, the angle α may be related to another angle Ψ whose limits, corresponding to s_1 and s_2, are zero and π, respectively. The relation between α and Ψ, can be determined from the trigonometry of Fig. (2.3-b) as follows:

$$a^2 = \rho^2 + b^2 - 2\rho\, b \cos\alpha\ ;\ \text{i.e. } \cos\alpha = \frac{b^2+\rho^2-a^2}{2b\rho}\ ; \qquad \ldots\ (2.9)$$

$$\rho^2 = a^2 + b^2 - 2ab\cos\Psi, \qquad \ldots\ (2.10)$$

or,

$$\cos\Psi = \frac{b^2 + a^2 - \rho^2}{2ab}\ ; \qquad \ldots\ (2.11)$$

and,

$$\frac{\sin\alpha}{\sin\Psi} = \frac{a}{\rho},\ \text{i.e. } \sin\alpha = \frac{a\sin\Psi}{\rho} \qquad \ldots\ (2.12)$$

By differentiating Eq. (2.9) with respect to ρ, and substituting Sin α from Eq. (2.12) into the resultant, then

$$\text{Sin } \Psi \frac{d\alpha}{d\rho} = \frac{b^2 - a^2 - \rho^2}{2a\rho b}$$

Differentiating Eq. (2.11) with respect to ρ, and dividing the above equation by the resultant, we have

$$\frac{d\alpha}{d\Psi} = \frac{b^2 - a^2 - \rho^2}{2\rho^2}$$

Equation (2.10) gives the value of ρ^2, and by simple re-arrangement, it also gives the value of $(b^2 - a^2 - \rho^2) = 2(ab\,\text{Cos } \Psi - a^2)$. Substituting these values into the last equation, gives eventually $d\alpha$ in terms of Ψ as follows:

$$d\alpha = \left(\frac{ab\,\text{Cos } \Psi - a^2}{a^2 + b^2 - 2ab\,\text{Cos } \Psi} \right) d\Psi \qquad \ldots\ (2.13)$$

Substituting $d\alpha$ into Eq. (2.8), then ϕ_p at any point for which $b > a$, is given by:

$$\phi_p = \frac{1}{2\pi} \int_{\Psi=0}^{\Psi=\pi} e^{-jks} \left(1 + \frac{z}{s}\right) \left(\frac{ab\,\text{Cos } \Psi - a^2}{a^2 + b^2 - 2ab\,\text{Cos } \Psi} \right) d\Psi \qquad \ldots\ (2.14)$$

where,

$$s = \sqrt{z^2 + \rho^2} = (z^2 + a^2 + b^2 - 2ab\,\text{Cos } \Psi)^{\frac{1}{2}} \qquad \ldots\ (2.15)$$

2-A.1.3 Analysis of the inside field region

The co-ordinate system used in the calculation of the field distribution in the inside region, where $b < a$, is shown in Fig.(2.4-a). The geometry involved in this calculation is shown in Fig. (2.4-b), from which it can be seen that, for each observation point P, there are two types of equi-distant elementary areas on the disc surface. One type of elements is represented by circular arcs of radius ρ and width $d\rho$, and the other is represented by complete circles of radius ρ' and width $d\rho$. As 'b' increases to approach 'a', the number of complete circle elements decreases, whereas that represented by circular arcs increases, and vice versa. Therefore, for a point P at a distance 'a' from the central axis, all the equi-distant elementary areas are represented by circular arcs, and those for a point on the central axis are only represented by complete circles.

For any point P in the inside field region, $\dot{\Phi}_p$ due to the whole disc area S equals to the summation of the contributions due to the complete circle elements $\dot{\Phi}'_p$, and the circular arc elements $\dot{\Phi}''_p$, i.e.

$$\dot{\Phi}_p = \dot{\Phi}'_p + \dot{\Phi}''_p$$

(i) Contributions due to the equi-distant circular elementary areas ($\dot{\Phi}'_p$):-

Let us consider a point P at a distance b from the central axis, where $b < a$, and at a distance s from any point on a circular elementary area dS. The limits of the radii (ρ')

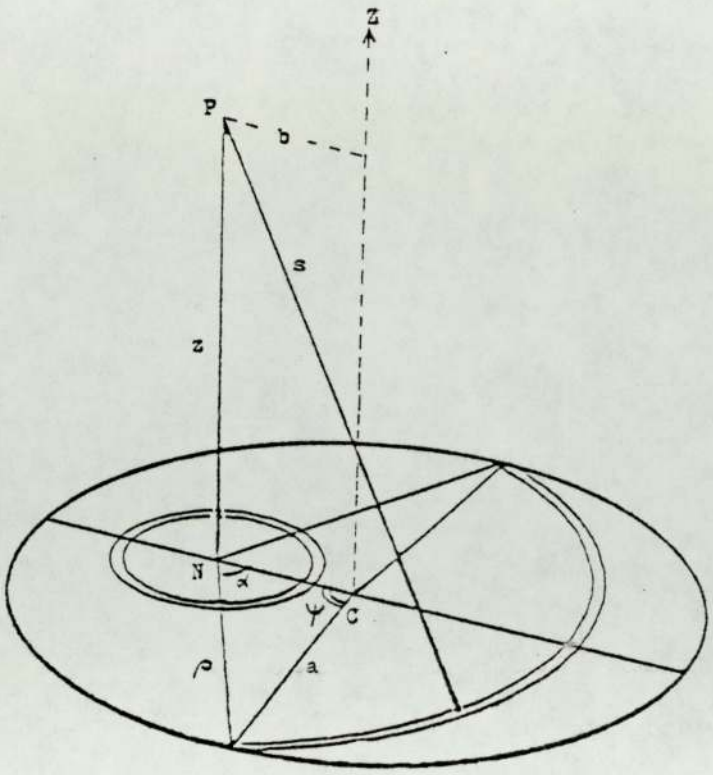

(a)

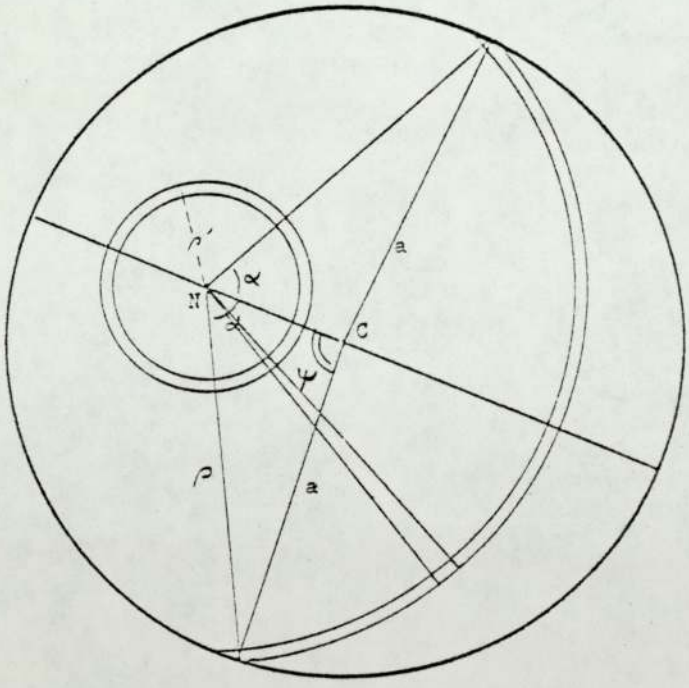

(b)

Fig. 2.4 Geometry used in calculating the distribution in the inside field region ($b < a$).

of these elements are $\rho_o = o$ and $\rho_1 = a-b$, as shown in Fig.(2.4-b). The elementary area dS, is given by:

$$dS = 2\pi\rho' \, d\rho$$

Since, $s^2 = z^2 + \rho'^2$; which by differentiating (where z is constant), gives:

$2sds = 2\rho' d\rho$. Therefore:

$dS = 2\pi s \, ds$. Substituting this value into Eq.(2.1), then

$$\Phi'_p = \frac{1}{2} \int_{s_o}^{s_1} e^{-jks} \left\{ jk\left(1 + \frac{z}{s}\right) + \frac{z}{s^2} \right\} ds$$

Where, $s_o = \sqrt{z^2 + o} = z$; and $s_1 = \sqrt{z^2 + \rho_1^2} = \sqrt{z^2+(a-b)^2}$

The solution of the above integral is similar to that given by Eq.(2.3).

Thus,

$$\Phi'_p = -\frac{1}{2} \left[e^{-jks} \left(1 + \frac{z}{s} \right) \right]_z^{s_1} \qquad \ldots.(2.16)$$

(ii) <u>Contributions due to the equi-distant circular arc elementary areas</u> (Φ''_p):-

For any point P (for which $b < a$), the limits of the radii of the circular arcs representing the equi-distant elementary areas (dS), are $\rho_1 = (a-b)$, and $\rho_2 = (a+b)$, as shown in Fig.(2.4-b).

Since, $dS = 2 \propto \rho \, d\rho$; and

$s^2 = \rho^2 + z^2$. By differentiation and substituting into the

above equation, then

$dS = 2\alpha s\, ds$. Substituting this value of dS into Eq.(2.1), gives

$$\phi''_p = \frac{1}{2\pi} \int_{s_1}^{s_2} e^{-jks} \left\{ jk\left(1+\frac{z}{s}\right) + \frac{z}{s^2} \right\} \alpha \, ds$$

Integrating by parts, and using the solution of the integral given by Eq.(2.3), then,

$$\phi''_p = \frac{1}{2\pi} \left[\left\{ -e^{-jks} \left(1+\frac{z}{s}\right) \right\} \alpha \right]_{s_1}^{s_2} - \frac{1}{2\pi} \int_{s_1}^{s_2} \left\{ -e^{-jks} \left(1+\frac{z}{s}\right) \right\} d\alpha$$

where, $s_1 = \sqrt{z^2 + \rho_1^2}$; and $s_2 = \sqrt{z^2 + \rho_2^2}$

The values of α corresponding to the limits s_1 and s_2, are π and zero, respectively. Substituting these limits of α into the above equation, and also substituting $d\alpha$ from Eq.(2.13), therefore,

$$\phi''_p = \frac{1}{2} \left\{ e^{-jks_1} \left(1+\frac{z}{s_1}\right) \right\} + \frac{1}{2\pi} \int_{\Psi=0}^{\Psi=\pi} e^{-jks} \left(1+\frac{z}{s}\right) \left(\frac{ab\cos\Psi - a^2}{a^2+b^2-2ab\cos\Psi} \right) d\Psi \qquad \ldots\ldots(2.17)$$

By the summation of Eqs.(2.16) and (2.17), we have

$\phi_p = \phi'_p + \phi''_p$, i.e.

$$\phi_p = e^{-jkz} + \frac{1}{2\pi} \int_0^{\pi} e^{-jks} \left(1+\frac{z}{s}\right) \left(\frac{ab\cos\Psi - a^2}{a^2+b^2-2ab\cos\Psi} \right) d\Psi \qquad \ldots(2.18)$$

where, $b < a$; and $s = \left(z^2+a^2+b^2-2ab\cos\Psi\right)^{1/2}$ (Eq.2.15).

By putting b=o into Eq.(2.18), gives the field distribution along the central axis, which agree with that given by Eq.(2.4).

2-A.1.4 Application of this theory to computation

From the above discussion, it can be seen that the calculation of the field distribution involves two cases, according to the position of the observation points (P), for which b is either more or less than a (Eqs. 2.14 & 2.18). In order to evaluate the results of this theory by computer, it is necessary for the real and imaginary parts (L and M), of each expression, to be given separately. The resultant r.m.s.value $Rp=\sqrt{L^2+M^2}$, is found in each case.

(i) Points in the outside field region (b>a):-

From Eq. (2.14), the real and imaginary parts are given by:

$$L=\frac{1}{2\pi}\int_0^{\pi} \text{Cos ks } (1+\frac{z}{s})(\frac{ab \text{ Cos } \psi - a^2}{a^2+b^2-2ab \text{ Cos}\psi})\, d\psi$$

$$M=\frac{1}{2\pi}\int_0^{\pi} -\text{Sin ks } (1+\frac{z}{s})(\frac{ab \text{ Cos } \psi - a^2}{a^2+b^2-2ab \text{ Cos}\psi})\, d\psi$$

(2) Points in the inside field region (b<a):-

From Eq.(2.18), the real and imaginary parts are given by:

$$L=\text{Cos kz} + \frac{1}{2\pi}\int_0^{\pi} \text{Cos ks } (1+\frac{z}{s})(\frac{ab \text{ Cos } \psi - a^2}{a^2+b^2-2ab \text{ Cos}\psi})\, d\psi$$

$$M=-\text{Sin kz} + \frac{1}{2\pi}\int_0^{\pi} - \text{Sin ks } (1+\frac{z}{s})(\frac{ab \text{ Cos } \psi - a^2}{a^2+b^2-2ab \text{ Cos}\psi})\, d\psi$$

where, $k=2\pi/\lambda$; and s is given by Eq.(2.15).

The Rp values for different points, parallel to the central axis and at a given distance b from it, are numerically evaluated by computer (ICL 1904S), using program(2) - appendix (B) for the outside field region (b>a), and program (3) for the inside region (b<a). These programs give also the plot of the results against the axial distances z, where z is expressed in terms of a.
In program (3), if b is set equal to zero, it gives the distribution along the central axis, which is indistinguishable from that given by program (1) (for calculation of the results obtained from analytical integration). Figures (2.5-a), (2.6-a), and (2.7-a) show the axial distributions for $a/\lambda=5$, 2.5, and 1, respectively.

Programs (2) and (3) have been used to obtain 38 curves of the field distribution parallel to the central axis, at given values of b, ranging from b=o to 1.5 a in 0.04 a steps, where the radius 'a' of the disc is taken to be 5λ. These curves were cut from pieces of cardboard, which are assembled together to give a three dimensional model of the field distribution, as shown in pictures (1) and (2).

Program (4) - in appendix (B), is a combination of programs (2) and (3). It gives the off-axis distribution, across the field (parallel to the face of the disc) by setting z at any given value. This program has been used to give the plots of the off-axis distribution, at z=0.2a, for $a/\lambda=5$, 2.5, and 1, as shown by the solid curves in Figs.(2.8), (2.9), and (2.10), respectively.

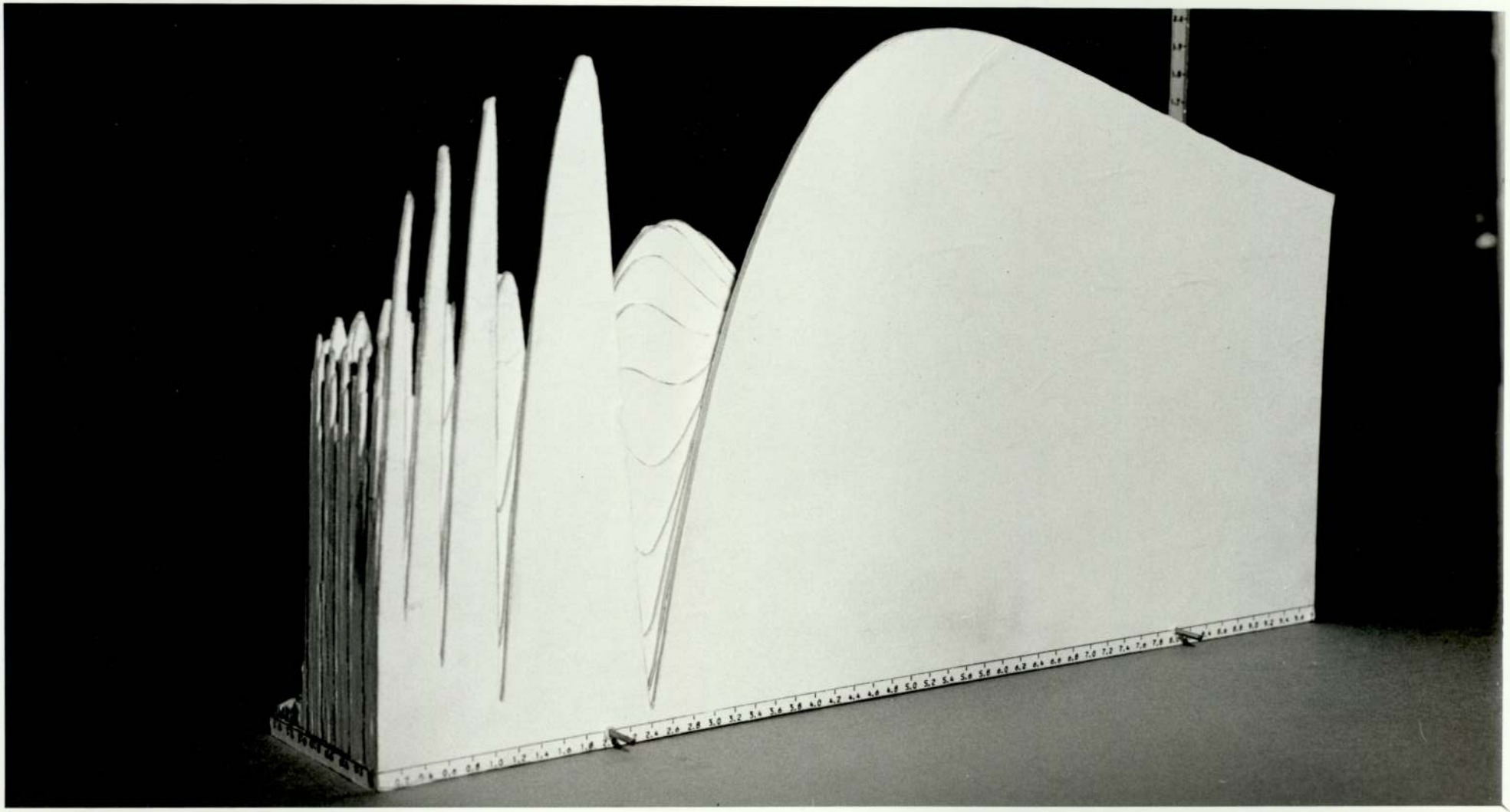

Picture (1) A view from inside

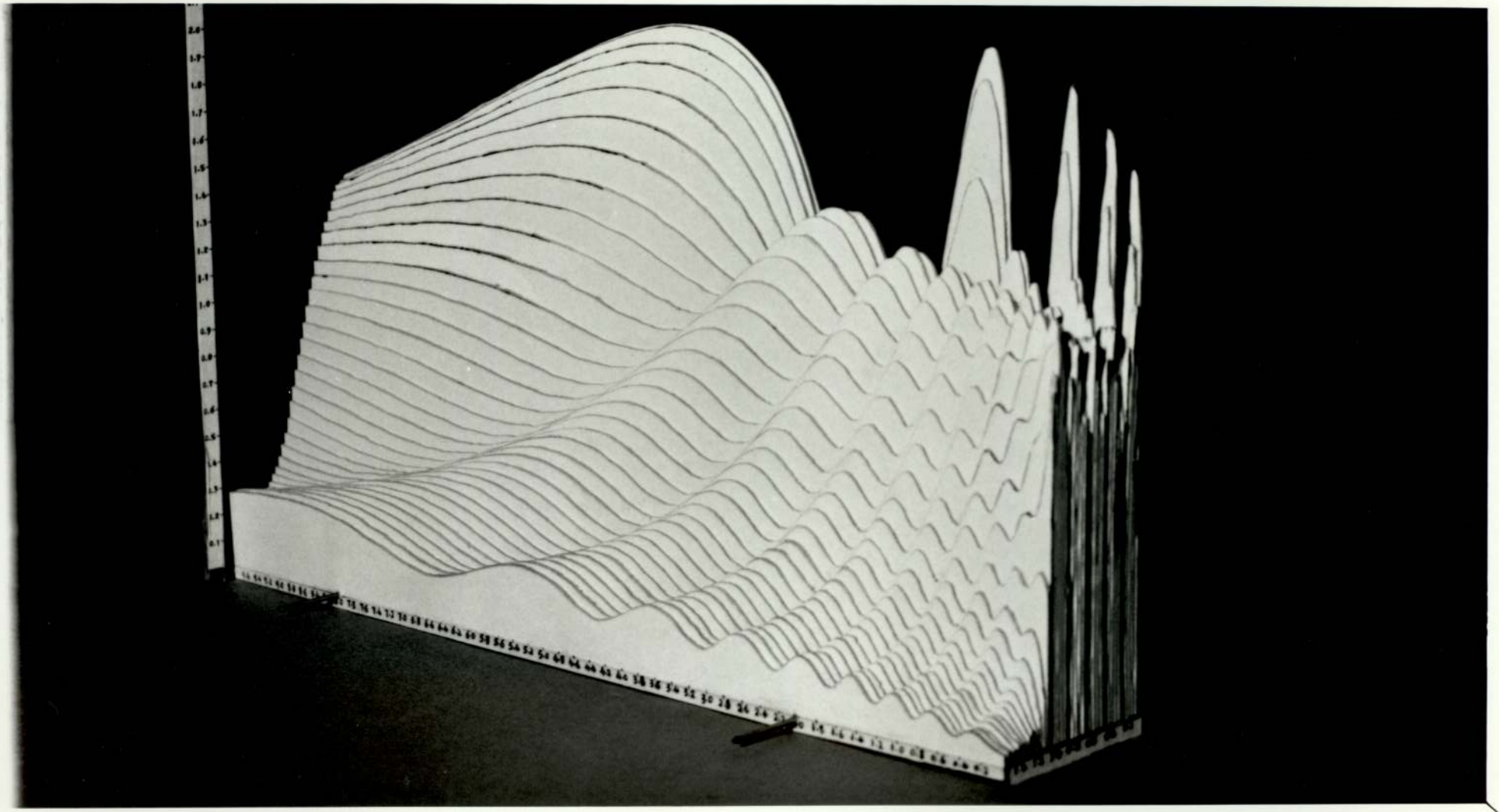

Picture (2) A view from outside

The off-axis distribution at the face of the disc transducer (z=o), for $a/\lambda=5$, and 1,are shown by the solid curves in Fig.(2.11).

Using the same method of geometrical analysis, explained in this section, but applying the Huygen's integral, it has been found that the results involve the replacement of the term z/s by unity. That is to say, the equations corresponding to those of (2.14) and (2.18), but using the Huygen's integral, are given as follows:-

For b>a:

$$\Phi p = \frac{1}{\pi} \int_{o}^{\pi} e^{-jks} \left(\frac{ab \cos \psi - a^2}{a^2+b^2-2ab \cos \psi} \right) d\psi \qquad \ldots\ (2.19)$$

For b<a:

$$\Phi p = e^{-jkz} + \frac{1}{\pi} \int_{o}^{\pi} e^{-jks} \left(\frac{ab \cos \psi - a^2}{a^2+b^2-2ab \cos \psi} \right) d\psi \qquad \ldots\ (2.20)$$

These equations have been applied for computation, in the same way as those of Eqs.(2.14) and (2.18).

Program (5) gives the field distribution in the inside region (b<a), using Eq.(2.20). In this program, b was set equal to zero in order to give the plots of the axial distribution for $a/\lambda=5$, 2.5, and 1, as shown in Figs.(2.5-b), (2.6-b), and (2.7-b), respectively.

Program (6) gives the plots of the off-axis distribution (using Eqs. 2.19 and 2.20), as shown by the dashed curves in Figs. (2.8), (2.9), (2.10), and (2.11).

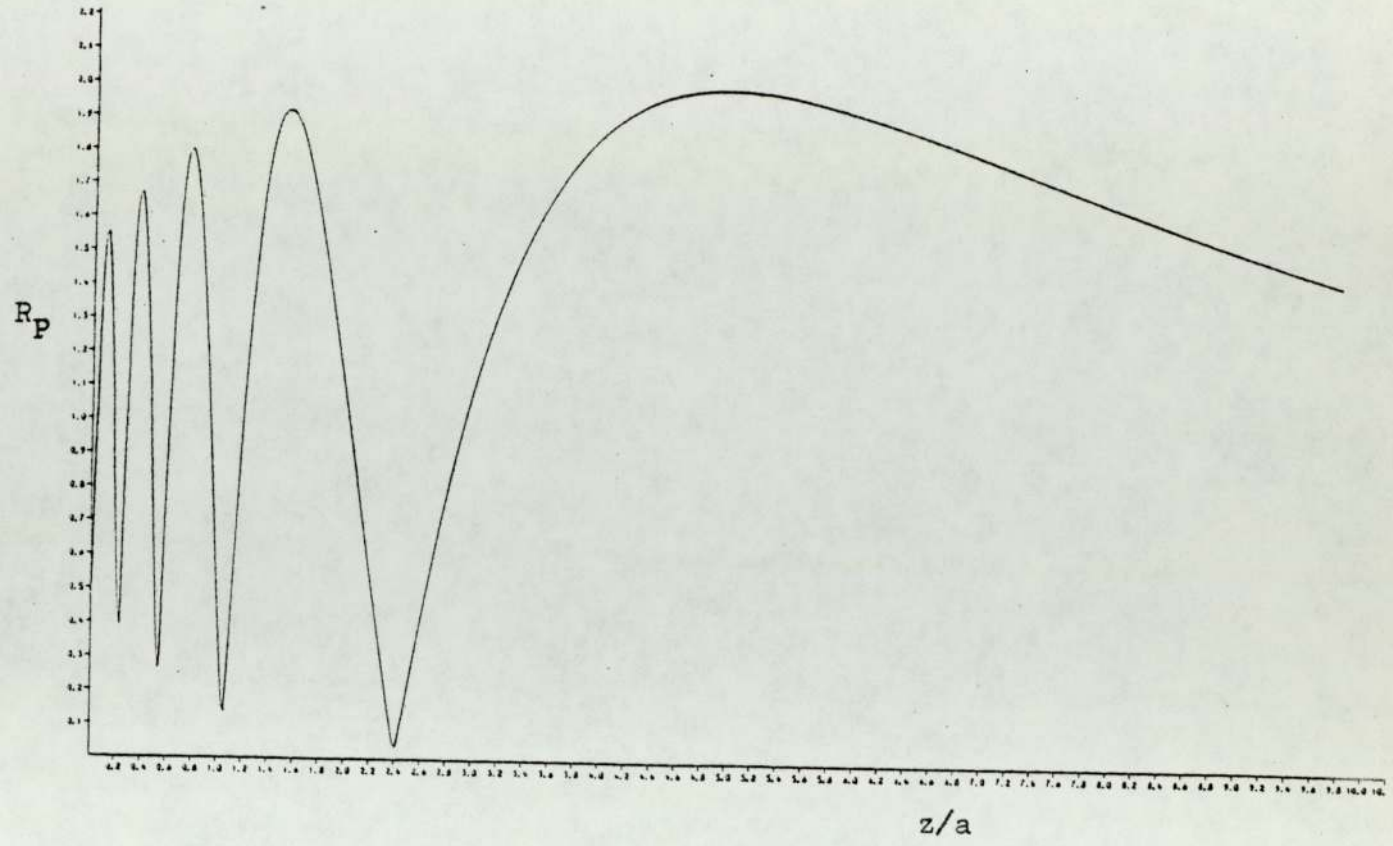

(a)

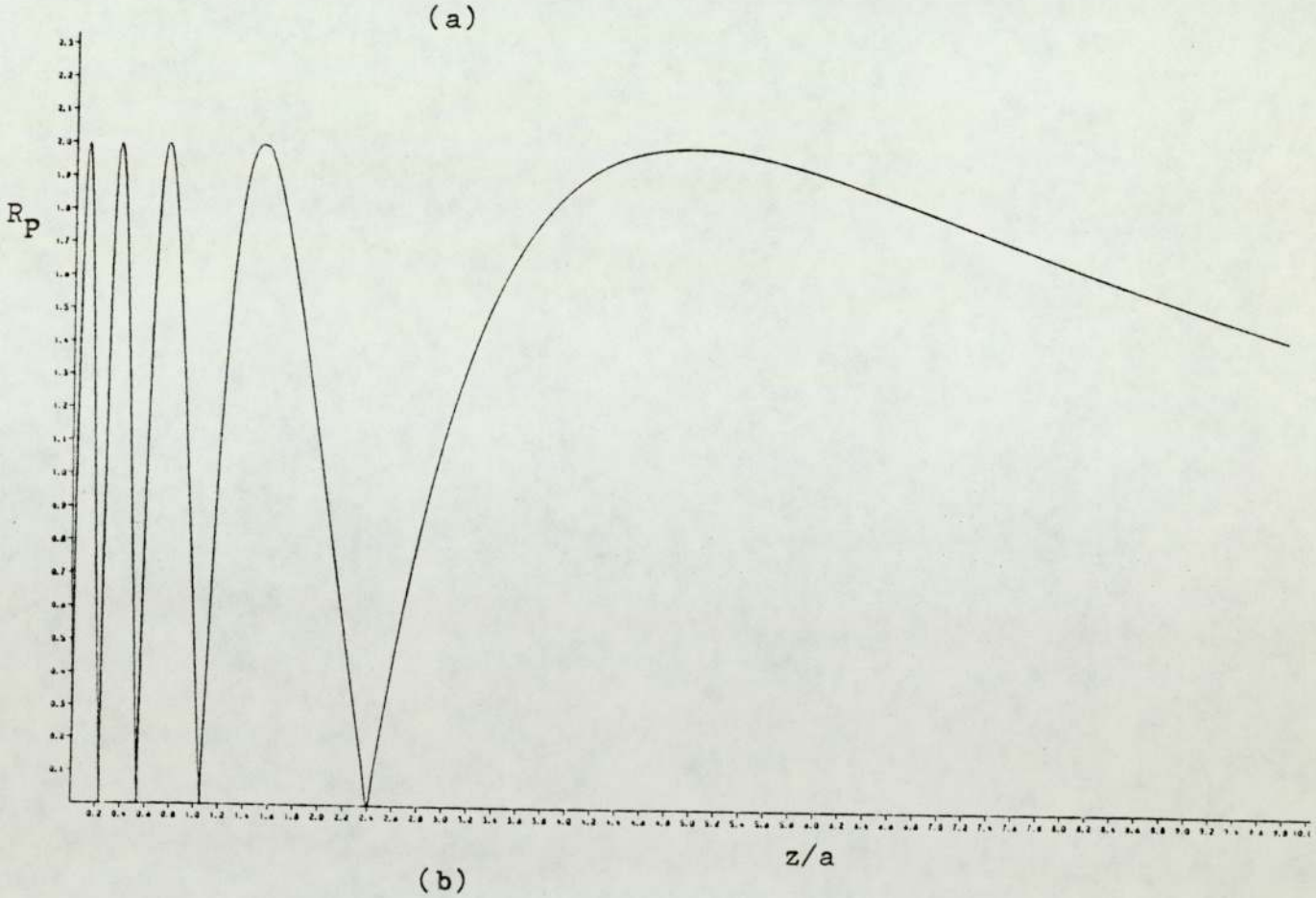

(b)

Fig. 2.5 Near- and farfield axial distribution ($a/\lambda = 5$)

(a) using Kirchhoff's integral

(b) using Huygen's integral

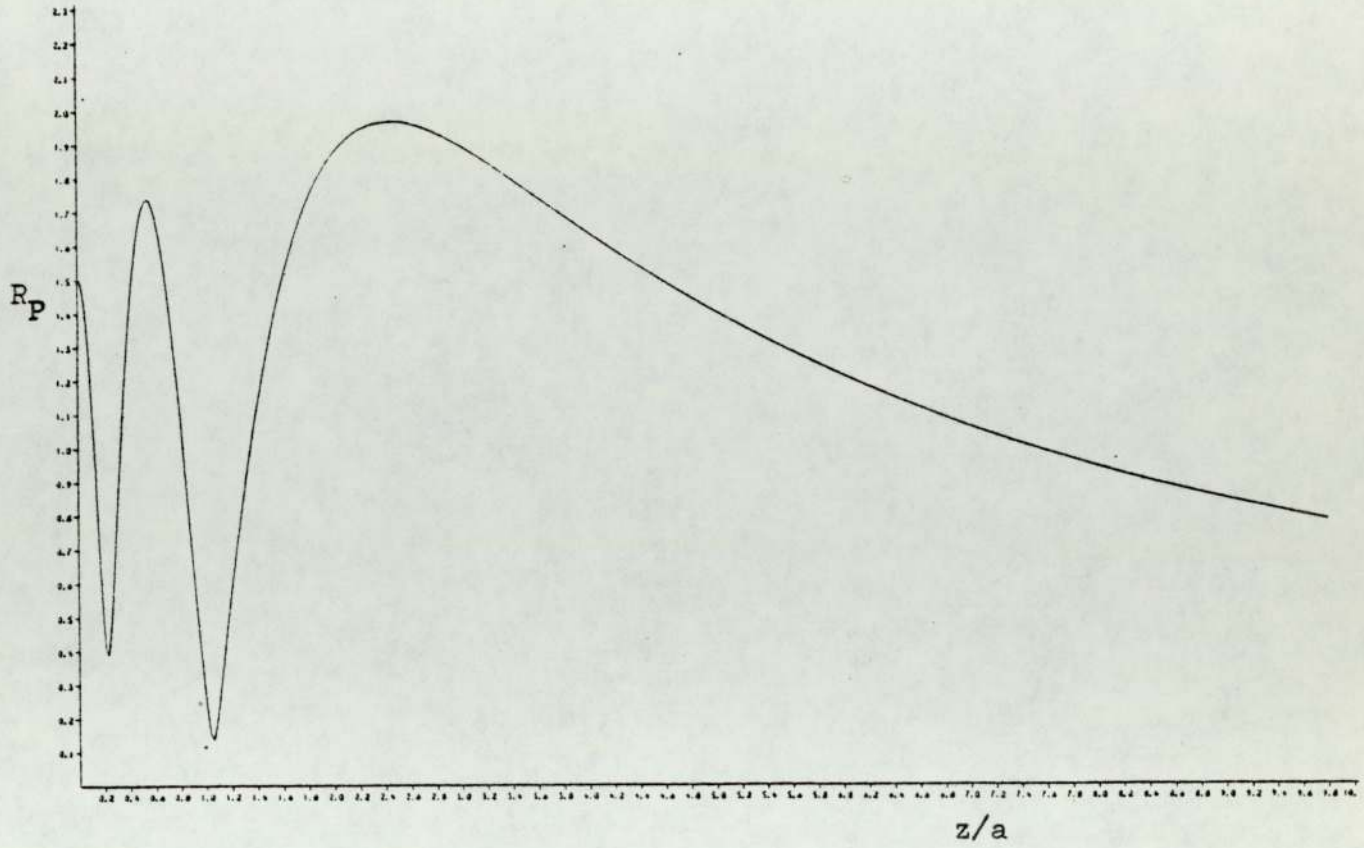

(a)

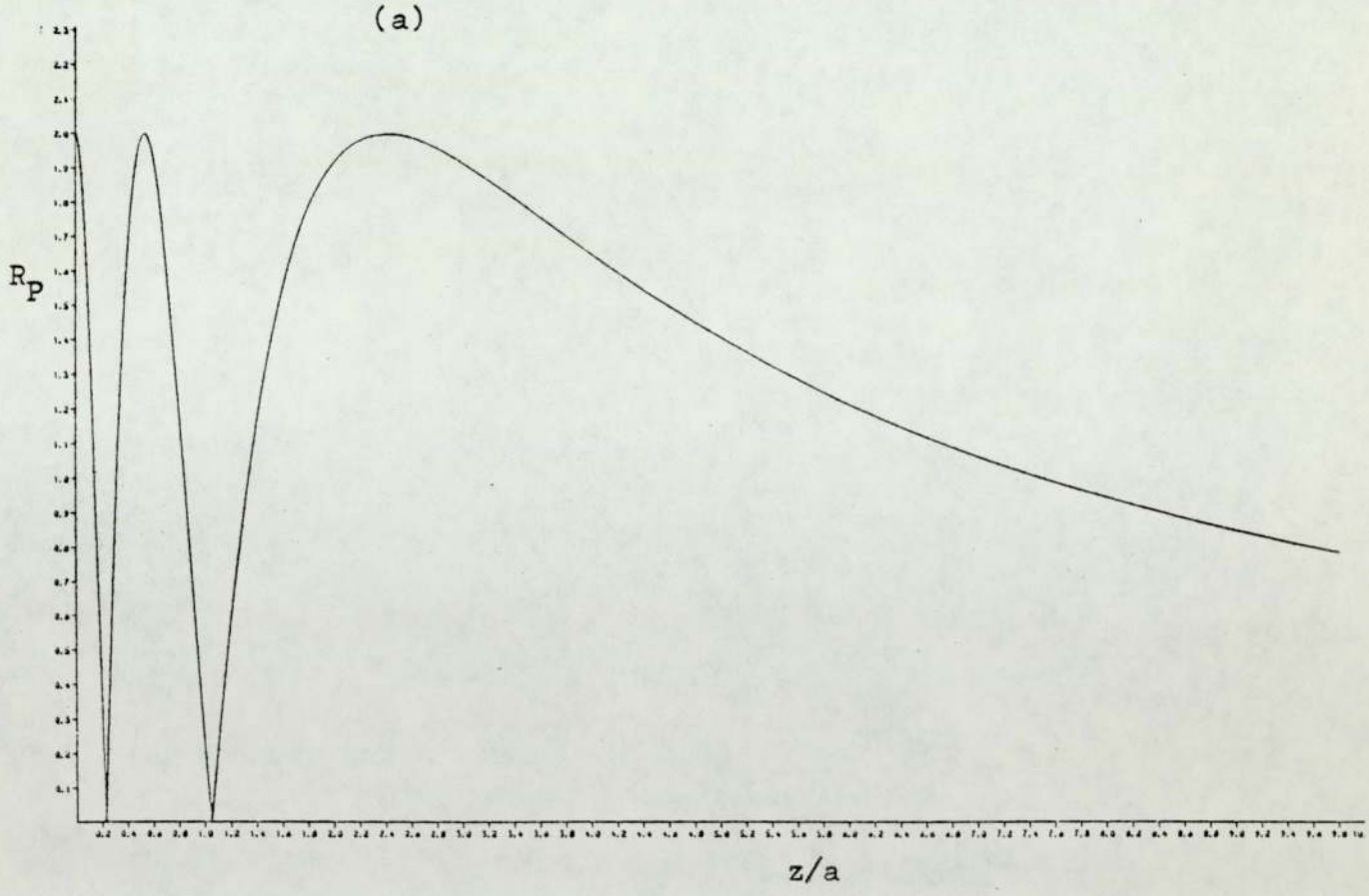

(b)

Fig. 2.6 Near- and farfield axial distribution ($a/\lambda = 2.5$)
(a)using Kirchhoff's integral
(b) using Huygen's integral

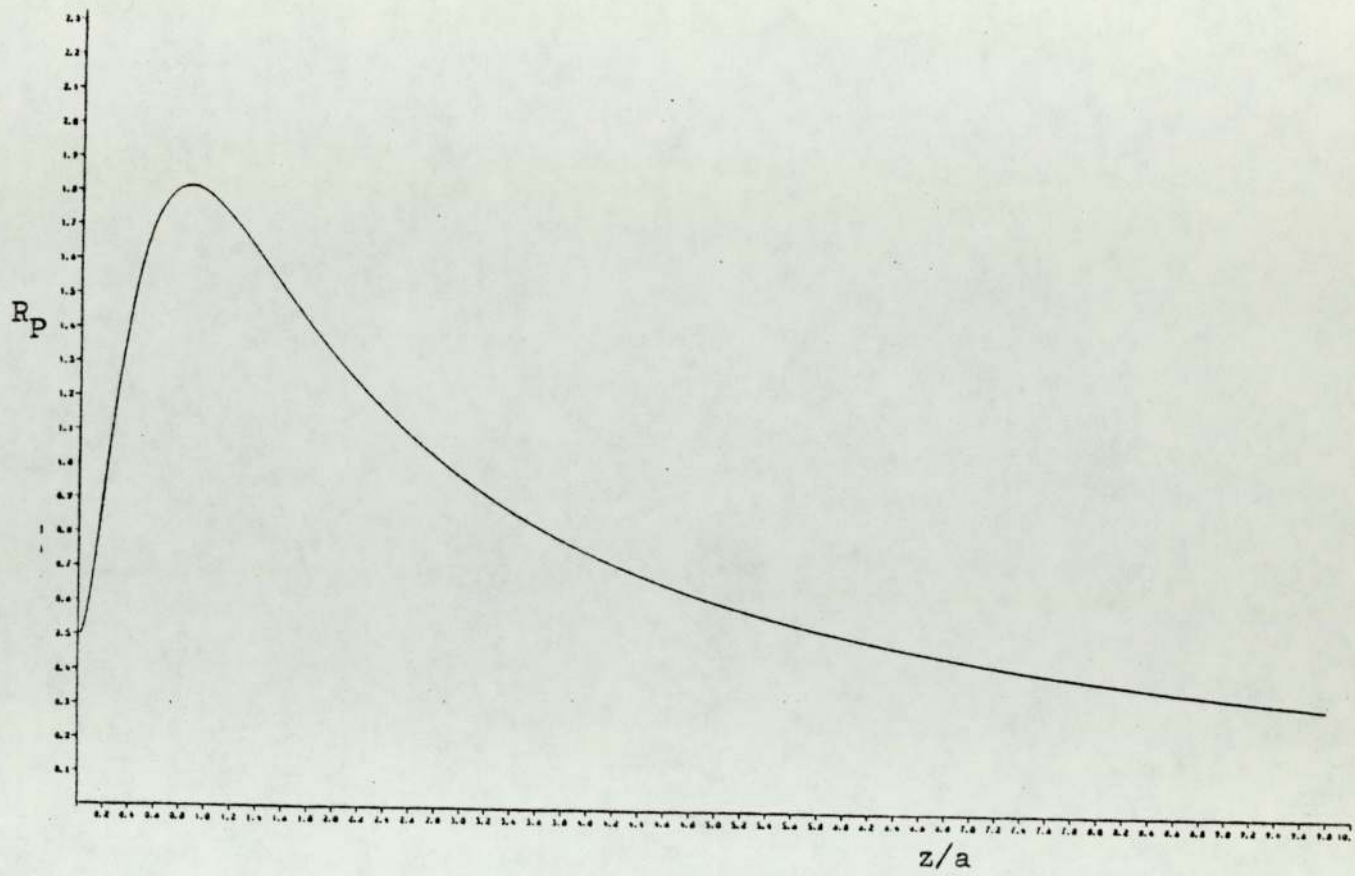

(a)

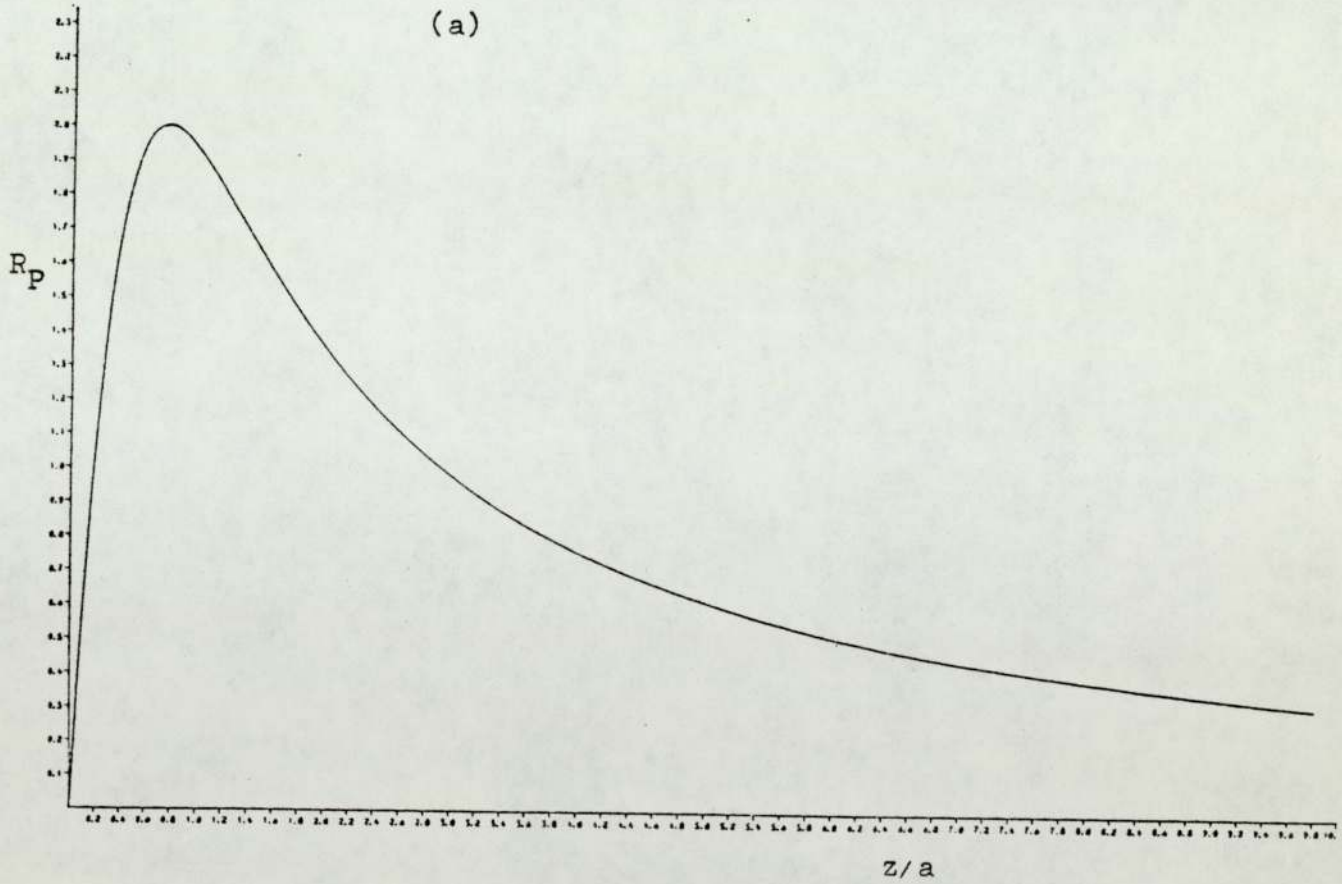

(b)

Fig. 2.7 Near- and farfield axial distribution ($a/\lambda = 1$)
(a) using Kirchhoff's integral
(b) using Huygen's integral

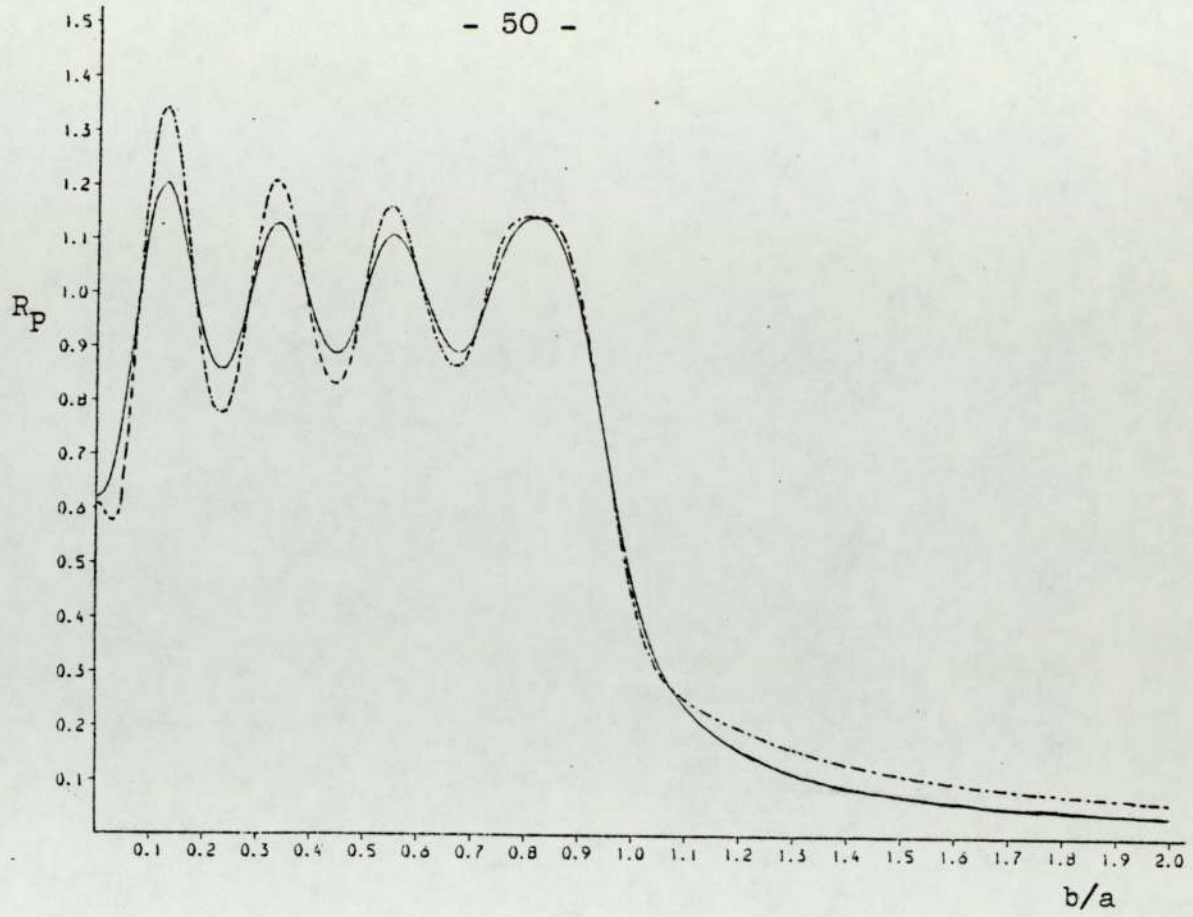

Fig. 2.8 Off-axis distribution at z= 0.2a.(a/λ =5)
—— using Kirchhoff's integral
----using Huygen's integral

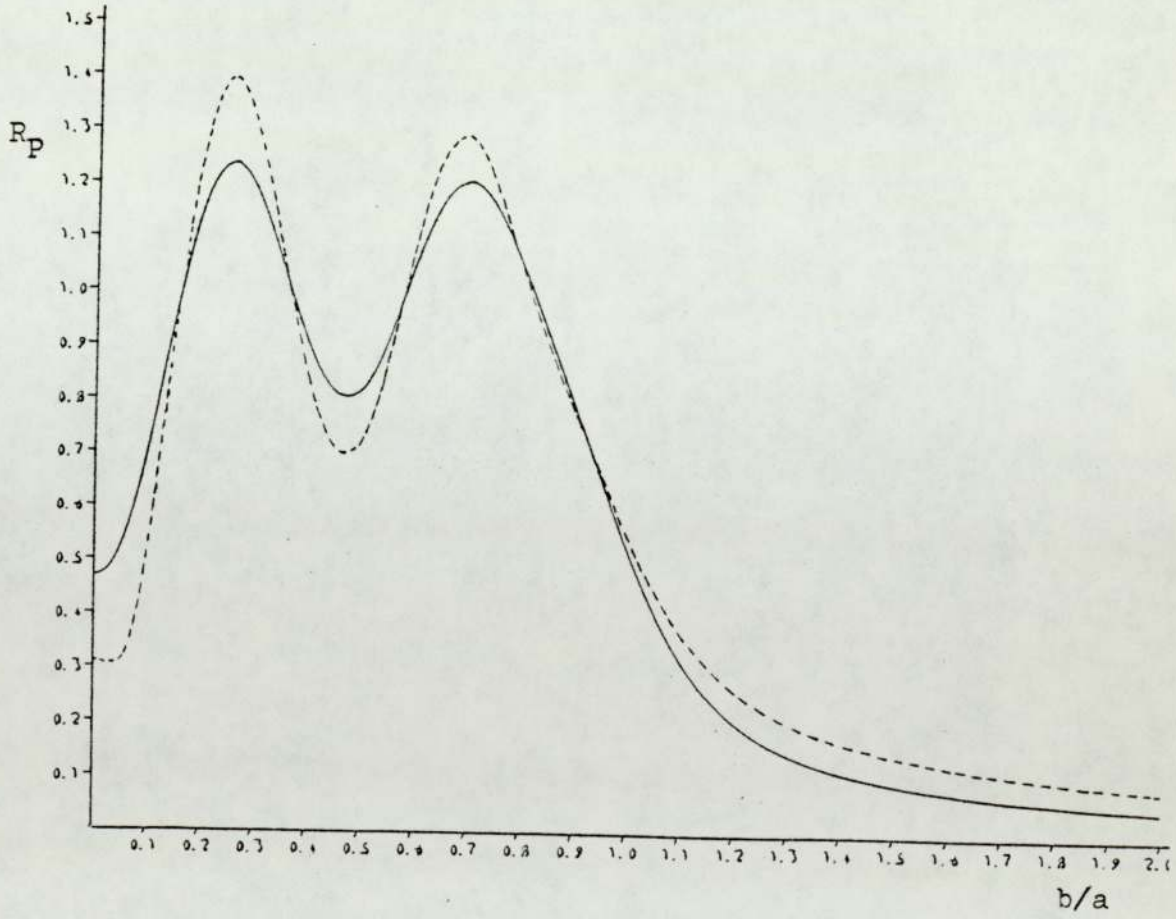

Fig. 2.9 Off-axis distribution at z=0.2a. (a/λ =2.5)
—— using Kirchhoff's integral
----using Huygen's integral

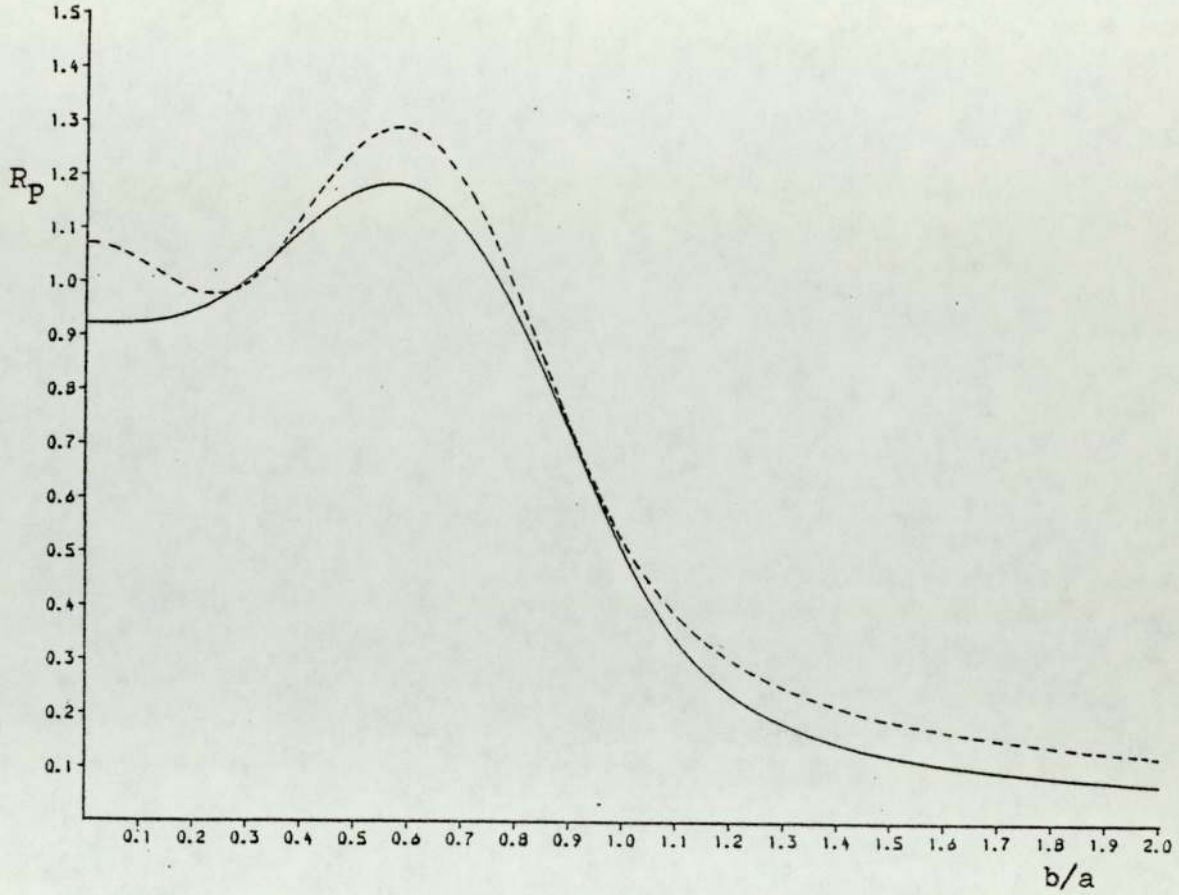

Fig. 2.10 Off-axis distribution at z= 0.2a.(a/λ =1)
—— using Kirchhoff's integral
----using Huygen's integral

From the previous discussion, using the Kirchhoff's integral, it can be concluded that:

1. The axial distribution shows minima which are not zero, at the same positions as the zeros given by the Huygen's theory (as shown in Figs. 2.5 to 2.7).
2. The relative variations between the off-axis maxima and minima in the inside field region (b<a), are less than those given by the Huygen's integral, as shown in Figs. (2.8) to (2.11).
3. The off-axis distribution in the outside field region (b>a), is less than that given by the Huygen's theory at the same value of b, as shown in Figs (2.8) to (2.11).

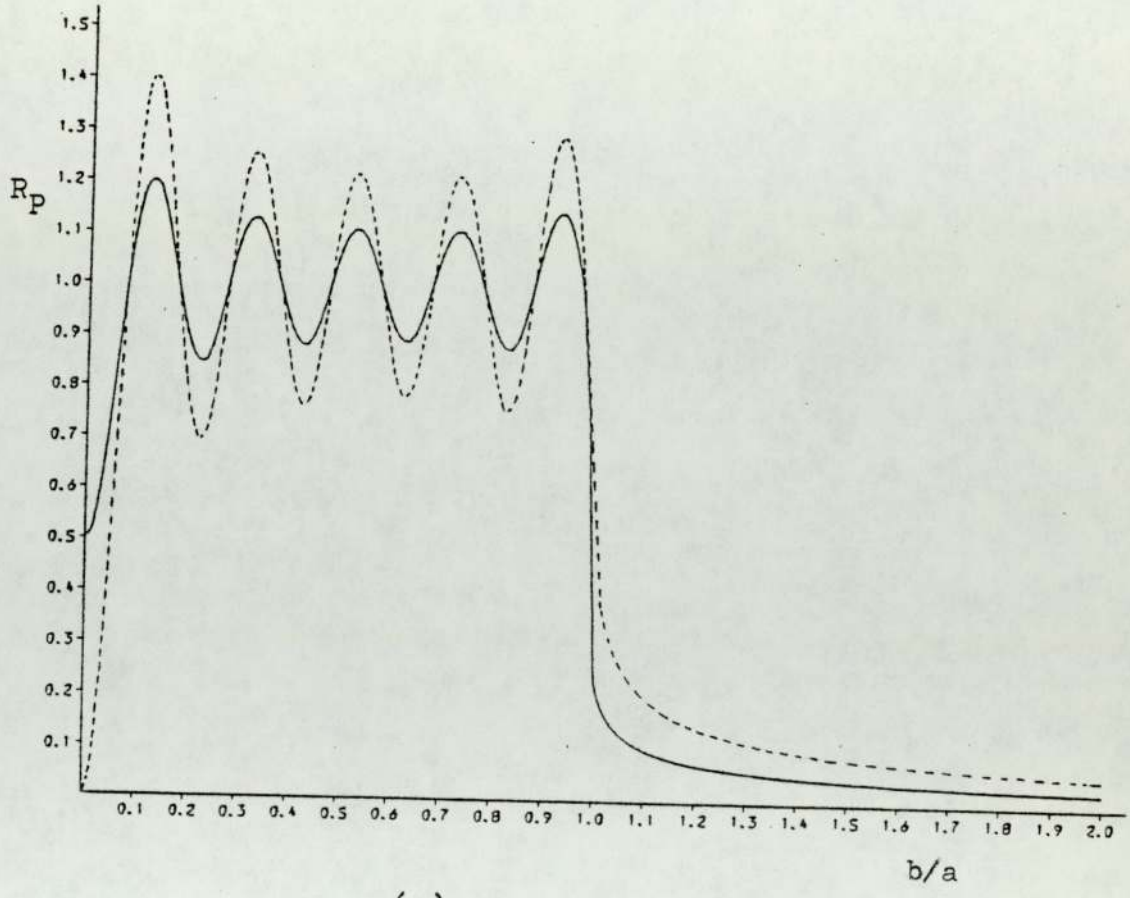

(a)

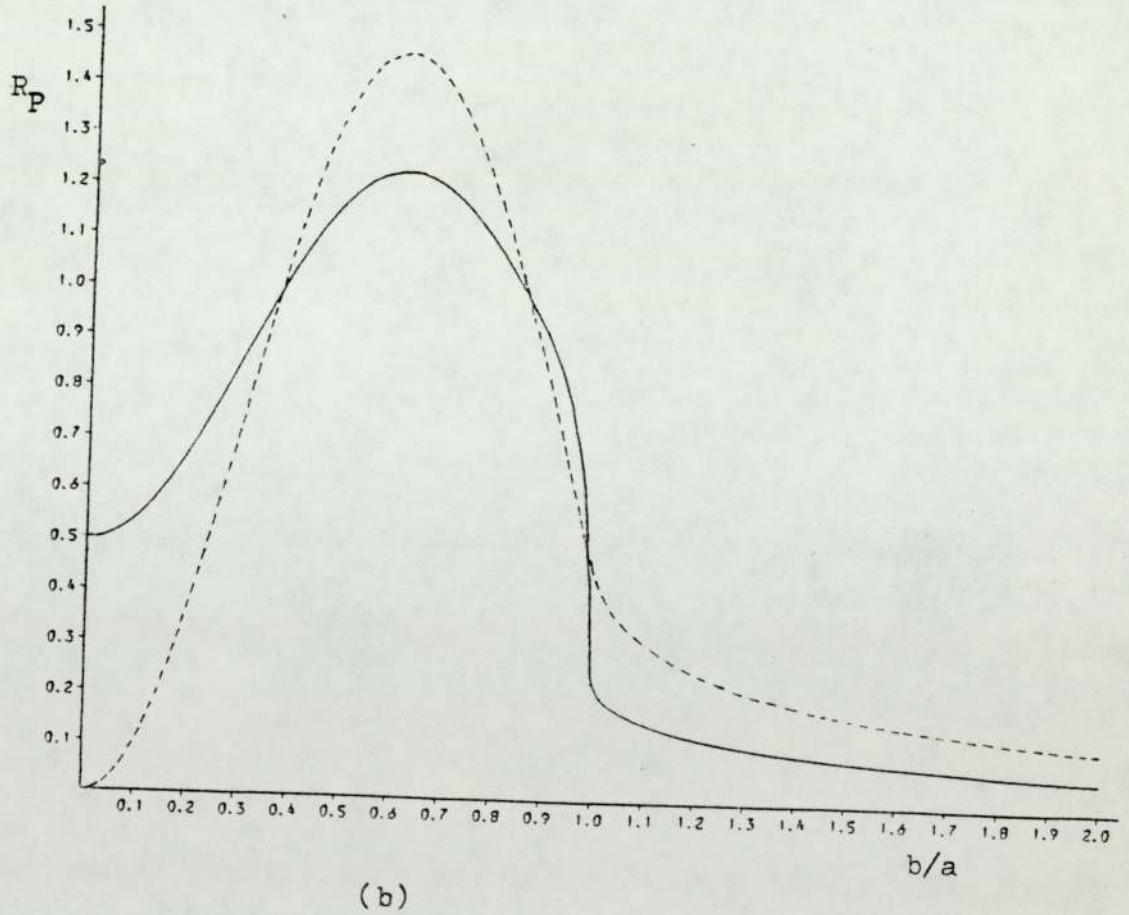

(b)

Fig. 2.11 Off-axis distribution at z= 0.0 of disc transducers:
(a) $a/\lambda = 5$, (b) $a/\lambda = 1$
—— using Kirchhoff's integral; ----using Huygen's integral

Since, at the start of this mathematical analysis, it has been assumed that the acoustic potential is unity at z=o, it was expected to get a constant distribution across the face of the disc transducer, which falls rapidly to zero at b=a. However, this has not been fulfilled as may be seen from Fig(2.11) which shows maxima and minima at the face of the disc.

This discrepancy is probably due to the fact that while the Kirchhoff theory related to the values of the acoustic potential (ϕ), there are no boundary conditions applied to the particle velocity.

An alternative reason may be due to the failure of mathematics to describe exactly a system with a discontinuity such as the edge of the vibrating disc, in a similar manner to that which occurs in the description of the square-wave by the Fourier series. In this case, the summation of the harmonics give rise to spikes at the edges of the square-wave, as shown in appendix B - Fig(B.1). As the number of harmonics added up increases, the width of the spike decreases, whereas its height remains the same. This is known as the Gibbs phenomenon.

2-A.2 A NEW APPROACH TO THE ULTRASONIC DISTRIBUTION IN THE FOCAL PLANE OF LARGE APERTURE BOWL TRANSDUCER

In the previous section, the full Kirchhoff's integral has been applied to determine accurately the field distribution for a flat disc transducer. In this section, the general relation giving the ultrasonic distribution in the central part of the focal plane, for any spherical concave transducer, will be determined accurately by applying the Huygen's integral, having in consideration the following assumptions:

1. The bowl transducer is vibrating in simple harmonic motion normal to its surface.
2. The observation points in the focal plane are not far from the central axis.
3. The radius of curvature of the bowl is large compared with the wavelength (λ) in the propagating medium.

Now, let us consider Eq.(2.1), which may be re-written as follows:

$$\phi_P = \frac{1}{4\pi} \int_S e^{-jks} \left\{ jk \left(\frac{1}{s} + \frac{\text{Cos}\,\theta}{s}\right) + \frac{\text{Cos}\,\theta}{s^2} \right\} dS \qquad \ldots.(2.1)$$

According to the first assumption, at the focal point $\theta=o$, and Cos $\theta=1$. For a point 'P' close to the focal point, Cos θ will remain very nearly unity. For instance, if the radius of curvature a=100 mm, then the deviation of Cos θ from unity, for any bowl transducer, will not exceed $1.25\text{x}10^{-3}$, provided that the observation point on the focal plane does not exceed 5mm from the central axis. If such a small deviation is neg-

lected, then Eq.(2.1) becomes

$$\phi_P = \frac{1}{4\pi} \int_S e^{-jks} \left(\frac{2jk}{s} + \frac{1}{s^2}\right) dS = \frac{1}{4\pi} \int_S e^{-jks} \left(\frac{4j\pi}{\lambda s} + \frac{1}{s^2}\right) dS$$

According to the third assumption, if $a \gg \lambda$; e.g. λ=o.2mm and a=100mm, then $\frac{1}{s^2} \simeq \frac{1}{a^2} = 10^{-4}$. Therefore, the term $\frac{1}{s^2}$, in the above equation, may be neglected. Hence,

$$\phi_P = \frac{1}{\lambda} \int_S \frac{e^{-jks}}{s} \, dS \qquad \ldots\ldots (2.21)$$

Thus, Huygen's integral can be applied accurately in order to determine the ultrasonic distribution in the central part of the focal plane of a bowl transducer.

The method used in this case for evaluation of the surface integral involves the use of cylindrical polar co-ordinates (instead of conventional spherical polars) and this enables a single integral to be obtained for computation.

Let us consider a spherical concave transducer for which:-

a, is the radius of curvature;

b, the radius of its circular boundary;

O, the centre of curvature, is the origin of the co-ordinate system, as shown in Fig.(2.12).

$P(o,o,z_1)$, is an observation point on the Z-axis at a distance z_1 from O.

Q(x,y,z), is any radiating point on the concave surface of the transducer.

s, is the distance between P and Q.

r, is the radial distance in the XY-plane, between Q and another point on the Z-axis, of the same z co-ordinate.

α, is the angle between the radial line r and the corresponding Y-axis.

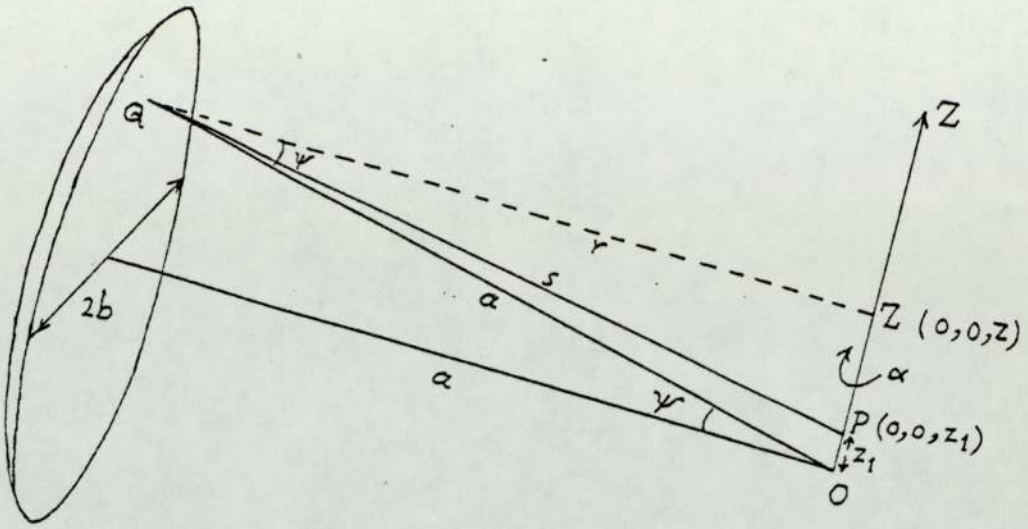

Fig. 2.12 Coordinate system used for surface integral of a concave bowl transducer.

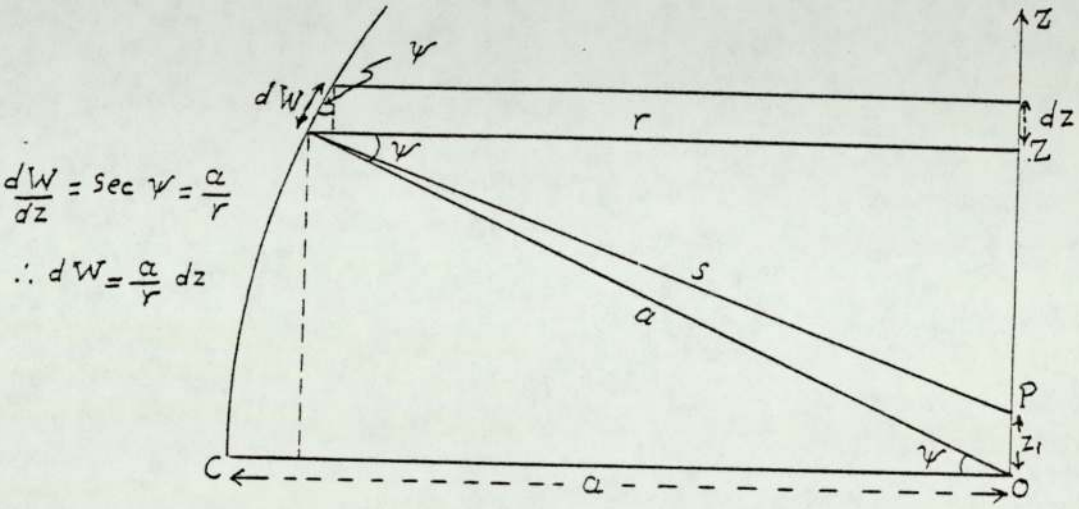

Fig. 2.13 Section through the Z-axis and the point Q on the concave surface.

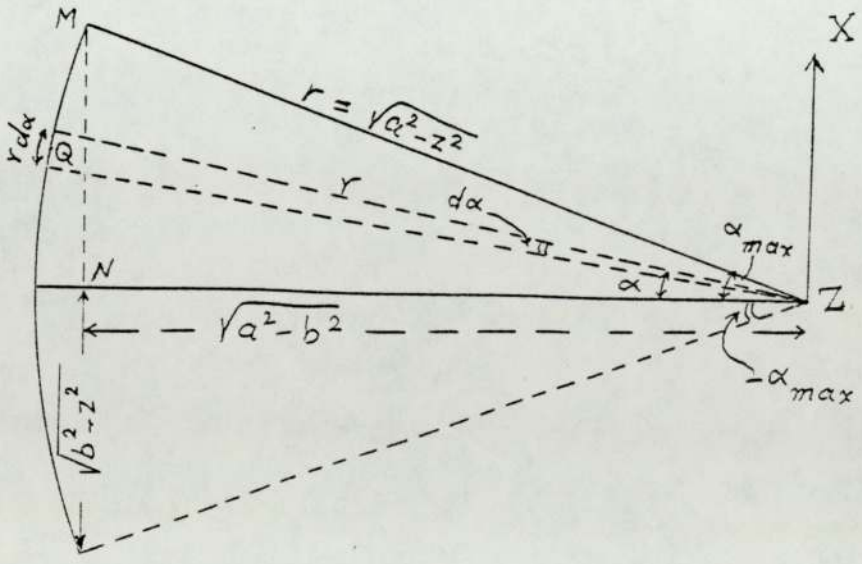

Fig. 2.14 Section in the XY-plane at the point Q on the concave surface.

Ψ, is the angle between r and the radius of curvature (a) from the same point Q.

The cylindrical co-ordinates of the point Q(r,α,z), are given by:

χ = r Sin α; y = r Cos α; and z.

From Fig.(2.12), we have

$$a^2=r^2 + z^2; \text{ and} \qquad \ldots\ldots (2.22)$$

$$s^2=r^2 + (z-z_1)^2 = r^2+z^2+z_1^2 - 2zz_1$$

$$s^2=a^2 + z_1^2 - 2zz_1 \text{ or, } s= \sqrt{a^2+ z_1^2 - 2zz_1} \qquad \ldots\ldots \quad (2.23)$$

Let us take a section passing through the point Q and the Z-axis, as shown in Fig(2.13), and another section in the XY-plane through the same point, as shown in Fig(2.14). At this point (Q), consider an elementary area dS whose dimensions in the planes of these sections are dW and rdα, as given by Figs.(2.13) and (2.14), respectively, where,

$\frac{dW}{dz}$ = Sec Ψ = $\frac{a}{r}$; or, dW = $\frac{a}{r}$ dz. Therefore,

$dS = rd\alpha\ dW = ad\alpha\ dz$

By differentiating Eq.(2.23), where a and z_1 are constants, then

$$dz = -\frac{s}{z_1} ds \qquad \ldots\ldots (2.24)$$

$$dS = -\frac{as}{z_1} d\alpha\ ds$$

Substituting this value into Eq.(2.21), gives

$$\phi_p = -\frac{a}{\lambda} \int_{s_1}^{s_2} \int_{\alpha_1}^{\alpha_2} \frac{e^{-jks}}{z_1} d\alpha\ ds \qquad \ldots\ldots (2.25)$$

The XY-section at the point Q (Fig.2.14), shows an arc on the concave surface whose radius is r. The points along this arc are all equi-distant from P. Its length can be determined by the maximum limits of α, i.e $\pm\alpha_{max}$, which depend on the z co-ordinate of Q. These may be found from Fig(2.14), in which: MN, is the normal from the edge of the arc M (at the bowl circumference) onto the corresponding Y-axis (ZN) at the point N.

Since the distance from the central axis to ZN is z, and that to the point M is b, therefore, $MN = \sqrt{b^2-z^2}$

$$\overline{ZN}^2 = r^2 - \overline{MN}^2 = r^2-(b^2- z^2)$$

Substituting from Eq. (2.22), then

$$ZN = \sqrt{a^2-b^2}$$

Thus,

$$\alpha_{max}=\pm \text{Sec}^{-1} \sqrt{\frac{a^2 - z^2}{a^2 - b^2}}$$

Substituting into Eq. (2.25), gives

$$\phi_P = - \frac{a}{\lambda}\int_{s_1}^{s^2} \frac{e^{-jks}}{z_1} \left[\text{Sec}^{-1} \sqrt{\frac{a^2-z^2}{a^2-b^2}} \right]_{-\alpha_{max}}^{\alpha_{max}} ds$$

$$= - \frac{a}{\lambda}\int_{s_1}^{s^2} \frac{e^{-jks}}{z_1} \left[2 \text{ Sec}^{-1} \sqrt{\frac{a^2-z^2}{a^2-b^2}} \right] ds$$

Substituting the value of $\frac{ds}{z_1}$ from Eq.(2.24) into the above equation, then

$$\phi_P = \frac{2a}{\lambda}\int_{-Z_{max}}^{+Z_{max}} \frac{e^{-jks}}{s} \text{ Sec}^{-1} \sqrt{\frac{a^2-z^2}{a^2-b^2}} \, dz$$

The limits of $\pm z_{max}$ are $\pm b$, thus

$$\phi_P = \frac{2a}{\lambda}\int_{-b}^{+b} \frac{e^{-jks}}{s} \; \mathrm{Sec}^{-1} \sqrt{\frac{a^2 - z^2}{a^2 - b^2}} \; dz \qquad \ldots\ldots (2.26)$$

Substituting the value of s, from Eq.(2.23), into the above equation, then the real and imaginary parts L and M, respectively, are given by:

$$L = \frac{2a}{\lambda}\int_{-b}^{+b} \frac{\mathrm{Cos}\; k\sqrt{a^2+z_1^2 - 2zz_1}}{\sqrt{a^2+z_1^2 - 2zz_1}} \; \mathrm{Sec}^{-1} \sqrt{\frac{a^2-z^2}{a^2-b^2}} \; dz$$

$$M = \frac{2a}{\lambda}\int_{-b}^{+b} \frac{-\mathrm{Sin}\; k\sqrt{a^2+z_1^2 - 2zz_1}}{\sqrt{a^2+z_1^2 - 2zz_1}} \; \mathrm{Sec}^{-1} \sqrt{\frac{a^2-z^2}{a^2-b^2}} \; dz$$

where, $k=2\pi/\lambda$; λ, denotes the wavelength in the propagating medium. The r.m.s. value (R_P) at any pcint P in the central part of the focal plane is given by:

$$R_P = \sqrt{L^2+M^2}$$

This equation was numerically evaluated by an ICL 1904S Computer, using programme (7) in appendix (B). This program gives the normalised off-axis R_P values in the focal plane, i.e. the ratios of R_P/R_o, where R_o is that value at the centre of curvature. These values are plotted against z_1 as shown in Figs.(2.15) and (2.16). In Fig.(2.15), curves (1), (2) and (3) represent the diffraction patterns for bowl transducers having the same radius of curvature (a=100mm) but different aperture diameters (2b), where b=25, 50, and 75mm, respectively, assuming λ to be 0.2mm in all cases. From these curves, it can be seen that the radii of the diffraction

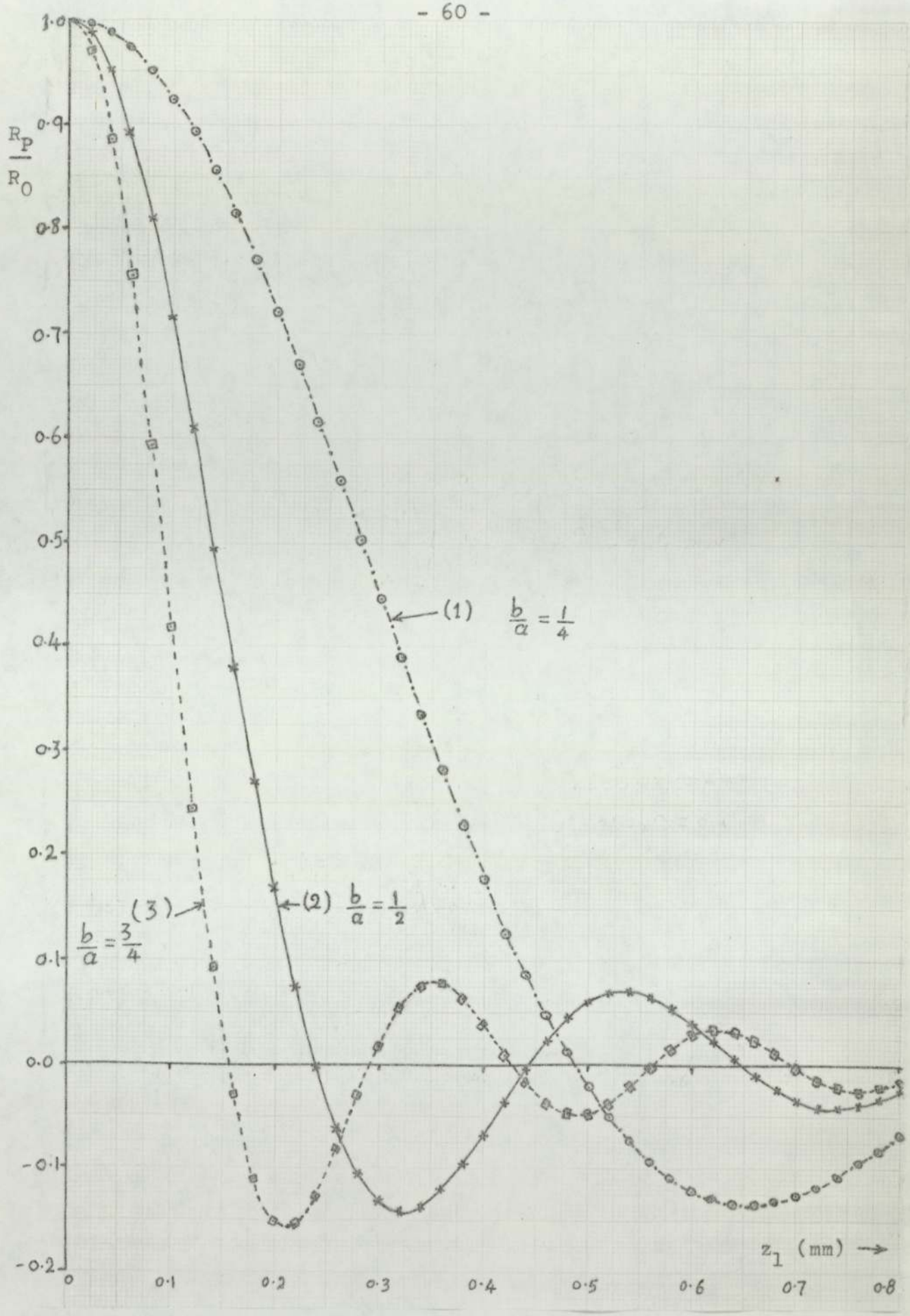

Fig. 2.15 Computed diffraction patterns for concave bowl transducers of different apertures. a=100 mm; λ=0.2 mm.

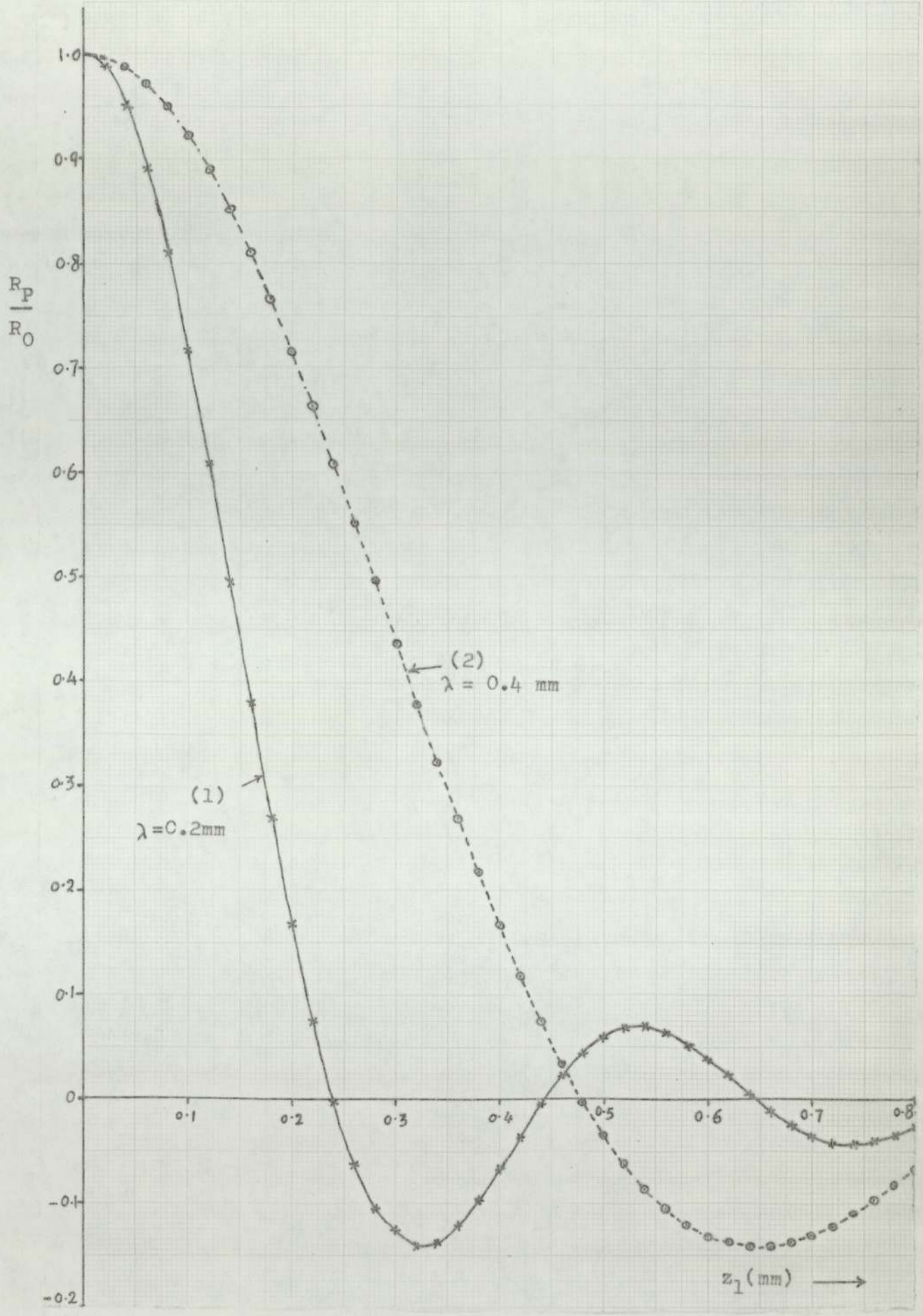

Fig. 2.16 Computed diffraction patterns of a bowl transducer (b=50 mm; a=100 mm) at 7.5 MHz and 3.75 MHz.

pattern nodes (r_n), where R_p=o, decrease progressively as b increases.

In other words, for the same wavelength (λ=O.2mm), curves (1), (2), and (3) represent the diffraction patterns for bowl transducers having the ratios b/a=$^1/4$, $^1/2$, and $^3/4$, respectively, from which it can be seen that, r_n is progressively decreasing as $^b/a$ increases.

In Fig.(2.16), curves (1) and (2) represent the diffraction patterns of a bowl transducer, for which $^b/a = ^1/2$ but driven at different frequencies, where λ=O.2 and O.4mm respectively. From this figure, it may be seen that r_n decreases as λ decreases. Therefore, from the above discussion, it may be concluded that, the radii of the diffraction pattern nodes (r_n) are progressively decreasing as the ratio $a\lambda/b$ decreases.

Before discussing the comparison between the diffraction pattern obtained by this method and that given by the classical theory, we shall consider first the special case of the concave bowl transducer, the hemi-sphere.

2-A.2.1 Hemi-spherical Bowl Transducer

In the case of a hemi-sphere, the limits of the angle α ($\pm\alpha_{max}$) are $\pm\pi/2$. Therefore, ϕ_p at any point in the central part of the focal plane, as given by Eq.(2.25), may be re-written as follows:

$$\phi_P = -\frac{a}{\lambda}\int_{s_1}^{s_2} \frac{e^{-jks}}{z_1}\left[\alpha\right]_{-\pi/2}^{+\pi/2} \quad ds$$

$$= -\frac{\pi a}{\lambda z_1}\int_{s_1}^{s_2} e^{-jks} \quad ds$$

$$= \frac{\pi a}{\lambda z_1}\frac{1}{jk}\left(e^{-jks_2} - e^{-jks_1}\right)$$

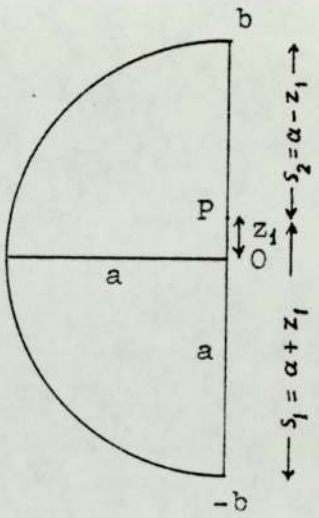

If, $y = e^{j\beta} - e^{j\gamma}$;

then $|y| = 2\,\mathrm{Sin}\left(\frac{\beta-\gamma}{2}\right)$. Similarly,

$$|\phi_P| = \frac{\pi a}{\lambda k z_1}\left\{2\,\mathrm{Sin}\,\frac{k}{2}\,(s_1 - s_2)\right\}$$

Since, $s_1 = a+z_1$; and $s_2 = a-z_1$. Then,

$$R_P = |\phi_P| = ka\,\frac{\mathrm{Sin}(kz_1)}{kz_1}$$

At the centre of curvature, where $z_1 = o$, $\mathrm{Sin}(kz_1)/kz_1 = 1$, and hence $R_o = ka$. Therefore,

$$R_P = R_o\,\frac{\mathrm{Sin}(kz_1)}{kz_1} \qquad \ldots\ldots (2.27)$$

This is the result obtained by analytic integration, which brought the realisation that an investigation of large aper ture bowl diffraction would be of value.

Due to Eq.(2.27), R_P falls from a maximum value R_o at the focus and then passes through several secondary maxima, with

equally spaced nodes at $kz_1 = \pm n\pi$, where n is a whole number. The radius (r_n) of the nth node is given by:

$$\frac{2\pi}{\lambda} r_n = n\pi, \text{ i.e } r_n = \frac{n\lambda}{2}$$

If, λ=0.2mm, the radius of the first node is 0.1mm, as shown in curve (1) of Fig.(2.17).

These relations are appreciably different from those given by the classical theory, where the directivity function for a hemi-spherical bowl is given by:

$$\frac{R_p}{R_o} = \frac{2J_1(\beta)}{\beta} = \frac{2J_1(kbz_1/a)}{(kbz_1/a)} = \frac{2J_1(kz_1)}{kz_1} \qquad \ldots\ldots (2.28)$$

where, J_1 is the Bessel's function of the first kind. According to this equation, the nodes do not occur at a whole number of π, but lie at points where kz_1 equal to certain values (Z_n) at which the J_1 function is zero. These values are determined from the tables of the J_1 Bessel's function. Therefore, the radius of the nth node is given by:

$$\frac{2\pi}{\lambda} r_n = Z_n \qquad \text{i.e, } r_n = \frac{Z_n}{\pi} \frac{\lambda}{2}$$

If, λ=0.2mm, then the radius of the central patch (where, Z= 3.832) equals 0.122mm, as shown in curve (2) of Fig.(2.17).

Therefore, it is obvious that the diffraction pattern obtained by this method is more narrow than that obtained by the classical theory. A comparison between the two methods, for bowl transducers of different aper tures, will be discussed in the following sub-section.

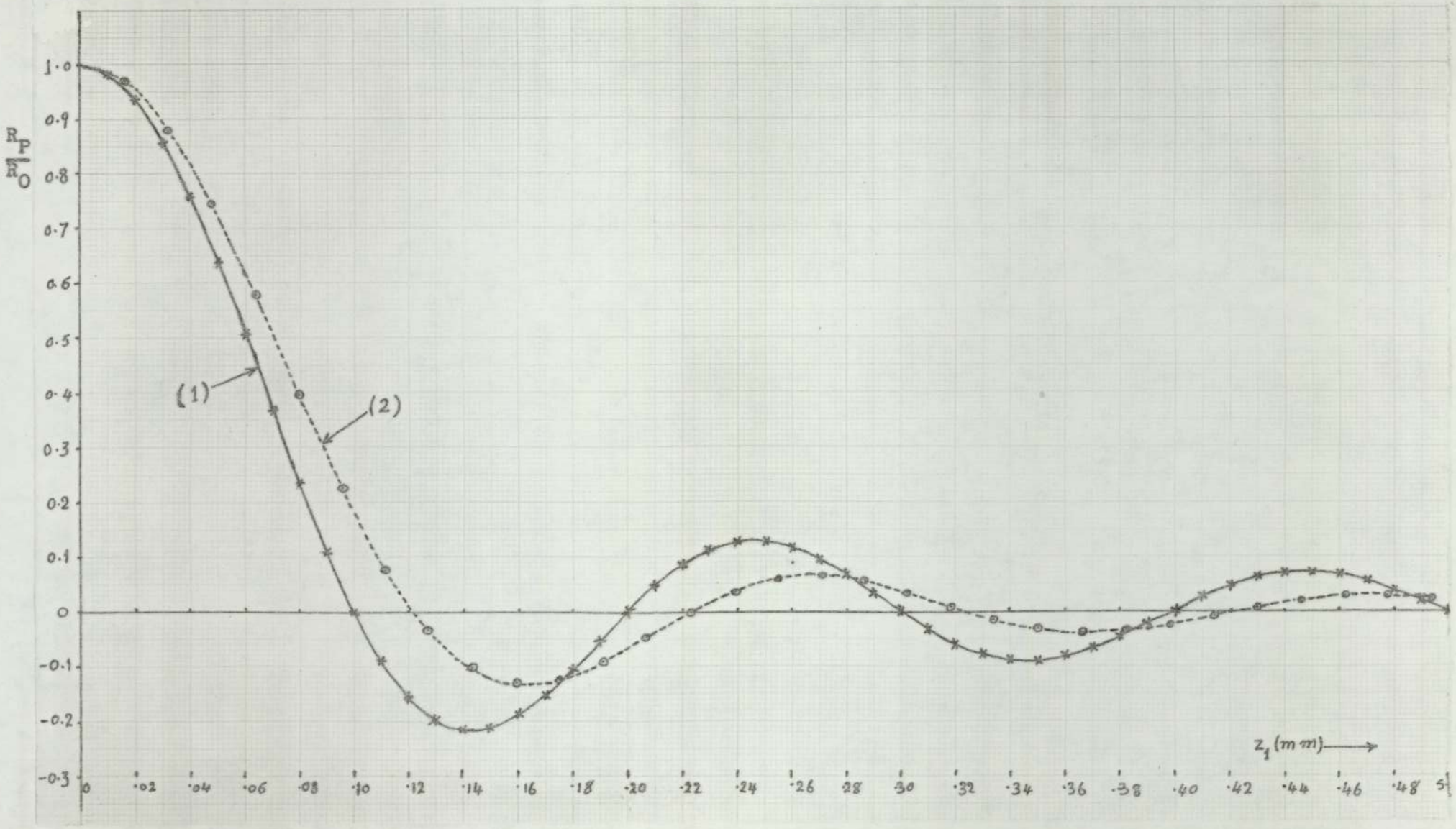

Fig. 2.17 Calculated diffraction patterns for a hemi-sphere (a = 100 mm, λ = 0.2 mm)
Curve (1) using Eq. (2.27); Curve (2) using classical theory (Eq. 2.28).

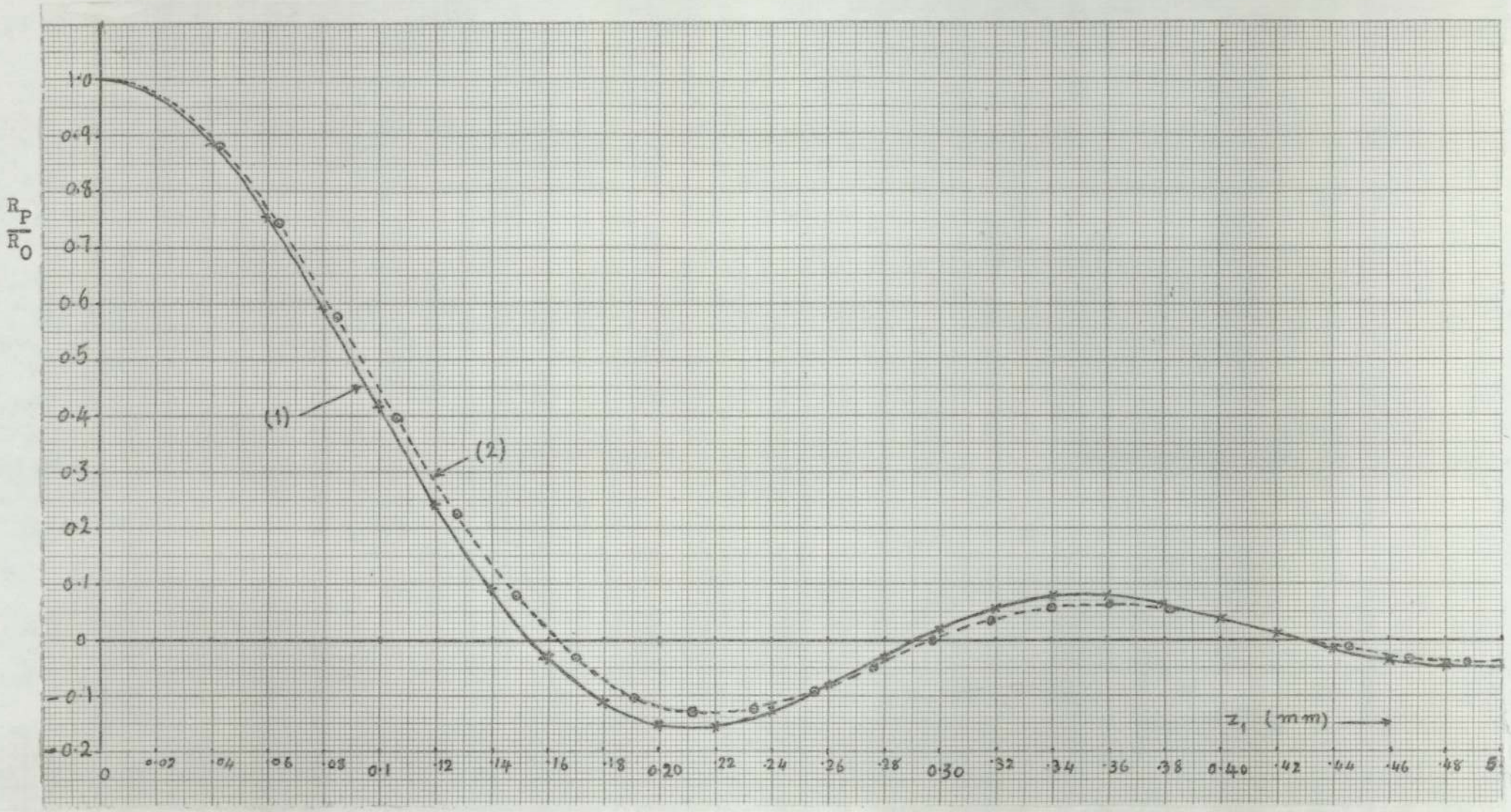

Fig. 2.18 Diffraction patterns for a bowl transducer, b= 75 mm, a=100 mm, and λ =0.2 mm

Curve (1) Computed results Curve (2) using classical theory (Eq. 2.28)

2-A.2.2 Comparison Between This Method and Classical Theory

For hemi-spherical bowl transducer, where λ=0.2mm, the diffraction patterns have been calculated by using this method (Eq.2.27), and the classical theory (Eq.2.28), as shown in Fig.(2.17). From this figure, it can be seen that the diffraction pattern obtained by this method (curve 1) is more narrow than that of the classical theory (curve 2). For instance, the radii of the first node differ by about 22%.

In Fig.(2.18), curve (1) shows the computed diffraction pattern (Eq.2.26) of a bowl transducer for which b=75mm, a=100mm, and λ=0.2mm. The corresponding diffraction pattern obtained by the classical theory, is represented by curve (2). From this figure, it can be seen that the difference, between the radii of the first node, is about 7%.

The radii of the diffraction pattern nodes (r_n), for bowl transducers of different aperture diameters (2b), using both methods, are given in Table (II.1). In each case, the radius of curvature a=100mm, and the wavelength λ=0.2mm.

TABLE II.1

Node Number	r_n (mm)							
	b=25mm		b=50mm		b=75mm		b=100mm	
n	Spherical Integration	Classical Theory	Spherical Integration	Classical Theory	Spherical Integration	Classical Theory	Spherical Integration	Classical Theory
1	0.485	0.488	0.238	0.244	0.153	0.164	0.100	0.122
2	0.890	0.893	0.444	0.447	0.290	0.298	0.200	0.223
3	-	1.295	0.645	0.648	0.430	0.432	0.300	0.324
4	-	1.696	0.845	0.848	0.563	0.565	0.400	0.424
5	-	2.097	-	1.049	0.698	0.699	0.500	0.524

From this table, it can be seen that the difference between the two methods decreases as the aperture diameter becomes smaller.

From the above discussion it may be concluded that:

1. For small aperture bowl transducers, where $^{b}/_{a} < ^{1}/_{2}$; as the aperture decreases the actual diffraction pattern approximates to that obtained by classical theory.
2. For large aperture bowls, $^{b}/_{a} > ^{1}/_{2}$; as the aperture increases, the difference between the actual diffraction pattern and that obtained by classical theory increases.
3. For $^{b}/_{a} > ^{3}/_{4}$; as this ratio increases the diffraction pattern approaches the expression of that obtained by the optical slit model, and becomes equal to it when $^{b}/_{a}=1$, as given by Eq.(2.27).

The relation of the optical slit diffraction pattern, is that for which the amplitude (R_P) at a point P in the central part of a plane at a distance (a) from the slit, is given by:

$$R_P = A \frac{\text{Sin } \beta}{\beta}$$

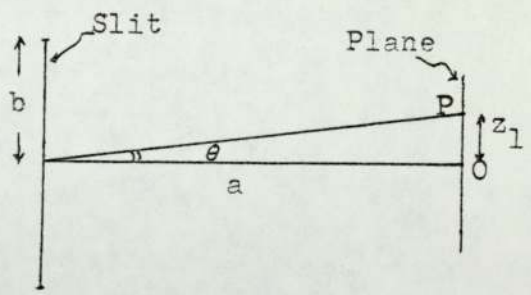

where,

$$\beta = kb \text{ Sin } \theta = kbz_1/a$$

i.e

$$R_P = A \frac{\text{Sin}(kbz_1/a)}{(kbz_1/a)} \qquad \ldots\ldots (2.29)$$

where, A, is constant. $k=2\pi/\lambda$; λ is the wavelength in the medium.

b, is half the length of the slit; z_1, is the distance between P and the central axis.

This equation represents the simplest mathematical expression

of a diffraction pattern, and is used later in connection with the analysis of pulse excitation.

2-A.3 EFFECT OF SHOCK EXCITATION ON THE DIFFRACTION PATTERN, IN THE FOCAL PLANE OF A BOWL TRANSDUCER

The steady state ultrasonic diffraction pattern, in the focal plane of a bowl transducer, has been described in the previous section (2-A.2). In this case the diffraction pattern is due to a single frequency, which is the driving frequency of the transducer. However, when a shock excitation is applied, there are very large number of different frequency components. The effect of these components on the resulting diffraction pattern will be discussed in this section.

In the following sub-section, a mathematical analysis is carried out in order to determine the Fourier series of the spike excitation.

2-A.3.1 Analysis of the Shock Excitation

Let us consider a spike whose width is W, and its amplitude is C at x=o, where

$$f(x) = C - \frac{2xC}{W}, \quad \text{when } o < x < \frac{W}{2};$$

$$f(x) = C + \frac{2xC}{W}, \quad \text{when } -\frac{W}{2} < x < o; \text{ and}$$

$$f(x) = o, \quad \text{when } \frac{W}{2} < x < (2\pi - \frac{W}{2})$$

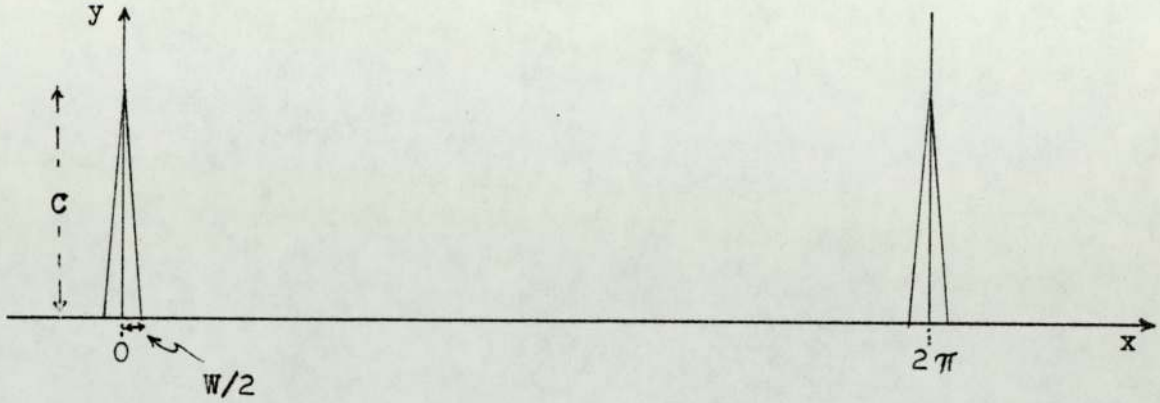

This function is periodic, with period 2π. Therefore, the Fourier series is given by:

$$y=f(x) = \frac{1}{2} a_o + a_1 \text{ Cos } x + a_2 \text{ Cos } 2x + a_3 \text{ Cos } 3x + \ldots + a_n \text{Cos } nx +$$
$$+ b_1 \text{ Sin } x + b_2 \text{ Sin } 2x + b_3 \text{ Sin } 3x + \ldots b_n \text{ Sin } nx.$$

where,

$$a_o = \frac{1}{\pi} \int_o^{2\pi} f(x)\, dx;$$

$$a_n = \frac{1}{\pi} \int_o^{2\pi} f(x) \text{ Cos } nx\, dx; \text{ and}$$

$$b_n = \frac{1}{\pi} \int_o^{2\pi} f(x) \text{ Sin } nx\, dx.$$

Since $\frac{a_o}{2}$ is equal to the mean value of f(x) in the range o to 2π, i.e. $\frac{a_o}{2} = \frac{CW}{4\pi}$. Also, b_n is (an even function, f(x) being) equal to zero, therefore

$$y=f(x)=\frac{CW}{4} + a_1 \text{Cos } x + a_2 \text{ Cos } 2x + a_3 \text{ Cos } 3x + \ldots + a_n \text{ Cos } nx \quad \ldots (2.30)$$

a_n can be determined as follows;

$$a_n = \frac{1}{\pi} \int_o^{W/2} \left(C - \frac{2xC}{W}\right) \cos nx\, dx + \frac{1}{\pi} \int_{-W/2}^{o} \left(C + \frac{2xC}{W}\right) \cos nx\, dx +$$
$$\frac{1}{\pi} \int_{W/2}^{(2\pi - \frac{W}{2})} (o) \cos nx\, dx$$

$$a_n = \frac{2}{\pi}\int_0^{W/2} \left(C - \frac{2xC}{W}\right) \text{Cos } nx \, dx$$

$$= \frac{2C}{\pi}\left\{\int_0^{W/2} \cos nx \, dx - \frac{2}{W}\int_0^{W/2} x \cos nx \, dx\right\}$$

Integrating by parts of the second term on the right-hand side of the above equation, then

$$a_n = \frac{2C}{\pi}\left\{\left[\frac{1}{n}\text{ Sin } nx\right]_0^{W/2} - \frac{2}{W}\left[\frac{x\text{Sin } nx}{n} - \int\frac{\text{Sin } nx}{n}\, dx\right]_0^{W/2}\right\}$$

$$= \frac{2C}{\pi}\left[\left(\frac{\text{Sin } nx}{n}\right) - \frac{2}{W}\left(\frac{x \text{ Sin } nx}{n} + \frac{\text{Cos } nx}{n^2}\right)\right]_0^{W/2}$$

$$= \frac{4C}{\pi W n^2}\left(1 - \text{Cos } \frac{nW}{2}\right)$$

$$= \frac{4C}{\pi W n^2}\left\{1 - \left[\left(1 - \frac{1}{2!}\left(\frac{nW}{2}\right)^2 + \frac{1}{4!}\left(\frac{nW}{2}\right)^4 - \frac{1}{6!}\left(\frac{nW}{2}\right)^6 + \ldots\right]\right\}$$

$$= \frac{4C}{\pi W}\left(\frac{W^2}{8} - \frac{n^2W^4}{384} + \frac{n^4W^6}{46080} - \frac{n^6W^8}{10321920} + \cdots\cdots\right)$$

Since if W is a very small fraction of 2π, the term $(n^2W^4/384)$ and also the subsequent terms, in the above equation, may be neglected.

Thence,

$$a_n = \frac{CW}{2\pi}$$

This means that a_n may be considered the same for each frequency, and therefore, Eq.(2.30) may be re-written as follows:

$$y = \frac{CW}{4\pi} + \frac{CW}{2\pi}\left(\text{Cos}\,\omega_o t + \text{Cos } 2\omega_o t + \text{Cos } 3\omega_o t + \ldots\ldots + \text{Cos } n\omega_o t\right)$$

or,

$$y = \frac{CW}{4\pi} + \frac{CW}{2\pi}\sum_{n=1}^{n=\infty} \cos n\,\omega_o t \qquad \ldots\ldots (2.31)$$

Therefore, there are infinite numbers of frequency components of the same amplitude, due to the shock excitation. This conclusion will be used in order to determine the resulting diffraction pattern, by applying the expression from the optical slit model (Eq.2,29), and that from the classical theory for a converging spherical wavefront(Eq.2.28).

2-A.3.2 Application of Slit Diffraction Pattern Expression

According to Eq.(2.29), the amplitude (R_p) due to the contribution of the nth frequency component, at a point P in the central part of a plane at a distance 'a' from the slit, is given by:

$$R_p = A \frac{\mathrm{Sin}(\frac{kbz_1}{a})}{(\frac{kbz_1}{a})} = A \frac{\mathrm{Sin}\ (\frac{n\omega_o}{c} \frac{bz_1}{a})}{(\frac{n\omega_o}{c} \frac{bz_1}{a})}$$

where, A is constant; $k=\frac{\omega}{c} = \frac{n\omega_o}{c}$; c denotes the velocity of sound in the propagating medium; b, is half the slit length; and z_1, is the distance between p and the central axis

The total contribution at P due to all the frequency components, is given by:

$$R_p = A \sum_{n=1}^{n=\infty} \frac{\mathrm{Sin}\ (\frac{n\omega_o bz_1}{ca})}{(\frac{n\omega_o bz_1}{ca})}$$

As ω_o is theoretically required to tend to zero, this effectively provides a continuum of frequencies and

therefore may be expressed as:

$$R_P = A \int_0^{\infty} \frac{\mathrm{Sin}\left(\frac{2\pi b z_1 f}{ca}\right)}{\left(\frac{2\pi b z_1 f}{ca}\right)} \, df$$

Theoretically, this integral can not be properly estimated with an upper limit of infinity.

Practically, there are at least five factors which impose an upper limit on the bandwidth. These are:

1. The upper limit of the power transistor giving the "spike" electrical signal.
2. The response of the transducer as a transmitter.
3. The effect of attenuation of ultrasonics in the propagating liquid, which is approximately proportional to the frequency squared.
4. The response of the transducer as a receiver.
5. The bandwidth of the receiving amplifier.

The most important effects among the above factors are those due to the attenuation and the bandwidth of the receiving amplifier. The effect of attenuation on the upper limit of the bandwidth, and hence on the resulting diffraction pattern, will be dealt with in a later sub-section (2-A.3.4). The receiving amplifier, on the other hand, may be designed so as to have a nearly flat response over a certain frequency region with given lower and upper limits.

Before discussing the detected diffraction pattern due to a limited bandwidth of the receiving amplifier, we shall

consider first the theoretical effect due to a wide bandwidth extending from a very low frequency limit (i.e. $f_1 \simeq o$) to an upper limit of a relatively high frequency (f_2). In this case, the contribution at any point P in the central part of the plane, may be written as follows:-

$$R_P = A \int_o^{f_2} \frac{\text{Sin } (\frac{2\pi bz_1}{ca})f}{(\frac{2\pi bz_1}{ca})f} \, df \qquad \ldots\ldots (2.32)$$

Let $(\frac{2\pi bz_1}{ca})f = \beta$ Hence, $df = (\frac{ca}{2\pi bz_1}) \, d\beta$

Substituting these values into the above equation, then

$$R_P = \frac{Aca}{2\pi bz_1} \int_o^{\beta_2} \frac{\text{Sin } \beta}{\beta} \, d\beta = \frac{Af_2}{\beta_2} \int_o^{\beta_2} \frac{\text{Sin } \beta}{\beta} \, d\beta \qquad \ldots\ldots (2.33)$$

The integral of Sin β/β, in the limits between zero and any value of β, can be determined from the tables (Jahnke, Emde; and Lösch, 1960).

The contribution at the centre of the plane (R_o), may be determined as follows:

Since, $\text{Sin } \beta = \beta - \frac{\beta^3}{3!} + \frac{\beta^5}{5!} - \ldots\ldots$

Substituting into Eq. (2.33) and integrating, then

$$R_p = \frac{Af_2}{\beta_2} \int_o^{\beta_2} (1 - \frac{\beta^2}{3!} + \frac{\beta^4}{5!} \ldots) \, d\beta = \frac{Af_2}{\beta_2} \left[\beta - \frac{\beta^3}{3x3!} + \frac{\beta^5}{5x5!} \ldots \right]_0^{\beta_2}$$

$$R_P = Af_2 \, (1 - \frac{\beta_2^2}{3x3!} + \frac{\beta_2^4}{5x5!} \ldots)$$

At the centre of the plane $z_1 = o$, and $\beta_2 = o$; therefore

$$R_o = Af_2$$

Dividing Eq.(2.33) by R_o, gives the normalised contribution (R_p/R_o), at any point P in the plane. Thus,

$$\frac{R_P}{R_o} = \frac{1}{\beta_2} \int_o^{\beta_2} \frac{\text{Sin } \beta}{\beta} \, d\beta = \frac{Q}{\beta_2} \qquad \ldots\ldots (2.34)$$

in which,

$$\beta_2 = \frac{2\pi b z_1}{ca} 10^6 F_2; \text{ and } Q = \int_o^{\beta_2} \frac{\text{Sin } \beta}{\beta} \, d\beta$$

where, F_2 is the frequency in MHz; and z_1, is the distance of P from the central axis.

The effect of this may be seen in a practical situation for a cylindrical transducer for which $b/a = 1/4$, operating into water for which $c = 1.5 \times 10^6$ mm/sec.
Assuming F_2 arbitrarily equal to 10 MHz, the values of β_2 for different values of z_1, have been calculated. The corresponding values of Q are determined from the tables, and the results of R_P/R_o are plotted against z_1, as shown by curve (1) in Fig.(2.19). From this curve it can be seen that the diffraction patter has no zero value.

Let us consider that the bandwidth of the receiving amplifier is arbitrarily limited between f_1 and f_2. In this case, both the lower and higher frequency components are excluded from the detection point of view. Therefore, the only contributions to be detected are those due to the components in this region, for which the resultant is given by:

$$R_p = A \int_{f_1}^{f_2} \frac{\text{Sin } (2\pi bz_1/ca)f}{(\frac{2\pi bz_1}{ca})f} df \qquad \ldots\ldots (2.35)$$

If $f_2 = mf_1$, then $\beta_2 = m\beta_1$. Therefore,

$$R_p = \frac{Aca}{2\pi bz_1} \int_{\beta_1}^{m\beta_1} \frac{\text{Sin } \beta}{\beta} d\beta = \frac{Af_1}{\beta_1} \int_{\beta_1}^{m\beta_1} \frac{\text{Sin } \beta}{\beta} d\beta \qquad \ldots\ldots (2.36)$$

or,

$$R_p = \frac{Af_1}{\beta_1} \left[\int_{o}^{m\beta_1} \frac{\text{Sin } \beta}{\beta} d\beta - \int_{o}^{\beta_1} \frac{\text{Sin } \beta}{\beta} d\beta \right] = \frac{Af_1}{\beta_1} Q' \qquad \ldots (2.36\text{-a})$$

where, Q' is the difference between the two integrals.

The contribution at the centre of the plane (R_o), can be determined by substituting the series of Sin β into Eq.(2.36), which gives:

$$R_p = \frac{Af_1}{\beta_1} \left[\beta - \frac{\beta^3}{3x3!} + \frac{\beta^5}{5x5!} \quad \ldots\ldots \right]_{\beta_1}^{m\beta_1}$$

$$R_p = Af_1 \left\{ (m-1) - \frac{(m^3-1)}{3x3!} \beta_1^2 + \frac{(m^5-1)}{5x5!} \beta_1^4 \quad \ldots\ldots \right\}$$

When $z_1 = o$, $\beta_1 = o$, and hence

$$R_o = Af_1 (m-1).$$

Dividing Eq.(2.36-a) by the above equation, then

$$\frac{R_p}{R_o} = \frac{Q'}{\beta_1 (m-1)} \qquad \ldots\ldots (2.37)$$

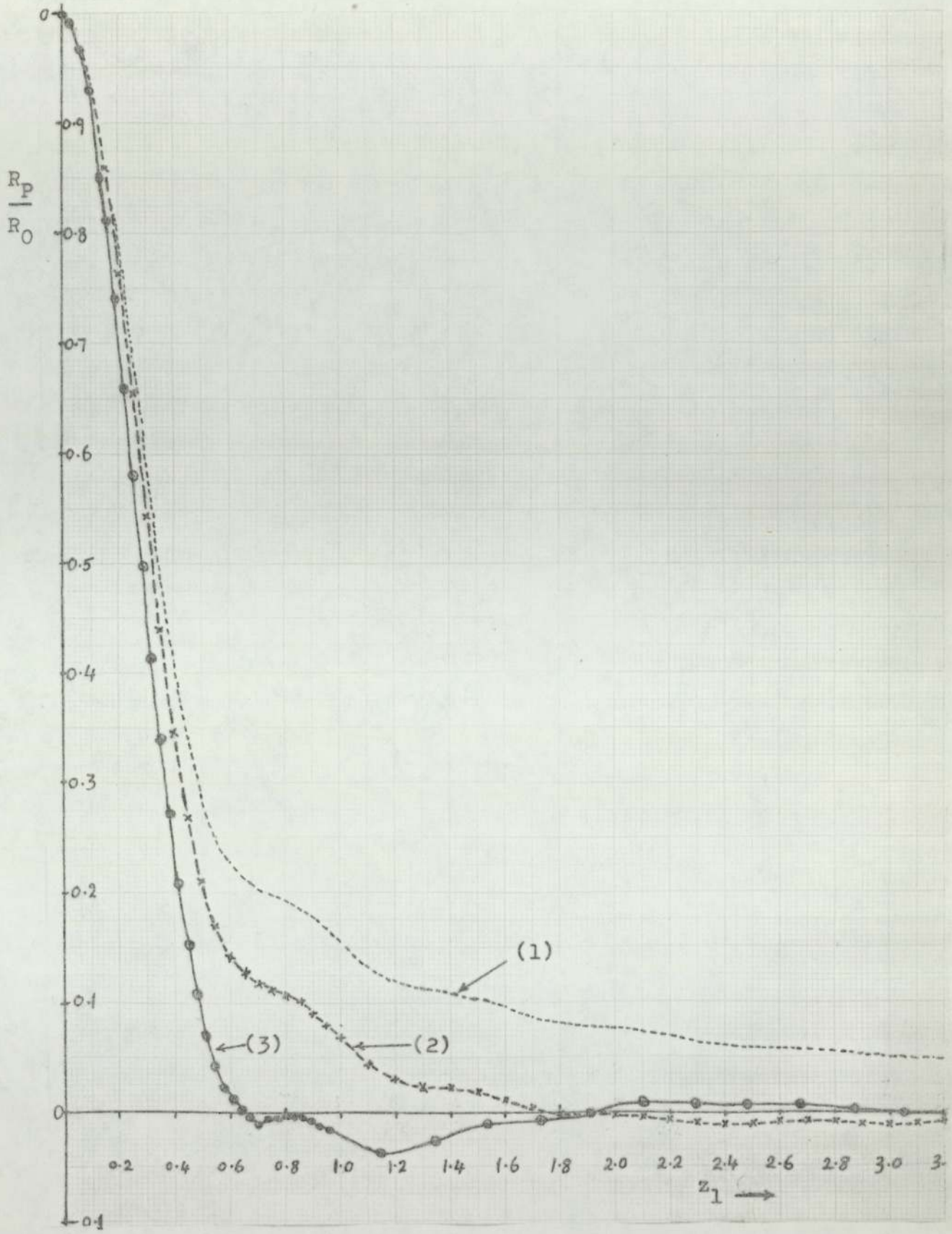

Fig. 2.19 Diffraction pattern due to a shock excitation, applying the expression from optical slit model (Eq.2.29), at different bandwidths: (1) 0 - 10 MHz; (2) 1 - 10 MHz; (3) 2.5 - 10 MHz.

where,

$m = \frac{f_2}{f_1} = \frac{F_2}{F_1}$; F_1 and F_2, denote the lower and upper limits of the bandwidth, in MHz.

$\beta_1 = \frac{2\pi b z_1}{ca} f_1$; for b/a =1/4, c = 1.5×10^6 mm/sec; then

$\beta_1 = \frac{\pi}{3} F_1 z_1$

Q', is the difference between the integrals in Eq.(2.36-a), which can be determined from the tables.

The results of R_p/Ro for two arbitrary bandwidths, i.e. 1-10 MHz, and 2.5-10MHz , are plotted against z_1 as shown by curves (2) and (3) in Fig.(2.19).

Equations (2.32) and (2.35) were numerically evaluated by computer, using program (8) - in appendix (B), which gave the same results as those obtained from Eqs.(2.34) and (2.37).

From Fig(2.19) - curves (2) and (3), it can be seen that, the first zero of the diffraction pattern becomes nearer to the centre as the lower limit of the bandwidth increases. From curve (3) it can be seen that the radius of the first node is about 0.65mm. This value corresponds to that which may be obtained from a steady state diffraction pattern for a single frequency of about 4.6MHz for the same system.

2-A.3.3 Application of the Classical Theory for a Bowl Transducer

According to the classical theory of the diffraction pattern (Eq.2.28), the normalised contribution due to a

single frequency component (f), at a point P in the central part of the focal plane of a bowl transducer, is given by:

$$\frac{R_P}{R_o} = \frac{2J_1(\beta)}{\beta}$$

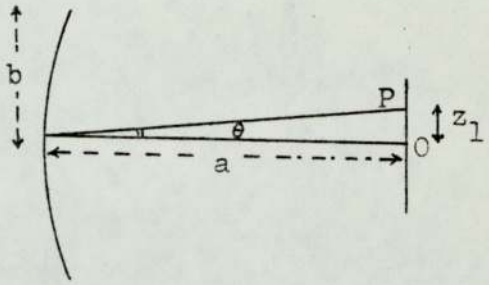

where,

$\beta = kb \sin\theta \simeq kbz_1/a$; in which

$$k = \frac{\omega}{c} = \frac{2\pi f}{c} = \frac{2\pi F}{c} \times 10^6$$

f, is the frequency in Hz; and F is that in MHz

c, is the velocity of sound in the propagating medium (in water $c \simeq 1.5 \times 10^6$ mm/sec.).

This theory was found (Section 2-A.2) to agree with the results for bowl transducers for which b/a is $< \frac{1}{2}$.

For a shock excitation applied to a bowl transducer, the normalised contribution at a point P, due to a bandwidth F_1 to F_2, will be:-

$$\frac{R_P}{R_o} = \int_{\beta_1}^{\beta_2} \frac{2J_1(\beta)}{\beta}\, d\beta = \int_{F_1}^{F_2} \frac{2J_1\left(\frac{2\pi bz_1}{ca} 10^6 F\right)}{\left(\frac{2\pi bz_1}{ca} 10^6 F\right)}\, dF \quad \ldots\ (2.38)$$

This equation was numerically evaluated by computer, using program (9) - in appendix (B), for bowl transducers of different apertures and for different bandwidths. The results are plotted against z_1 as shown in Figs(2.20) and (2.21).

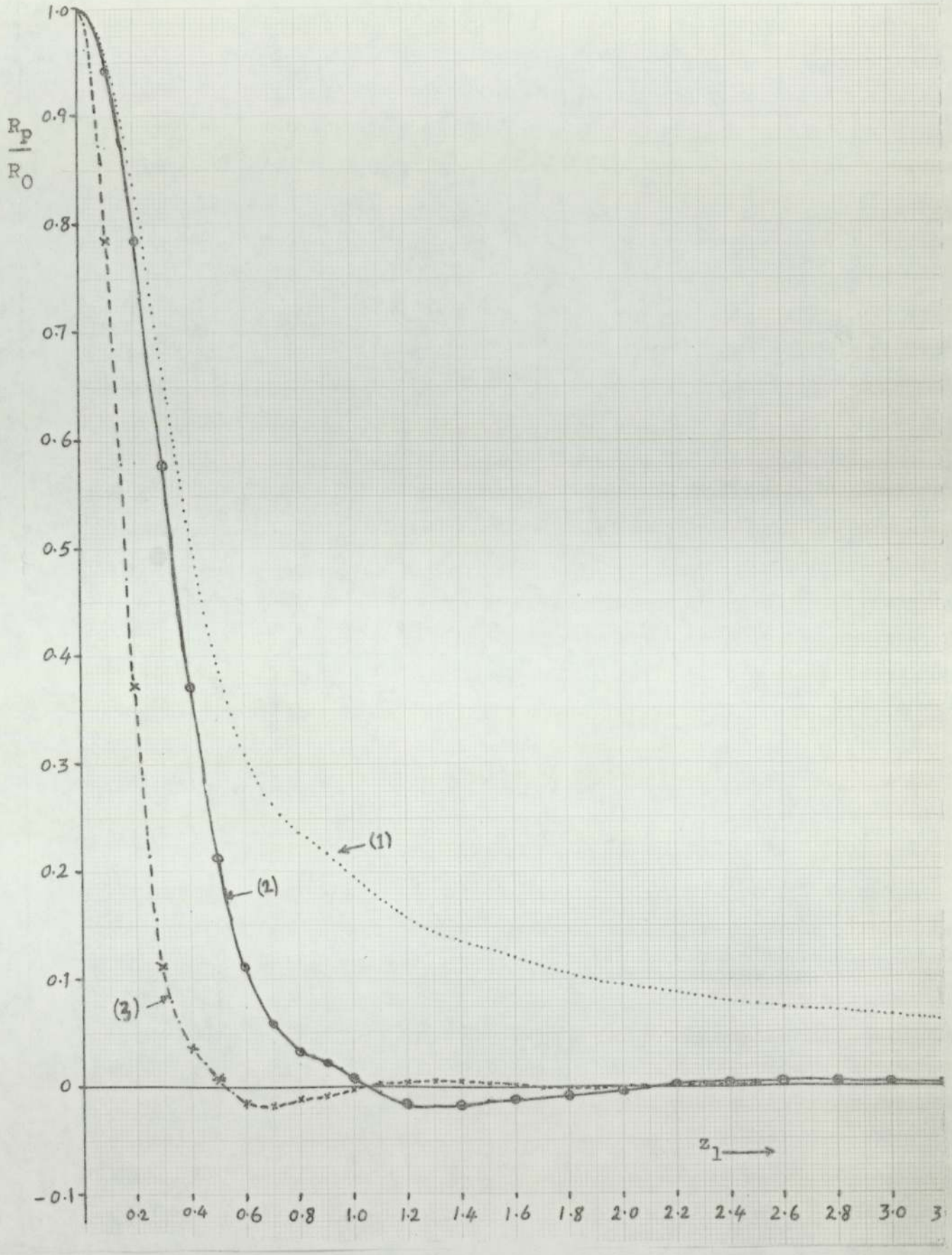

Fig. 2.20 Diffraction patterns of two bowl transducers, due to shock excitation and different bandwidths

(1) b/a =1/4 , 0 -10 MHz; (2) b/a = 1/4 , 2.5 - 10 MHz;

(3) b/a =1/2 , 2.5 - 10 MHZ.

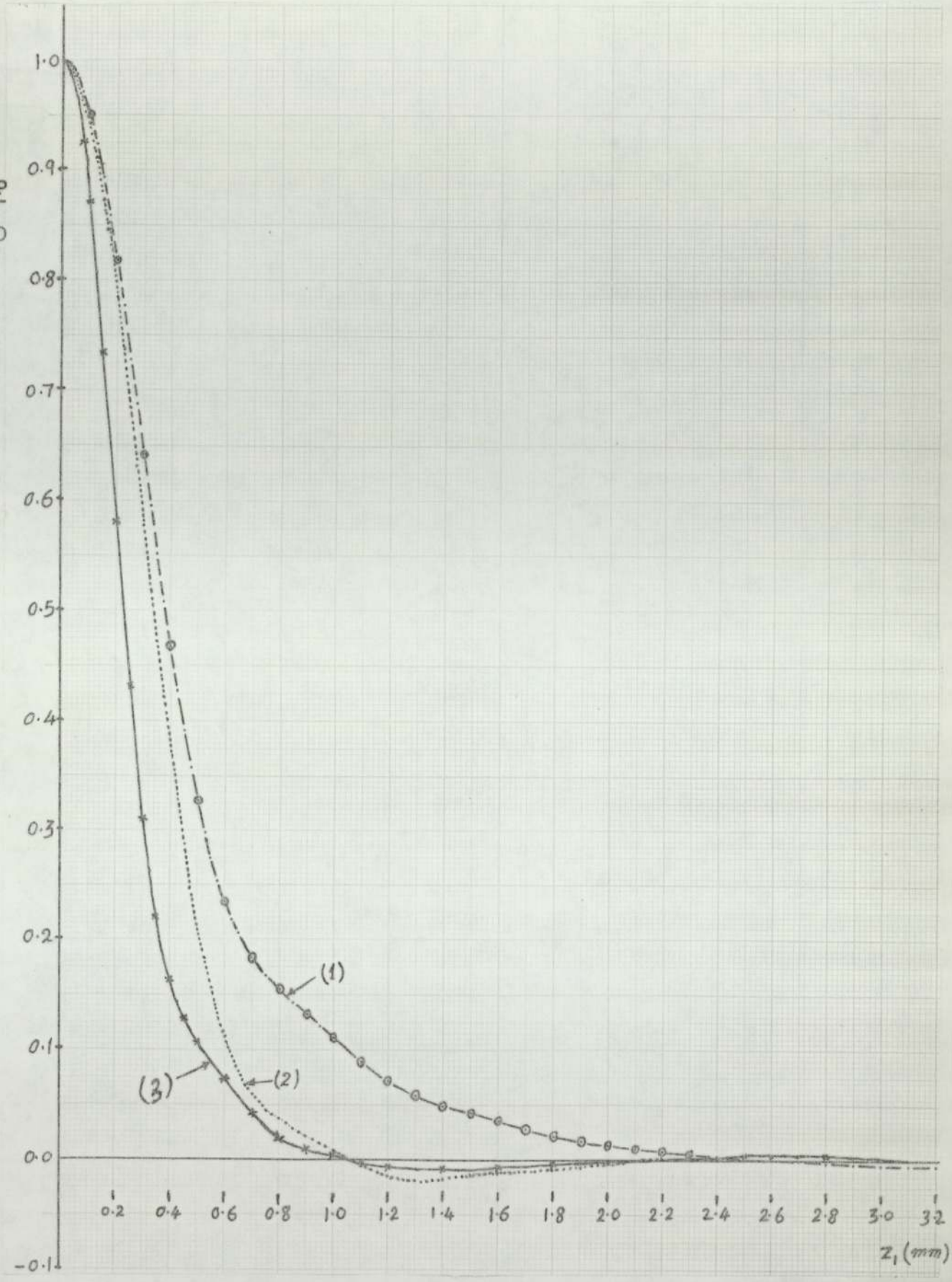

Fig. 2.21 Diffraction pattern for a bowl transducer (b/a =1/4) due to shock excitation and different bandwidths:

(1) 1 - 10 MHz (2) 2.5 - 10 MHz (3) 2.5 - 16 MHz.

In Fig.(2.20), curve (1) shows the theoretical effect due to a broad bandwidth, where F_1=o and F_2=10MHz, for a bowl transducer whose b/a=1/4. From this curve it can be seen that the diffraction pattern has no zero value.
Curves (2) and (3) - Fig.(2.20), show the results due to a limited bandwidth (F_1=2.5, and F_2 = 10MHz), for two bowl transducers of different apertures , where b/a = $^1/4$ and $^1/2$. From these curves, it can be seen that the diffraction pattern becomes more narrow as the aperture increases, as it does in the steady state.

Figure (2.21) shows the diffraction patterns of a bowl transducer, for which b/a = $^1/4$, due to different limits of bandwidth.
From curves (1) and (2), it can be seen that, as the lower limit of the bandwidth increases, the radius (r) of the central patch of the diffraction pattern decreases. By comparing curves (2) and (3), which have the same lower limit of bandwidth, it can be seen that, as the higher limit increases, the central patch becomes more narrow whereas its radius (r) remains the same.

2-A.3.4 Attenuation Effects

From the above discussion, it has been shown that, in the case of spike excitation applied to a spherical bowl transducer, there are an infinite number of frequency components of constant amplitude. However, in travelling through a medium, the amplitude of each component will be attenuated depending on its frequency. Since, the absorption co-efficient

(α) in water is very nearly proportional to the frequency squared, therefore,

$$A=A_o\, e^{-\alpha x} = A_o\, e^{-CF^2x}$$

where,

A_o and A, are the amplitudes before and after attenuation, respectively.

x, is the distance traversed, which may be considered equal to the radius of curvature of the bowl transducer, i.e. x=a;

F, is the frequency in MHz; and

C, is a constant, for water C=0.00025 nepers/cm. $(MHz)^{-2}$ (Kaye and Laby).

Eq.(2.38) may be modified to take absorption into account, thus becomes

$$\frac{Rp}{Ro} = \int_{F_1}^{F_2} \frac{2J_1\left(\frac{2\pi bz_1}{ca}\, 10^6 F\right)}{\left(\frac{2\pi bz_1}{ca}\, 10^6\right) F}\, e^{-F^2a/4000}\, dF \qquad \ldots\ldots (2.39)$$

This equation was numerically evaluated by computer, using program (10) - in appendix (B), for a bowl transducer whose aper ture radius b=2.5 cm, and its radius of curvature a=10 cm. The results are shown in Fig(2.22). Curve (1) shows the diffraction pattern for a shock excitation with attenuation in water and a limited bandwidth between 2.5 to 16MHz. Curve (2) shows the diffraction pattern due to a bandwidth with a lower frequency (F_1) of 2.5 MHz, and an unbounded upper frequency which shows the effect of attenuation by water only. This was shown by putting F_2 equal to 40 MHz and 50 MHz for computation and obtaining identical results.

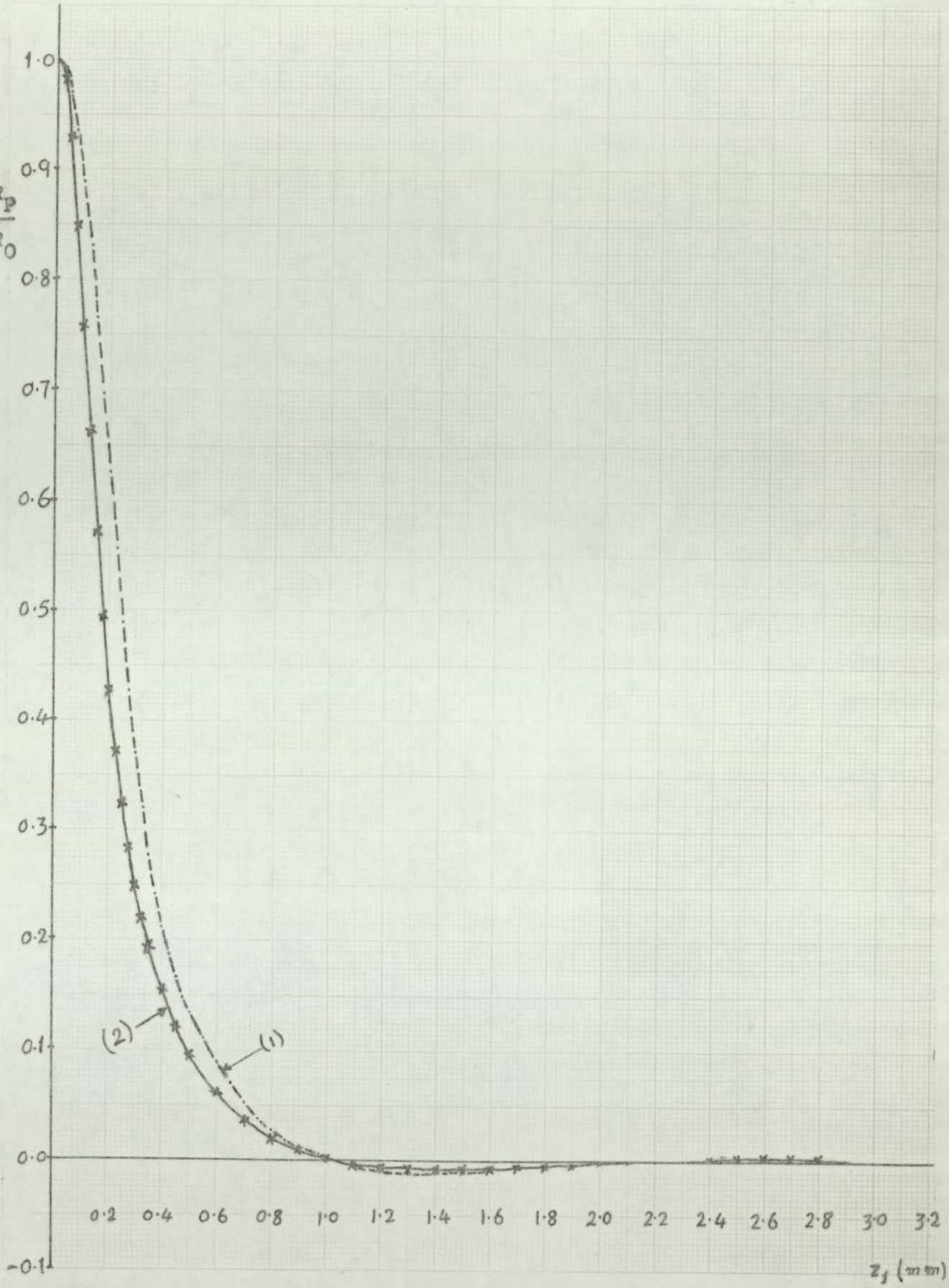

Fig. 2.22 Diffraction pattern for a bowl transducer (b/a = 1/4) due to shock excitation with attenuation in water.

(1) 2.5 - 16 MHz (2) 2.5 - 40 MHz.

From the previous discussion, of the diffraction pattern due to a pulse excitation applied to a bowl transducer, it can be concluded that:-

1. The lateral resolution increases as the aperture diameter increases (curves (2) and (3) - Fig.2.20), in a similar manner to the steady state condition (section 2-A.2).
2. The resolution is mainly dependant on the increase of the lower limit of the bandwidth of the receiving amplifier (curves (1) and (2) - Fig.2.21).
3. The position of the first zero, for a given bowl transducer and a given lower frequency limit, is independent of increase of the upper limit, above 10 MHz.
4. There is no benefit in extending the upper frequency of the receiving amplifier beyond 30-40 MHz, where the major path is in water.

2-A.3.5 Effects of Attenuation and a Bell-Shape Bandwidth of the Receiving System

So far we were dealing with an arbitrary flat bandwidth of the receiving amplifier, terminated by a lower and upper frequency limits. However, in practice, the bandwidth of the receiving system may have any shape which in turn may affect the diffraction pattern due to a shock excitation applied to a bowl transducer.

A theoretical analysis has been carried out, in Chapter V (Section 5.4), in order to determine the bandwidth of the coupling circuit to the receiving pre-amplifier, as given by Eq.(5.4) and shown in Fig(5.7). From this figure it can be seen that the bandwidth of this circuit is represented by a

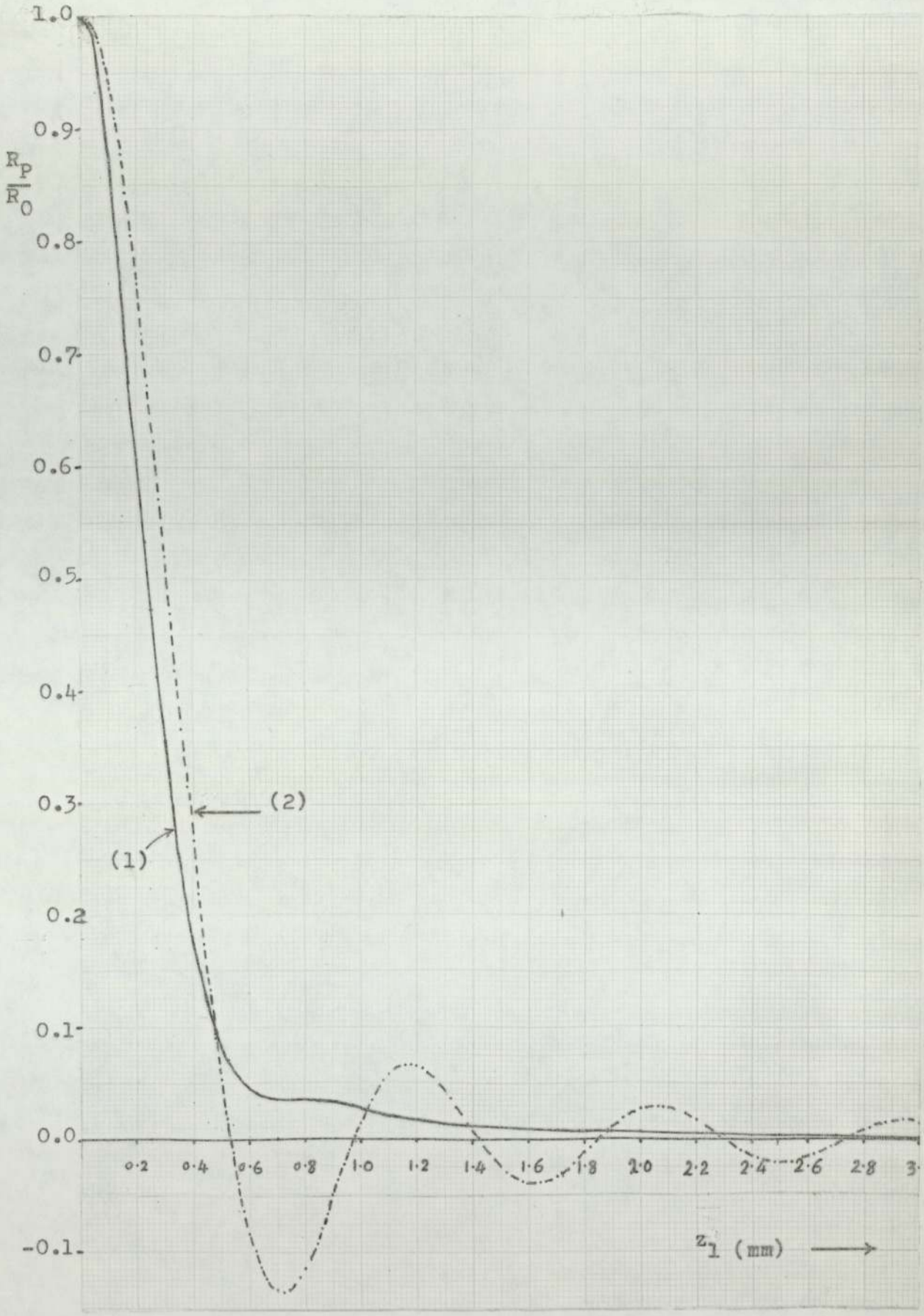

Fig. 2.23 Diffraction pattern for a bowl transducer (b/a = 1/4)

(1) Due to shock excitation, with attenuation in water and a bell-shape bandwidth.

(2) Due to steady state condition at 6.85 MHz.

bell-shape curve, in the high frequency region (with a peak at 9MHz.).

As this coupling circuit imposes the principle restriction on the bandwidth of the receiving amplifier, its bandwidth effect on the diffraction patterns of the bowl transducers, for which $b/a=1/4$, used in this system, will be discussed in this sub-section.

According to Eq.(5.4), the bandwidth of the coupling circuit may be re-written as follows:

$$\left|\frac{V_2}{V_1}\right| = \frac{0.212F}{\left\{(1-0.02F^2)^2+(0.212F)^2(1-0.01F^2)^2\right\}^{\frac{1}{2}}} \qquad \ldots(2.40)$$

For F=0.02MHz, the ratio $\left|\frac{V_2}{V_1}\right|$ is about 0.004, i.e. 0.4%.

Eq.(2.39), incorporating the effect of attenuation, may be modified to take this expression of the bandwidth (Eq.2.40) into account, thus becoming:

$$\frac{R_p}{R_o} = \int_{F_1}^{F_2} \frac{2J_1\left(\frac{2\pi bz_1}{ca}10^6\right)F}{\left(\frac{2\pi bz_1}{ca}10^6\right)F} e^{-F^2a/4000} \frac{0.212F}{\left\{(1-0.02F^2)^2+(0.212F)^2\ (1-0.01F^2)^2\right\}^{\frac{1}{2}}} dF \qquad \ldots\ldots (2.41)$$

This equation was numerically evaluated by computer, using program (11) - in appendix (B). For computation, F_1, is put equal to 0.02MHz, and F_2 is put equal to 40MHz. The results are shown by curve (1) in Fig.(2.23). In this figure, curve (2) represents the diffraction pattern in the steady state condition, for the same bowl transducer ($b/a=1/4$) which is driven at 6.85MHz.

2-A.4 AXIAL DISTRIBUTION AROUND THE CENTRE OF CURVATURE OF A BOWL TRANSDUCER - AT A STEADY STATE CONDITION

For a concave bowl transducer radiating into water, the ultrasonic radiation will not be focused at a point but rather will be spread both along and across the axis around a focal centre, so that the effective focus may be thought of as occupying a volume.
The distribution in the direction perpendicular to the axis, i.e. the diffraction pattern in the focal plane, has been discussed in section (2-A.2).

O'Neil (1949) has developed a theory from which the axial distribution around the centre of curvature may be determined. In this section, an easy method will be discussed, in which the Huygen's integral is applied, in order to determine the effective length of the focus. The geometry involved in the mathematical analysis, is shown in Fig.(2.24); where,
a, is the radius of curvature of the concave transducer;
b, is the radius of its circular boundary;
P, is an observation point on the central axis; and
ℓ is the distance of P away from the centre of curvature O, and ℓ is not too large so that the Huygen's integral can be applied accurately, as explained in Section (2-A.2). For instance, if b=25 mm and a=100mm, the deviation of Cosθ from unity does not exceed 7×10^{-5} if ℓ is not more than 5mm, and 2.6×10^{-4} if ℓ is not more than 10mm.

In order to determine the acoustic potential (ϕ_P) at the point P due to the total contribution from the whole area S

of the concave surface, consider a circular elementary band whose radius is (a Sin α) and its width is (adα), as shown in Fig.(2.24). All points on this element, are equi-distant (s) from P.

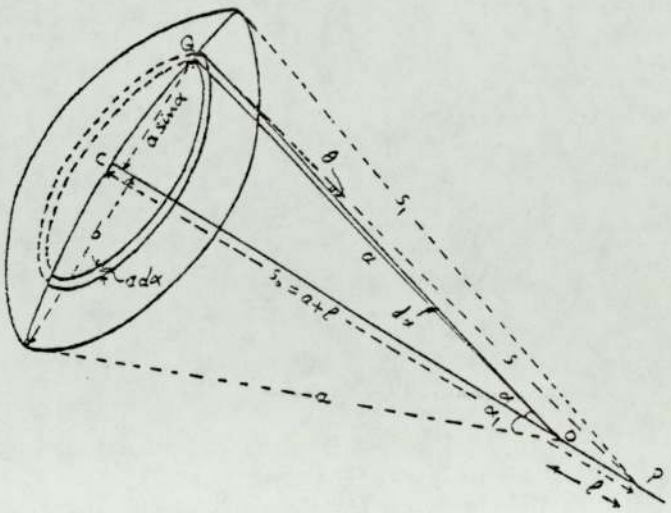

Fig. 2.24 Geometry used in calculating the axial distribution around the centre of curvature of a bowl transducer.

The area of the elementary band (dS) is given by:

$$dS = 2\pi\, a^2 \text{ Sin } \alpha\, d\alpha$$

Substituting this value into Eq.(2.21), then

$$\phi_p = \frac{2\pi a^2}{\lambda} \int_{\alpha=0}^{\alpha=\alpha_1} \frac{e^{-jks}}{s} \text{ Sin } \alpha\, d\alpha \qquad (2.42)$$

where,

α, is the angle between the radius of curvature from any point Q on the elementary band, and the central axis.

α_1, is the angle between the radius of curvature from the boundary of the concave surface, and the central axis.

From the trigonometry of Fig(2.24), we have;

$s^2 = a^2 + \ell^2 + 2a\ell \cos \alpha$, which by differentiating gives

$$\text{Sin } \alpha\, d\alpha = - \frac{s}{a\ell}\, ds$$

Substituting into Eq.(2.42), then

$$\phi_p = -\frac{2\pi a}{\ell\lambda}\int_{s_o}^{s_1} e^{-jks}\,ds = \frac{2\pi a}{\ell\lambda k}\left[e^{-jks_1} - e^{-jkso}\right]$$

$$\left|\phi_p\right| = \frac{a}{\ell}\left[2\,\mathrm{Sin}\,\tfrac{1}{2}\,(kso - ks_1)\right] = \frac{2a}{\ell}\,\mathrm{Sin}\,\frac{\pi}{\lambda}\,(So - s_1)$$

Substituting the value of so and s_1, where

$$so = a+\ell; \text{ and } s_1 = \sqrt{a^2+\ell^2+2a\ell\,\cos\alpha_1}$$

Therefore,

$$\left|\phi_p\right| = \frac{2a}{\ell}\,\mathrm{Sin}\left[\frac{\pi}{\lambda}\left\{(a+\ell) - (a^2+\ell^2+2a\ell\,\cos\alpha_1)^{\frac{1}{2}}\right\}\right] \quad \ldots\ (2.43)$$

In order to determine the positions of the first axial nodes on each side of the centre of curvature, where $\phi_p = o$, we require

$$\frac{\pi}{\lambda}\left\{(a+\ell)-(a^2+\ell^2+2a\ell\,\cos\alpha_1)^{\frac{1}{2}}\right\} = \pm\pi$$

i.e.,

$$(a+\ell)-(a^2+\ell^2+2a\ell\,\mathrm{Cos}\,\alpha_1)^{\frac{1}{2}} = \pm\lambda$$

For $+\pi$, where the first axial node beyond the centre of curvature, then

$$\ell = \frac{2a\lambda-\lambda^2}{2a(1-\cos\alpha_1)-2\lambda} \quad \ldots\ (2.44)$$

For $-\pi$, where the first axial node infront of the centre of curvature, then

$$\ell = -\frac{2a\lambda+\lambda^2}{2a(1-\cos\alpha_1)+2\lambda} \quad \ldots\ (2.45)$$

Equation (2.43) has been used to calculate the axial distribution around the centre of curvature of a bowl transducer, for which b=25mm, a=100mm, and λ=0.2mm. The normalised values ϕ_p/ϕ_o (ϕ_o, being the value at the centre of curvature)

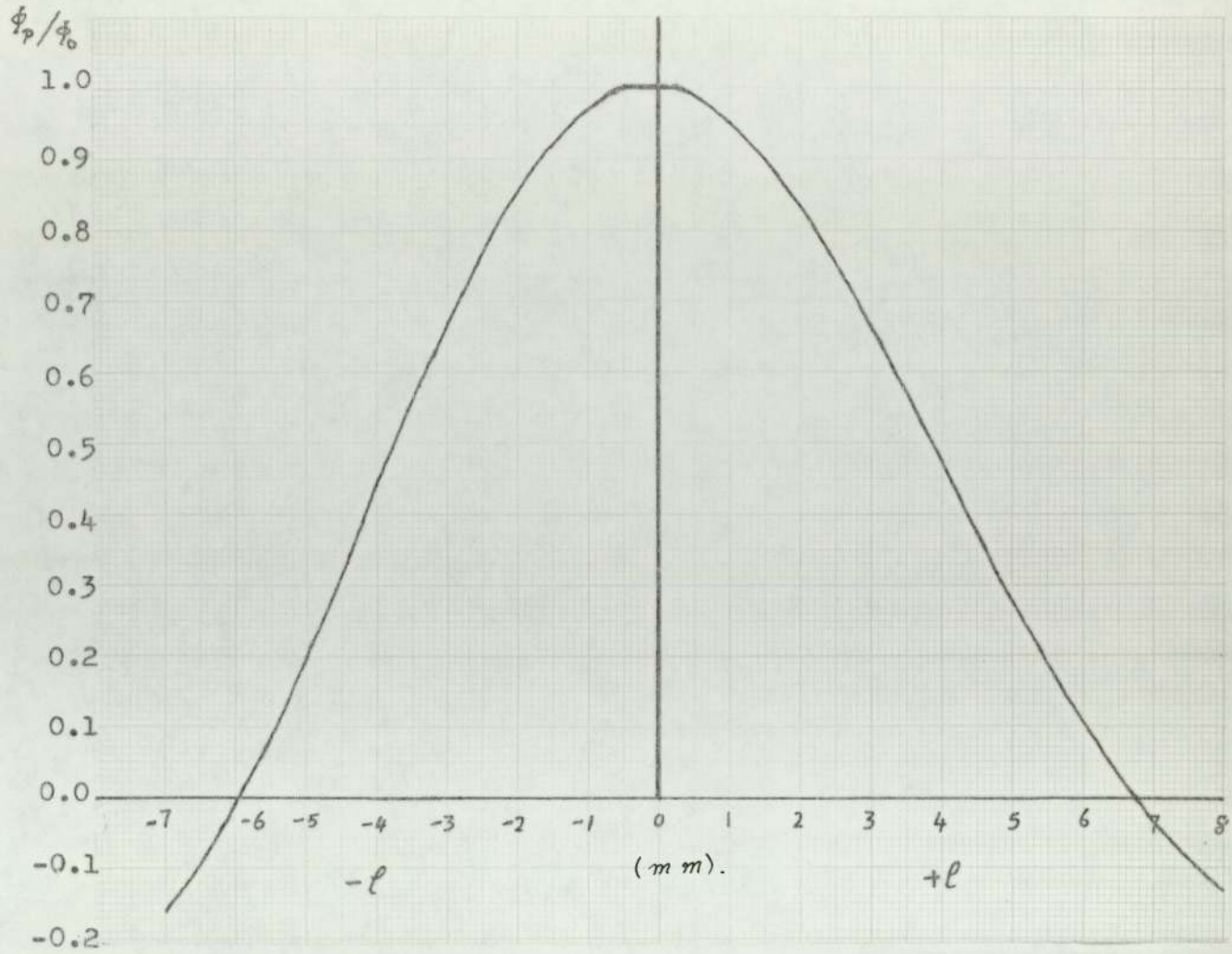

Fig. 2.25 Axial distribution around the centre of curvature of a concave bowl transducer (b/a = 1/4; λ =0.2 mm).

Table II.2 Normalised Axial potential distribution infront of and beyond the centre of curvature

Infront of the centre of curvature (-ℓ)		Beyond the centre of curvature (+ℓ)	
ℓ(mm)	ϕ_p/ϕ_o	ℓ(mm)	ϕ_p/ϕ_o
-1.00	0.96770	0.05	0.9994
-0.80	0.98100	0.10	0.9986
-0.60	0.99080	0.15	0.9976
-0.40	0.99720	0.20	0.9964
-0.20	1.00030	0.40	0.9895
-0.15	1.00053	0.60	0.9795
-0.13	1.00056	0.80	0.9665
-0.12*	1.00057	1.00	0.9505
-0.10	1.00056		
-0.05	1.00040		
0.00			

* The point of maximum axial intensity

are plotted against ℓ, as shown in Fig(2.25).
From this figure it can be seen that, there is a region of nearly constant intensity around the centre of curvature (about 1mm in length), of almost the maximum value.
The positions of the first axial nodes infront of, and beyond the centre of curvature, are $-\ell$=5.93mm, and ℓ=6.72mm, respectively.

The values of (ϕ_p/ϕ_o) in the region close to the centre of curvature, for the same bowl transducer, are given in Table (II.2). From this table it can be seen that:

1. The position of the maximum axial intensity is infront of the centre of curvature, at a distance ℓ=0.12mm.
2. The value of the maximum axial intensity is very close to that at the centre of curvature.
3. In practice, the axial distribution over about 2mm, may be considered very nearly constant. This conclusion led to the development of a new method for measuring the velocity of sound in solid materials, which will be discussed in Chapter IV.

It must be noted that the length of the focus does not affect the axial resolution of the bone tomography, which depends on the timing of the sharp onset of a pulse excitation, as will be discussed in part (B) of this chapter. On the other hand, this length provides a degree of tolerance in setting up the system.

PART (B)

PROVISIONAL CONCEPTS FOR THE OPERATION OF THE SYSTEM

2-B.1 General Possibilities

From the previous discussion, it would appear that ultrasonic radiation could be used for the purpose of bone tomography, if a bowl transducer for which the ratio of the aperture diameter to the radius of curvature is large enough so as to obtain a high lateral resolution.

Although the decrease in radius of curvature gives a high resolution and also, minimizes the effect of ultrasonic attenuation, it will be limited by the mechanical construction and the clearance required for the transducer to rotate around the limb. Therefore, the radius of curvature was chosen to be about 10cm.

A large aperture diameter of the transducer, beside giving a higher resolution, also enables a great proportion of the reflected ultrasonic waves to be collected when the transducer operates as a detector.
The largest ceramic bowl transducers available, are those for which the aperture diameter is about 5cm. Attempts have been carried out in order to construct a large capacitative bowl transducer, for which both the aperture diameter and radius of curvature are equal to 10cm, as will be explained later in Chapter III (Section 3.3.1). Unfortunately, we have some difficulties in applying a high polarizing voltage to it.

Therefore, it was decided to use the available ceramic bowl transducers, whose aperture diameter is 5cm and the radius of curvature is 10cm. The lateral resolution of these transducers seems to be satisfactory for our purpose, as shown earlier in part (A) of this chapter.
In order to preserve the lateral resolution, the transducer must execute a radial movement to maintain its focus at the bone surface.

In order to obtain a scan of the ulna cross-section profile, it is necessary for the transducer to move around the arm so as to look at a series of points on the surface of the ulna at the required level of cut. While the transducer is moving in its circular path, the echoes from the reflecting targets on the bone surface are received at delay times proportional to their distances from the centre of the transducer.

There are two systems by which the distances of the targets from the transducer can be determined:

(a) A timing mechanism; or

(b) a reference system.

A timing mechanism, such as a quartz crystal oscillator, needs a calibration from a known value of velocity of sound in the coupling medium (water). As the velocity of sound in water is temperature dependent, as shown in Fig.2.26 (Kossoff et al, 1964), any variation in the water temperature is equivalent to changing the time of the ultrasonic path. For instance, $10^{o}c$ change in temperature gives a change in velocity of about 35m/s. This is equivalent to about 2.4mm change in a path

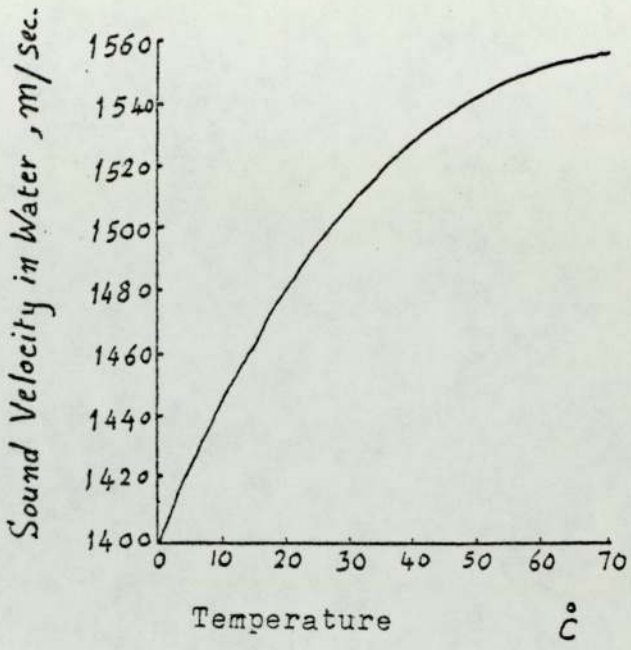

Fig. 2.26 Temperature dependence of velocity of sound in water.

length of 100mm.

The possibility of using a thermostatic control was considered, but it was realised that the requirement of inserting the hand from the bottom of the tank, necessitates that it must be filled with water each time, hence makes the control of temperature difficult.

The error due to variation of sound velocity, however, could be overcome by using a reference system in the same water bath. This system consists of a concave bowl transducer (exactly matching the scanning transducer) with a fixed reflecting rod, present at its focus. Both the scanning and reference transducers are pulsed simultaneously to operate as transmitters. The returning echoes from the bone surface and reference rod, are detected by the corresponding transducer at delay times proportional to their ultrasonic path lengths. As the distance between the reflecting rod and the reference transducer is always constant (equal to the radius of curvature) the echoes from the bone surface may arrive earlier or later than the reference echoes, depending on whether the distance

of the targets from the scanning transducer is shorter or longer than the radius of curvature.
This system gives a method for the comparison of the delay times of the echoes from the bone surface, and hence removes the errors in range introduced by the change in velocity of ultrasonics with water temperature.
Furthermore, with the case of shock excitation, the two echoes from bone and reference rod will have a similar shape, since they will have similar frequency spectra which makes it feasible to compare the reflection times.

If consideration is to be given for precise location of the bone surface in the radial direction, i.e. a maximum axial resolution, it will be seen that this depends on the accuracy of assessment of the time interval between the two echoes detected by the scanning and reference transducers.

2-B.2 The Display System

The movement of the scanning transducer as it goes around the limb follows the shape of the reflecting bone surface, at the level at which scanning is performed. The transducer could be made to draw its display as it goes, by one of the following systems:-

(i) a remote external plotter of a pen on a chart;

(ii) a cathode-ray tube; or

(iii) a direct mechanical coupling of the transducer to a pen on a drawing paper, attached to the frame of the apparatus.

The accuracy of the result depends on the type of the display used. For example, the remote display system involves r and θ, and the transmission of their values onto paper could give rise to errors in the plotting system. In the second display system, the magnification ratio on a cathode-ray tube is limited by the size of the screen. Also, a cathode-ray tube could give a distorted picture. For a permanent record, it is necessary to photograph the cathode-ray display, which is a further disadvantage of this system.

The direct mechanical coupling display system is, therefore, more desirable than the other systems for the following reasons:-

1. The backlash error in the angular plot is zero.
2. The backlash error in the radial co-ordinate would be less than in a system with remote display.
3. Any desired magnification ratio can be achieved, so that the error in taking measurements due to the thickness of the plotting pen will be minimized by increasing this ratio.
4. It gives directly a permanent record of the display on a drawing paper, without photography and its associated problems.
5. The drawing papers are much cheaper than photographic films.

Therefore, the scanning transducer is to be made to transfer its movement by a coupled screw drives to a pen writing on a paper attached to the frame of the apparatus. A suitable

magnification ratio of the plot can be obtained by using suitable gear boxes.

2-B.3 The Scanning System

The intention is now to use a scanning bowl transducer moving around the arm, and a fixed matching reference transducer with a reflecting rod present at its focus, in the same water bath.

In order to preserve the required lateral resolution of the scanning transducer, its focus must be always maintained at the bone surface. This means that, during its circular movement, the scanning transducer must execute in addition radial movement towards and away from the limb, correcting for the ultrasonic path difference. The information to do this can be obtained from the time interval between the two echoes detected by the scanning and reference transducers.

Therefore, provision must be made for movement of the scanning transducer in:

(i) a circular movement around the limb; and

(ii) a radial movement towards and away from the limb, so as to maintain its focus at the bone surface.

2-B.4 Information to Control the Radial Movement

It is intended to determine the path difference by the comparison of reflection times from the reference and scan-

ning transducers and their respective targets for a distinct event. It is necessary for the comparison of the two echo pulses that they are amplified to about the same value before applying to the discriminator.

Any system to be used in this manner requires the receiving amplifier dealing with the bone signal to have a variable gain to allow for change of the strength of the reflected signal. A voltage signal controlling the gain, could be derived from a continuous wave-train transmitted before the event.

In the original scheme, it was intended to obtain the event from the abrupt cessation of a continuous wave. For accurate assessment of the time intervals, the wave-trains should be sharply terminated, which requires that the decay time of the transducers must be as short as possible. Considerable work has been carried out with regard to the construction of backing and matching layers (Chapter III), but the cessation of the wave-trains could not be made abrupt enough to provide distinct events.

This difficulty may be overcome by using a shock excitation with a sharp onset, after the end of the transmitted pulses. The signals derived from the reflections of these shocks can give an accurate estimate of the time interval between the two echoes.

These signals are to be fed into a discriminator in order to determine which of the two pulses returns earlier. The information from the discriminator provides the input for a

servomechanism, which operates in such a way so as to maintain the focus of the scanning transducer on the bone surface, by radial movement. If the bone surface at any point on the circular scan, is at a distance from the vertex of the scanning transducer, greater than its radius of curvature, then the transducer will be moved towards the bone surface by the servomechanism, and vice versa. The detailed operation of the servomechanism and the electronic circuits of the apparatus, will be discussed in Chapter V.

2-B.4.1 The Axial Resolution

It has been observed experimentally that the rise time of the onset of the shock excitation echo, is about $\frac{1}{8}\mu$s. Since the velocity of sound in water is about 1500 m/s., this time corresponds approximately to

$$1500 \times 10^{3} \times \tfrac{1}{8} \times 10^{-6} \simeq 0.2\text{mm}.$$

This therefore, gives an estimate of the maximum error in determining the radial movement.

2-B.5 The Circular Movement

The circular movement can be achieved by mounting the scanning transducer vertically beneath a rotating drum, in such a way that its axis is directed towards the centre of rotation of the system. The limb is placed vertically opposite to the scanning transducer in such a way to allow for the rotation of the transducer around it. The limb must be held

normal to the axis of the transducer, in order to obtain an accurate tomographs.

The scanning plane, is the plane generated by the axis of symmetry of the transducer. This plane has to be adjusted in the required plane of cut, at which the cross-section profile of the ulna is to be determined.

A reasonable way for setting up the patient, which minimizes any physical movements of the limb during the scanning period without discomfort to the paient, will be discussed in Chapter VI (Section 6.4).

In order to arrive at a provisional estimate of the speed of the rotating drum, i.e. the speed of the circular movement of the scanning transducer, the following requirements must be taken into consideration.

1. The time required for each complete scan must be as short as possible, in order to minimize the errors due to any physical movement, and also to reduce the discomfort of the patient.
2. As the servomechanism requires a finite time to respond, a high rotational speed of the drum could result in an error in plotting the radial co-ordinate.
3. The speed must be as slow as possible in order to reduce the turbulence in the water bath, which in turn may disturb echoes.

2-B.5.1 The use of two separate 275° Scanning

In practice, the single complete rotation of 360° scanning of the ulna is impossible to achieve, since the radius bone

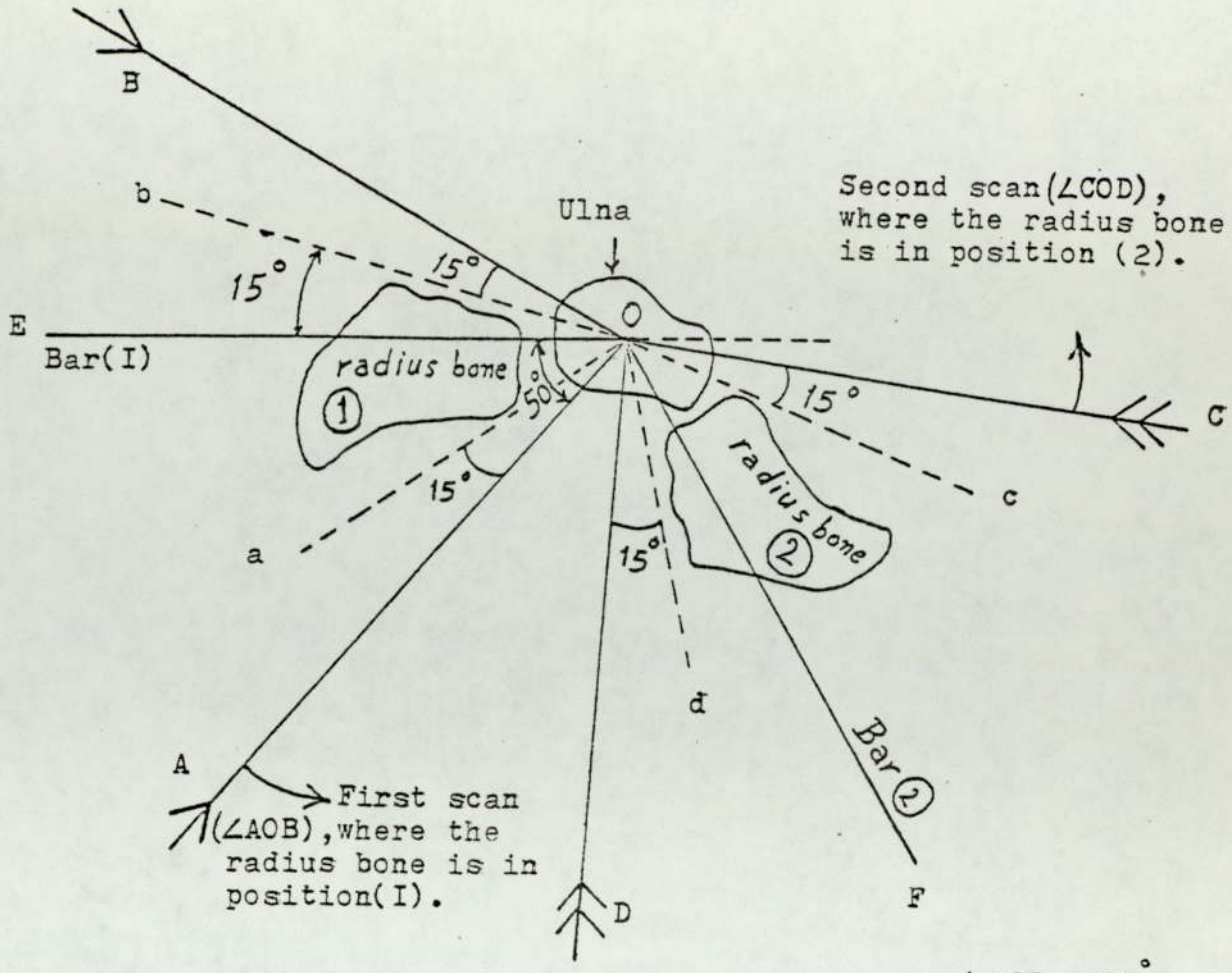

∠ AOB = 275°
∠ COD = 275°
∠ EOF = 120°
∠ EOA = 50°
∠ FOC = 50°

Fig. 2.27 Section of left forearm bones(seen from hand).
(I) Supinated
(2) Pronated

presents a complete obstacle to the ultrasonic waves at some parts of the ulna surface. According to the anatomy of the limb, the relative position of the radius bone with respect to the ulna can be changed by twisting the forearm by 90-120°, while the elbow remains fixed.

Figure(2.27) is a life-size section of the left forearm bones, seen from the hand, when the arm is supinated (position 1), and when it is pronated through 120° (position 2).
In the first position, the surface of the ulna shadowed by the

radius bone is that portion represented by the angle aOb, which is about 50-55°. When the arm is pronated through 120° (position 2), the portion of the ulna surface covered by the radius bone, is that represented by the angle cOd, which is also about 50°.

Therefore, it could be possible to use two separate scans (each about 275°), one for each position of the arm. In the first scan, the patient's arm is held stationary in the supinated position, and the scan is carried out through the angle AOB≈275°. For the second scan, the patient's hand is turned by 90-120° (while the elbow remains in the same position) and then the scan is carried out through the angle COD≈275°. The missed portion of the ulna in the first scan (which is represented by the angle AOB≈85°), is now shown in the second scan.

Having the two scans, it could be possible to superimpose the plotted outlines by fitting the repeated portions on each other, in order to obtain the complete cross-section profile.

CHAPTER III

EXPERIMENTAL WORK ON DAMPING OF TRANSDUCERS

3.1 Introduction

In the old scheme, it was intended to obtain the distinct events from the abrupt cessation of the long duration pulse echoes. The work described in this chapter was, therefore, aimed at achieving a maximum damping of the transducers. This implies little reflection at both front and back surface of the transducer. This may be achieved by:

1. Using a highly absorbent backing material with an acoustic impedance similar to that of the ceramic, placed in contact with the rear surface of the transducer in order to absorb all the energy incident on this surface; and
2. Using transition or matching layers, attached to the front surface of the transducer, which acts as an acoustic transformer. These matching layers allow for a maximum power transfer into the loading medium (water).

Since, the construction of the matching layers depends on the ultrasonic frequency (i.e. each layer must be a quarter wavelength thick or multiple thereof), and because the distinct events are now obtained from the sharp onset of pulse excitation, the matching layers mentioned later (section 3.3) have been abandoned.

3.2 BACKING LAYER

The main purpose of the backing layer is to let the energy incident at the rear surface of the transducer pass into it and be

absorbed. This requires:

(a) the material cemented at the back of the transducer should offer an acoustic impedance similar or comparable to that of ceramic; and,

(b) its attenuation co-efficient must be as high as possible.

One of the early attempts (Goldman, 1962) to achieve these requirements, was that in which the transducer is backed up with multiple alternate layers (each a wavelength thick or multiple thereof) of fibreglass and tungsten filled rubber. However, in employing multiple backing layers of any kind, it is often difficult to achieve a good impedance match with high absorption. Also, it is difficult to cement a large number of layers on the convex back surface of the transducer, using very thin layers of cement, without serious gaps between the layers themselves and/or between them and the transducer. Furthermore, reflections will occur at the interfaces due to the acoustic mismatching of the cement layers.

It has been found (Marklein; G.E.C.; U.S.A.) that some non-piezoelectric ceramic materials (fine grained fused alumina) have a density (ρ) and sonic velocity (c) which vary considerably with firing temperature, as shown in Fig(3.1). In addition their attenuation can be controlled with firing temperature or by the addition of some substances which increase the porosity. Therefore, a ceramic piezoelectric transducer may be backed up by a single alumina block (which is fired in a graded temperature furnace), whose characteristics are graded

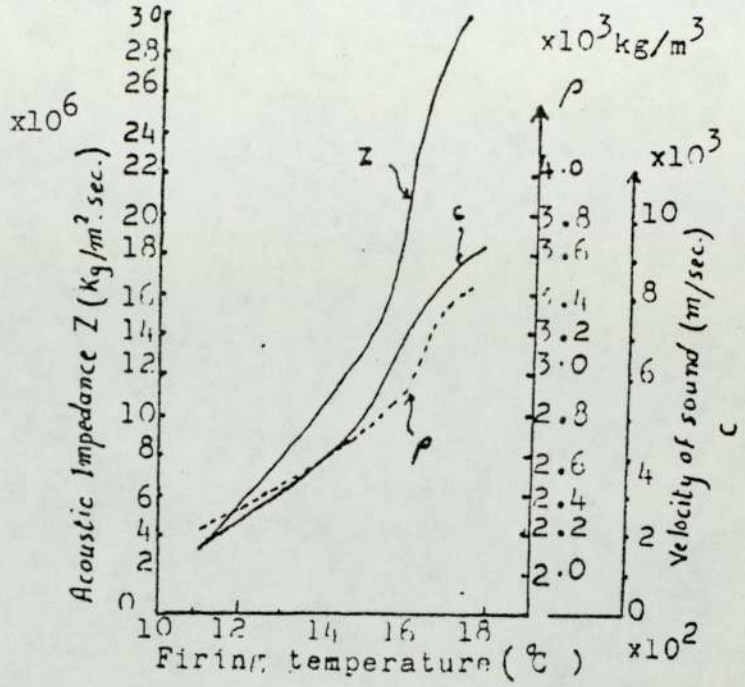

Fig. 3.1 Velocity of sound, density, and impedance of a pure fine-grained fused alumina versus firing temperature.

continuously from a region of controlled impedance ρc (fired at 1620°C) at the transducer surface, to a region of controlled attenuation (fired at 1100°C) at the rear surface of the backing block.

The advantage of this method is that there is only one cement joint between the transducer and its backing. Unfortunately, not much information about the composition and technical procedures is published.

3.2.1 Experimental Observation

Attenuation of Ultrasonic Radiation in Lead

It is known from tables that lead has an acoustic impedance (27.4×10^6 Kg/m^2.s) almost equal to that of the ceramic transducer, PZT-5A (28.4×10^6 Kg/m^2.s). Also, it has been found, experimentally, that when a lead sheet, about 2mm thick is applied to the face of a 7.7 MHz ultrasonic transducer, the transmitted ultrasonics have been observed to have suffered considerable attenuation, which was found to be about 14 nepers/cm.

Some other experiments have been carried out in order to determine the degree of attenuation of ultrasonics in lead more exactly, for the purpose of using it as a backing layer. Two ceramic transducer discs, whose fundamental resonant frequencies are 1 MHz were used, one as a transmitter and the other as a receiver. The transmitting transducer was cemented (using a very thin layer of perspex cement) to one end of a lead rod (1.6 cm in diameter and 6.5 cm long). This transducer was driven at its 7th harmonics, using a 7 MHz oscillator. The receiving transducer is coupled (using a very thin layer of a coupling oil) to the far surface of the rod. Each transducer was connected to a preamplifier and then to one channel of an oscilloscope.

It was found impossible to detect any of the driving frequency ultrasonic waves at the receiving transducer. When the rod was shortened, by cutting it into halves, i.e. 3.2, 1.6, and 0.8cm, the same result was obtained even with the shortest speciment (0.8cm).

When however, the experiment was repeated using a perspex rod instead of lead, it was possible to detect the waves reaching the receiving transducer. The amplitude of these waves, was found to increase as the perspex length decreases, which showed that the system was working.
When measurements were carried out using aluminium rods, waves reaching the receiving transducer were detected with very little attenuation.

From these experiments, it was therefore, concluded that ultrasonic radiation is attenuated by at least 10^3 times by

a path length of lead, about 0.8 cm. This led to the concept of the possibility of using lead as a backing layer for ceramic bowl transducers.

3.2.2 Lead as a backing layer

From the above experiments it is evident that lead imposes a high absorption on ultrasonic radiation and that a one-centimetre thickness of lead is sufficient to absorb all the incident ultrasonic waves.

For this purpose, two similar plano-concave blocks of lead have been constructed, having a diameter equal to that of the transducers, i.e. 4.8 cm., and a thickness of 1 cm at the edges. They have been machined so that their concave surfaces have exactly the same curvature of the convex surfaces of the transducers. The concave surfaces of lead were rubbed down with the convex surfaces of the transducers, and then checked by using a blue engineering marker in order to achieve a good contact over the whole area without any gap between them. These backing layers were then cemented to the back surface of the transducers by using a very thin layer of araldite.

Two matching layers, quarter-wavelength thick of aluminium and perspex, were cemented on the front of each transducer (this will be explained in a later section in this chapter). Finally the transducers were assembled in their cases and sealed off to prevent any water leak to the inside.

These transducers were tested, separately, in a water bath in which a glass plate is placed vertically at the focus. The transducers were driven at their 7th harmonics in order to produce 7.7 MHz ultrasonic pulses (120us) by using an

oscillator and a pulse time generator whose repetition frequency is $\frac{1}{500}$ sec. The transducer is also connected to a preamplifier and to an oscilloscope in order to detect the returning echoes reflected on the glass plate.

Unfortunately, we could not detect any reflected echoes, even when the transducers were driven at their 5th and 3rd harmonics, and also at their principal resonant frequency (1.1MHz).

This negative information was attributed to the possibility of production of shear waves in lead, or the transducers may be depolarized due to their heating to 48°C during the process of cementing. Because of the last probability, i.e. the depolarization of the transducers, and also because it was difficult to detach the lead backing layers from the transducers without damage to the latter, we therefore ordered further new transducers from Vernetron. This time they offered us the possibility of manufacturing new transducers with a principal resonant frequency of 2.285 MHz instead of the 1.1 MHz of the original ones. The diameter of each transducer is 4.9 cm and the radius of curvature is 10 cm. It was decided to order these new ceramic bowl transducers, as they can be driven more easily at their 3rd harmonics in order to produce 6.85 MHz ultrasonic radiation.

3.2.3 The Effects of Backing on the Performance of Ceramic Transducers

The effects of backing on the performance of a transmitting and receiving ceramic transducer, radiating into water,

have been analysed by Kossoff (1966). For a backed transducer with no matching to load, the effects of backing are shown in figures 3.2, 3.3 and 3.4.

The voltage transfer functions for a backed transmitting and receiving transducer, versus the fractional frequency deviation f/f_o, are shown in Figs. 3.2 and 3.3, respectively, where f_o is the resonant frequency. In these figures the zero dB reference level applies to an output $F=V_i$ and $V_o=2F$, where V_i is the input applied voltage, F is the force exerted by the transducer face, and V_o is the output voltage of the receiving transducer. Fig. 3.4 is a plot of the decay time (μs) versus the fractional frequency deviation f/f_o.

From Figs. 3.2 & 3.3, it can be seen that the air-backed transducer has the maximum output, but the smallest bandwidth. The narrow bandwidth of an air-backed transducer limits its sensitivity in pulse detection applications. From Fig. 3.4, it can be seen that the decay time of an air-backed transducer at resonance is quite large (5μs) which gives a considerable ringing after the main echo.

Low impedance absorbing backings, such as araldite ($z=3\times10^6$ Kg/m^{2}s), widen the bandwidth, giving a symmetrical response and also give a decay time of the order of 2μsec.

Higher impedance absorbing backings, such as tungsten in araldite (10×10^6Kg/m^{2}s) give a lower output, but a wider bandwidth. A transducer backed with such an impedance has a better response and a shorter decay time of the order of 0.5μs.

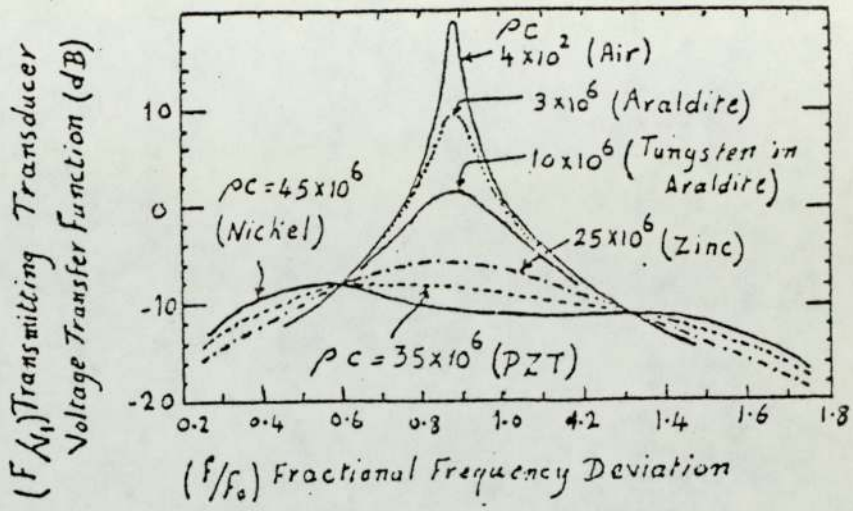

Fig.3.2. Backed transmitting transducer voltage transfer function.

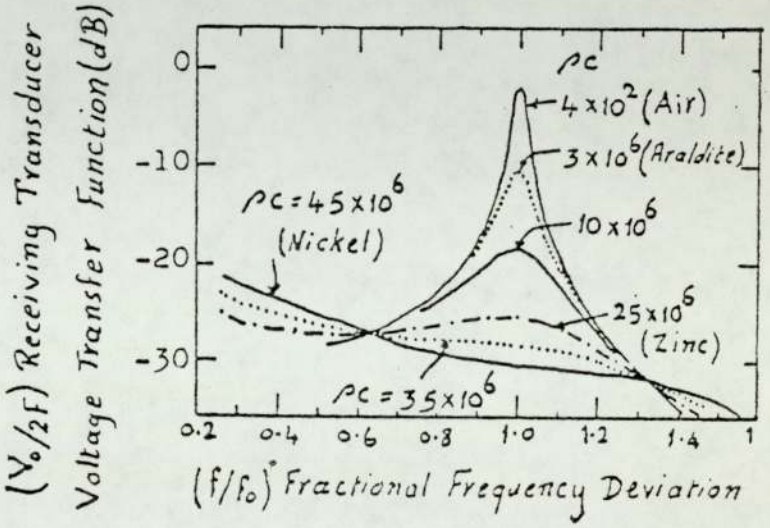

Fig. 3.3 Backed receiving transducer voltage transfer function.

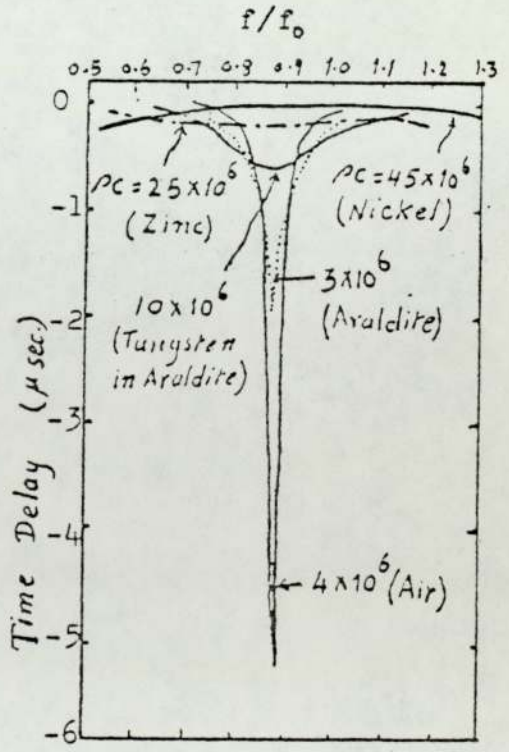

Fig. 3.4 Time delay of transmitting transducer.

By a further increase in the acoustic impedance of the backing material ($25x10^6 Kg/m^2s$ or more) it can be seen (Fig. 3.2 - 3.4) that although the decay time is considerably decreased and hence achieving a high damping, on the other hand, the output is considerably decreased, and the voltage transfer function loses its symmetry. Hence the maximum response is shifted to a lower frequency. This means that the increase in the acoustic impedance of the absorbing backing material, to a high value, close to or more than that of the transducer; would considerably increase the damping, but this will be at the expense of the sensitivity of the transducer. This conclusion with regard to high acoustic impedance materials could explain the failure to obtain a signal from ceramic bowl transducers back with lead.

Therefore, for a reasonable damping without loss of the response of the ceramic transducer, the backing layer should have a moderate acoustic impedance, i.e. 10 to $16x10^6 Kg/m^2 s$, and it must have a high absorption coefficient. These conditions can be achieved by using a mixture of tungsten in rubber, or tungsten in araldite (Kossoff 1966 & Fry et al 1968). Tungsten-araldite mixture has been fabricated (Kossoff) by mixing fine tungsten powder (0.5 microns or less) with epoxy resins and centrifuging the mixture to give a high packing ratio. The characteristic impedance of mixtures made from 100-200 gms of tungsten powder in 40 cc of araldite (100 parts of casting Resin D and 50 parts of Polyamid 75, Ciba) and spun at 3000 r.p.m. varies from 6 to $16x10^6 Kg/m^2s$.

3.2.4 Tungsten-Rubber Mixture Backing Layer

Rubber has a higher attenuation coefficient for ultrasonic radiation than araldite. The use of rubber with as much as possible tungsten powder, milled into it, gives a mixture of high acoustic impedance, which provides a higher attenuation for ultrasonics than tungsten-araldite mixtures. The time of polymerisation of rubber is longer than that of araldite. Such a long time gives a chance of good and homogeneous mixing, and also allows the mixture to be cast easily and accurately to the required shape.

For these reasons, it has been found reasonable to use tungsten-rubber mixture for the purpose of backing layers for our ceramic bowl transducers. The mixture has been fabricated by mixing fine tungsten powder with silicone rubber (ρ=1.065gm/cc), and stirring the mixture to give a high packing ratio. It has been found that the appropriate ratio by weight is between 7 parts to 10 parts of tungsten, and one part of rubber. The resulting solid mixture has a density between 5.8 to 6.9 gm/cc.

The manufacturing procedure for the solid mixture backing layers of the ceramic bowl transducers was as follows.

Tungsten powder (216 gm) was added gradually to the required amount of silicone rubber (21.5 gm).
The mixture was stirred by using a slow speed rotating stainless steel rod. During the process of stirring, some drops of petroleum ether were added in order to decrease the viscosity of the mixture. This makes the process of mixing easier and

the mixture more homogeneous. The mixture is then cast into a mould, by putting it in a perspex cylinder, 7 mm high, and 4.8 cm inside diameter. The transducer is placed on the top of the soft mixture, with its convex surface downwards. The mixture is subjected to a small static pressure (4-5 Kgm weights), by using a soft plano-convex pad on the concave surface of the transducer, in order to avoid any possible damage to the latter. At least 24 hours were allowed for solidification to occur with the pressure applied, in order to avoid cavities during the shrinking process, and also to make the surface of the solid mixture retain the same curvature as that of the back surface of the transducer. The resultant solid backing layer, is then cemented to the back of the transducer, using a very thin layer of permabond liquid which gives a good adhesion.

The transducers backed with this mixture were checked in a water bath by means of the pulse reflection method, when a high damped echo with a considerable amplitude has been detected.

3.3 MATCHING LAYERS

The problem of disparity of the specific acoustic impedances of ceramic and water, may be dealt with by the use of transition (matching) layer which behave as an acoustic transformer. Such transformer takes the form of one or more transition layers, attached to the front face of the transducer. The composition and thickness of these layers must be precisely controlled to achieve maximum power transfer, into and from the loading medium, and thus giving maximum damping and also maximum sensitivity.

The matching layer, or layers, offering maximum transmission of ultrasonic waves, must have the following characteristics:

1. The attenuation co-efficient must be as small as possible
2. The thickness (ℓ) of each layer must be a quarter-wavelength or multiple thereof, i.e. $\ell = m\lambda/4$, where m is an odd number. In practice, however, it is preferable to use a quarter-wavelength thickness rather than its multiple, since the latter contributes more attenuation as the thickness increases.
3. The input impedance (Z_{iY}) for any number (Y) of layers, must be equal to the specific acoustic impedance of transducer (Z_t), by suitable choice of the acoustic impedances of the materials forming the layers. This relation may be given by:

   (i) If Y is an even number, i.e. Y=2n, where n is an integer, then

$$Z_{iY} = Z_w \left(\frac{Z_2 Z_4 \ldots Z_{2n}}{Z_1 Z_3 \ldots Z_{2n-1}}\right)^2 = Z_t \qquad \ldots\ldots\ldots (3.1)$$

   (ii) If Y is an odd number, i.e. Y=2n+1, where n=0,1,3, etc., then

$$Z_{iY} = \frac{1}{Z_w} \left(\frac{Z_1 Z_3 \ldots Z_{2n+1}}{Z_2 Z_4 \ldots Z_{2n}}\right)^2 = Z_t \qquad \ldots\ldots\ldots (3.2)$$

where, Z_w is the specific acoustic impedance for water.

From Eq.(3.2) the relation for a single matching layer, where Y=1, and n=0, is given by

$$\frac{Z_1^2}{Z_w} = Z_t, \text{ or } Z_1 = \sqrt{Z_t\ Z_w} \qquad \ldots\ldots (3.3)$$

The derivation of the above equations, are given in appendix (c).

For any given application, the increase in transmission obtained by the matching layers must be carefully balanced against the increase in absorption caused by each additional layer of material. Therefore, it is preferable to use the least possible number of matching layers, with low absorption co-efficients.

3.3.1 Construction of a Capacitative Transducer with no matching layers

The requirement we require is to use the least possible number of matching layers. This led us to think of using a transducer with no matching layer i.e. a capacitative transducer. The construction of this capacitative bowl transducer consists of a brass bowl of constant thickness (about 7 mm), whose radius of curvature is 10 cm, and its aperture diameter is also 10 cm. A quarter wavelength thick (0·07 mm) polythene layer, is to be kept over and in contact with the concave surface of the brass bowl, by applying a vacuum through a very tiny hole at the centre of the latter. On the outside surface of the polythene layer, a very thin layer of evaporated gold is deposited, which is then electroplated with a very thin layer of silver, so as to be a good electrical conductor. The main purpose of constructing this capacitative concave

transducer is that it does not need any matching layer since the specific acoustic impedance of polythene (ρc = 1,75 x 10^6 $Kg/m^2.sec.$) is nearly equal to that of water (ρc=1,5 x $10^6 Kg/m^2 s$) Furthermore, it would give a high lateral resolution, and also avoids the difficulty of making a damping layer,

Unfortunately, we have found some difficulties in applying a high polarising voltage to this transducer, Therefore it has been found reasonable to use ceramic bowl transducers instead of the capacitative transducer, with the least possible number of matching layers,

3.3.2 One Matching Layer

As described before, the optimum matching using a quarter-wavelength matching layer can be obtained if the characteristic impedance of the material forming the layer (Z_1) is equal to the geometric mean of the impedances of the transducer (Z_t) and the loading medium (Z_w), as given by Equation (3.3). Therefore, with a ceramic transducer (Z_t= 28.4 x $10^6 Kg/m^2 sec$) radiating into water (Z_w= 1,5 x $10^6 Kg/m^2$. sec), the acoustic impedance of the material of the matching layer, Z_1 must be equal to

$$Z_1 = \sqrt{28.4 \times 1.5 \times 10^{12}} = 6.53 \times 10^6 kg/m^2 s.$$

A matching layer with an acoustic impedance of this order (5.5 x $10^6 Kg/m^2 s$) has been fabricated by Kossoff (1966) by mixing 1.5 parts by weight of fine aluminium powder with one part of araldite. However, as we noted before in the backing material, that the use of powdered metals adds a very high attenuation. As we require a maximum power transfer and hence a minimum absorption coefficient of the matching layer, it has been found that aluminium-araldite mixture

is not suitable for this purpose. Therefore, we found that it may be more reasonable to determine other suitable materials for the construction of two matching layers, instead of only one.

3.3.3 Two matching layers

As described before, equation 3.1 , that for optimum matching between the transducer (Z_t) and the loading medium (Z_w), using two $\lambda/4$ matching layers, the specific acoustic impedances Z_1 and Z_2 of the materials forming the layers must be carefully chosen so that

$$Z_t = Z_w \left(\frac{Z_2}{Z_1}\right)^2$$

or

$$\frac{Z_2}{Z_1} = \sqrt{\frac{Z_t}{Z_w}} \qquad (3.4)$$

From the tables, it has been found that there are two metals of intermediate acoustic impedances between ceramic and water, namely aluminium (Z_{Al}= 17,3) and magnesium (Z_{Mg}=10). These metals can be machined to the required thickness and shape. Therefore , it has been thought to use either aluminium or magnesium for the construction of one of the two matching layers, for our ceramic bowl transducers. This metallic layer,

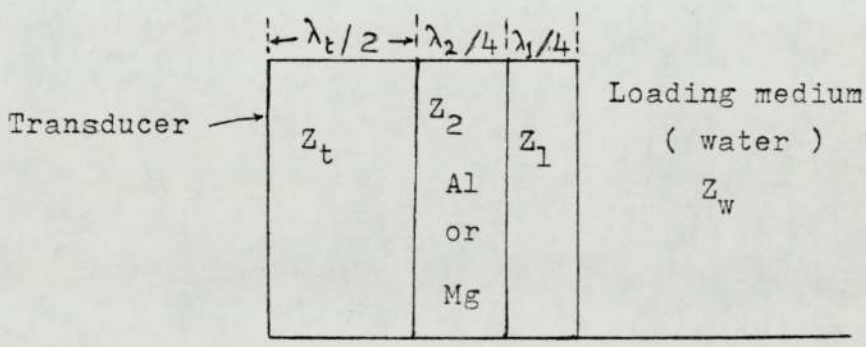

Fig. 3.5 Two matching layers.

will be that one which is in contact with the transducer. A considerable number of experimental trials have been carried out to determine the other material to be used with aluminium or magnesium, so that their specific acoustic impedances fulfil the above equation (3. 4).

3.3.3.1 Determination of the other material to be used with aluminium

From equation (3.4) the specific acoustic impedance (Z_1) of the other material to be used with aluminium for the construction of two matching layers, in order to obtain an optimum matching, is given as follows :

$$Z_1 = Z_{Al}\sqrt{Z_{w/Z_t}} = 17.3 \times 10^6\sqrt{\frac{1.5\times10^6}{28.4\times10^6}} = 3.98\times10^6 Kg/m^2s.$$

Polytetrafluoroethylene PTFE was thought to be useful for this purpose since its characteristic acoustic impedance is about $3.6\text{-}3.8 \times 10^6 Kg/m^2s$. However, it has been found difficult to cement the PTFE permanently to aluminium by using any kind of the usual bonding materials.

Some experiments have been carried out to polymerise some plastic materials, in order to determine a suitable material which has the required acoustic impedance (3.98×10^6 Kg/m^2s).

Experiment (1) : Polymerization process

The polymerization process of the liquid polymer was carried out as follows:

A suitable amount of the liquid polymer (about 5cc) and 1-2% by weight (about 70-100 mg) of benzoyl peroxide, as a catalyst, are mixed together in a test tube. The test tube

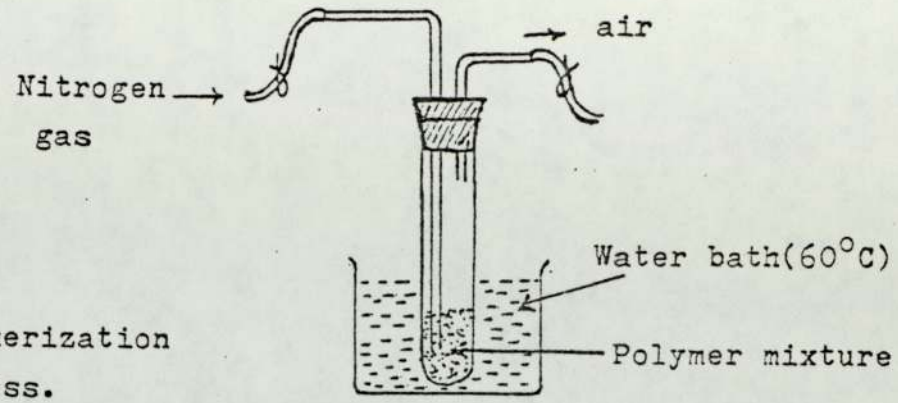

Fig. 3.6 Polymerization process.

is covered with a rubber stopper through which there are two bent glass tubes with rubber tubes at the other ends, as shown in Fig. 3.6. A little suction is applied for a short period and a small stream of nitrogen gas is passed through for a short period in order to get rid of any oxygen present in the tube. The rubber tubes are closed tightly, using strong clips to prevent any air leaking into the tube. The mixture is then polymerized in the absence of oxygen by putting the tube in a water bath at 60°C and left at this temperature for 16-24 hours, until the mixture becomes very viscous or solid. The density of the resultant lump of the polymerized material is determined by Archimedes method.

Experiment (2) Measurement of the velocity of sound in the polymer

The velocity of sound in the resulting polymerized material was determined by making a thin tapered wedge. A small piece of the polymerized material was dissolved in chloroform ($CHCl_3$) to form a thick solution. The solution was put on a slightly tilted flat glass surface and then left to dry. The resulting wedge was placed at the common focus of two opposite ceramic bowl transducers. One transducer was used as a transmitter and the other used as a receiver for the transmitted

ultrasonic waves through the wedge. The wedge was moved slowly and carefully across the beam in a direction perpendicular to the central axes of the transducers.

Maximum transmission of the ultrasonics through wedge will occur when the focal spot falls on those points of the wedge whose thicknesses are $n\frac{\lambda}{2}$, where "n" is an integer i.e. 1 , 2, 3, 4, 5, ... etc. Minimum transmission occurs at those points whose thicknesses are $m\frac{\lambda}{4}$; where, "m" is an odd number i.e. 1, 3, 5, .. etc.

By measuring the thickness of the wedge at these points it is possible to determine the wavelength λ of the ultrasonic beam (f=5.4MHz or 7.6MHz) in the wedge material. Determine the mean value of λ from which the velocity of sound "c" in the wedge material can be calculated where $c=\lambda f$. The detailed description of this method will be explained in the next chapter (Chapter IV).

Experimental results for different polymers

(i) Bromostyrene 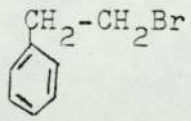

The bromostyrene liquid has been polymerized by the method in experiment (1). The density of the resulting polymer was measured by the Archimedes method and found to be 1.583 gm/cm^3 or $1.583 \times 10^3 Kg/m^3$. A thin tapered wedge of the polymer was prepared and the mean value of the wavelength λ (for 7.6MHz) in the wedge material was determined as explained in experiment (2).

The wavelength λ was found to be 0.04 cm. Therefore, the velocity of sound c in bromostyrene is given by

$$c = \lambda f = 0.04 \times 7.6 \times 10^6 \text{ cm/sec}$$

$$= 3040 \text{ m/sec.}$$

The acoustic impedance of bromostyrene is given by

$$Z = \rho c = 1.583 \times 10^3 \times 3040 = 4.74 \times 10^6 \text{Kg/m}^2\text{s}$$

(ii) A mixture of bromostyrene and perspex

Since the specific acoustic impedance of bromostyrene was found to be greater than the required value (3.98×10^6) it has been thought to use a mixture of bromostyrene and perspex ($\rho c = 3.2 \times 10^6 \text{Kg/m}^2\text{s}$) in the ratio 3:5 by weight, which may give the required value of acoustic impedance. Two pieces of bromostyrene polymer and perspex were dissolved, separately, in chloroform so that they have the ratio 3:5 by weight. The two solutions were mixed together. A wedge of the resulting mixture was prepared, as explained in experiment (2).

It has been found that the resulting wedge was not homogeneous, having some bubbles. Therefore, this mixture was found unsuitable for our purpose.

(iii) Chloroethyl methacrylate

The chloroethyl methacrylate liquid was polymerized by the method explained in experiment (1). The density of the resulting polymer is found to be 1.33 gm/cm^3.

It has been found that the resulting polymer does not dissolve in chloroform, or any other usual organic solvent,but forms an emulsion. For this reason, a suitable amount of chloroethyl methacrylate liquid was polymerized in a wedge-like form. The mixture of chloroethyl methacrylate liquid and 1-2% benzoyl peroxide (as a catalyst), was put into a

flat groove in a PTFE slab, through which two tiny holes were provided for the suction process and to pass the nitrogen gas. The mixture was covered with a glass plate and clamped strongly to the PTFE slab. A silicone rubber has been applied to the glass plate edges, in order to prevent any air, or water leak to the mixture. The PTFE slab (with the mixture in its groove) is placed into a water bath ($60^{o}C$) in such a way that it is tilted at the required angle to make the wedge.

After the polymerization process (16-24 hours), a thin tapered wedge of chloroethyl methacrylate has been obtained. The wavelength of the ultrasonic beam (5.4 MHz) in the wedge material, has been determined, as explained in experiment (2) and found to be 0.034 cm. The velocity of sound c in chloro-ethyle methacrylate is given by:

$$c = \lambda f = 0.034 \times 5.4 \times 10^{6} = 1836 \text{ m/s}$$

Therefore the acoustic impedance $\rho c = 1.33 \times 10^{3} \times 1836 = 2.45 \times 10^{6} Kg/m^{2}.s.$

It is obvious that this value is much less than that required, $3.98 \times 10^{6} Kg/m^{2}.s.$

(iv) Chlorostyrene 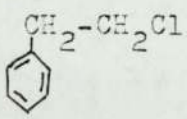

The chlorostyrene liquid was polymerized in the same way as explained in experiment (1). The density of the resulting polymer was measured and found to be 1.242 gm/cm^{3}. A small piece of the resulting polymer was dissolved in chloro-form, in order to prepare a thin tapered wedge. The wavelength λ of the ultrasonic beam (5.4 MHz) in the wedge material has been determined, as explained in experiment (2) and found to be 0.051 cm. The velocity of sound $c = \lambda f = 0.051 \times 5.4 \times 10^{6} = 2750$ m/s.

Therefore, the acoustic impedance of chlorostyrene is given by:

$$\rho c = 1.24 \times 10^3 \times 2750 = 3.42 \times 10^6 Kg/m^2 s$$

This figure is smaller than the required value of specific acoustic impedance.

It has been, therefore, thought that it might be reasonable to polymerize a mixture of bromostyrene and chlorostyrene liquids, using a proper ratio which could give the required value of acoustic impedance.

(v) Polymerization of a mixture of Bromostyrene and Chlorostyrene

A mixture of bromostyrene and chlorostyrene liquids, in the ratio 2:5 by weight, was polymerized in the same way as explained in experiment (1), using 1% by weight of benzoyl peroxide as a catalyst.

The density of the resulting polymer mixture was measured and found to be 1.32 gm/cm^3.

A small piece of the resulting polymerized mixture was dissolved in chloroform in order to make a thin tapered wedge. The wavelength in the wedge material, using a 5.4 MHz ultrasonic beam, has been determined (as explained in experiment 2) and found to be $\lambda = 0.0537$ cm. The velocity of sound in the mixture $c = \lambda f = 0.0537 \times 5.4 \times 10^6 = 2900$ m/s. Therefore, the acoustic impedance of the mixture is given by:

$$\rho c = 1.32 \times 10^3 \times 2900 = 3.85 \times 10^6 Kg/m^2 s.$$

Although this mixture has an acoustic impedance which is nearly equal to the required value ($3.98 \times 10^6 Kg/m^2 s$), it has been found to be brittle and therefore not suitable for the construction of $\lambda/_4$ thick matching layers.

(vi) Polymerization of a mixture of Bromostyrene, Chlorostyrene and 2-Ethoxy ethylemethacrylate (as a softener)

It has been found that a mixture of bromostyrene and chlorostyrene polymers, can be made more flexible by adding 5-10% by weight of a softener, such as lauryl methacrylate, cetostearyl methacrylate, n-butyl methacrylate, or 2-ethoxy ethylmethacrylate. These softeners reduce the rigidity of the resultant polymerized material, as shown in Fig. 3.7 . Many experiments have been carried out in order to find out a suitable construction of the mixture which gives rise to a reasonable flexible material, with an acoustic impedance as close as possible to the required value. The best mixture achieved was that which consists of 30.2% by weight bromostyrene, 63.5% chlorostyrene, 5.3% 2-ethoxy ethyl methacrylate (as a softener) and 1% benzoyl peroxide (as a catalyst). The mixture has been polarized in the same way as explained in experiment (1). The density of the resulting polymerized material, was measured and found to be 1.318 gm/cm^3.

A small piece of the resulting polymerized material was dissolved in chloroform in order to make a thin tapered wedge. The wavelength in the wedge material, using 5.40 MHz ultrasonic beam, was found to be 0.0534 cm.

The velocity of sound in the material is given by:

$c=\lambda f = 0.0534 \times 5.4 \times 10^6 = 2880$ m/s.

The acoustic impedance of the material is given by

$$\rho c = 1.318 \times 10^3 \times 2880 = 3.80 \times 10^6 \text{Kg/m}^2\text{s}.$$

This material, however, was brittle and developed cracks spontaneously.

The experimental results of the density (ρ), velocity of sound (c), and the corresponding values of acoustic impedances (ρc) for the above mentioned polymers, are summarised in Table III.1.

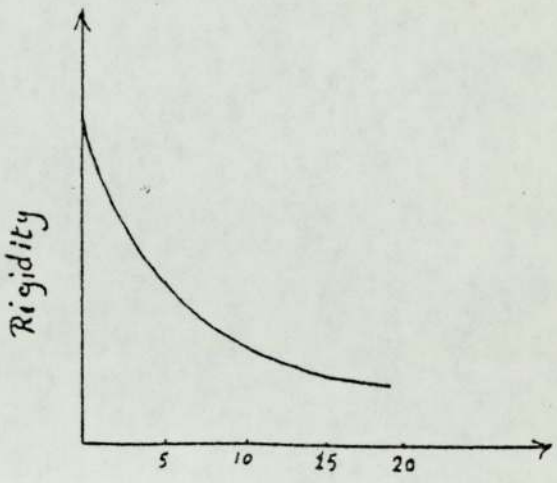

fig. 3.7 Variation of the rigidity of the polymer with the addition of a softener.

Table III.1. The density(ρ), velocity of sound(c),&acoustic impedance(ρc) for different polymers.

Polymer	Molecular weight	ρ gm/cm^3	c m/sec.	ρc kg/m^2.s.
1- Polystyrene 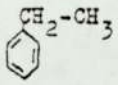	106	1.055	2350	2.48
2- Chloroethyl methacrylate		1.33	1836	2.45
3- Bromostyrene 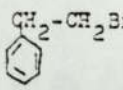	185	1.58	3040	4.74
4- Chlorostyrene 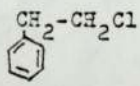	140	1.24	2750	3.42
5- A polymerized mixture of chlorostyrene and bromostyrene (5 : 2 parts by weight)		1.32	2900	3.85
6- A polymerized mixture of chlorostyrene, bromostyrene, & 2-ethoxy ethyl methacrylate(63.5%,30.2%, 5.3%)		1.318	2880	3.8
7- Perspex		1.19	2736	3.25

Use of perspex as a second matching layer with aluminium

A trial has been carried out to use perspex with aluminium for the construction of two matching layers for the ceramic bowl transducers. Although perspex has an acoustic impedance ($3.25 \times 10^6 Kg/m^2.s.$), whose value is less than that required ($3.98 \times 10^6 Kg/m^2s$), it is found possible to cut quarter wavelength thick (0.09mm) sheets which are more flexible than the previous polymers. A perspex layer was cemented on the outer surface of each aluminium layer, where the latter was cemented on the concave surface of each bowl transducer. However, after using the transducers in a water bath, the perspex layers parted spontaneously.

It has been found necessary therefore to use magnesium instead of aluminium and to determine the other suitable material which can be used with it in order to make two matching layers.

3.3.3.2 Determination of the other material to be used with Magnesium

Magnesium was found to be more easily machinable to the required thickness and shape than aluminium. Magnesium was obtained from the market in the form of sheets (18 thou. i.e. 0.45 mm thick) containing 2% by weight of manganese (Mn) and 1% zinc (Zn). The density of magnesium is 1.7-1.74 gm/cm^3, the velocity of sound in it is 5700-5750 m/s, and its acoustic impedance ρc is $9.8\text{-}10 \times 10^6 Kg/m^2s$.

Now, since we are using two ceramic bowl transducers, whose fundamental frequency is 2.28 MHz and driven at their

third harmonics in order to generate 6.84 MHz ultrasonic waves therefore the wavelength in magnesium is given by

$$\lambda_{Mg} = \frac{5750 \times 100}{6.84 \times 10^6} = 0.084 \text{ cm} = 0.84 \text{ mm}$$

$$(\lambda/_4)_{Mg} = 0.21 \text{ mm}$$

Two quarter-wavelength magnesium discs, 0.21 mm thick and 4.8 cm diameter, have been cut, annealed by heating to 500°C, and then stamped to the required curvature of the concave surfaces of the bowl transducers. Each disc was cemented, using permabond, to the concave surface of the corresponding transducer.

From equation (3.4), in order to achieve the optimum matching between the ceramic transducer (Z_t) and water loading (Z_w), the characteristic acoustic impedance (Z_1) of the material to be used with magnesium, for the construction of two matching layers (see Fig. 3.5), is given by:

$$Z_1 = Z_{Mg} \sqrt{\frac{Z_w}{Z_t}} = 9.8 \times 10^6 \sqrt{\frac{1.5 \times 10^6}{28.4 \times 10^6}} = 2.18 \times 10^6 \text{Kg/m}^2\text{s}$$

(i) Use of Kynar as a second matching layer with Magnesium

Kynar was found to have good physical properties which may be useful for this purpose. It is stronger and more flexible than perspex, its density is 1.77 gm/cm^3, the velocity of sound in it is 1218 m/s, and its acoustic impedance is 2.16×10^6 Kg/m^{2}s, which is nearly equal to the required value (2.18×10^6).

The wavelength λ in kynar, using 6.8 MHz ultrasonic radiation, is 0.18 mm, and $\lambda/_4$ is equal to 0.045 mm. It has been found difficult to achieve such a small thickness (0.045 mm) of

kynar layers. Therefore, it has been decided to use layers of kynar, whose thickness is $\frac{3\lambda}{4}$, instead of $\lambda/_4$, i.e. 0.135mm thick.

Each three-quarter wavelength thick kynar layer was cemented, using permabond, to the magnesium layer, which in turn is stuck to the concave surface of the transducer. After operating the transducers for a few times in water, unfortunately the kynar layers became detached, and no permanent adhesion between kynar and magnesium layers could be achieved.

(ii) Use of Polythene as a second matching layer with Magnesium

Polythene is softer and more flexible than kynar. Its density is 0.92 gm/cm^3, the velocity of sound in it is 1950-2000 m/s., and its acoustic impedance is 1.75-1.8 x 10^6Kg/m^{2}s. The wavelength λ in polythene, using 6.8 MHz ultrasonic radiation, is equal to 0.29mm and $\lambda/_4$ is 0.0725mm (which is greater than the corresponding value in kynar). Polythene sheets, whose thickness is $\frac{\lambda}{4}$ (i.e. 0.072 mm), have been obtained from the market.

Although the acoustic impedance of polythene is less than the required value (2.18x10^6Kg/m^{2}s), a good and permanent adhesion has been achieved (by Dr. Archer-Hall) between polythene and the selenium coating on the magnesium. Two magnesium discs (one for each transducer) 48mm in diameter have been machined, from one side, to the required thickness (i.e. $\frac{\lambda}{4}$ = 0.21mm); leaving the other side with its selenium coating. Each magnesium disc was annealed by heating to 500^{o}C, and then left to cool down to the room temperature. A

quarter-wave length thick polythene disc (0.07 mm thick and 48mm in diameter) is placed on the top of the selenium coating surface of the magnesium disc, and then heated together to 150°C. A static pressure is applied on the top of the two layers, using some weights, and then left to cool down to the room temperature. The two layers are now stuck together. They are stamped between brass concave and convex surfaces, whose curvature is exactly the same as that of the concave surface of the transducers so that the convexity is on the magnesium side and the concavity is on the polythene side. Each pair of layers is then cemented (using permabond) to its corresponding transducer, so that the convex surface of magnesium is stuck to the concave surface of the transducer. With this technique, a permanent adhesion has been obtained between polythene and magnesium, and between the latter and the transducer.

The performance of the assembled transducers, having their backing layers of tungsten-rubber (as explained before) has been examined and found to be satisfactory. Their decay time was found to be about $\frac{2}{3}\mu$ sec.

It has therefore been decided to use shock excitation with a sharp onset, in order to obtain the abrupt event (as will be explained in Chapter V). The use of matching layers have been abandoned.

CHAPTER IV

DETERMINATION OF THE VELOCITY OF SOUND IN SOLID MATERIALS USING A THIN WEDGE WITH HIGH FREQUENCY ULTRASONICS

4.1 Theoretical Considerations

Consider a system in which we have a transducer generating acoustic waves in a liquid, and a parallel sided plate of thickness "ℓ", is placed in the path of the beam and normal to it, as illustrated in Fig 4.1. As we consider a normal incidence of the acoustic waves, this plate of transition layer may be looked as a transmission line, for which the input impedance Z_{in} (at the side ab) is given by the general transmission line equation.

$$Z_{in} = Z_m \frac{Z_w + jZ_m \tan k\ell}{Z_m + jZ_w \tan k\ell} \qquad (4.1)$$

or

$$Z_{in} = Z_m \frac{Z_w \cos k\ell + jZ_m \sin k\ell}{Z_m \cos k\ell + jZ_w \sin k\ell} \qquad (4.2)$$

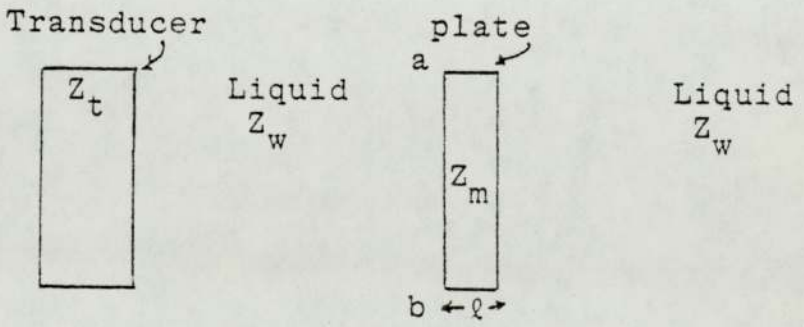

Fig.4.1. Transmission through a thin plate in a liquid (normal incidence).

where,

Z_m is the specific acoustic impedance of the material forming the plate,

Z_w is the specific acoustic impedance of the surrouding liquid, and $k = 2\pi/\lambda$, where λ denotes the wavelength of the acoustic waves in the plate material.

According to equation 4.2, there are three special cases of the thickness ℓ of the plate.

1. A very thin plate or membrane, whose thickness is very small compared with the wavelength λ in its material, i.e, $\ell \ll \lambda$. In this case the value of sin $k\ell$ becomes very small and approximate zero, and cos $k\ell$ approximates unitv.

   Therefore, the input impedance Z_{in} (as given by equation 4.2), will be equal to the acoustic impedance of surrounding liquid Z_w. This means that, such a layer acts as if it is not present and thus allows for a maximum transmission of acoustic waves through it.

2. If the plate is a half-wavelength thick or its multiples, i.e, $\ell = \frac{n\lambda}{2}$, where n is an integer, 1,2,3,4, etc. In this case sin $k\ell = 0$, cos $k\ell = 1$, and hence the input impedance Z_{in} will be equal to that of the liquid Z_w. This means that, such a plate acts as though it is not present and hence allows for a complete transmission of acoustic energy (except for the internal losses by absorption in the plate material.

3. If the plate is a quarter wavelength thick or its multiples i.e. $\ell = m\lambda/4$, where m is an odd number 1,3,5 etc., In this case, $\sin k\ell = 1$, $\cos k\ell = 0$, and hence the input impedance $Z_{in} = z_m^2/Z_w$. This means that the input impedance of the plate is different from that of the liquid. Thus, some of the incident energy is reflected back, and the remainder is transmitted through the plate.

These conclusions can be looked at more generally as follows: If a beam of acoustic waves travelling in a semi-infinite medium (1) whose specific acoustic impedance is Z_1, falls normally on the boundary between medium (1) and another semi-infinite medium (2) whose acoustic impedance is Z_2, it will be transmitted as

$$T = \frac{I_2}{I_1} = \frac{4Z_1 Z_2}{(Z_1 + Z_2)^2} \qquad (4.3)$$

Where I_1 and I_2, are the intensities of the incident and transmitted waves, respectively. T, is the transmission coefficient or intensity transmissivity. The reflection coefficient or intensity reflectivity R = 1 - T, is given by

$$R = \left\{ \frac{Z_2 - Z_1}{Z_2 + Z_1} \right\}^2 \qquad (4.4)$$

In order to calculate the transmission through the plate, let us consider it as a lossless transmission line (i.e, we neglec the internal loss of acoustic energy by absorption in the material of the plate), for which the input impedance Z_{in}, as given by equation 4.1, may be rewritten as follows:

$$Z_{in} = r\, Z_w \frac{1 + jr \tan k\ell}{r + j \tan k\ell} \qquad (4.5)$$

where,

$$r = Z_{m/Z_w}$$

The reflected energy at the liquid-solid interface can be determined by using equation 4.5 into equation 4.4, putting $Z_2 = Z_{in}$, and $Z_1 = Z_w$, so eventually we have:

$$R = \frac{\frac{1}{4}\,(r - \frac{1}{r})^2 \sin^2 k\ell}{1 + \frac{1}{4}(r - \frac{1}{r})^2 \sin^2 k\ell} \qquad (4.6)$$

After finding R, we can determine the transmissivity T, since T = 1-R , i.e.

$$T = \frac{1}{1 + \frac{1}{4}\,(r - \frac{1}{r})^2 \sin^2 k\ell} \qquad (4.7)$$

The variation of the transmissivity T with the thickness ℓ of plate, whose specific acoustic impedance Z_m relative to that of the surrounding liquid Z_w is equal to 6 (i.e, $Z_{m/Z_w} = r = 6$), is shown in Fig 4.2. From this figure, it can be seen that, for certain values of ℓ for which $\sin k\ell = 0$ (i.e, $\ell = n\lambda/2$, where n = 0,1,2,3 etc), the transmissivity is theoretically equals unity. In effect the plate is then acting as a half-wave transformer, where its input impedance equals that of the liquid, so there is no reflection occurrs i.e, R = 0.

On the other hand, for $\ell = m\lambda/4$, where m is an odd number, the transmissivity T has its minimum value. The plate is now acting as a quarter wavelength transformer for which the input

impedance Z_{in} (as given by equation 4.2) may be written as:

$$Z_{in} = Z^2_{m/Z_w} = r\, Z_m \qquad (4.8)$$

From this equation (4.8), for a plate of $m\lambda/4$ thick, as the specific acoustic impedance of the material forming the plate decreases to approach that of the surrounding liquid, the ratio r decreases to approach unity, and the input impedance Z_{in} approximates that of the liquid; consequently, the transmissivity increases to approach unity.

Therefore, the value of minimum transmissivity varies from a material to another; in the same liquid, so that it increases as the ratio r decreases. The variation of transmissivity T with thickness of plates of different materials (i.e, with different values of r), as calculated from Eq.(4.7), is shown in Fig.(4.3).

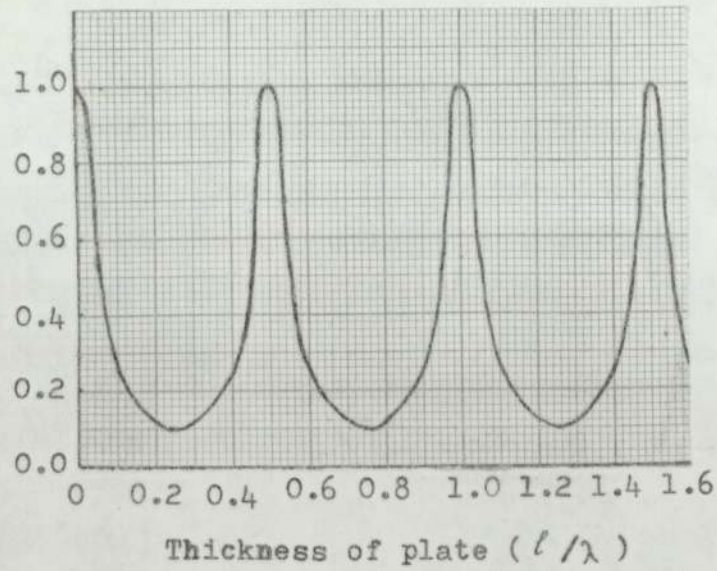

Fig. 4.2 Transmissivity as a function of plate thickness (ℓ/λ)

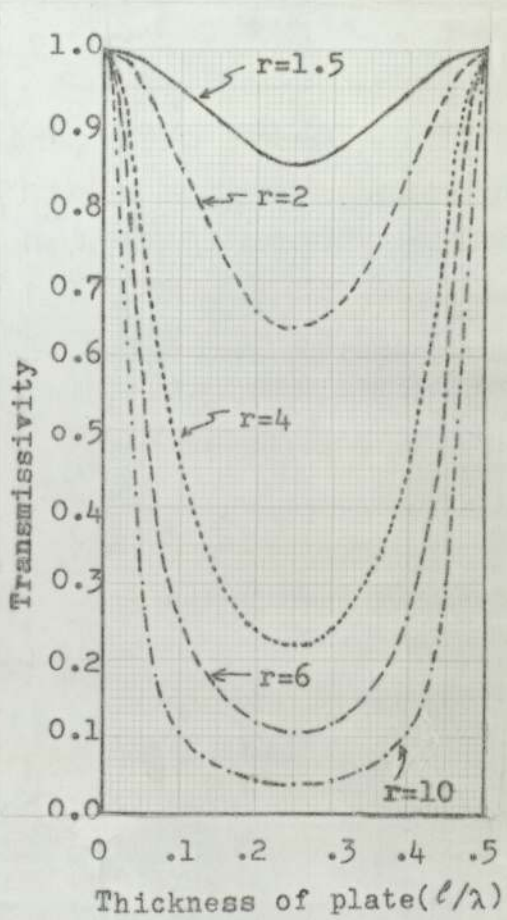

Fig. 4.3 (Right) Transmissivity as a function of ℓ/λ for different plate materials.

4.2 Ultrasonic Beam in the Focal Region of a Concave Bowl Transducer

As explained in Chapter II, the ultrasonic distribution in the focal region of a bowl transducer, may be thought as occupying a volume, which is nearly cylindrical in shape. Its radius is determined by the lateral resolution of the bowl transducer (Section 2-A.2), and its length equals to that of the effective focus (Section 2-A.4).

In other words, the transmitted radiation from a bowl transducer, is propagated in the focal region in a narrow beam of finite length and width, with almost a uniform intensity. This means that, the direction of propagation of ultrasonics may be considered normal to the focal plane.

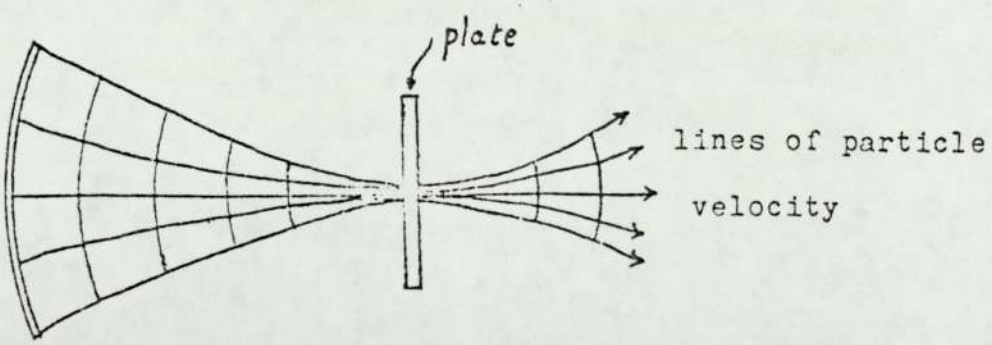

Fig. 4.4 Normal incidence of ultrasonic radiation on a thin plate at the centre of curvature of a concave transducer.

Thus, a system in which a parallel sided plate is placed at the focal plane of a bowl transducer, as shown in Fig.(4.4) is similar to that of Fig.(4.1). Such a system can be therefore, treated with the transmission line theory, explained in the previous section.

4.3 Transmission through a thin tapered wedge in the focal plane of a concave transducer

Consider a system in which a concave transducer is radiating into a liquid, and a thin tapered wedge is placed at the focus, so that its face "abde" (Fig.4.5-a) opposite to the transducer, is at the focal plane. In this case, the ultrasonic waves fall normally on the liquid-solid interface, represented by the line ab in Fig.(4.5-b). From the geometry of this figure it can be seen that, the angle of incidence on the solid-liquid interface (ac), is equal to the angle of the wedge (θ_1). If the angle of refraction in the liquid is θ_2, the velocity of sound in liquid is c_2 , and that in the wedge material is c_1 ; then according to Snell's law we have:

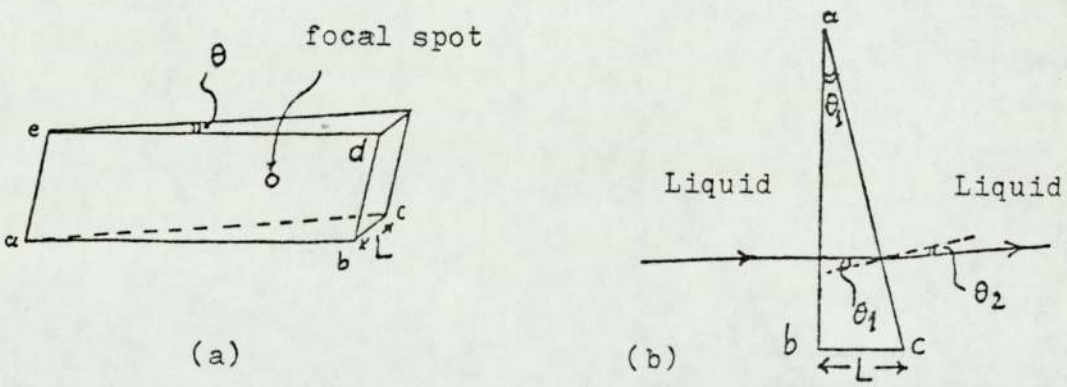

Fig. 4.5 . Transmission of a normally incident beam of ultrasonics through a thin tapered wedge in a liquid .

$$\frac{\text{Sin } \theta_1}{\text{Sin } \theta_2} = \frac{c_1}{c_2} \text{ , i.e.}$$

$$\text{Sin } \theta_2 = \text{Sin } \theta_1 \ \frac{c_2}{c_1} \qquad \ldots\ldots (4.9)$$

The error in transmission, through a wedge, produced by its angle θ_1, depends on the departure of cos θ_2 from unity. Suppose an aluminium wedge of angle $\theta_1 = 10^\circ$, and that the

surrounding liquid is water. Since the velocity of sound in aluminium, c_1=6420 m/s, and that in water c_2=1500 m/s, then from Eq.(4.9), we have

$\theta_2 \simeq 2.33^\circ$; cos 2.33=0.9992

The percentage error in transmissivity $\simeq \frac{0.0008}{1} \times 100 \simeq 0.08\%$

Suppose a perspex wedge of the same angle $\theta_1=10^\circ$, and also in water. Since the velocity of sound in perspex c_1=2736 m/s, then from Eq.(4.9) we have:

$\theta_2 \simeq 5.46^\circ$; cos $\theta_2 \simeq$ 0.9955

% error$\simeq$ 0.45%

Therefore, it can be seen that the percentage error in transmissivity of normally incident ultrasonic waves, through a wedge whose angle is 10°, in water, is very small and can be neglected. This error can be made even smaller, by further decreasing the angle of the wedge.
It can be also seen that, for the same angle of wedge, and the same surrounding liquid, the produced error decreases as the velocity of sound in the wedge material increases.

Thus, it may be concluded that, a thin tapered wedge, placed in a liquid, on which an ultrasonic beam is normally incident, may be looked at as a transmission line. This conclusion is based on the assumption that the angle of the wedge must be as small as possible so that:

1. The error produced by this angle is negligible, and

2. The thickness of the wedge becomes as small as possible, in order to decrease the internal losses of the acoustical energy by absorption in its material, so as to be negligible.

Fulfilling these conditions, the transmission through this wedge will behave in the same way like that through a parallel-sided plate. This means that the transmissivity through the wedge will be a maximum if its thickness ℓ is equal to $n\lambda/2$, and it will be a minimum if the thickness ℓ' is equal to $m\lambda/4$, where n is 0, 1, 2, 3, 4, etc., and m is an odd number.

If the wedge is moved in the focal plane, in a direction perpendicular to the axis of symmetry of the concave transducer, a number of transmission maxima and minima will occur. The number of transmission maxima, through a finite length of a tapered wedge, depends on two main factors, namely the angle of the wedge, and the ratio of the wedge thickness at the thick edge "L" to the wavelength λ in its material, i.e, L/λ.

1. The angle of the wedge must be very small to decrease the error produced by it, and also to obtain a very thin wedge in which the internal absorption is negligible.

2. In order to obtain an "n" number of transmission maxima, through a finite length of a thin wedge, its thickness at the thick edge "L" must be at least $n\,\lambda/2$, i.e, $L/\lambda \geqslant n/2$, as illustrated in Fig 4.2. However, for the first requirement of a very thin wedge, L should be kept as small as possible. Therefore, the only factor to be

varied in order to achieve the second requirement, (i.e, $L/\lambda \geqslant n/2$) is the wavelength λ in the wedge material, which can be decreased as required by increasing the frequency "f" of the ultrasonic beam, where $\lambda = c/f$; C, is the velocity of sound in the wedge material.

However, the increase of the frequency of the ultrasonic beam will be on the expense of its maximum range, since the attenuation of ultrasonics in the surrounding liquid (water) is proportional to the square of the frequency. The reasonable frequency to be used without great attenuation in water is about 5 - 8 MH_2.

4.4 Determination of the Velocity of Sound in Solid Materials Using a thin tapered wedge and a Converging Beam of Ultrasonics

From the previous discussions it can be seen that, if a thin tapered wedge (made from the material for which the velocity of sound is to be determined) is moved slowly in the focal plane of a concave transducer, in a direction perpendicular to its axis of symmetry, a number of transmission maxima and minima can be observed.

If the thickness of the wedge at any of these points is measured, it will be possible to determine the wavelength "λ" of ultrasonics in the material of the wedge.

Since the thickness "ℓ" of the wedge corresponding to the n^{th} transmission maximum is equal to $n\lambda/_2$, then thewavelength is given by:

$$\lambda = 2\ell/_n$$

Also, as the thickness (ℓ') of the wedge corresponding to the m^{th} transmission minimum is equal to $m\lambda/_4$, then the wavelength λ is given by:

$$\lambda = 4\ell'/_m$$

where, n is an integer, and m is an odd number.

Finding the wavelength λ in the wedge material, and if the frequency (f) of the ultrasonic beam is known, then it will be possible to calculate the velocity of sound c in the material of the wedge, where

$$c = \lambda f \qquad (4.10)$$

The accuracy of determining the wavelength λ depends on the width of the used ultrasonic beam. The resolution of fine details requires to look at one little patch of the wedge surface, at each time. Therefore, in order to achieve the required resolution, conducting to accurate measurements, a concave transducer of a good lateral resolution must be used. The ceramic bowl transducer used for this purpose, has an aper ture diameter of 4.9cm, its radius of curvature is 10cm, and its fundamental resonant frequency is 1.09 MHz. This transducer was driven at its 7^{th} harmonics in order to produce a 7.6 MHz ultrasonic beam.

The calculated lateral resolution of such a transducer, was found to be about 0.4mm. This has been checked experimentally, while the transducer is operating in a water bath, by holding a thin straight wire (about 0.4mm in diameter) vertically above the focus. Another matching concave transducer is fixed in the water bath, so that the two transducers are facing and parallel to each other, with their foci coinciding on each other. The second transducer is used as a detector for the received ultrasonic waves from the first one.

Where the wire is brought down to intersect the focus, it has been found that more than 80% of the transmitted radiation from the first transducer has been stopped from reaching the second transducer (receiver). This means that the experimental result of the lateral resolution agree with the calculated figure.

There are two methods for determining the wavelength λ in the wedge material, for which the velocity of sound c is to be determined:

(i) either detecting the transmission maxima and minima through the wedge,

(ii) or by detecting the reflection maxima and minima at the surface of the wedge.

4.4.1 The first method: Detection of the transmissivity maxima and minima through the wedge

In order to determine the points on the wedge at which maximum or minimum transmission occur, two matching ceramic bowl transducers of a good lateral resolution (0.4 mm), have been used. The two transducers are fixed onto a perspex base "B" in a water bath, so that they are parallel to each other, with their central axes in the same horizontal line and their foci coinciding on each other at the same point (the common focus of the two transducers). At the common focus, and normal to the central axes of the two transducers, there is a groove "G" in the perspex base "B" as shown in Fig.(4.6).

One of the transducers is used as a transmitter by connecting it to a 7.6 MH_z oscillator. The other is used as a detector by connecting it to a pre-amplifier and an oscilloscope, in order to detect ultrasonic waves transmitted through the wedge.

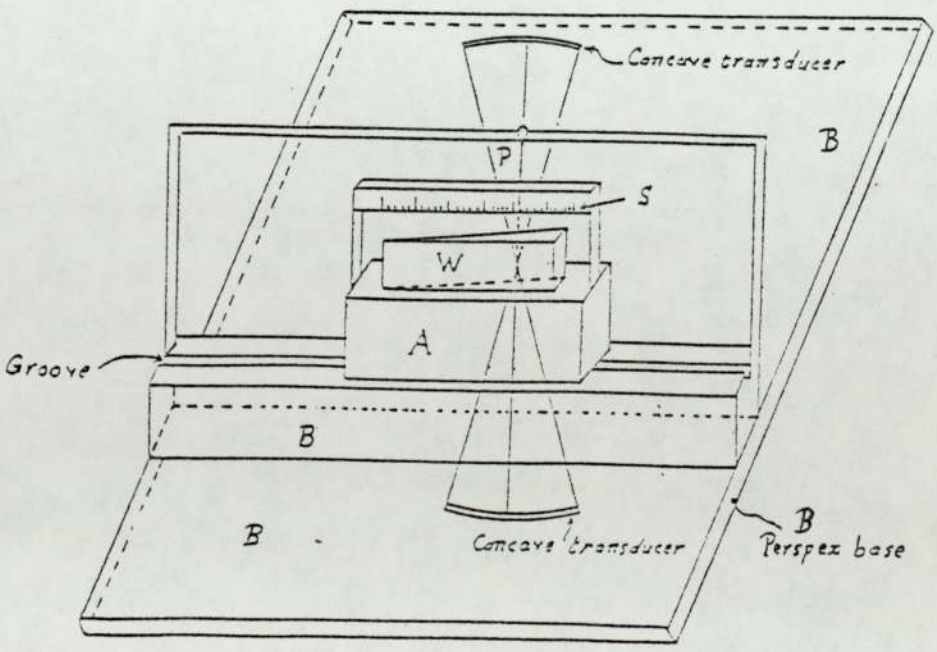

Fig. 4.6 Determination of the velocity of sound in the material of the wedge.

The position of the common focus must be determined accurately. This has been done by holding a thin wire vertically above the focus. The wire is slightly moved until a position is obtained at which most of the ultrasonic waves are stopped from reaching the receiving transducer. Finding this position of the focus, a vertical pointer P, above the water level, is set at this position and remains fixed there with respect to the transducers and the perspex base B.

The thin tapered wedge W (of the required material for which the velocity of sound is to be determined), is fixed on a piece of perspex A which slides into the groove G. The wedge is fixed on the sliding perspex A in such a way so that its surface facing the transmitting transducer must be in the focal plane, and the focus is at the mid-line of this surface.

Above the wedge and parellel to its surface, there is a scale S, fixed onto the sliding perspex A, and opposite to the pointer P. The reading given by the pointer on the scale when a maximum or a minimum transmission is detected, shows accurately the corresponding position on the wedge.

The procedure of determining the wavelength λ in the wedge material is described as follows:

The sliding perspex A is set first, so that the focus falls on the tapered edge of the wedge, which is considered to be very thin, relative to the wavelength λ . In this case, a maximum transmission, corresponding to nearly a zero thickness, will be observed on the oscilloscope. If the sliding perspex is moved

slowly into the groove, the transmissivity decreases to a minimum, when the focus falls at a point on the wedge surface whose thickness (ℓ') is equal to $\lambda/_4$. Take the reading of the scale given by the pointer P, which shows the position on the wedge corresponding to the first minimum (i.e, m = 1). Move the sliding perspex slowly in the same direction, the transmissivity will increase to a maximum value, when the focus falls at a point on the wedge surface whose thickness (ℓ) is $\lambda/_2$. Take the reading of the scale, which shows the position on the wedge surface corresponding to the first maximum (i.e, n = 1). Further movements of the sliding perspex into the groove across the focus give rise to a number of transmission minima and maxima.

After taking as many as possible readings of the scale, corresponding to the distinguishable transmission maxima and minima lift out carefully the sliding perspex, with its attachments (i.e, the wedge and the scale) remaining in place, from the water bath. Measure the wedge thicknesses corresponding to the scale readings, by using a micrometer onto which two small ball-bearings are attached by means of two small rubber tubes. By this method, it is possible to measure the thickness of the wedge at a point (which corresponds to the scale reading) instead of a finite area which depends on the thickness of the micrometer.

Calculate the value of the wavelength λ in each case where,

(a) for the n^{th} transmission maximum for which the thickness is ℓ , λ is given by:

$$\lambda = 2\ \ell/_n \qquad (4.11)$$

(b) for the m^{th} transmission minimum for which the thickness is ℓ', λ is given by:

$$\lambda = 4\,\ell'/_m \qquad (4.12)$$

where n is an integer and m is an odd number.

Determine the mean value of λ, from which the velocity of sound "c" in the wedge material can be calculated by using equation 4.10 i.e,

$$c = \lambda f$$

where f the frequency of the ultrasonic beam is known (f=7.6 MHz).

4.4.2 The Second Method: Detection of the reflectivity maxima and minima at the wedge surface

The points on the wedge surface through which a maximum transmission of ultrasonics occur, and whose thicknesses $\ell = n\lambda/_2$, are those points at which there is a minimum reflection. On the other hand, the maximum reflection occurs at those points, at which there is a minimum transmission, i.e, at points whose thicknesses $\ell' = m\,\lambda/_4$.

In order to detect the reflectivity maxima and minima, only one ceramic bowl transducer is used as a transmitter and receiver, for the returning echoes from the wedge surface. In this case, the transducer is connected to a 7.6 MH_z oscillator and a pulse time generator (whose repetition frequency is $1/_{500}$ sec) in order to produce 7.6 ultrasonic pulses (120 μs). The transducer is

also connected to a pre-amplifier and an oscilloscope, in order to detect the echo pulses from the wedge surface.

The focal point of the transducer is determined by using a vertical thin wire about the focus. The position of the wire at which a maximum reflection is observed on the oscilloscope is that of the focus. The pointer P (Fig 4.6) is adjusted at this position and remains fixed there with respect to the transducer where the latter is fixed onto the base B in the water bath.

The wedge is fixed on the sliding perspex A, and the same procedures, described in the first method, are carried out in order to determine the thicknesses of the wedge at which reflectivity maxima and minima are observed.

Calculate the wavelength λ, where:

(a) for the n^{th} reflectivity minimum (for which the thickness is ℓ), λ is given by: $\lambda = 2\ell/_n$.

(b) for the m^{th} reflectivity maximum (for which the thickness is ℓ'), λ is given by: $\lambda = 4\ell'/_m$

Determine the mean value of λ, from which the velocity of sound c can be calculated.

These two methods have been carried out under the same conditions and using the same wedge. Although the two methods differ in the technique for detecting the maxima and minima of either the transmissivity or the reflectivity, they give the

same results, and therefore, they may be considered as one method.

4.5 Experimental Results of the Velocity of Sound in different Solid Materials

The above mentioned methods have been carried out for some materials, such as perspex and aluminium (in which the velocities of sound are known), for the purpose of determining the efficiency of this method , when the results are compared with the published data. Also, the velocity of sound in some polymers have been determined by this method , for the purpose of constructing matching layers. The results of these experiments are given in chapter III.

4.5.1 Determination of the velocity of sound in Aluminium

A thin tapered wedge of aluminium has been constructed by using a milling machine. The length of the resultant wedge is 12cm, its thickness at the tapered edge is 0.09mm, the thickness at the thick edge is 0.16cm. Both the above mentioned methods have been carried out using this wedge, in order to determine the velocity of sound in aluminium. The frequency of the used ultrasonic radiation f=7.6 MHz.

The measured thickness of the wedge at those points corresponding to maximum and minimum transmissivity and also corresponding to minimum and maximum reflectivity, are given in table IV-1. It must be noted that the thickness of the wedge at

the n^{th} transmissivity maximum has found to be the same as that obtained at the n^{th} reflectivity minimum, and vice versa, i.e, the thickness at the m^{th} transmissivity minimum is the same as that at the m^{th} reflectivity maximum. The calculated values of λ, from each measured thickness, are shown in table IV-1. The mean value of λ is found to be 0.0844 cm.

The frequency "f" of the ultrasonic beam generated by the transducer has been measured accurately by using a frequency computer, which is found to be 7.6 MH_z. Therefore, the velocity of sound **c** in aluminium is given by:

$$c = \lambda f = \frac{0.0844}{100} \times 7.6 \times 10^6 = 6414 \quad m/sec$$

This figure of the velocity of sound in aluminium is nearly the same as that of the published data which is between 6400 - 6420 m/sec.

4.5.2 The Velocity of Sound in Perspex

The perspex wedge can be machined by using a milling machine. It also can be constructed by dissolving a piece of perspex in chloform. A flat groove, 2cm wide, 13cm long, and 0.5cm deep, is made in a poly tetra fluoro ethylene, (PTFE) slab. The PTFE slab is placed tilted on a horizontal flat surface, to the required angle "θ", as shown in Fig.(4.7). The perspex solution is then poured in the groove, which is covered with a glass plate, leaving a small outlet to allow the chloroform vapours to escape. The solution is then left to dry slowly. After 24 hours, the perspex wedge is lifted out carefully.

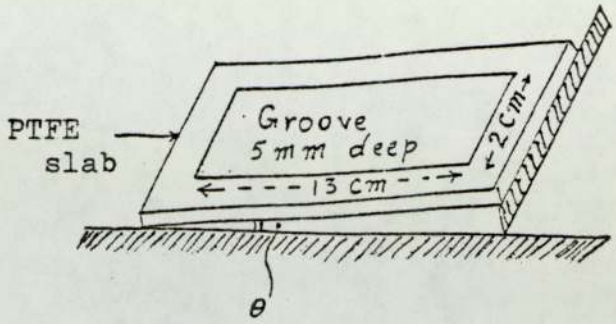

Fig. 4.7 PTFE slab with a groove, tilted at an angle θ for making a thin tapered wedge of perspex.

Table IV.1 Thicknesses of aluminium wedge corresponding to maximum and minimum transmissivity.

Maximum transmision	n	Thickness ℓ (cm)	$\lambda = 2\ell/n$ (cm)	Minimum transmission	m	Thickness ℓ' (cm)	$\lambda = 4\ell'/m$ (cm)
1st maximum	1	0.0425	0.0850	1st minimum	1	0.0211	0.0844
2nd maximum	2	0.0842	0 0842	2nd minimum	3	0.0630	0.0840

Table IV. 2 Thicknesses of perspex wedge corresponding to maximum and minimum transmissivity.

Maximum transmission	n	Thickness ℓ (cm)	$\lambda = 2\ell/n$ (cm)	Minimum transmission	m	Thickness ℓ' (cm)	$\lambda = 4\ell'/m$ (cm)
1st maximum	1	0.0180	0.0360	1st minimum	1	0.0095	0.0380
2nd maximum	2	-	-	2nd minimum	3	0.0255	0.0340

The measured thicknesses of the wedge at which the transmission maxima and minima occur, are given in table IV-2. The corresponding calculated values of the wavelength λ, are given in the same table.

The mean value of the wavelength λ = 0.036 cm. Since the frequency f of the used ultrasonic beam is 7.6 MH_z, the velocity of sound in perspex is given by:

$$c = \lambda f = \frac{0.036}{100} \times 7.6 \times 10^6 = 2736 \text{ m/sec}$$

From the texts the velocity of sound in perspex is 2700m/sec. Therefore, the two figures are very nearly the same, within the experimental errors.

From the previous experiments, it can be seen that this method is accurate enough and reliable for determining the velocity of sound in solid materials.

CHAPTER V

ELECTRONICS

The theoretical consideration and principles of construction of the ultrasonic bone tomograph, have been discussed in Chapter II. The electronic procedures for determining the time difference of the returning echoes, from bone surface and reference rod, and its transfer to the recording system, will be considered in this chapter.

Figure(5.1) is a block diagram of the electronic circuits of the apparatus. The scanning and reference transducers are acoustically coupled via the ultrasonic path to the patient and the reflecting rod, respectively. Both transducers are electrically coupled to a transmitter, which consists of an oscillator and a transmitting amplifier. Each transducer is also electrically coupled to its own receiver. Both re-receivers consist of similar amplifying stages including an integrated circuit. The integrated circuit of the scanning transducer, has a variable AGC bias which provides a gain control to compensate for the differences of the voltage amplitudes of the two pulse echo signals.

These signals are fed into a servomechanism, which consists of a discriminator and a motor switch circuit. The servomechanism operates in such a way so as to maintain the focus of the scanning transducer at the soft tissue-bone interface. If the bone surface at any point on the circular scan is at a distance from the vertex of the scanning transducer,

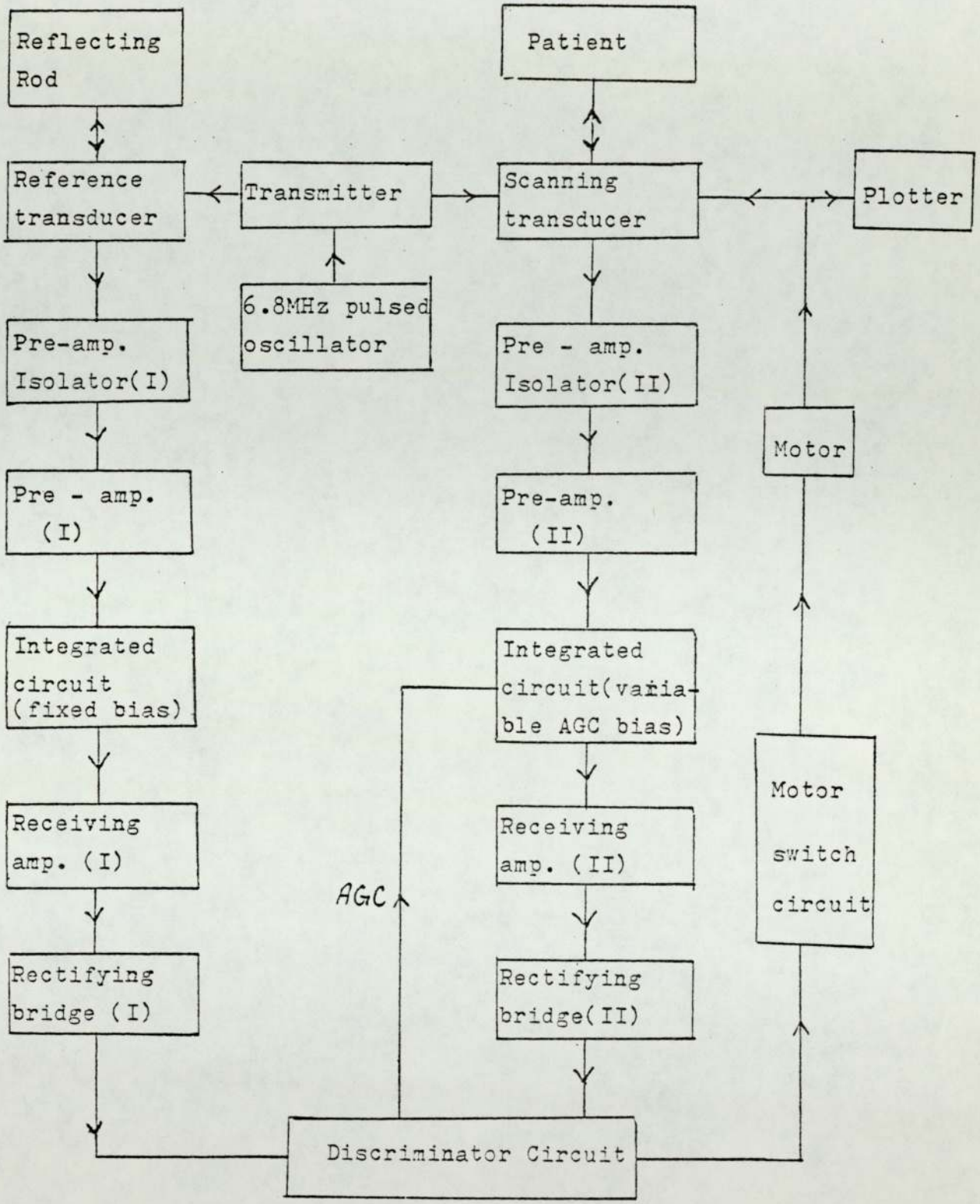

Fig. 5.1 A block diagram of the ultrasonic bone tomograph .

greater than its focal length, then the scanning transducer will be moved to the bone surface by the servomechanism, and vice-versa.

The scanning transducer movement is transferred to a plotter by a direct mechanical coupling, as described in Chapter VI.

The detailed electronics of the apparatus will be described in the following sections.

5.1 Pulse Repetition Frequency Generator

The time pulse generator has been built to provide the required pulses for operating the electronic circuits at the correct times. The circuit of the pulse generator is illustrated in Figure 5.2, which consists of:

(1) PNP astable multivibrator (timer), circuit I in Figure 5.2. It produces square pulses, whose duration is 146μs, with a repetition frequency f=500 pulses/s (i.e. the period of each oscillation is 2ms). The resulting pulses of the timer, P1, P2 and P3 are shown in Figure 5.3. The pulse P3 is a sharp square negative-going pulse which is used to trigger another three monostable circuits.

(2) Two pnp monostable multivibrators, circuits II and III in Figure 5.2. These circuits are triggered by the negative-going edge (at t = o) of pulse P3. The unstable state of circuit II is adjusted to be 120 μs. The resulting pulses of this circuit P4, P5 and P(5A) are shown in Figure 5.3.
The unstable state of the other pnp multivibrator (circuit III), is adjusted to give pulses of longer duration, i.e. 240 μs. These pulses are P7, P8, P9 and P10.

(3) NPN monostable multivibrators (circuit IV in Figure 5.2), is triggered by the positive-going edge (at t = 146 μs) of the timer pulse P3. The unstable state of the circuit was adjusted to be 130 μs i.e. from t =146 to t =276 μs. The resulting pulses, P11, P12, P13 are shown in Figure 5.3.

(4) Some stages of pch FETS have been triggered from the pulses P3, P5, P9, or P12 in order to give other inverted pulse or pulses with different output voltages.
These stages are shown in Figure 5.2.

Figure 5.3 gives the wave forms of the different pulses produced by the pulse time generator. Table 5.1 gives a summary of the uses of these pulses in the electronic circuits.

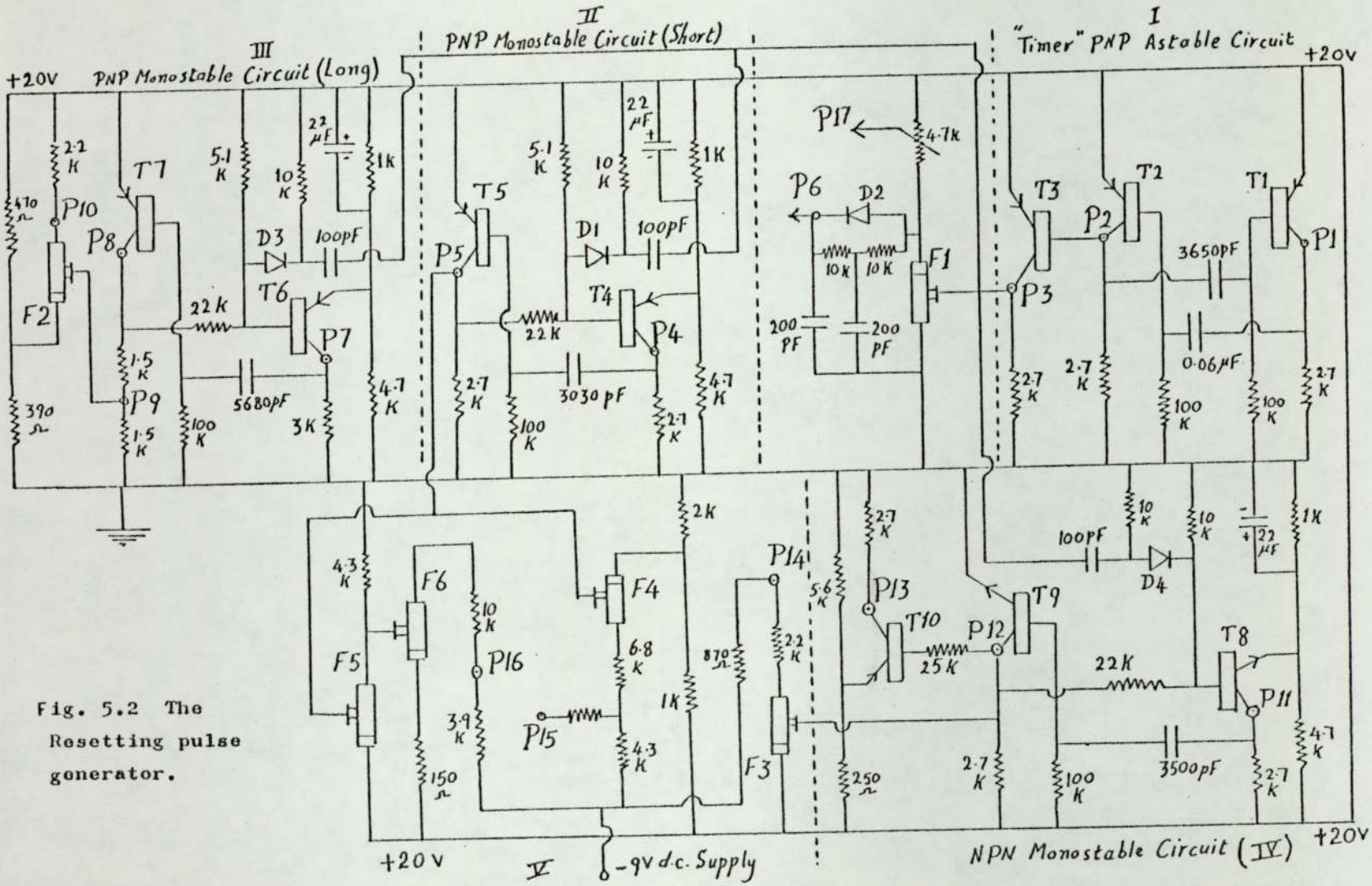

Fig. 5.2 The Resetting pulse generator.

List of electronic components of Fig. 5.2 :-

(a) Bipolar transistors:

TI- T7 ,pnp (BFX48)

TIO , pnp (BCY7I) ;

T8 &T9 ,are npn (BSX39)

(b) Field effect transistors :

FI,F3,F4,&F5 are p ch FETs(3NI55A),

F6, is p ch FET (3NI57A);

F2, n ch FET (2N4859A)

(c) Diodes :

DI- D4,(IGPIO)

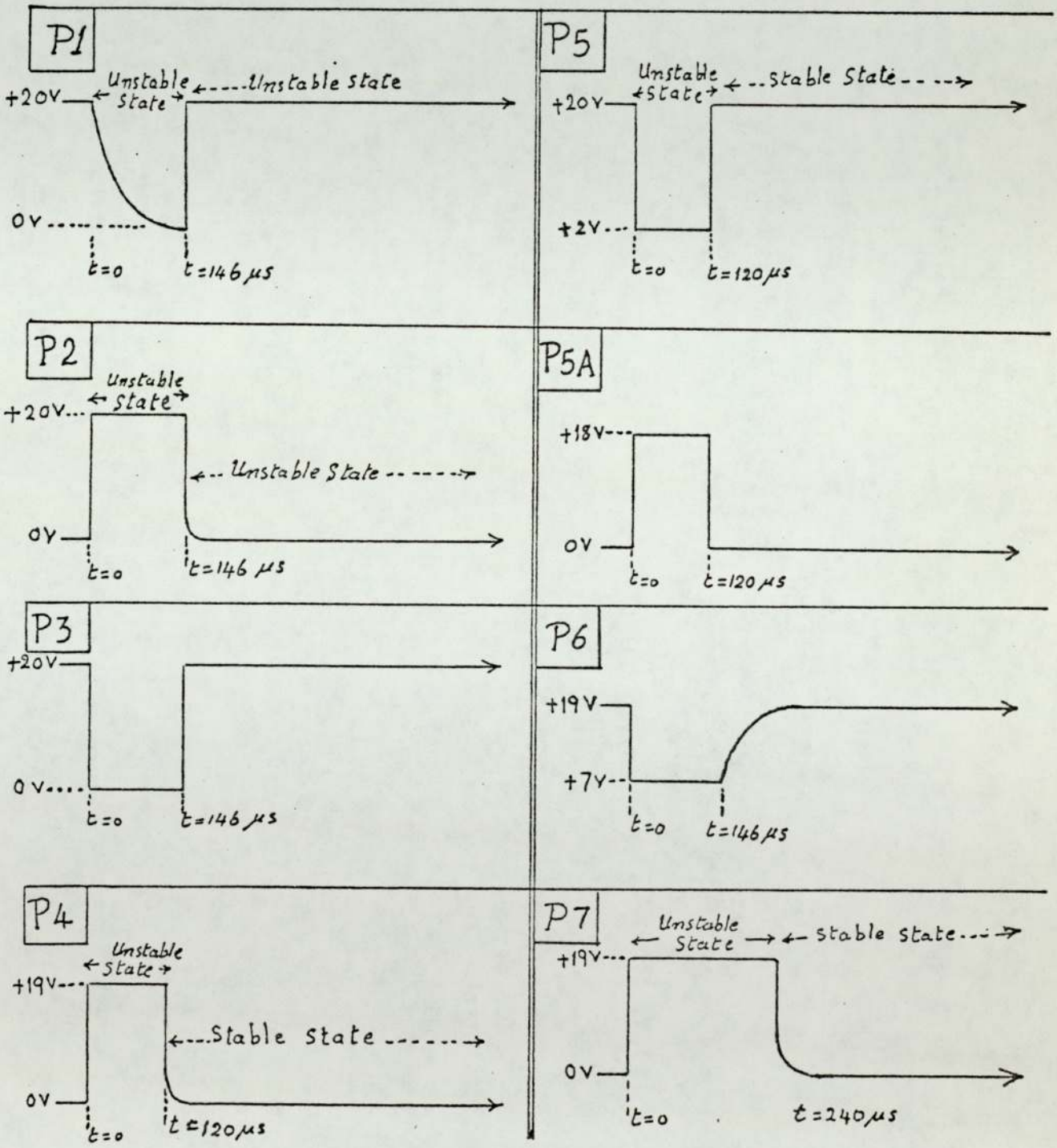

Fig. 5.3. Wave forms of the pulses of Fig. 5.2.

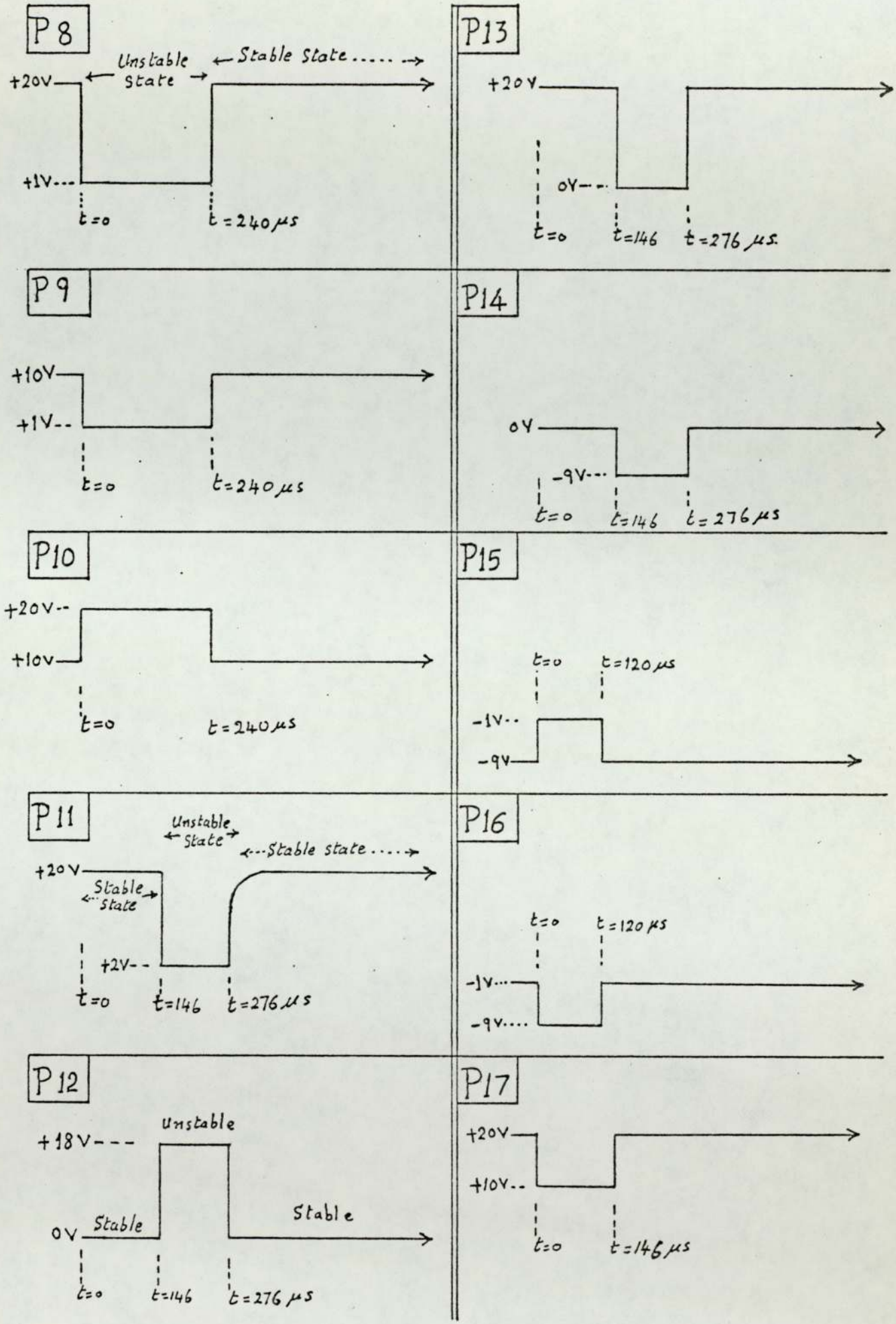

Fig.5.3. (continue) waveforms of pulses of Fig. 5.2.

TABLE 5.1: The uses of the pulses of the pulse generator into the electronic circuits

Pulse No	Duration	Its use in the electronic circuit
1	0 - 146 μs	
2	0 - 146 μs	
3	0 - 146 μs	
4	0 - 120 μs	
5	0 - 120 μs	
5A	0 - 120 μs	Oscillator Chopper
6	0 - 146 μs	Transmitter Bias Chopper
7	0 - 240 μs	
8	0 - 240 μs	AGC Bias Lock In
9	0 - 240 μs	PNP reset, in the discriminator
10	0 - 240 μs	NPN reset, in the discriminator
11	146 - 276 μs	Bias Guard, of the AGC
12	146 - 276 μs	Nch Guard, in the discriminator
13	146 - 276 μs	PCh Guard, in the discriminator
14	146 - 276 μs	Pre-amplifier isolator
15	0 - 120 μs	Transmitter power transistor chopper
16	0 - 120 μs	Main transmitter chopper
17	0 - 146 μs	Pre-amplifier isolator

5.2 $7MH_Z$ Sinusoidal Pulsed Oscillator

The intention is to send pulses of 6.8 MH_Z ultrasonic waves by the two transducers, simultaneously, for 120 μs. A $7MH_Z$ pulsed oscillator has been built as shown in Figure 5.4, and shielded in a separate box in order to reduce any possibility of radiation coupling during the transmission. It consists of a

tuned transformer LL´ . The frequency-determining section is represented by the LC network, which is tuned to the required resonance frequency i.e. 6.85 MH_Z. A fine adjustment of the tunning can be obtained by screwing the core of the coils through a hole in the lid of the box. The maintaining section of the oscillator is npn transistor amplifier T1 (BC 184L), which has a sufficient gain to offset the attenuation of the frequency-determining section. T2, npn transistor (BSx39), is a buffer amplifier emitter follower. A 1k potentiometer is connected as an emitter load to control the output amplitude.

The pulsed oscillations are obtained by using a switching pch FET "F1", connected accross the coil L´ . A signal will only be received on the base of T2, and hence on its emitter load, provided that F1 is not conducting. This will depend on the V_{GS} potential, i.e. the signal on the gate of F1, which is derived from the pulse "P5A" (given in Figure 5.3). Since this pulse is +20V during the transmission period from t=o to t = 120μs, the FET F1 will be non-conducting during this period, and hence an output oscillations will be obtained. After this period, i.e. 120μs, the gate potential is negative with respect to the source, so that F1 will be in its conducting mode, shortening the coil L´ and hence no output oscillations are obtained until the start of the next pulse.

5.3 The Transmitting Driving Amplifier

The transmitting circuit is illustrated in Figure 5.5. The output of the pulsed oscillator is fed into a single pnp transistor amplifier T1, which has a tuned coil as an output load. The output of this stage is fed into two similar

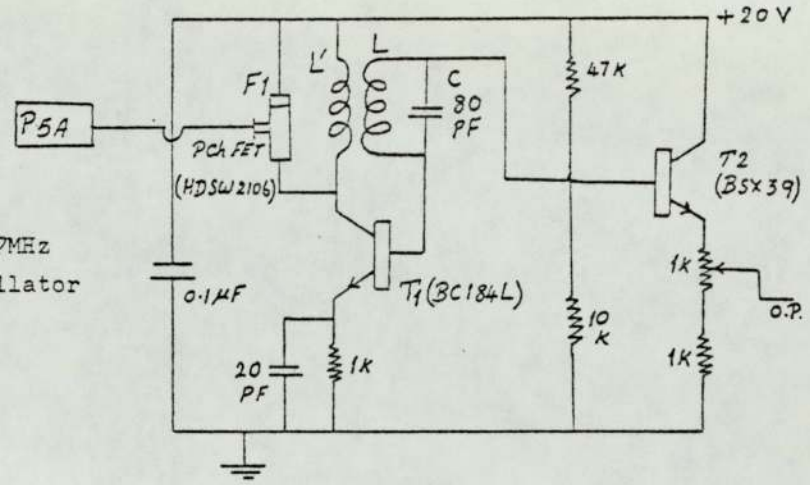

Fig. 5.4. 7MHz pulsed oscillator

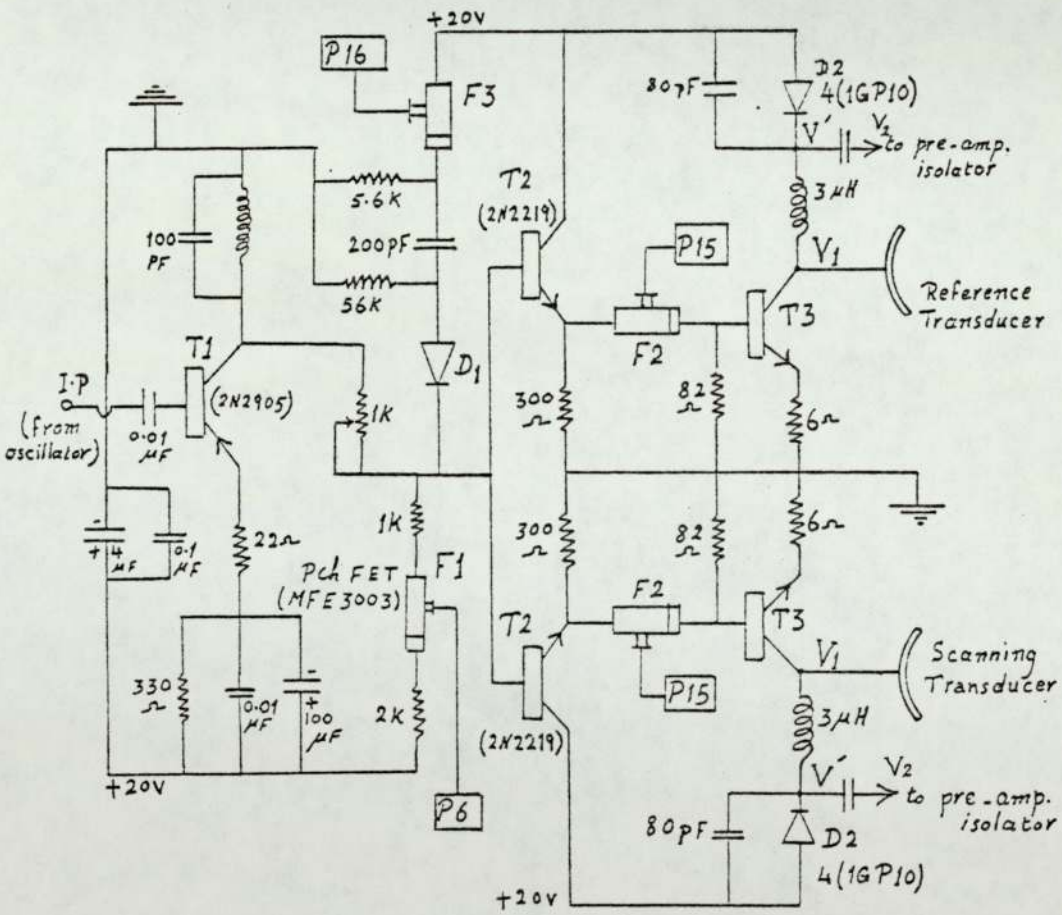

Fig.5.5. Transmitting driving amplifier

T3,npn power transistors ;F2 &F3,nch J FETs (2N4859A) ;
DI& D2, diodes (IGPIO)"

Darlington circuits, located in separate housings. Each circuit consists of an intermediate power transistor T2 (2N2219), and a power transistor T3 (D44 C3) which is used in the output stage. Due to power dissipation in these transistors, small heat sinks are mounted on the cases of the intermediate power transistors T2, whereas the power transistors T3 are mounted with their collectors in good thermal contact with thick (0.5cm) aluminium plates of large area (about 7x10 cm).

The switching FETS, F1 and F2 are in their conducting mode during the transmission period, t = o - t = 120μs, depending on the V_{GS} of each FET. The signal on the gate of the pch bias chopper F1 is derived from the negative-going pulse P6 (as shown in Figure 5.3), allowing the FET to conduct during the transmission time (until t = 146μs, after which the bias will be cut off until the start of the next pulse. The signal on the gates of the nch FETS "F2", the power transistor choppers, is derived from the positive-going pulse P15, so that these FETS will be conducting during the transmission period, after which they will be cut off until the start of the next pulse.

It was intended to derive the information from the abrupt cessation of the signals. Considerable experimental work has been carried out with regard to the construction of backing and matching layers for the transducers to be critically damped, in order to obtain the abrupt cessation of the signals. However, the cessation of the wave trains could not be made to provide a sufficiently distinct event.

The intention now is to provide a steep fronted impulse by using a very sharp jump in the d.c. level, at the end of transmission. During the transmission period, from t=o to t=120μs, the FET "F3" will be cut off by means of the pulse P16 applied to its gate. At t=120μs F3 starts to conduct giving a spike with a jump in the d.c. level. The sharp cut of the spike is provided by the power transistor choppers F2. The distinct event will be reproduced at the ends of the returning echoes, which gives an accurate method to estimate the time delay between the two returning signals, and also to operate the discriminator so that the motor moves in the correct direction.

A resistive load was used in the output stage of each driving power transistor "T3", but it was impossible to avoid step pulses to the transducers at the start and end of transmission. This also produced flexural modes of vibrations. However, it has been found satisfactory to use an inductance as an output load instead of a resistive load. The value of the inductance (L=3μH) has been chosen so that its impedance (Z) at the driving frequency (6.85MHz) is considerably larger than the resistance of the ceramic transducer (about 4 Ω), where

$$Z = \omega L = 2\pi f L = 130\ \Omega$$

This means that almost all the driving signal (V_1) will be applied to the transducer. The diode D_2, shown in Figs.(5.5) and (5.6), has been used to reduce the signal (V_2) applied to the pre-amplifier, during the transmission period, to a small value as possible. This depends on the low resistance of D_2 to a.c. when it is also passing d.c.

The coupling circuit (shown in Fig.5.6), between the transmitting and receiving circuits, must therefore fullfil the following requirements:-

(1)The ratio of V_2/V_1, is to be as small as reasonably possible during the transmission period so as not to apply an excessive signal to the receiving pre-amplifier.

(2)The ratio of V_2/V_1, must be as large as possible when derived from the returning signal during the receiving period.

For the second requirement, a theoretical analysis of the coupling circuit between the transmitting and receiving circuits will be dealt with in the following section.

5.4 Theoretical Analysis of the Coupling Circuit to the Pre-amplifier

The coupling circuit to the receiving pre-amplifier is illustrated in Fig.(5.6-a), and its equivalent circuit is shown in Fig.(5.6-b). The inductance of the coil L is equal to 3μH, and C2 is a blocking condenser for the pre-amplifier whose input impendance R=400 Ω . The equivalent capacity C_1 of the actual condenser C' and the capacity contributed by the assembly of the four diodes (1GP10), in parallel with C', in the non-conducting state (i.e. after the transmission period), is equal to 84 PF. From the circuit of Fig.(5.6-b), we have

$$V' = I_2 \left(R + \frac{1}{j\omega C_2}\right) = I_1 \frac{1}{j\omega C_1} \quad ; \text{ from which:}$$

$$I_1 = \left(j\omega C_1 R + \frac{C_1}{C_2}\right) I_2, \text{ and}$$

$$V_1 = (I_1 + I_2)\, j\omega L + V'$$

substituting for I_1, and V' from the above equations we have:

$$V_1 = j\omega L \left(1+\frac{C_1}{C_2} + j\omega C_1 R\right) I_2 + I_2\left(R+\frac{1}{j\omega C_2}\right) \qquad \ldots\ (5.1)$$

since, $V_2 = I_2 R$, therefore

$$\frac{V_2}{V_1} = \frac{R}{j\omega L \left(1+\frac{C_1}{C_2} + j\omega C_1 R\right) + \frac{1}{j\omega C_2} + R}$$

$$\frac{V_2}{V_1} = \frac{j\omega C_2 R}{1-\left(1+\frac{C_1}{C_2}\right)\omega^2 LC_2 + (1-\omega^2 LC_1)\, j\omega C_2 R}$$

The accuracy of the system for reproducing an abrupt signal, depends on the following conditions:-

(1)The ratio V_2/V_1 must have as large magnitude as possible and to cover an adequate bandwidth.

(2)The value of V_2 must fall to zero as rapidly as possible after the cessation of the reflected pulse.

For the first requirement, if C_1 and C_2 are equal, then

$$\frac{V_2}{V_1} = \frac{j\omega CR}{1-2\omega^2 LC + (1-\omega^2 LC)\, j\omega CR} \qquad \ldots\ (5.2)$$

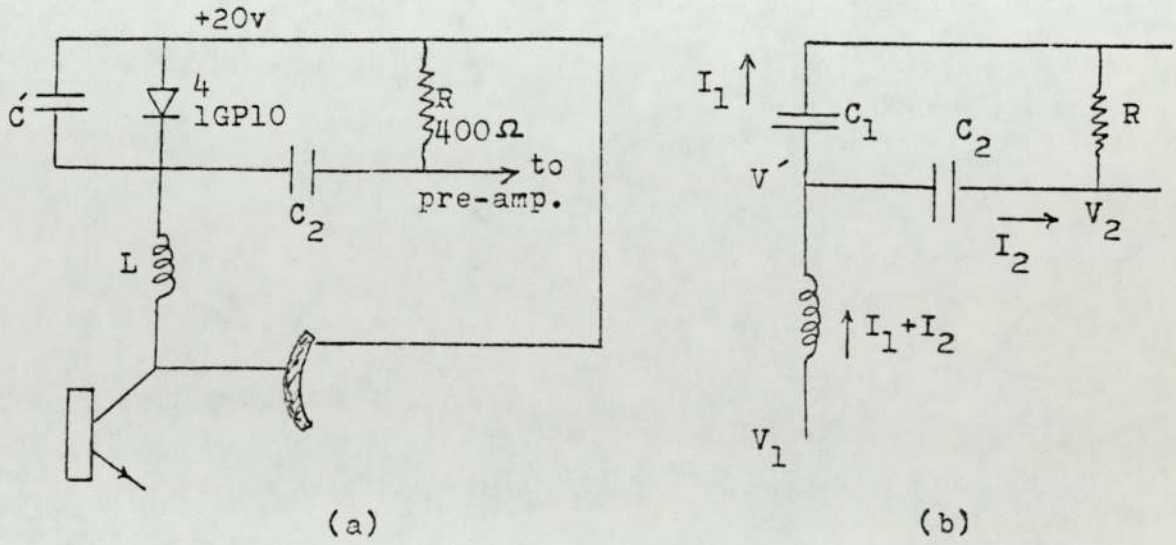

Fig. 5.6 The coupling circuit between the transmitter and the receiving pre-amplifier.

If $\omega^2LC=1$ at 10 MHz, then the ratio V_2/V_1 at this frequency is given by:

$$\frac{V_2}{V_1} = \frac{j\omega CR}{-1}$$

Substituting the values of $L=3\times10^{-6}$H, C=84pF, and R=400 Ω then the value of ωCR at 10 MHz is equal to 2.12. Therefore, at any other frequency, n×10 MHz, the ratio V_2/V_1 is given as follows:

$$\frac{V_2}{V_1} = \frac{2.12\ n}{1-2n^2+(1-n^2)\times 2.12nj} \qquad \ldots\ (5.3)$$

The modulus of this complex number is given by:

$$\left|\frac{V_2}{V_1}\right| = \frac{2.12n}{\sqrt{(1-2n^2)^2+(2.12n)^2(1-n^2)^2}} \qquad \ldots\ (5.4)$$

The values of the ratio V_2/V_1, as given by Eq.(5.4) have been calculated for different values of n. The results are plotted against the corresponding frequencies, as shown in Fig.(5.7).

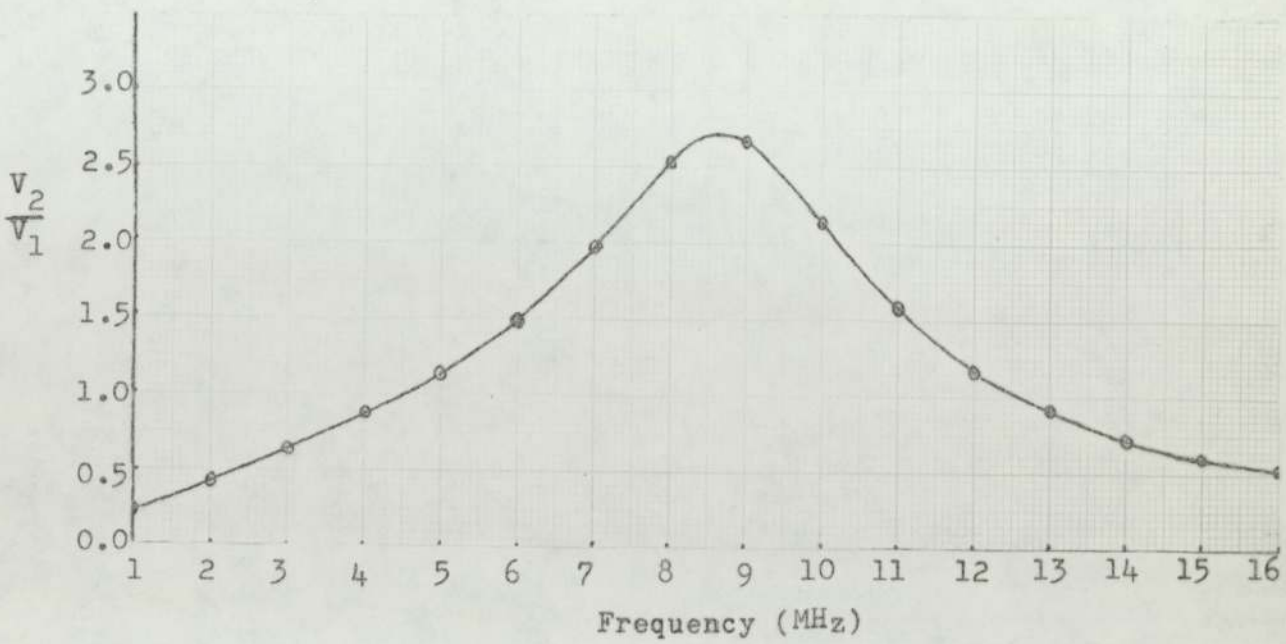

Fig. 5.7 Frequency bandwidth during the receiving period.

5.4.1 Consideration of Damping

For optimum damping V_2 must fall as rapidly as possible after the cessation of the reflected wave-train. The damping effect of the system will be determined, assuming that C_1 and C_2 are equal (Figure 5.6). From equation 5.1, the value of V_1, if C_1 and C_2 are the same and equal to C, is given by:

$$V_1 = \left\{ jwL(2 + jwCR) + \left(R + \frac{1}{jwC}\right) \right\} I_2 \qquad \ldots\ldots\ldots (5.5)$$

$$= \left\{ RC^2L\,(jw)^3 + 2LC\,(jw)^2 + RC\,(jw) + 1 \right\} I_2/jwC \qquad \ldots\ldots\ldots (5.6)$$

If $V_1 = o$, equation (5.6) may be written as

$$(RC^2LD^3 + 2LCD^2 + RCD + 1)\, I_2 = o$$

where $jw = D$

Substituting for the values of R, C and L, where $R = 400\,\Omega$, $C = 84pF$, and $L = 3\mu H$, then we have:

$$8.46 \times 10^{-24}\, D^3 + 5.04 \times 10^{-16}\, D^2 + 3.36 \times 10^{-8}\, D + 1 = o$$

Let $10^{-8}\, D = x$, then

$$8.46\, x^3 + 5.04\, x^2 + 3.36\, x + 1 = o$$

This equation may be divided by $(x + 0.375)$ to give the following quadratic equation

$$8.46\, x^2 + 1.8675\, x + 2.66 = o$$

or

$$x^2 + 0.2207x + 0.3144 = o$$

The solution of this equation is given by:

$$x = -0.1103 \pm \sqrt{(0.1103)^2 - 0.3144}\,, \text{ i.e.,}$$

$$x = -0.1103 - 0.55j\,, \text{ or,}$$

$$x = -0.1103 + 0.55j$$

Therefore:

$$D = jw = -0.375 \times 10^8$$

$$\text{or} \quad = (-0.1103 + 0.55j) \times 10^8$$

$$\text{or} \quad = (-0.1103 - 0.55j) \times 10^8$$

Let us put $0.375 \times 10^8 = \alpha$; $0.1103 \times 10^8 = p$; and, $0.55 \times 10^8 = q$; then

$$V_2 = Ae^{-\alpha t} + Be^{(-p+jq)t} + Ce^{(-p-jq)t}$$

$$= Ae^{-\alpha t} + e^{-pt} (Be^{jqt} + Ce^{-jqt})$$

$$= Ae^{-\alpha t} + e^{-pt} G \cos (qt + \phi)$$

Substituting the values of α, p & q, this equation may be written as:

$$V_2 = Ae^{-0.375 \times 10^8 t} + Ge^{-0.1103 \times 10^8 t} \cos (0.55 \times 10^8 t + \phi) \ldots \ldots \ldots \ldots (5.7)$$

In one half cycle of the signal principal frequency (6.85 MH_Z), i.e. $\frac{10^{-6}}{13.7}$ second, we have:

(a) The first term of equation (5.7), which represents an exponential decay, is reduced by a factor

$$e^{-0.375 \times 10^8 \times \frac{10^{-6}}{13.7}} = e^{-2.73} = 0.064$$

(b) In the same time the amplitude of the second term, which represents an oscillation decay, is reduced by a factor:

$$e^{-0.1103 \times 10^8 \times \frac{10^{-6}}{13.7}} = e^{-0.81} = 0.45$$

For critical damping, the attenuation in one half-cycle of the principal frequency (6.85 MH_Z) can be calculated as follows:

$y = (D^2 + 2kD + \omega^2)y_o = o$, from which:

$$D = -k \pm \sqrt{k^2 - \omega^2}$$

If $k = \omega$ at critical damping, then

$D = -k = -\omega$, therefore

$$y = Ae^{-\omega t} + Bte^{-\omega t} = (A + Bt)\, e^{-\omega t} \qquad .....(5.8)$$

$$\frac{dy}{dt} = -\omega (A + Bt)\, e^{-\omega t} + Be^{-\omega t} \qquad .....(5.9)$$

If $dy/dt = o$ for $t = o$, then from equation (5.9), we have

$$-\omega A + B = o, \text{ or}$$

$$B = \omega A = 2\pi fA = 2\pi A/\tau$$

where, τ is the time of each cycle (i.e., $\frac{10^{-6}}{6.85}$ sec.)

Substituting the value of B into equation (5.8), therefore

$$y = A\left(1 + \frac{2\pi t}{\tau}\right) e^{-\omega t} = A\left(1 + \frac{2\pi t}{\tau}\right) e^{-\frac{2\pi t}{\tau}}$$

Since, for a half cycle $t/\tau = \frac{1}{2}$, therefore

$$y = A\,(1 + \pi)\, e^{-\pi}$$

Thus, for critical damping, the attenuation in one half cycle is given by the following factor:

$$(1 + \pi)\, e^{-\pi} = 4.14\, e^{-3.14} = 0.179 \approx 0.18$$

The damping is not as good as critical damping but it is acceptable.

5.5 Pre-amplifier Isolator

Considerable difficulty was experienced in providing isolation of the transmitted signal pulse from the pre-amplifier. Some circuits were tried with FETS, but trouble was experienced with spikes resulting from the operation of the gate voltages. The circuit which found to be satisfactory is that shown in Fig.5.8. The pulse P14 is applied to the gate of F1 so it will be cut off during the receiving period, from t=146 to t=276μs, and it will be conducting at other times. While F1 is in its conduction mode, it provides the bias making transistor T1 conduct. The function of T1 is to provide a short circuit, i.e. a low resistance path, for unwanted signals during periods other than the receiving period.

The signal applied to the gates of F2 and F3 is derived from the pulse P17. This means that F2 and F3 will be cut off during the transmission period (from t=o to t=146), then they start conducting until the start of next transmission period.

Two pre-amplifier isolators have been built, each one is located in its corresponding pre-amplifier housing.

5.6 Receiving Amplifying Circuits

The returning echoes from bone and reference rod, are received by the corresponding transducer at delay times pro-

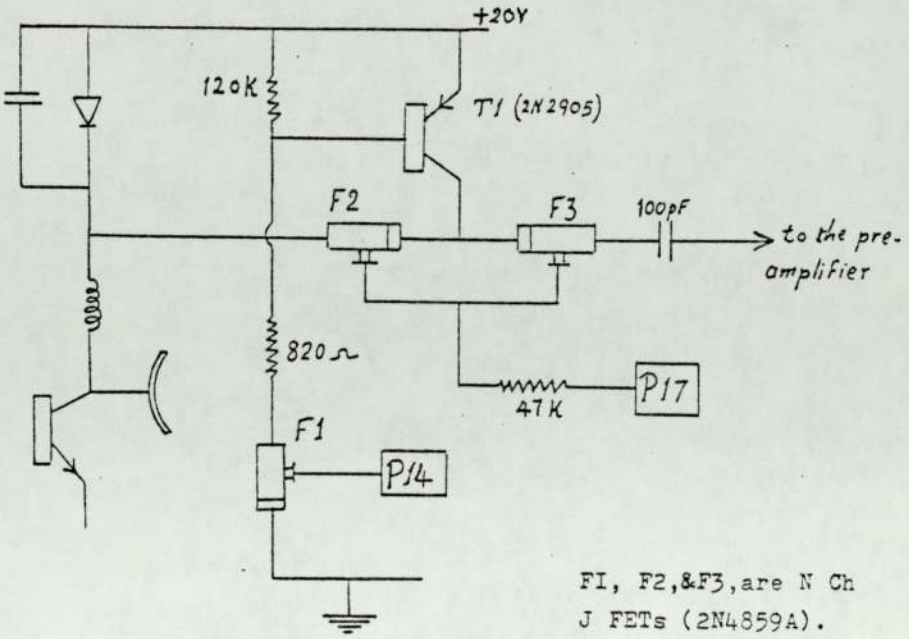

Fig.5.8. Pre-amplifier Isolator

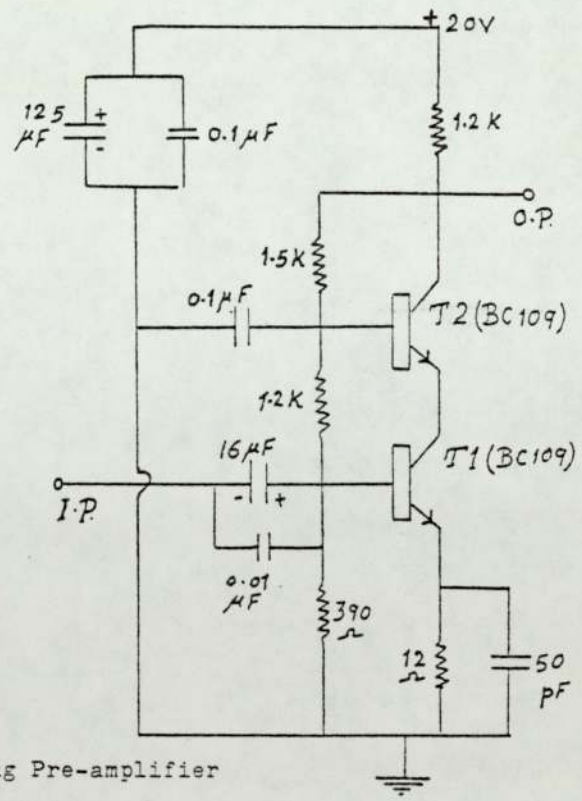

Fig. 5.9. Receiving Pre-amplifier

portional to the path length traversed. About 10-15μs worth of the start of the wave-train signals are chopped by the pre-amplifier isolators, allowing the remaining tail end of each signal (i.e. from t=146 to t=276μs) to be fed into the corresponding amplifying circuit. Both signals are amplified separately by two similar amplifying circuits, each consists of a pre-amplifier, an integrated circuit, a single stage amplifier and a high voltage pulse output stage.

5.6.1 The Pre-amplifier

The tail ends of the received signals from bone and reference system are amplified separately by two similar pre-amplifiers. Each consists of two npn transistors, T1 and T2, connected in cascade as shown in Fig. 5.9. The bandwidth of each pre-amplifier is about 1-15 MHz. The received signal from each transducer can be about 1/400vp.p. The gain of each pre-amplifier is about 18-20, giving an output of about 0.05v p.p. The output of the pre-amplifier of the reference system is fed into an integrated circuit with a fixed bias (Fig. 5.10). The output of the pre-amplifier of the bone system is fed into a similar integrated circuit, but with a variable bias (Fig. 5.11).

5.6.2 The Integrated Circuits

Two similar wideband (up to 20 MHz) integrated circuits with AGC (MC1590G) are used, each located in a separate housing. One integrated circuit "I" with a fixed bias is

used for the signals of the reference system, (Fig. 5.10), and the other "II" with a variable bias for the signals of the bone system (Fig. 5.11). The series of resistors, shown in Figs. (5.10) and (5.11), are made to provide the necessary bias for the integrated circuits.

The purpose of the integrated circuit "I" with a fixed bias (Fig. 5.10) is to provide a standard gain, giving an output of about 0.5v peak to peak.

The integrated circuit "II" (Fig. 5.11), provides a gain control that compensates for the difference in voltage amplitudes, which may appear at the end of the amplification, of the two signals from bone and reference system. If the signal from bone is greater than that from the reference system, the difference between them will give rise to positive d.c. signal at the point B in the discriminator circuit (see Fig. 5.14). This positive d.c. signal is fed into the point E (the source of F1) shown in Fig. (5.11).

The voltage at the point E is applied to the gate of F3 during the period when F1 and F2 are conducting (t=o to t=240μs), as a result of the negative going pulse P8. F3 function as a source follower amplifier whose output is directly connected to the integrated circuit.
When F1 and F2 cease to conduct, the gate potential of F3 is maintained, until after the event has been observed, by the 50pF capacitor. The gain of the integrated circuit varies according to the d.c. bias as shown by Fig(5.12).

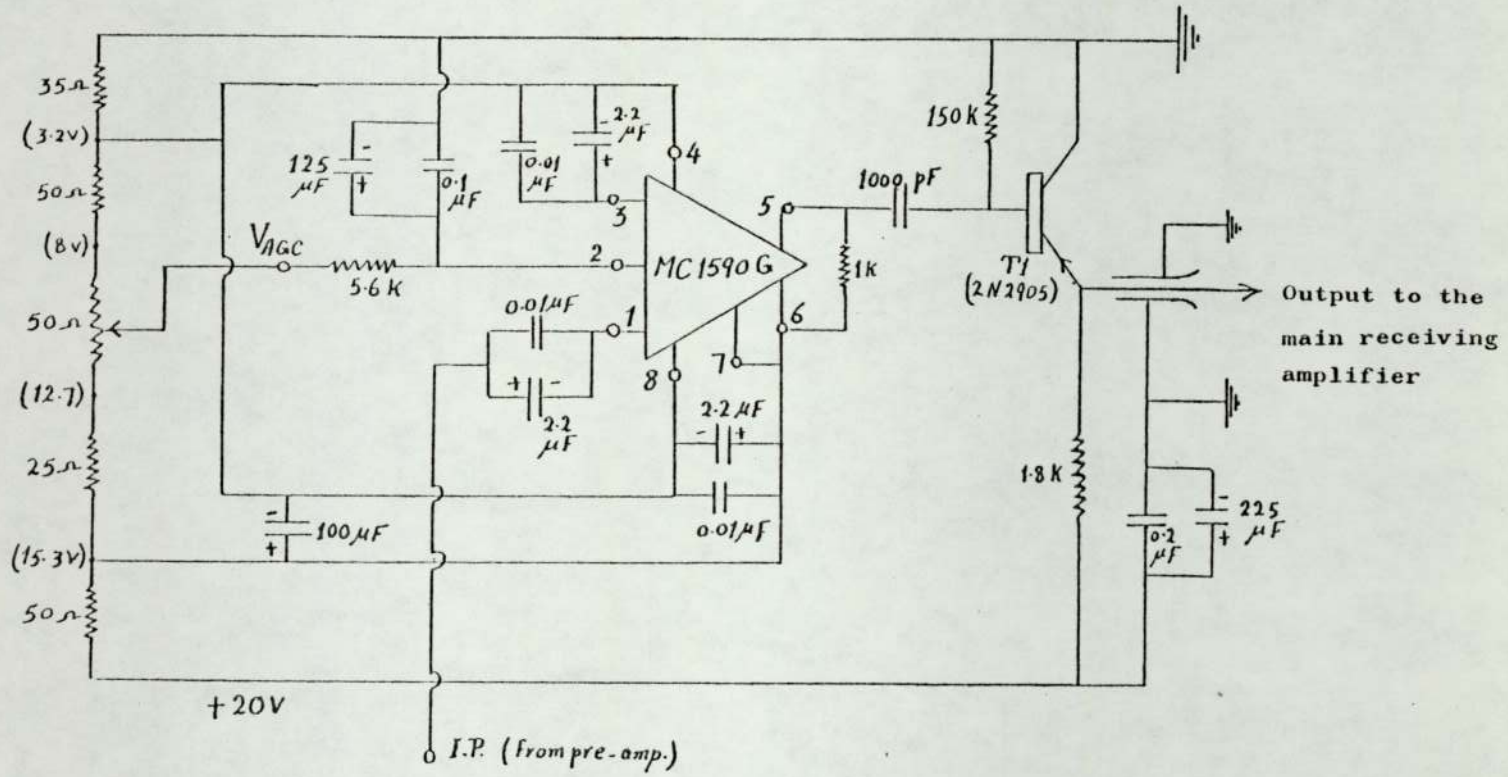

Fig. 5.10 Integrated circuit I (fixed bias).

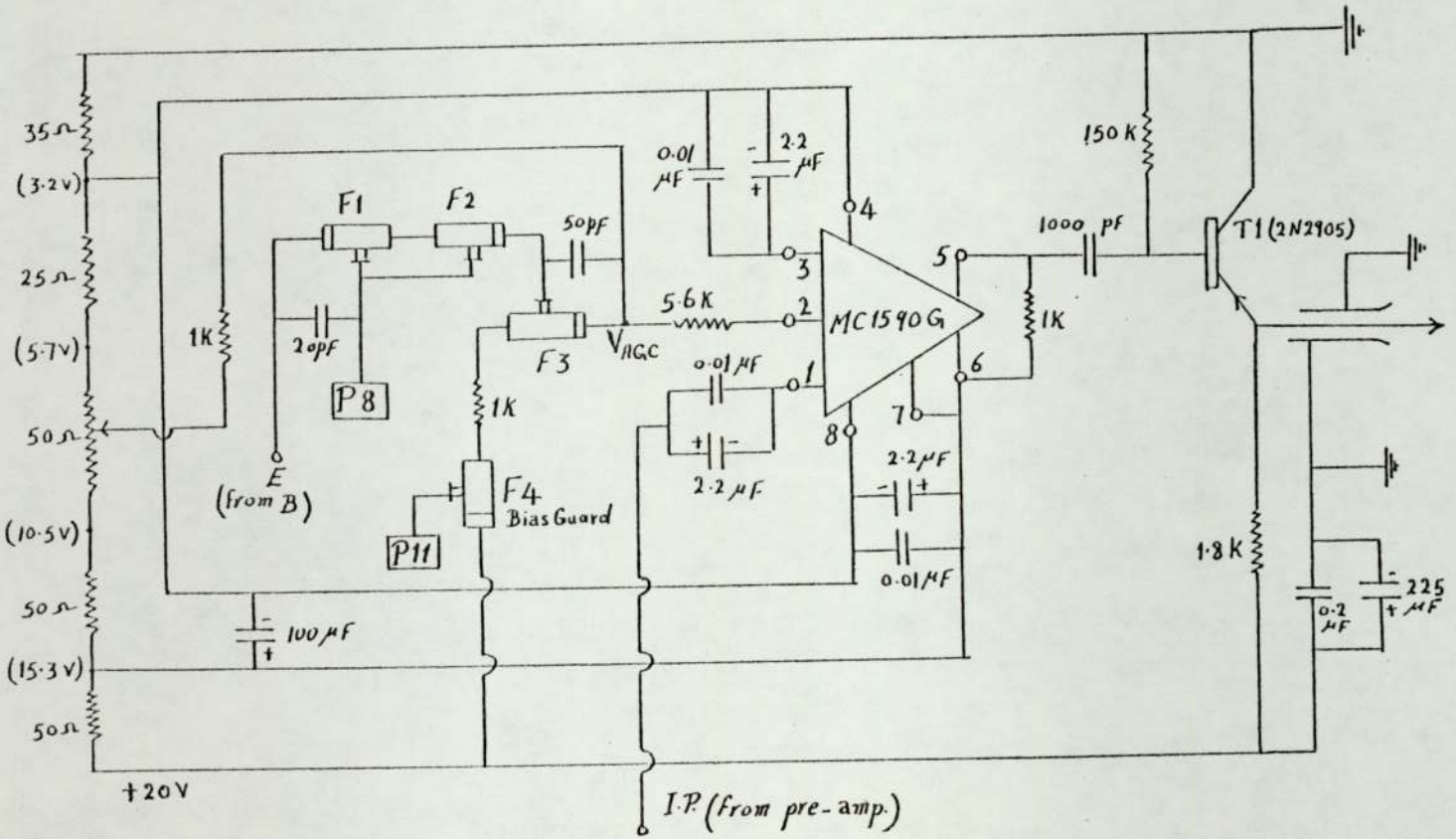

Fig. 5.11 Integrated circuit with a variable AGC bias, for the bone system.

F1, F2,&F4, Pch FETs (3N157A); F3, NChJFET(2N3821)

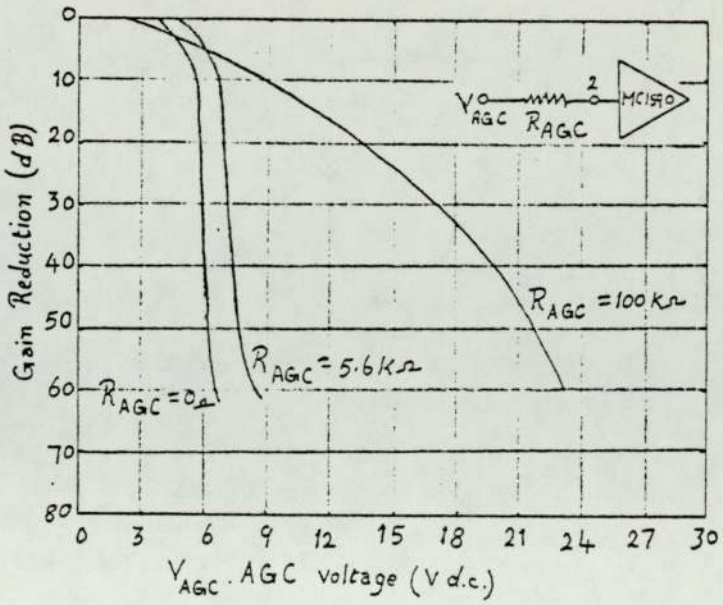

Fig. 5.I2. Gain reduction versus AGC voltage ,for MCI590G (after Motorola).

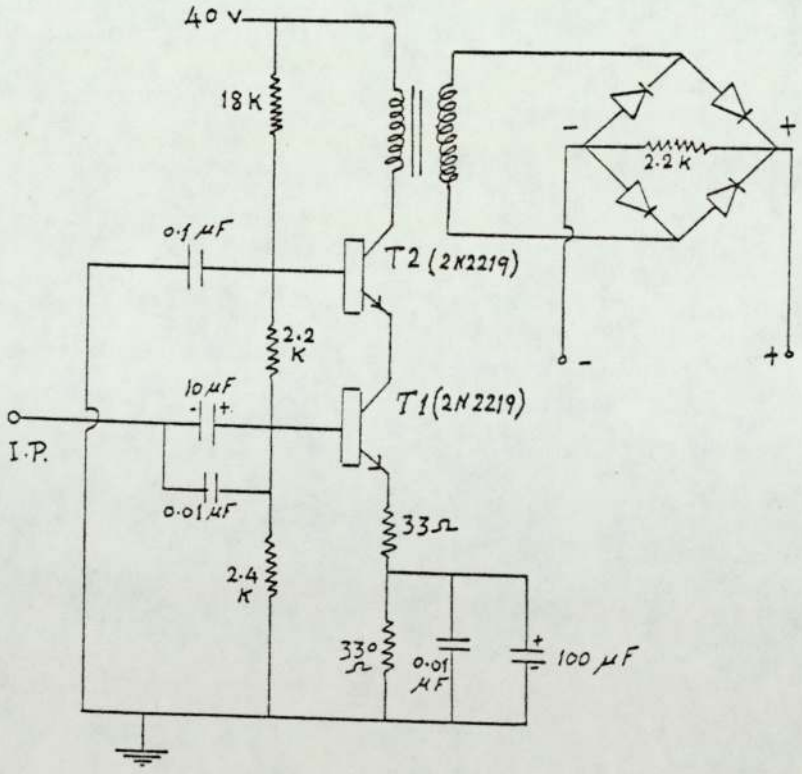

Fig. 5.13 Final Receiving Amplifier.

The output of each integrated circuit is fed into a single transistor amplifier T1 (as shown in Figs. 5.10 and 5.11), whose output is fed into a final stage amplifier.

5.6.3 The Final Stage Amplifier

Two similar amplifiers have been constructed, each located in a separate housing. The gain of each amplifier is about 28. The circuit of the final stage amplifier is illustrated in Fig. (5.13), which consists of two npn transistors T1 and T2, connected in cascade in the similar way as in the case of the pre-amplifier. The supplying voltage in this case is +40v d.c., which is obtained from an auxillary power pack, shown in Fig. (5.16).

The output of each amplifier feeds a transformer, whose primary coil is connected to the collector of T2. The secondary coil of the transformer is connected to a full-wave rectifying bridge which can give about 6-7v d.c. across 2.2kΩ.

5.7 The Discriminator

After the received signals from bone and reference system have been amplified by means of two separate matching receiving amplifying stages, they are rectified separately by two similar full-wave rectifying bridges. The negative ends of the two rectifying bridges are connected together and the positive ends are connected to the points A and B in the

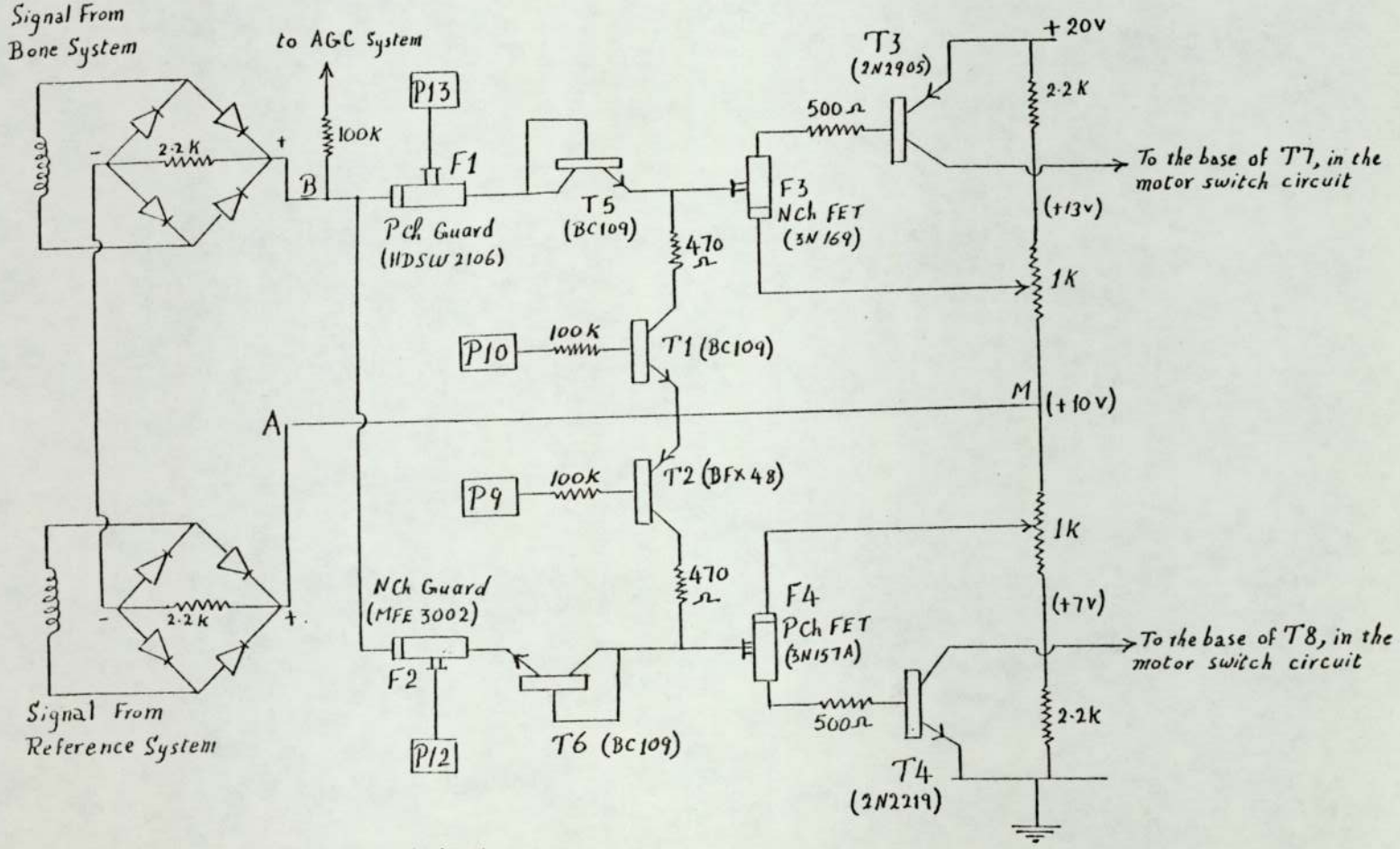

Fig. 5.14 The Discriminator

discriminator circuit, as shown in Fig.(5.14).

In the discriminator, the two FET guards F1 and F2 are in their conduction mode during the receiving period, t=146 to t=276μs, by the signals applied to their gates, which are derived from the pulses P13 and P12 respectively.

The npn transistors(BC109) T5 and T6 act as diodes, where the base of each is connected to its collector. The leakage of these transistors is lower than any diode. The npn and pnp transistors T1 and T2 are conducting during the period t=o to t=240μs, by means of the signals applied to their bases, which are derived from the pulses P10 and P9 respectively. During this period no signal can be applied to F3 and F4.

The function of the discriminator is explained as follows: After t=240μs until the start of the next cycle at t=o both transistors T1 and T2 are in the non-conducting state since their bases and emitters are at the same potential, (i.e. + 10v.) During the period t=240μs to t=276, both guard FETS, F1 and F2 are in their conducting mode due to the pulses P13 and P12 applied to their gates. Suppose that the returning echo from the bone surface arrives earlier than that of the reference system. The positive sharp spike at the tail end of the bone signal will be conducted through the pch guard FET "F1" and the diode transistor T5 to the gate of the Nch FET "F3" making the latter and hence the pnp transistor T3 conduct. When this happens the potential of the mid-line

"AM" becomes more positive so that the pnp transistor T2 conducts while the npn transistor T1 is still cut off. The output at the collector of T3 is fed into the base of npn power transistor T7, in the motor switch circuit (Fig.5.15), causing the motor to rotate so as to drive the scanning transducer away from the bone surface.

On the other hand, if the echo returning first is that from the reference rod, the negative sharp spike will be conducted through the NCh guard FET "F2" and the diode transistor T6 to the gate of the PCh FET "F4" making the latter and also the npn transistor T4 conduct. Then the potential of the mid-line becomes now more negative so that the npn transistor T1 conducts while the pnp transistor T2 is till cut off. The output at the collector of T4 is fed into the base of pnp power transistor T8 in the motor switch circuit (Fig.5.15), causing the motor to rotate so as to drive the scanning transducer towards the bone surface.

5.8 The Motor Switch Circuit

A motor whose armature has a little moment of inertia, is used to drive the scanning transducer towards and away from the bone surface according to the signal derived from the discriminator. The field coil current is always in the same way. The direction of the current through the armature and hence its direction of rotation is controlled by the motor switch circuit (Fig. 5.15), which acts as a double switch.

The motor switch circuit is a four transistor bridge which consists of two pairs of complementary npn and pnp power transistors. The applied signal from the discriminator makes one pair of transistors conduct, while the other pair are cut off allowing the current to flow through the armature in one way and consequently it rotates in one direction. When the process is reversed, by the other signal from the discriminator, the current through the armature and the direction of rotation is reversed.

If the early returning signal is that from bone surface, then the pnp transistor T3, in the discriminator conducts applying a positive signal on the base of the npn power transistor T7, in the motor switch circuit (Figure 5.15). This positive signal makes T7 and consequently T9 conduct, allowing the current to flow in the armature in the "ba" direction. The motor then rotates so as to drive the scanning transducer away from the bone surface. On the other hand, if the early signal is that from the reference system, the npn transistor T4, in the discriminator conducts applying a negative signal on the base of the pnp power transistor T8, in the motor switch circuit. This negative signal makes T8 and consequently T10 conduct allowing the current to flow in the armature in the direction "ab". The motor then rotates so that it moves the scanning transducer towards the bone surface.

A resistor, 17Ω, is connected across the motor to provide dynamic electric damping. Also, any sudden voltage which appears across the motor, may find a leak through this resistor.

A condenser, 2μF, is connected across the motor in order to stop sparking at the brushes. No supply is available to the motor until a control button operating a relay is pressed.

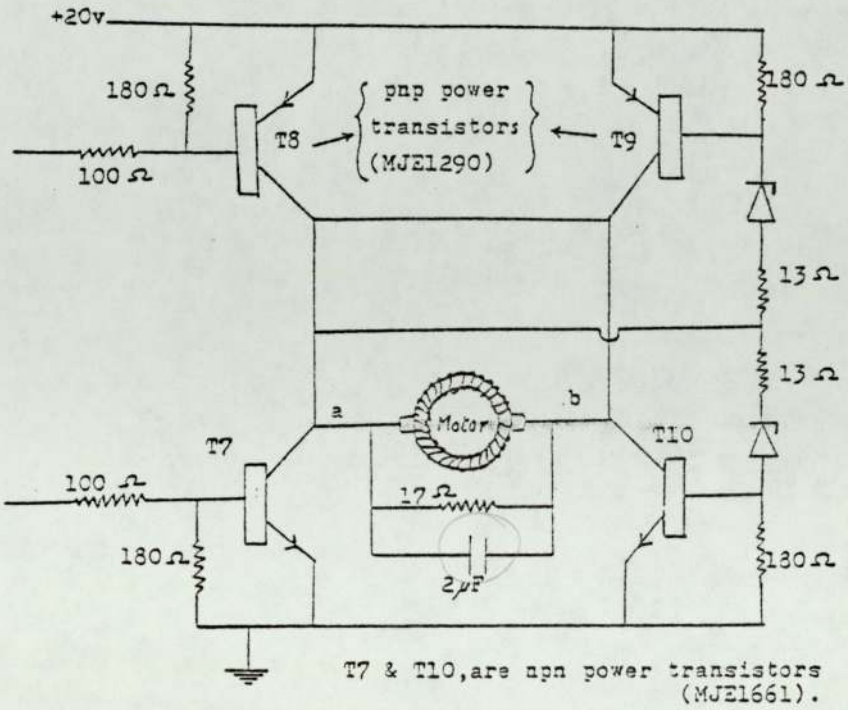

Fig. 5.15 The motor switch circuit.

5.9 The Voltage Supplies

Three supplying d.c. voltages, + 20v, 40v and -9v are used in the electronic circuits of this apparatus. The + 20v supply is used for most of the electronic circuits and also in the auxillary power pack which is constructed to provide the other supplying d.c. voltages i.e. +40v and -9v. The +40v supply is used for the receiving amplifiers. The -9v supply is used in the pulse repetition frequency generator (circuit V, in Figure 5.2), in order to provide the pulses P14, P15 and P16 which vary between 0 and -9v as shown in Figure 5.3.

5.9.1 The +20v d.c. Supply

This d.c. supply is achieved from a Farnell stabilised power unit which is operated from the mains supply (240v a.c.). Its output has two terminals. One terminal, the common zero connection is used as earth. The other provides +20v with respect to the common zero connection. This is connected to the rotating system by two large copper strip rings.

5.9.2 Auxillary Power Pack (+40v and -9v d.c. Supply)

This power pack was built in order to convert power from the +20v d.c. of the Farnell unit, to a higher voltage (+40v) and also to a lower d.c. voltage (-9v) with respect to the common zero connection (earth). The circuit of the auxillary power pack is shown in Figure 5.16 . T1 and T2 are npn (BC184L) transistors, which are used as an astable multivibrator where each collector is coupled to the base of the other through a capacitor (1800pF). This astable oscillator generates rectangular waves of frequency about $4kH_Z$. The collector of T2 is directly coupled to the base of T3 (npn transistor, BC184L), which acts as a monostable triggered from the astable circuit. The resultant rectangular oscillations are driven through a power npn transistor (BD121), to the primary coil L_1 of two transformers L_1L_2 and L_1L_3 ,where L_1L_2 is a stepping up transformer and L_1L_3 is a stepping down transformer.

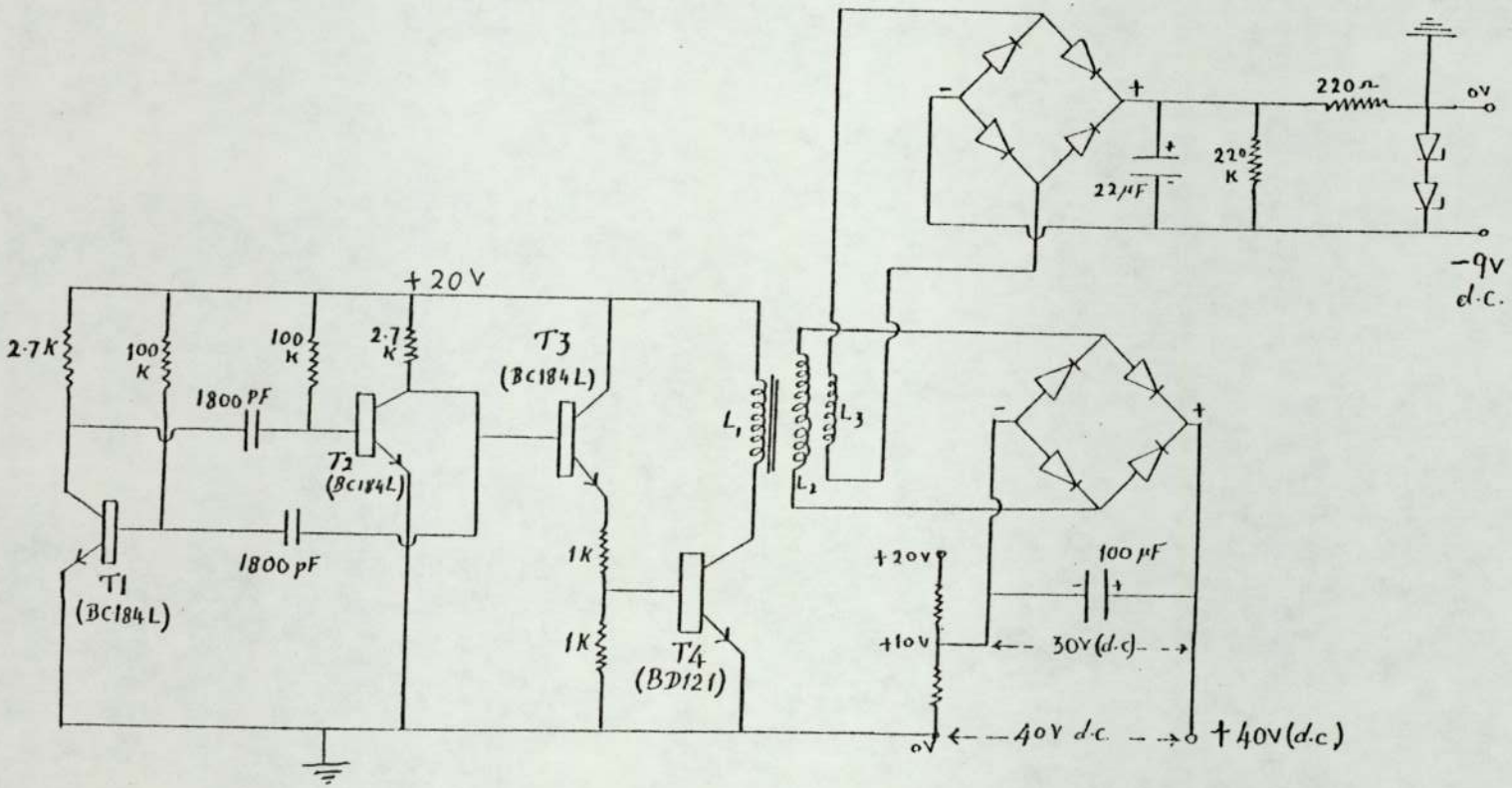

Fig. 5.16 Auxillary power pack (+40 and -9 v D.C)

(a) + 40v d.c. Supply

The oscillations are stepped up in voltage by the transformers L_1L_2, to give a high voltage which is rectified and smoothed by using a full-wave rectifying bridge and capacitor 100μF in order to obtain a high voltage d.c. output about 30-32v. The negative terminal of the bridge is connected to +10v, which is obtained by a potential divider (connected between 0v and +20v of the Farnell unit). The output voltage between the positive terminal of the bridge and the common zero connection, is now 40-42v.

(b) -9v d.c. Supply

The oscillations are stepped down by the transformer L_1L_3 to give a low voltage which is rectified and smoothed by using a full-wave rectifying bridge and a capacitor (22μF), in order to give a low d.c. voltage, about 9v. The positive terminal of the bridge is connected to the common zero connection (earth). The output d.c. voltage between the negative terminal of the bridge and earth is -9v.

CHAPTER VI

MECHANICAL CONSTRUCTION OF THE BONE TOMOGRAPH AND ITS OPERATION

6.1 General Description of the Apparatus

The mechanical construction of the ultrasonic bone tomograph, is shown in pictures (1) to (3), and also illustrates in figures 6.1 to 6.6. The apparatus consists of a rotating dural drum, of two horizontal and parallel discs which are separated by three equi-spaced pillars. The two discs are similar and match each other. The layout of the top and lower discs of the rotating drum, is a mirror image. Holes are provided in each disc for the monitoring motor shaft and for the necessary electrical connections. This motor provides the radial drives described later.

Two similar square dural plates are fixed, horizontally to the frame of the apparatus. The top plate provides a seat for a ball race on which the top disc of the drum rests, as shown in Figures 6.2 and 6.3. The circular movement of the drum is achieved by a motor, which is operated from the mains supply, 240 v a.c. The rotating motor is supplied by on-off, and reversing switches located in a box which is fixed to the frame of the apparatus. The time for each complete rotation (360°) of the drum is about 25 seconds.

At the periphery of each disc of the drum, there is a copper ring for the electrical connections of the d.c. supply.

The upper copper ring is embodied into the top surface of the upper disc for the zero volt connection, where the common zero voltage (earth) is connected to the body of the apparatus. The lower copper ring is insulated from the edge of the lower disc by a thick perspex ring, in order to provide +20v d.c. connection to the electronic circuit elements. The electrical connections to these copper rings are obtained by using silver brush contacts. On the upper disc, the auxillary power-pack is mounted.

On the lower disc, all the electronic circuit elements are mounted. The monitoring motor is mounted vertically between the two discs of the drum. The two ends of the motor shaft are connected to stepping down worm boxes at the other sides of the discs. The worm box, fixed on the top disc, has a ratio of 10:1 whereas that attached to the bottom of the lower disc, has a ratio of 100:1. A long screw (about 22cm) is connected at one end to each worm box, and rests at the other end in a bearing block, as shown in Figure 6.6. On each screw there is a carrier block which transfers the rotation of the screw to radial movements. For accurate monitoring and recording, the carrier movements must be smooth. Therefore, each carrier rests on a guide rod in order to avoid errors due to the carrier twist and bearing play.

The scanning transducer is mounted vertically into an aluminium tube attached to the carrier block at the bottom of the lower disc. The reference transducer is mounted into a similar aluminium tube which is fixed at the bottom of the

lower disc and near to its periphery. A reference metallic rod is fixed at 10cm away from the reference transducer and also at the periphery of the lower disc. Each transducer has a long copper tube (about 17 cm long), which can slide freely into the aluminium tube, for the initial adjustment of the transducers to the required direction and level. The scanning transducer must be directed towards the centre of rotation of the drum, and the reference transducer towards its reference rod. Both transducers and the reference rod are immersed in the same water bath, which is fixed to the frame of the apparatus below the rotating drum as shown in Figure 6.1 and picture (1). After the initial adjustment of the transducers, they are kept fixed in their tubes by means of a captive screw ring at the end of each aluminium tube. The transmitted and received signals to and from each transducer are fed into a coaxial cable, through a hole in the lower disc, to the electronic circuits mounted on this disc above the transducers.

Onto the carrier block at the top of the upper disc of the rotating drum, an L-shaped pen is fixed with its nib pointing upwards. A perspex cover rests on the top of the apparatus frame with a drawing paper attached to its bottom surface so that the paper is over the nib of the pen and just touching it. The circular movement of the drum and also, the linear movement of the top carrier block with the pen are thus registered on the drawing paper, giving an outline cross-section of the examined object. Since the linear movement of the top carrier is 10 times greater than that of the scanning transducer, the resulting outline will be magnified by the ratio 10:1.

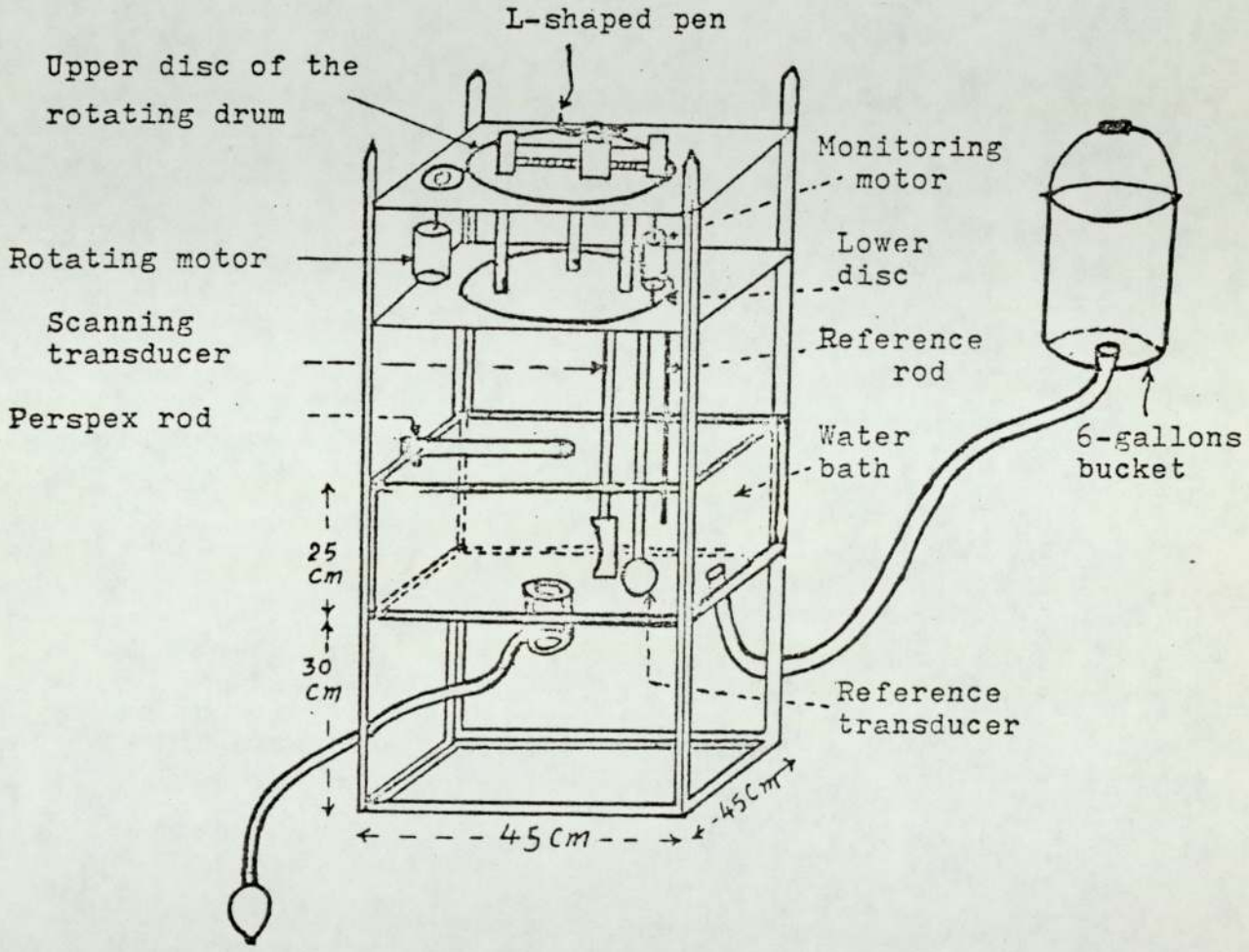

Fig. 6.1 Schematic diagram of the ultrasonic bone tomograph .

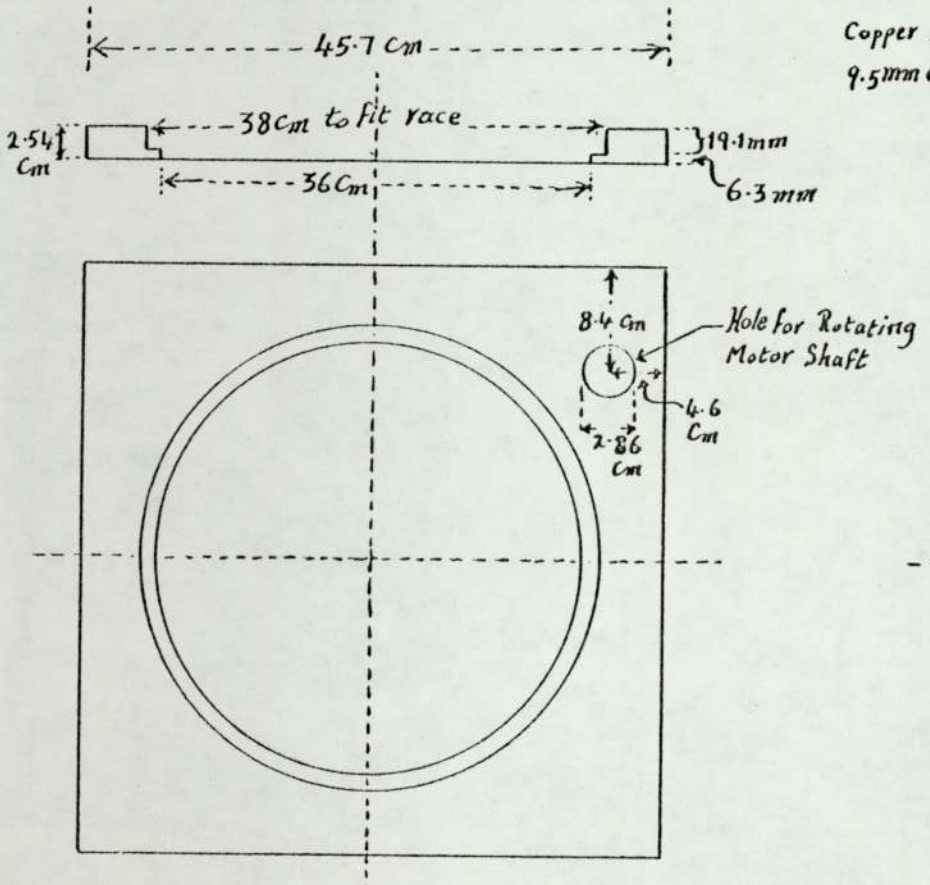

Fig.6.2 Square dural plate which provides a seat for the ball race.

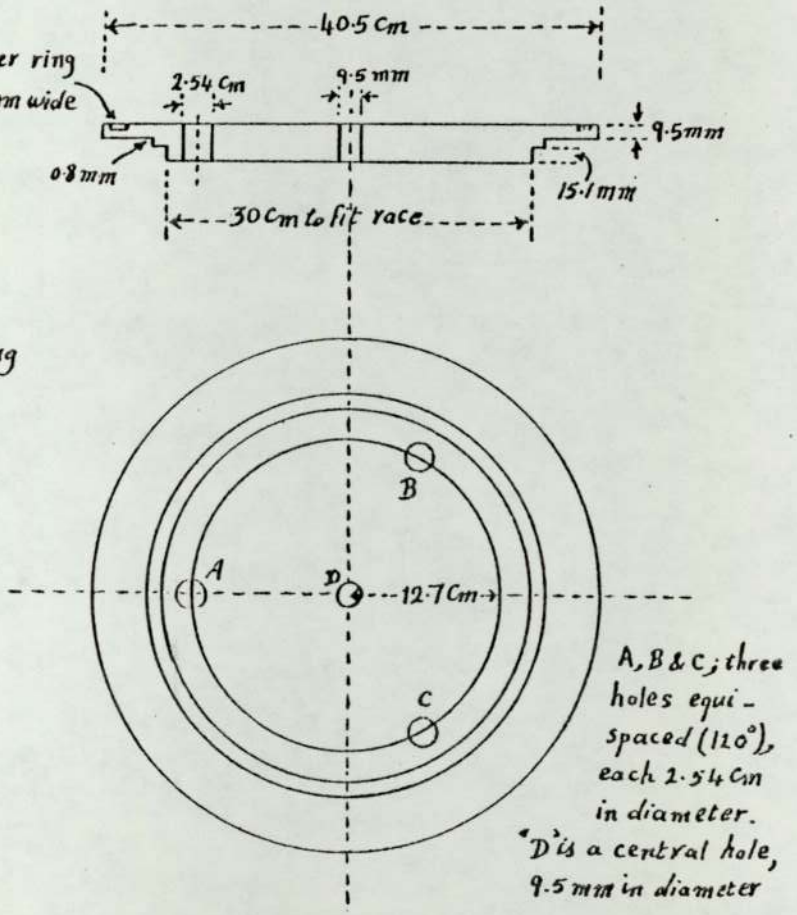

Fig.6.3 View of the top disk

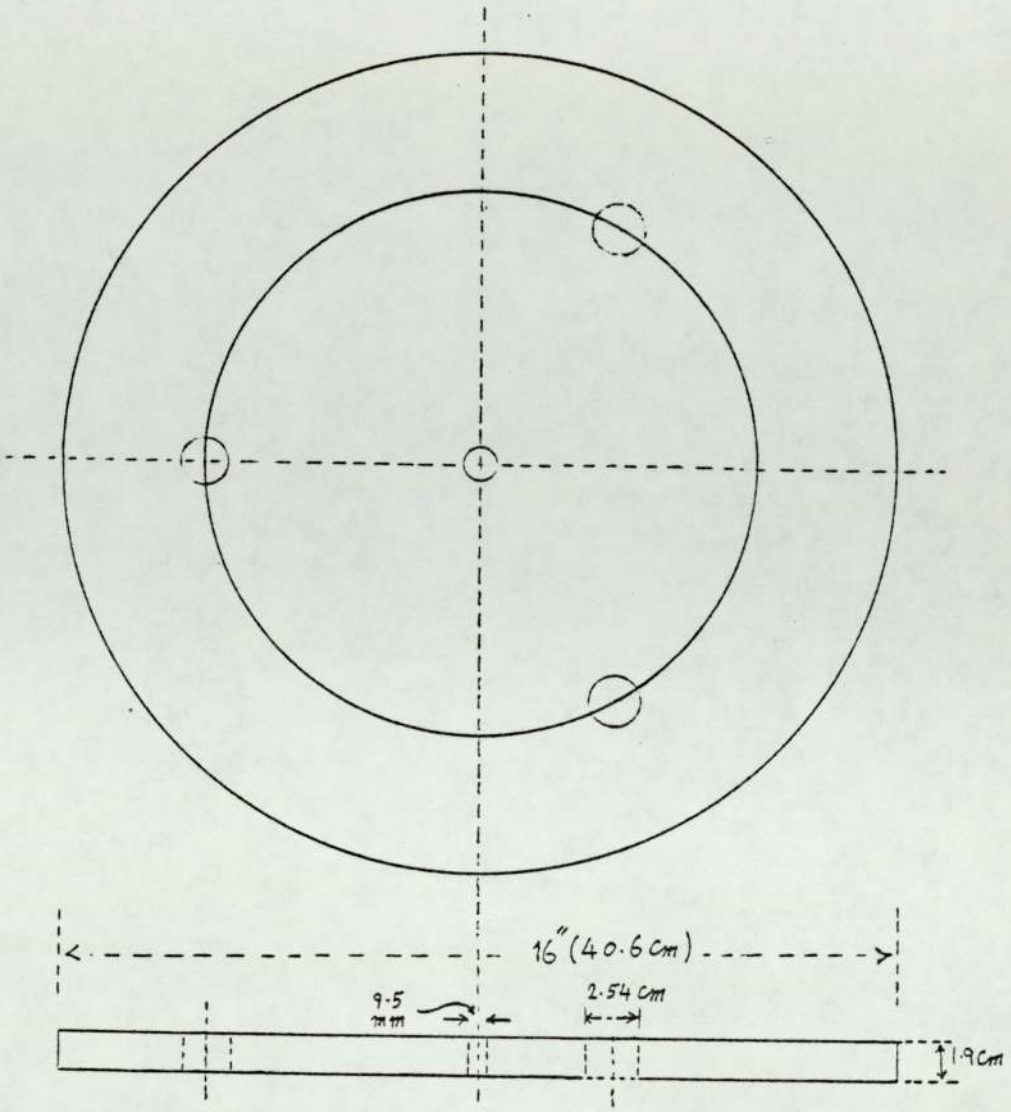

Fig. 6.4. View of the lower disc.

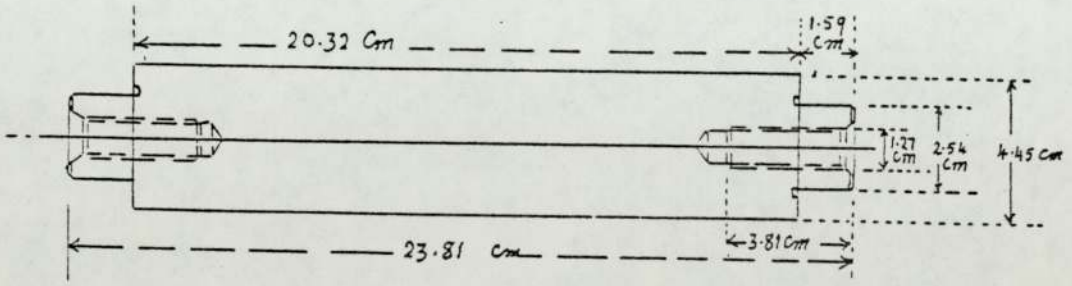

Three off- Dural Pillars

Fig. 6.5. Diagram of the pillars.

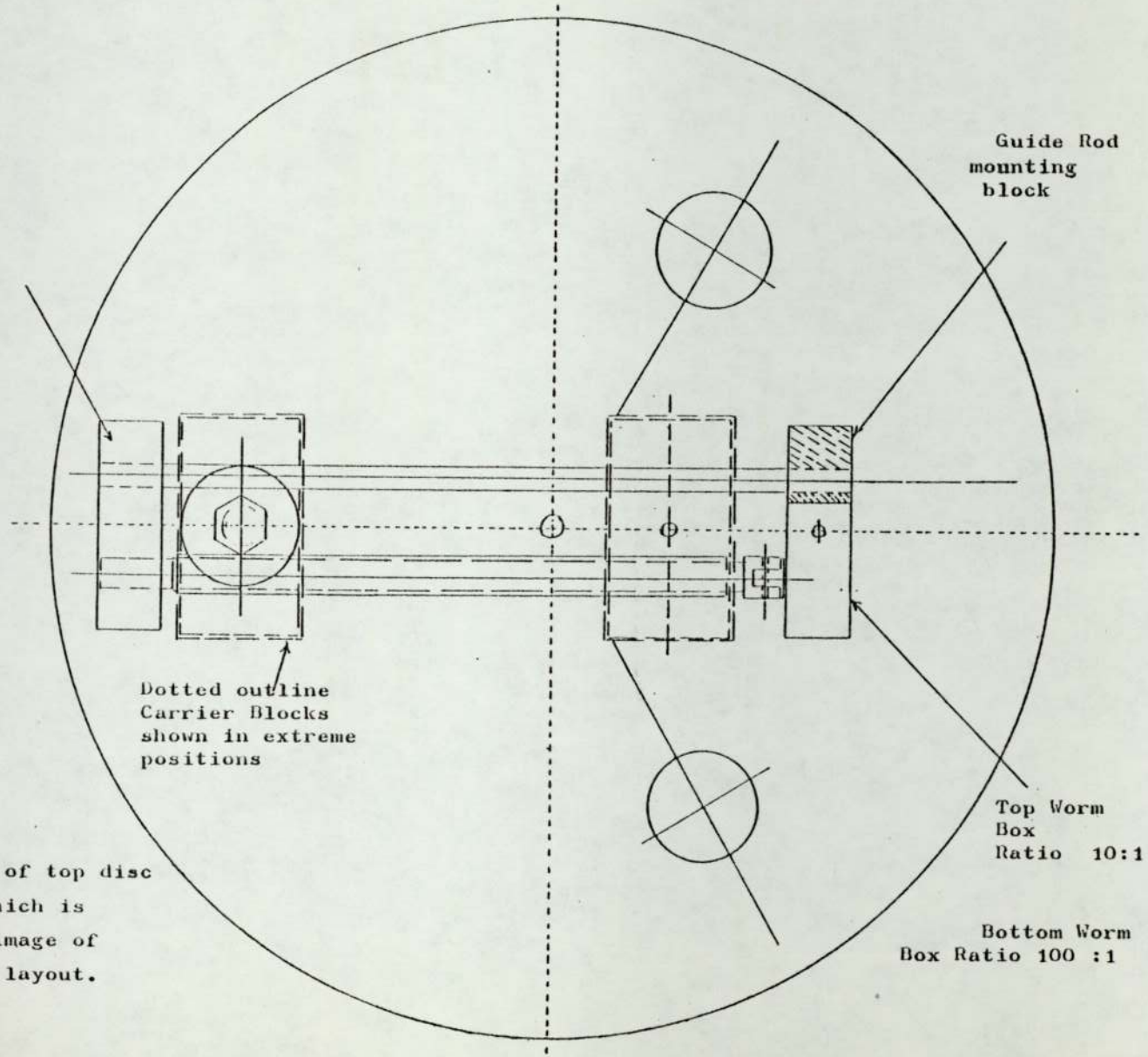

Fig. 6.6 Plan view of top disc layout ,which is a mirror image of lowerdisc layout.

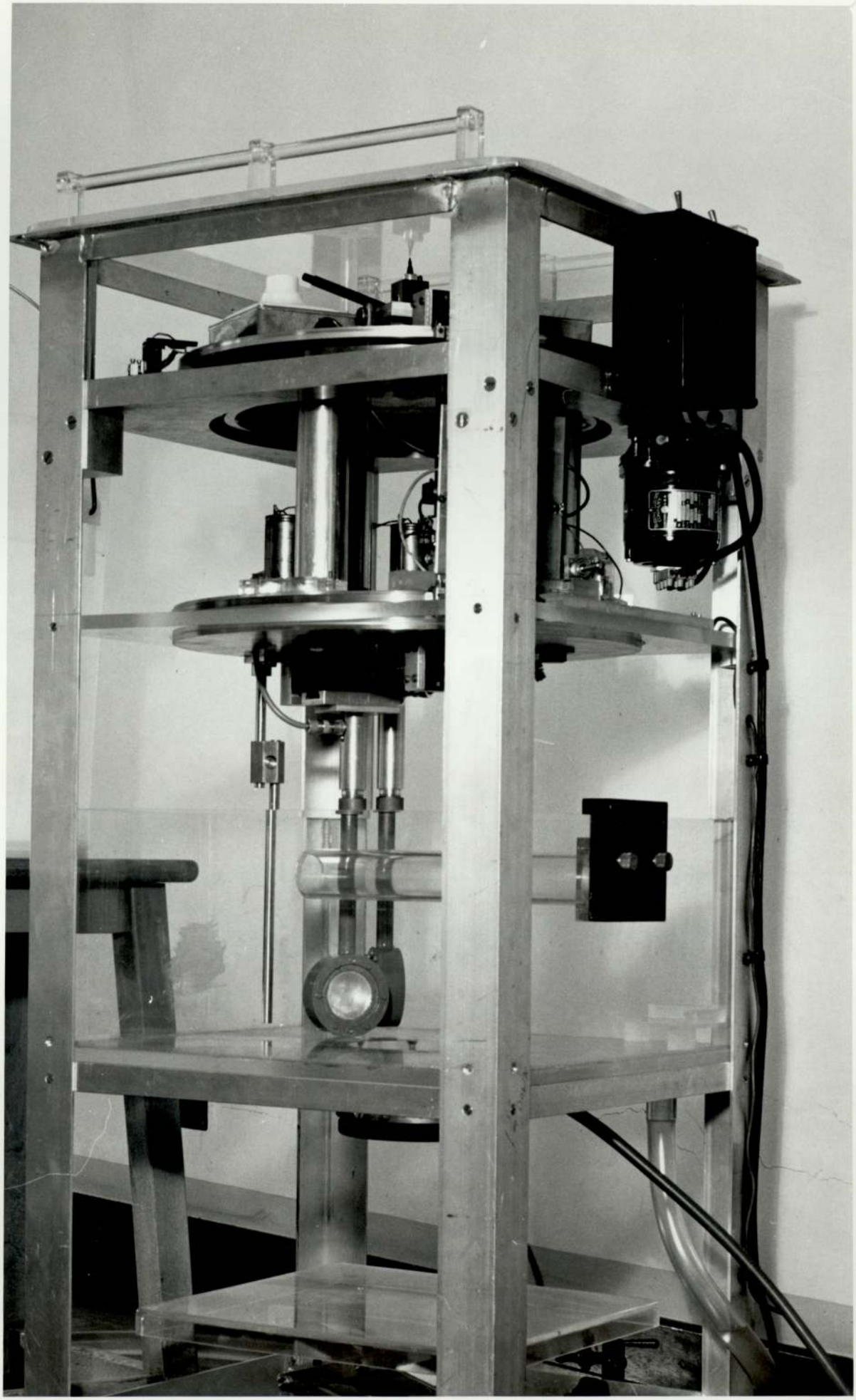

Picture (1) General view of the ultrasonic bone tomograph (electronics absent).

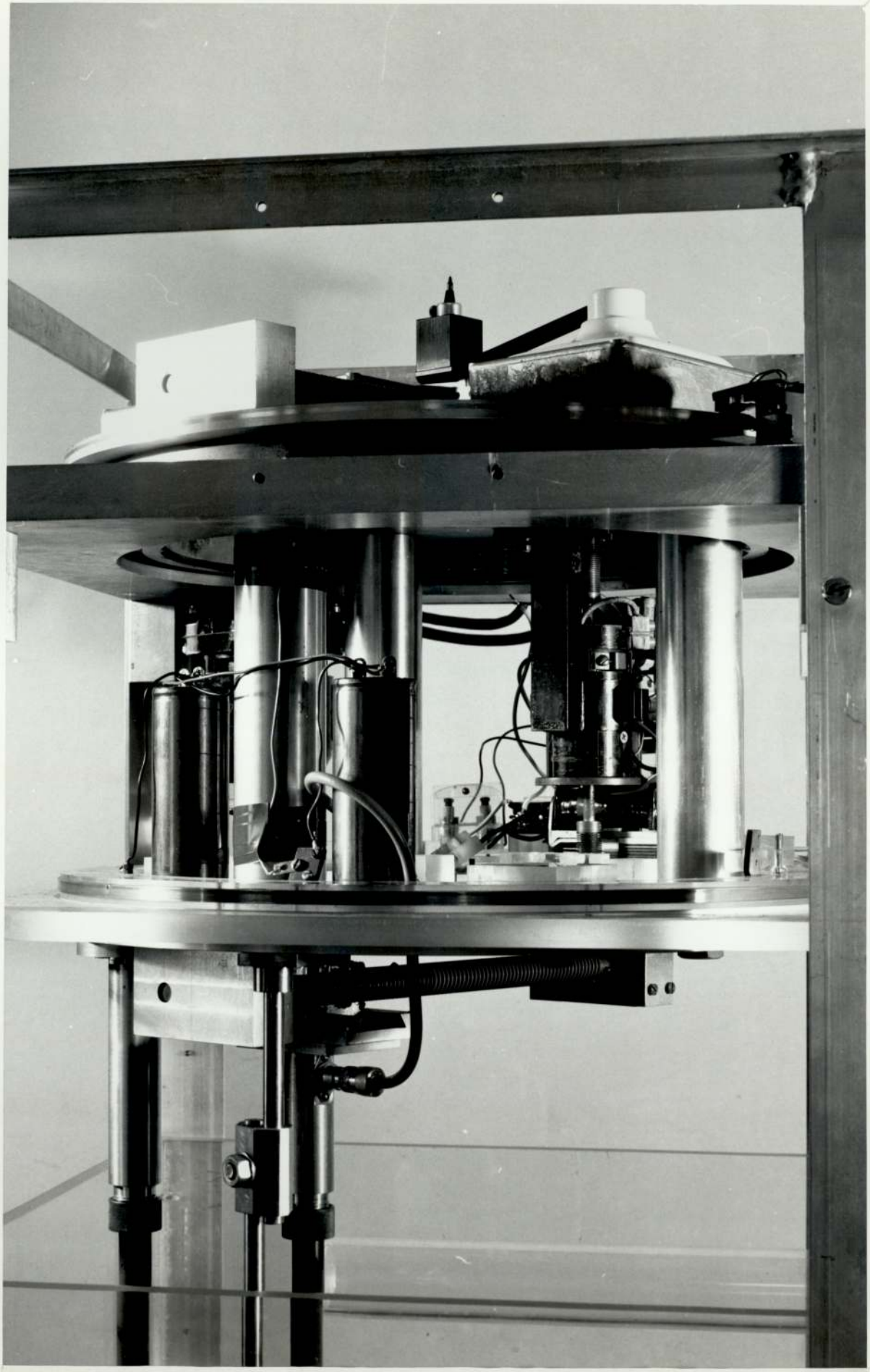

Picture (2) Close up view to show the rotating system (electronics absent).

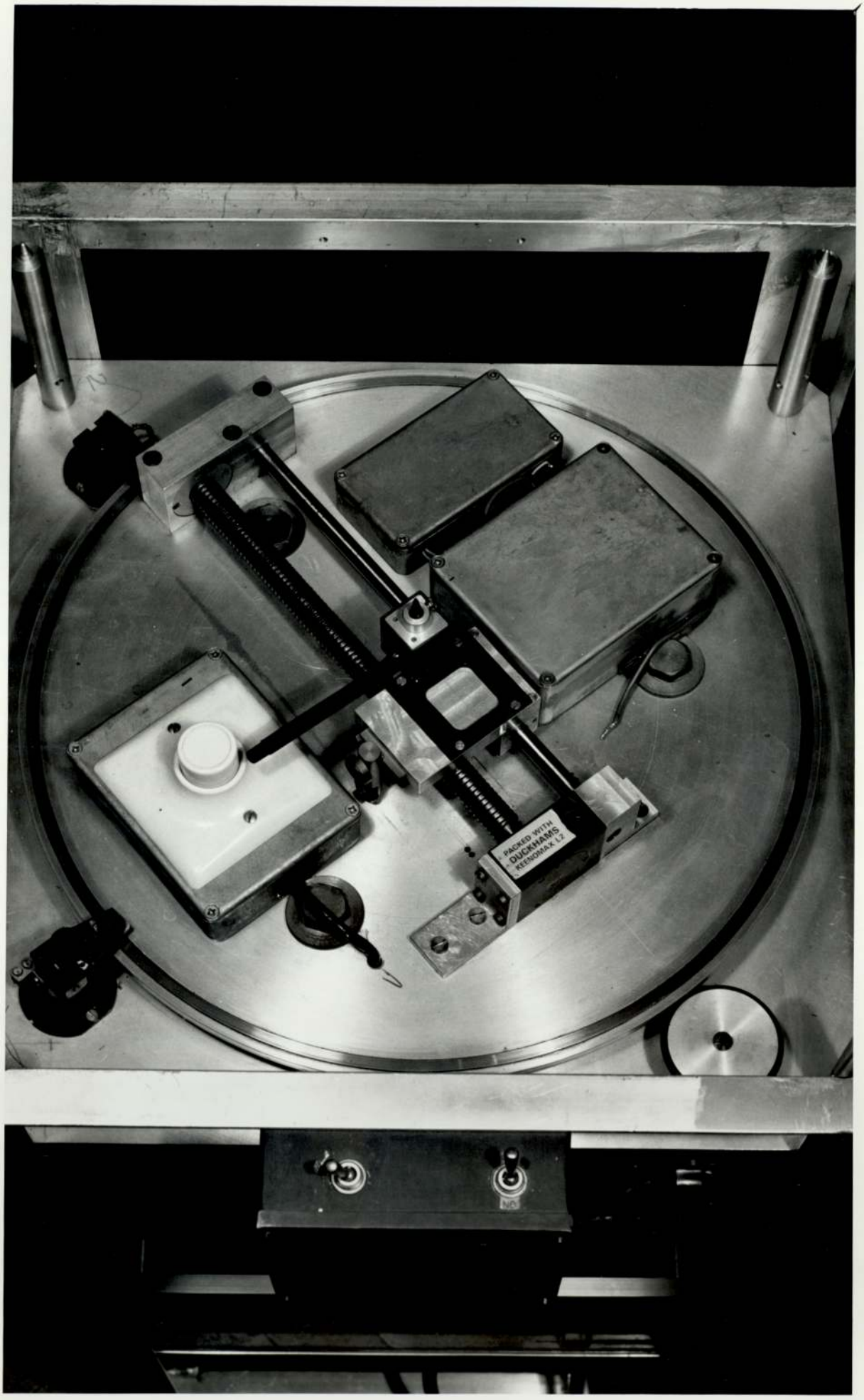

Picture (3) A view of above, showing the pen carriage.

6.2 The Transducer Housing

Both the scanning and reference ceramic bowl transducers are similar and match each other. The diameter of each ceramic bowl transducer is 4.9cm, and its radius of curvature is 10cm. Each transducer is backed with a layer of tungsten-rubber mixture, about 0.8cm thick.

The construction of the housings for both transducers, is the same which is illustration in Figures 6.7 to 6.9 and shown in pictures (4) and (5). Each housing consists of an outside strong brass case and an inside perspex case on which the transducer is mounted, with its back surface insulated from the outside brass case.

The outside case is machined by using a brass cylinder (3.1mm thick, and 7cm inside diameter), which is cut to the required height, 2.3cm. A wide hole was bored in the wall of the cylinder. A long copper tube (about 17cm long) is soldered to the wall of the cylinder and over the hole by using silver solder whose melting point is high (about 800°C). A brass disc with six equi-spaced holes (for 6BA screws) was then soldered to the bottom of the brass cylinder by using a lower melting point solder (such as lead-tin solder, its m.p is 170°C). The heads of the screws were also soldered to the brass disc in order to avoid any water leak to the back of the transducer.

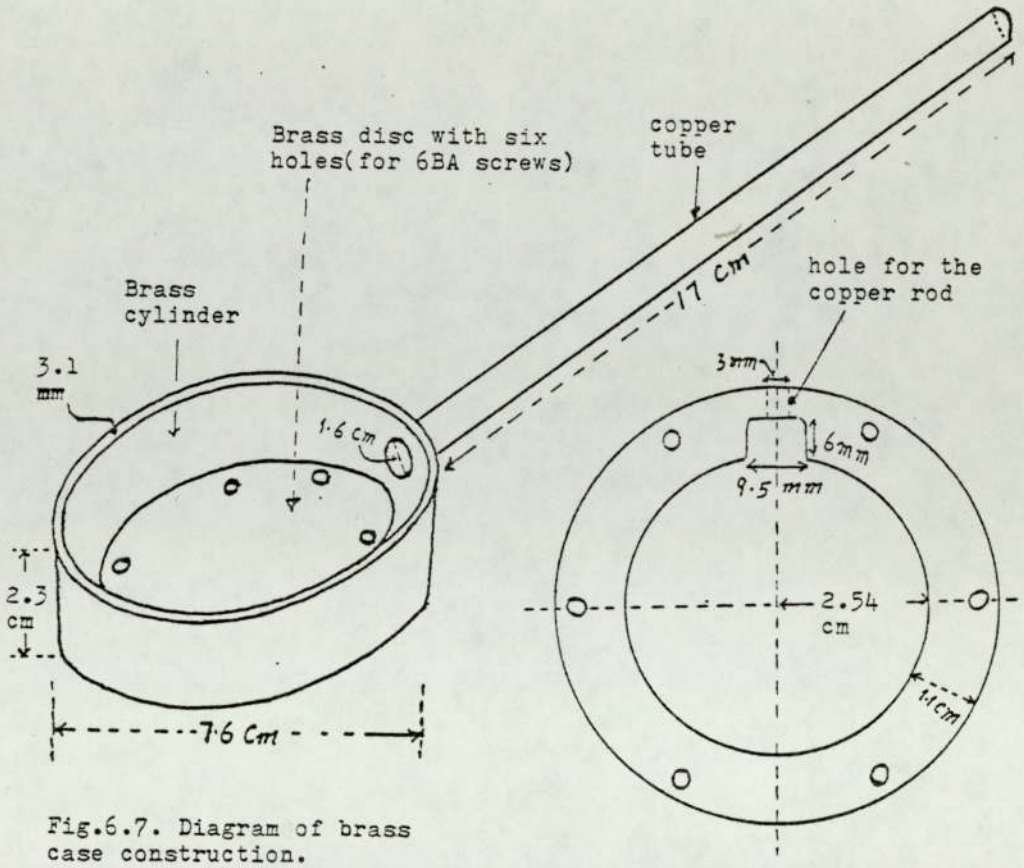

Fig.6.7. Diagram of brass case construction.

Fig.6.8. Diagram of perspex case construction.

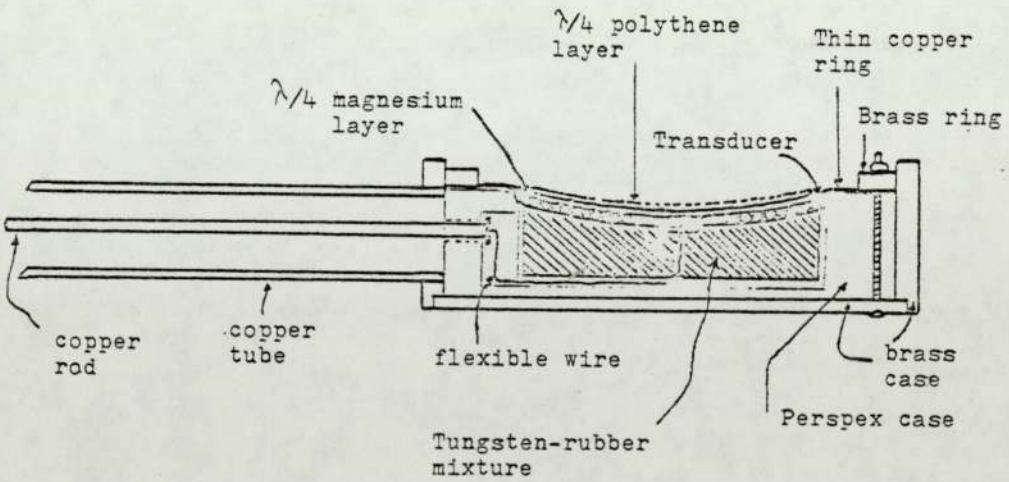

Fig.6 9. Schematic diagram of transducer housing.

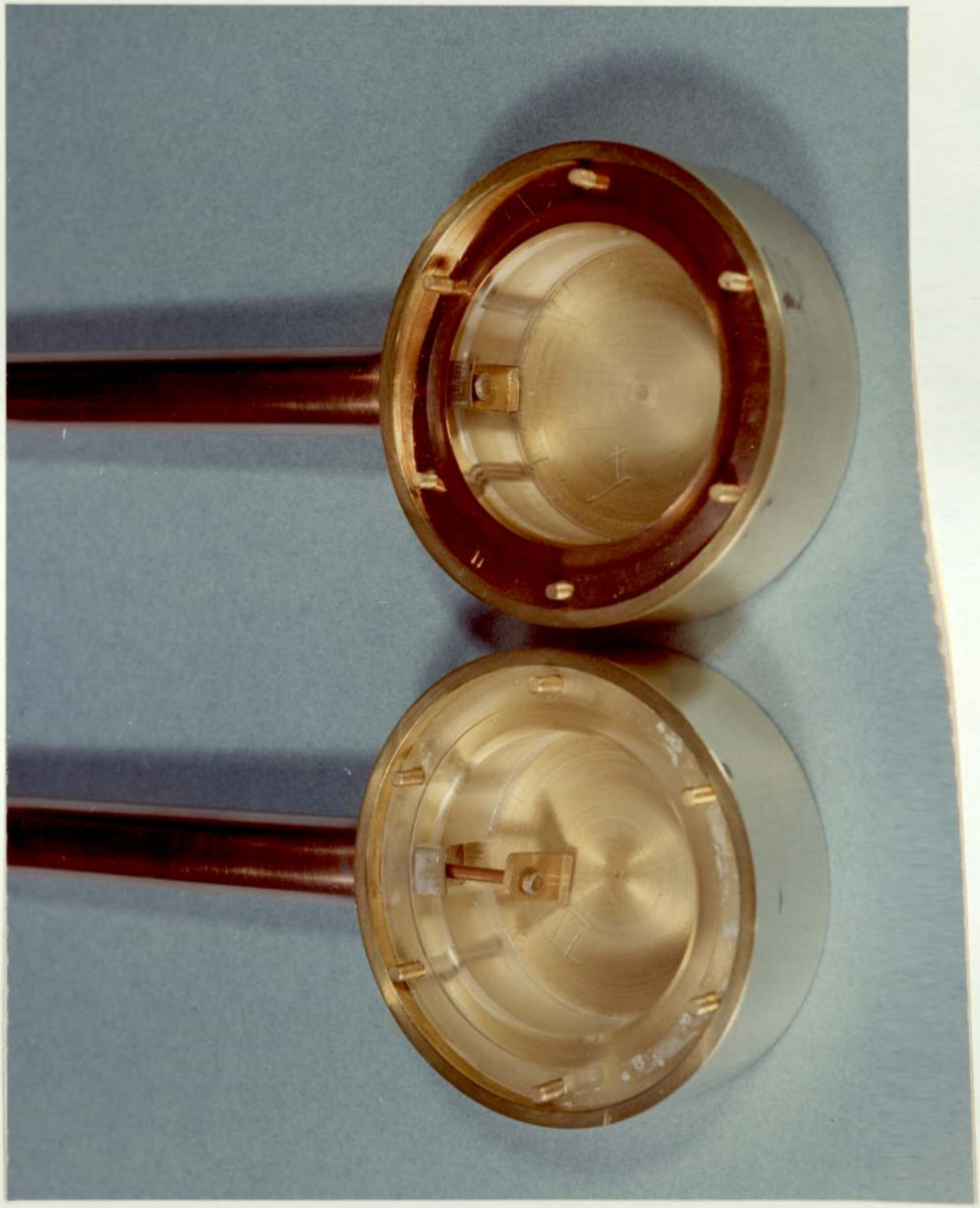

Picture (4) Transducer case.

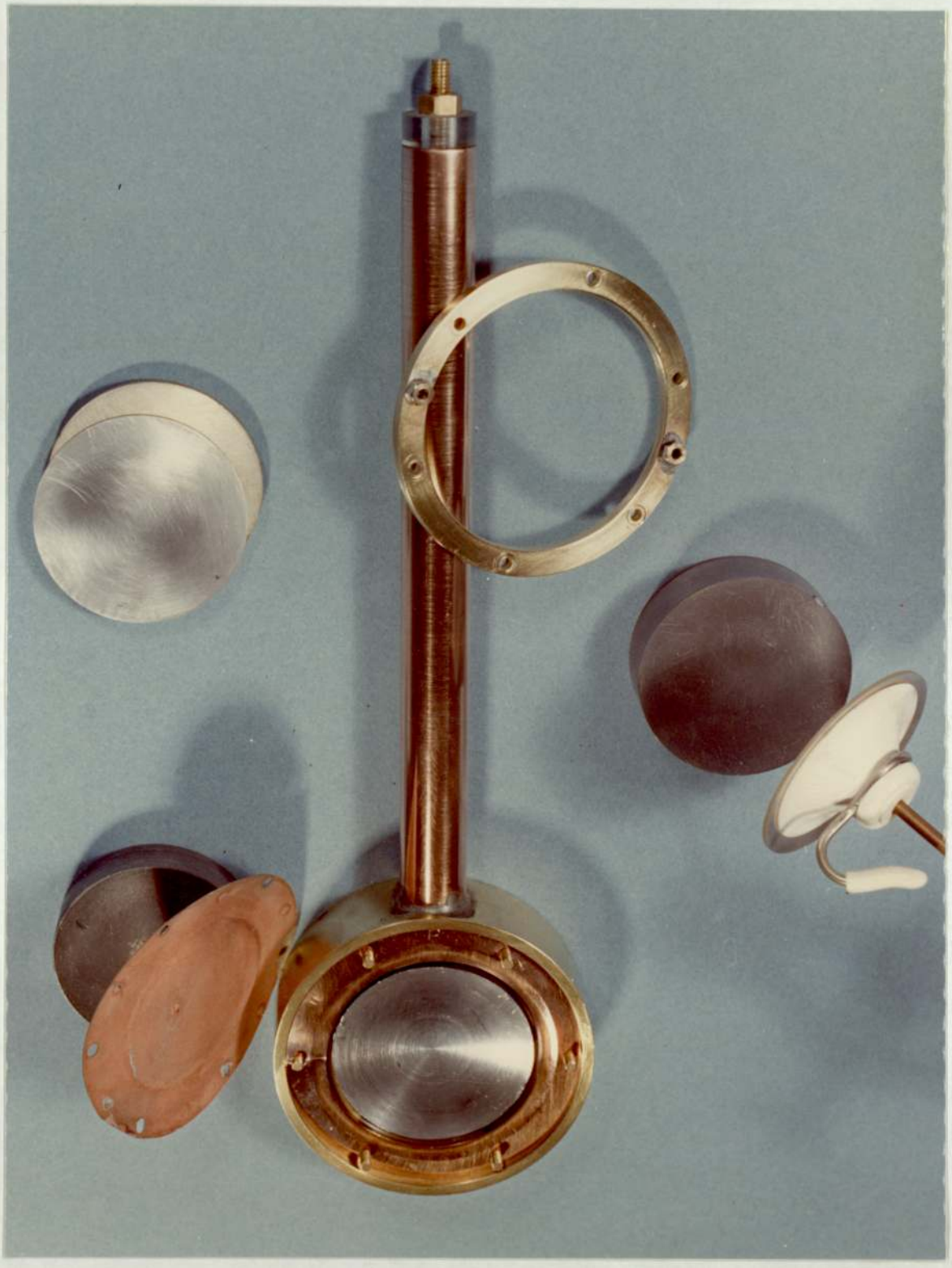

Picture (5) Transducer, its case , backing and matching layers.

The inside perspex case consists of a thick wall (1.1cm thick, and 2cm high) and a thin base (1.5mm thick). Through the perspex wall there are six equi-spaced vertical holes, with enough clearance for the "6BA" screws to get through. A small groove is machined through the perspex wall (as shown in Figure 6.8, so as to be opposite to the hole in the brass case. A small horizontal hole (3mm wide) is bored through the perspex wall and at the centre of the groove so that it will be opposite to the middle of the copper tube. A copper rod (2.5mm in diameter, and 19 cm long) is held at the middle of the copper tube and insulated from it. The copper rod is therefore, resting at one end in the hole of the perspex case, and at the other end in a perspex collar, which is tightly fixed at the top end of the copper tube. The copper rod is used to make the electrical connection to the silver on the back of the transducer, the active electrode. A small disc (5mm in diameter) of copper foil is soldered at the centre of its surface to one end of a flexible wire. The other surface of the disc is cemented at its edge (so that its middle is in good electrical contact with the silver coating) to the middle of the back surface of the transducer. The wire is threaded into the backing layer, while the latter is still soft. After the backing layer was completely dry it has been cemented to the back surface of the transducer using a very thin layer of permabond. The other end of the wire is then soldered to the copper rod end, in the perspex groove. The far end of the copper rod is connected to the transmitting and receiving circuits through a coaxial cable.

A thin copper ring (1.2cm wide), with six equi-spaced holes fits onto the screws so that it rests on the top of the perspex case. The inside edge is cemented (using a very thin layer of permabond) to the outside rim (about 1mm wide) of the front surface of the transducer. A brass ring (about 5mm wide and 3mm thick) with six equi-spaced holes, is secured on the top of the outside rim of the copper ring by nuts on the screws.
By this method a good electrical conductivity has been achieved between the front surface of the transducer and the brass case which is earthed.

Finally, the front surface of the housing is painted in order to avoid any water leak to the back of the transducer.

6.3 The Water Bath

The water tank is constructed from thick perspex sheets (0.5 inch thick), having dimensions shown in Figure 6.1. It is mounted below the rotating drum and fixed to the frame of the apparatus, about 30cm above its base. There is a large hole (about 15cm in diameter) in the tank base, to accommodate the patient's limb with the forearm upwards in the tank and the elbow below it. Around this hole there is a rubber ring which can be blown up in order to hold the limb in place and to prevent any water leak.

Provision has been made for filling up and emptying the water bath by using a 5-6 gallons bucket which is connected to a small hole at the bottom of the tank, via a long rubber

tube, as shown in Figure 6.1. This gives an easy and quick method for filling up and emptying the water bath by moving the bucket above or below the level of the tank.

6.4 Setting up the Patient

The patient's limb to be accommodated in the water bath through the hole at its bottom, so that the elbow is resting on an adjustable level below the tank, and the forearm is upwards. The patient's arm is adjusted in place so that the axis of symmetry of the scanning transducer is normal to the ulna and at the required level of cut at which the cross-section profile is to be determined. The patient is to grasp a horizontal perspex rod, which is fixed at the top of the water tank (as shown in Figure 6.1 and pictures 1 and 2) with the arm in the suprinated position. The rubber ring around the arm (at the bottom hole) is blown up to hold the arm in place and to prevent water leaking when the tank is filled up with water. Finally, the tank is filled with water or saline solution from the bucket after being adjusted to the required concentration and controlled to the required temperature, if necessary.

6.5 The Scanning Procedure

As described in Chapter II, the radius bone presents a complete obstacle of some parts of the ulna surface. However, the relative positions of the radius bone with respect to the ulna can be changed by twisting the forearm by 90-120°. This

means that the portion of the ulna surface obstacle by the radius bone when the arm is in the first position, i.e. when it is supinated, will be seen by the scanning transducer in the second position when the arm is twisted by 90-120°, i.e. when it is pronated.

Therefore, it has been thought reasonable to use two separate scans, each of 270°. When the first scan is finished, with the arm supinated, the forearm is to be twisted by 90-120°, while the limb is still held by the rubber ring at the bottom of the water bath. The patient grasps the perspex rod at this position where his arm is pronated and the second scan is carried out for 270°.

Having the two scans, it will be possible to superimpose the plotted outline of the repeated scanned positions of the ulna on each other in order to obtain the complete cross-section profile of the ulna.

CHAPTER VII

GENERAL CONCLUSIONS AND RECOMMENDATIONS

7.1 General Conclusions

The work described in this thesis involves a general study of ultrasonic wave diffraction, and the construction of an ultrasonic bone tomograph for the purpose of determination of the ulnar cross-section profile.

As a part of this study, a way has been found to apply the Kirchhoff's integral, without approximation, to a plane disc transducer. The results show significant differences from previous investigations.

A new approach has been taken to the diffraction pattern in the focal plane of a concave bowl transducer, in the steady state conditions. From this analysis, it has been shown that for bowl transducers for which the ratio of the aperture radius (b) to the radius of curvature (a), is greater than $\frac{1}{2}$, the diffraction pattern departs from that given by classical theory, where as for $b/a < \frac{1}{2}$, it approaches the value of that obtained by classical theory.

The expression given by classical theory has been used in the analysis of the diffraction pattern due to shock excitation applied to a bowl transducer. It has been found that the lateral resolution is dependent on the increase of the lower frequency limit of the bandwidth of the receiving system. It

also depends on the ratio b/a of the bowl transducer in a similar manner to that in steady state conditions.
An analysis of a system in which the bandwidth is limited by a function closely resembling that imposed by the circuit used, has been carried out as shown by curve (1) - Fig.(2.23). The resolution resulting from this system is comparable to that given by the same bowl transducer in the steady state condition at 6.85 MHz (curve 2 - Fig. 2.23).

The ultrasonic bone tomograph is not as yet operating satisfactorily. Preliminary runs have been carried out using a reflecting cylindrical metallic rod, almost concentric with the rotation system. It has been found that the apparatus is capable of drawing a plot of the profile of the rod with an error of only the thickness of the plotting line, i.e. 1mm. As the plot is 10 times the actual size, this is compatible with the estimated resolution of about 0.2mm, based on time discrimination of $^{1}/_{8}\mu s$.
When the reflecting rod surface is too oblique due to being too excentrically placed, the apparatus fails to follow the contour of the rod. This is due to the fact that the AGC system is not compensating enough for weak echoes.

7.2 Recommendations

If the apparatus is to function properly it is clearly necessary that the performance of the AGC amplifier must be further investigated.

The replacement of the scanning bowl transducer by one of a larger aperture , e.g. b/a=½, would enable a larger proportion of the reflected waves to be collected, giving a more reliable response with obliquity of the reflecting surface.

The apparatus could be tried first by using some reflecting metallic rods of different profiles, and also by using some post-mortem ulnas, in order to determine its response and accuracy.

APPENDIX "A"

ARTIFICIAL BONE-LIKE MATERIAL AS A REFERENCE FOR THE BONE DENSITOMETER

A.1 Introduction

As described in the preface, ivory was found to be unsatisfactory for the purpose of construction of a reference step wedge for the bone densitometer. The intention is now to produce an artificial bone-like material which can be used for this purpose, instead of ivory. The requirements we require for this material, are:-

1. Its density and elemental composition, must be as close as possible to those of bone, and precisely known.

2. It must be homogeneous, without any air between the particles of the constituent materials.

3. It should be solid, rigid, compact, and easily machinable to the required shape.

4. This material must be water-proof, i.e. insoluble in water and has no tendancy to absorb it.

The approach to these requirements can be achieved by using:-

(i) A homogeneous mixture of very fine powders of different

materials, chemically inert, insoluble in water, and of known elemental composition; and,

(ii) A water-proof adhesive or binding material, of known elemental composition, in order to bind the particles of the materials forming the mixture firmly together.

The mixture of the powders and the binding material, must be homogeneously mixed, and any air or moisture present must be removed before the final adhesion is obtained. This process depends on the type of the binding material used. Three types of adhesive have been tried for this purpose.

(a) In the first type, a low viscosity liquid (resin) is homogeneously mixed with the mixture powders, and using another liquid material as a hardener. The total mixture is then put under vacuum, with a continuous stirring to obtain a uniform distribution of the hardener, and to get rid of air and moisture. After a certain period, a hard solid adhesion is obtained. An example of this type of binding material is araldite resin (resin AY105, and hardener HY951).

(b) The second type, is a powder binding material, which is homogeneously mixed with the mixture powders, heated to melt, and then left to cool down forming a solid adhesion. An example of this type, is shellac powder (m.p. about 85^{o}C).

(c) The third type, is a powder binding material, which can be melted and polymerized by heating, forming a hard solid

adhesion, e.g. araldite epoxy resin AT1 (m.p about 80°C; polymerisation occurs at about 130°C).

The last two types, i.e. the powder binding materials are more desirable than the first, for the following reasons:-

1. A homogeneous distribution of the binding material in the mixture powders, can be easily achieved by mixing powders only, rather than powders and low viscosity liquids.

2. The expulsion of air from the mixture can be carried out by applying suction and compression to the powder mixture. This is an easier method than stirring under vacuum, which is elaborate and complicated.

3. The mixing of the binding material into the powder mixture, and the expulsion of air and moisture from it, can be carried out over unlimited period before the heating process; whereas in the first type, there is a time limit after the addition of the hardener.

In order to decide upon the materials to form the mixture and their proportions, it is necessary to know the chemical composition of bone. Bone consists of organic and inorganic materials. The percentage by weight of the organic materials, in dry defatted bone, is about 25-26%, and that of the inorganic materials is about 74-75%. The inorganic material in bone is present as calcium hydroxy apatite molecules, $\left[Ca_3(PO_4)_2\right]_3 \cdot Ca(OH)_2$.

The percentages by weight of the different elements in bone (femur), are given in table A.1 (H.E.Johns, 1961).

Among the calcium salts which are insoluble in water, and have no tendancy to absorb it, are, Calcium Orthophosphate $Ca_3(PO_4)_2$, and Calcium Hydroxide $Ca(OH)_2$, which can be obtained as very fine powders.

Table (A.1) The percentages by weight of the different elements in bone:

Element	Atomic weight	% by weight in bone
Calcium (Ca)	40.08	14.70
Phosphorus (P)	30.975	7.10
Carbon (C)	12.011	27.80
Nitrogen (N)	14.000	2.70
Oxygen (O)	16.008	40.88
Hydrogen (H)	1.008	6.40
Magnesium (Mg)	24.320	0.22
Sulphur (S)	32.066	0.20

A.2 A Mixture of Calcium orthophosphate, Calcium hydroxide, and Shellac

In the first experimental trial of making the artificial bone-like material, the inorganic contribution (i.e, 75% by

weight) has been introduced in the mixture by using calcium orthophosphate $Ca_3(PO_4)_2$and calcium hydroxide $Ca(OH)_2$ powders. These salts were used in the same proportions as they exist in the calcium hydroxy apatite, i.e. 3 molecular weights of $Ca_3(PO_4)_2$ and 1 molecular weight of $Ca(OH)_2$. Since the molecular weight of $Ca_3(PO_4)_2$ is 310.19, and that of $Ca(OH)_2$ is 74.08, therefore their ratio by weight will be 12.6 : 1, respectively.

The organic matter (i.e. 25%) in the artificial bone, has been introduced by using shellac powder, which is also used as a water-proof adhesive, although its elemental composition is not known. Therefore, the percentages by weight of the constituent materials in the mixture are, 25% shellac, 69.5% $Ca_3(PO_4)_2$, and 5.5% $Ca(OH)_2$.

The powders of these materials were homogeneously mixed, and left for 48 hours under a bell-jar, with phosphorus pentaoxide in a separate glass pot, in order to absorb any moisture that may be present in the mixture. Small quantities (about 30 gms each) were compressed under different pressures (5-30 tons), in a stainless steel cylinder, while the suction of air is carried out, as shown in Fig A.1. The compressed specimen is taken out of the cylinder, heated gradually in an oven for ½ to 1 hour at 110°C, and then left to cool down slowly.

All the resultant specimens were found to have some cracks, which arise during the heating process. However, the resulting material was rigid enough, easy to cut and machinable. The weights of the resultant specimens were checked before and

after putting them in water for 48 hours. It has been found that there is no decrease in the weights, which means that the material is insoluble in water. A very small increase in the weight, about 0.4% was observed, which means that this material has a very small, almost negligible tendancy to absorb water.

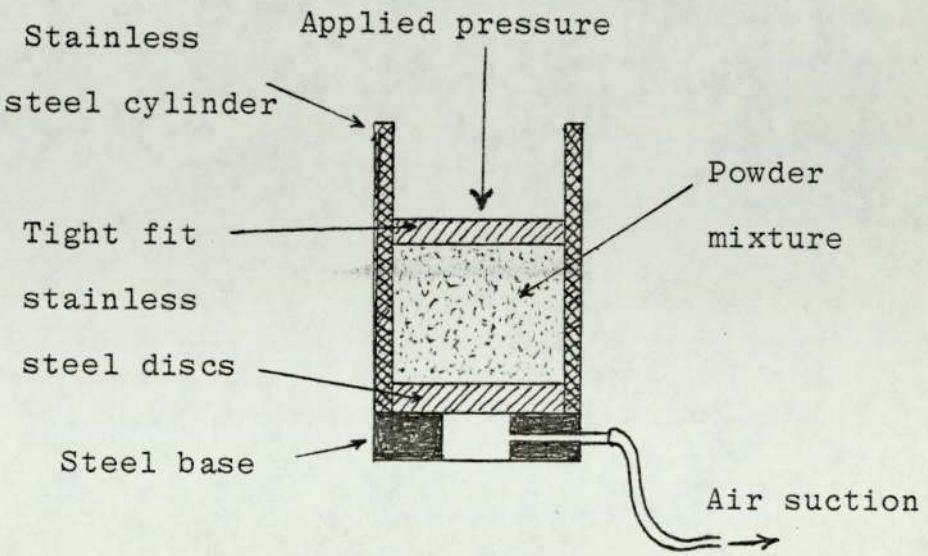

Fig.A.1 Compression of the powder mixture

The densities of the specimens are determined and found to be 1.45-1.6 gm/cm^3. Due to the cracks in the resulting specimens, and also because the elemental composition of shellac is not known and need to be determined by chemical analysis which is elaborate, shellac was abandoned. It is, therefore, necessary to use other organic material, rather than shellac, of known elemental composition and has the property of forming a water-proof adhesion. Araldite epoxy resin powder A.T.1, has found to be suitable for this purpose.

Among the nitrogen organic compounds, chemically inert and water insoluble, is melamine polymer (63.8% nitrogen). This

material has been used, primarily in order to introduce most of the required percentage of nitrogen in the mixture. Also, small amounts of magnesium oxide (MgO) and sulphur (S), which are water insoluble, have been added to themixture in order to introduce the small percentages of magnesium (0.22%) and sulphur (0.20%). The method of calculations of the proportions of the different materials in the mixture, will be explained in the next section.

A.3 A mixture of Calcium orthophosphate, Calcium hydroxide, Araldite resin, Melamine polymer and Magnesium oxide

A.3.1. Method of calculation of the amount of each material

In order to calculate the required amounts (percentages by weights) of the materials in the mixture, so that the latter has the same elemental composition as bone, let us consider that the total weight of the mixture is 100 gm . The constituent elements, in this amount of mixture, must have, therefore, the values given in table A.1. The calculation procedure is carried out in the following steps:-

(i) The amount of calcium orthophosphate $Ca_3(PO_4)_2$

The amount of phosphorus (P) in the mixture is only introduced by $Ca_3(PO_4)_2$, where each molecule of the latter contains two atoms of phosphorus. This means that each molecular weight of $Ca_3(PO_4)_2$, i.e. 310.19 gm contains $2 \times 30.975 = 61.95$ gm P Therefore, the weight of $Ca_3(PO_4)_2$, which gives the required

percentage of P in the mixture (7.1%), is given by:

$$\%W_{Ca_3(PO_4)_2} = \frac{310.19}{61.95} \times 7.1 = 35.55\%$$

Since each molecular weight of $Ca_3(PO_4)_2$ i.e. 310.19, contains 3x40.08 = 120.24 gms of Ca, therefore, the weight of calcium present in 35.55 gms of $Ca_3(PO_4)_2$ is given by:

$$\frac{120.24}{310.19} \times 35.55 = 13.78 \text{ gms of Ca}$$

From table (A.1) the calcium difficiency is equal to 14.70 - 13.78 = 0.92 gm, which can be compensated by using a proper amount of calcium hydroxide.

(ii) The amount of calcium hydroxide $Ca(OH)_2$

The amount of calcium hydroxide necessary to compensate for the calcium difficiency i.e. 0.92%, is given as follows:

Since the molecular weight of $Ca(OH)_2$, i.e. 74.08 contains 40.08 gms of Ca, therefore, the amount of $Ca(OH)_2$ which contains 0.92 gms Ca, is given by

$$\%^{W}\, Ca(OH)_2 = \frac{74.08}{40.08} \times 0.92 = 1.7\%$$

(iii) The amounts of araldite epoxy resin (AT1) and melamine Polymer

The araldite AT1 epoxy resin consists of carbon, nitrogen, oxygen, and hydrogen in the percentages by weight given in table A.2. The melamine polymer consists of carbon, nitrogen and

hydrogen in the percentages by weight, given in the same table (A.2).

Table A.2 Araldite AT1 epoxy resin, and Melamine polymer compositions (% by weight).

Material / Element	Araldite AT1 resin	Melamine polymer
Carbon "C"	75.60	32.81
Nitrogen "N"	0.25	63.80
Hydrogen "H"	6.85	3.39
Oxygen "O"	17.30	

The percentages by weight of carbon and nitrogen in bone (table A.1), are 27.80% and 2.70%, respectively.

In order to calculate the percentages by weight of the araldite resin and the melamine polymer in the mixture, which give the same contributions of carbon and nitrogen elements as those in bone; consider $W_{(R)}$ and $W_{(M)}$ are the required weights of araldite resin and melamine, respectively, in 100 gms of the mixture. Suppose that the carbon and nitrogen contributions in the mixture due to $W_{(R)}$ gms of araldite resin, are $C_{(R)}$ gms, and $N_{(R)}$ gms, respectively. Therefore, the carbon contribution in the mixture due to $W_{(M)}$ gms melamine, should be $C_{(M)}=(27.8 - C_{(R)})$ gms. Also, the nitrogen contribution due to $W_{(M)}$ gms melamine, should be $N_{(M)}=(2.7 - N_{(R)})$ gms.

Since the percentages by weight of carbon and nitrogen in the araldite resin (table A.2), are 75.6% and 0.25%, respectively, therefore, the required weight of the resin $W_{(R)}$ in 100 gms of the mixture, is given by:

$$W_{(R)}=\frac{100}{75.6}\ C_{(R)}\ \text{gms} \qquad (1)$$

or,

$$W_{(R)}=\frac{100}{0.25}\ N_{(R)}\ \text{gms} \qquad (2)$$

From equations (1) and (2), we have

$$N_{(R)}=\frac{0.25}{75.6}\ C_{(R)} \qquad (3)$$

Also, the percentages by weight of carbon and nitrogen in the melamine polymer (table A.2), are 32.81% and 63.8%, respectively, therefore, the required weight of melamine $W_{(M)}$ in 100 gms of the mixture is given by:

$$W_{(M)}=\frac{100}{32.81}\ C_{(M)} = \frac{100}{32.81}\ (27.8 - C_{(R)}) \qquad (4)$$

or,

$$W_{(M)}=\frac{100}{63.8}\ N_{(M)} = \frac{100}{63.8}\ (2.7 - N_{(R)} \qquad (5)$$

From equations (4) and (5), we have

$$N_{(R)}=2.7 -\left\{\frac{63.8}{32.81}\ (27.8 - C_{(R)})\right\} \qquad (6)$$

From equations (3) and (6), the carbon contribution $C_{(R)}$ in the mixture due to $W_{(R)}$ gms of resin, is given by:

$$C_{(R)} = 26.456\ \text{gms} \qquad (7)$$

Substituting this value of $C_{(R)}$ into equations (1) and (4), give the required percentages by weight of araldite $W_{(R)}$ and melamine $W_{(M)}$ in the mixture. Thus the percentage by weight of the araldite epoxy resin AT1 in the mixture is,

$$W_{(R)} = 34.935\%$$

and,

the percentage by weight of the melamine polymer in the mixture is:

$$W_{(M)} = 4.221\%$$

(iv) The amount of magnesium oxide (MgO) in the mixture

The required percentage of magnesium (Mg) in the mixture i.e. 0.22%, can be introduced by using magnesium oxide (MgO) powder, which is insoluble in water. Since each molecular weight of MgO i.e. 40.32, contains one atomic weight of magnesium (24.32), therefore, the percentage by weight of MgO in the mixture, which gives the required percentage of Mg i.e, 0.22%, is given by:

$$\%W_{MgO} \text{ in the mixture} = \frac{40.32}{24.32} \times 0.22 = 0.365\%$$

A.3.1.1 The oxygen contribution in the mixture due to calcium orthophosphate, calcium hydroxide, araldite AT1 resin, and magnesium oxide

(a) Calcium orthophosphate $Ca_3(PO_4)_2$:

Since each molecular weight of $Ca_3(PO_4)_2$ i.e. 310.19, contains 8 atomic weights of oxygen (8x16=128); therefore, the oxygen contribution due to 35.55% $Ca_3(PO_4)_2$ is:

$$\%O_{Ca_3(PO_4)_2} = \frac{128}{310.19} \times 35.55 = 14.72\%$$

(b) Calcium hydroxide $Ca(OH)_2$:

Each molecular weight of $Ca(OH)_2$, i.e, 74.08, contains two atomic weights of oxygen (2x16=32). Therefore, the oxygen contribution due to 1.7% $Ca(OH)_2$ is given by:

$$\%O_{Ca(OH)_2} = \frac{32}{74.08} \times 1.7 = 0.73\%$$

(c) Araldite (AT1) epoxy resin:

From table A.2, the oxygen content in araldite is 17.3%, therefore, the oxygen contribution due to 34.935% of araldite resin is given by:

$$\%O_{resin} = \frac{17.3 \times 34.935}{100} = 6.06\%$$

(d) Magnesium oxide (MgO):

Each molecular weight of MgO (40.32) contains one atomic weight of oxygen; therefore, the oxygen contribution due to 0.365% of MgO, is given by:

$$\%O_{MgO} = \frac{16}{40.32} \times 0.365 = 0.15\%$$

Therefore, the total oxygen contribution in the mixture, is given by:

$$\%O_{mix} = 14.72 + 0.73 + 6.06 + 0.15 = 21.66\%$$

The oxygen deficit in the mixture = 40.88 - 21.66 = 19.22%

A.3.1.2 The hydrogen contribution in the mixture due to calcium hydroxide, araldite and melamine

(a) Calcium hydroxide $Ca(OH)_2$:

Each molecular weight of $Ca(OH)_2$ contains 2 atomic weights of hydrogen (2x1=2). Therefore, the hydrogen contribution in the mixture due to 1.7% $Ca(OH)_2$ is given by:

$$\%H_{Ca(OH)_2} = \frac{2}{74.08} \times 1.7 = 0.05\%$$

(b) Araldite (AT1) epoxy resin:

From table A.2, the hydrogen content in araldite is 6.85%; therefore, the hydrogen contribution due to 34.935% araldite resin, is given by:

$$\%H_{resin} = \frac{6.85}{100} \times 34.935 = 2.4\%$$

(c) Melamine polymer:

From table A.2, the hydrogen content in melamine is 3.39%; therefore, the hydrogen contribution due to 4.221% melamine, is given by:

$$\%H_{mel} = \frac{3.39}{100} \times 4.221 = 0.14\%$$

Therefore, the total hydrogen contribution in the mixture is given as follows:

$$H_{mix} = 0.05 + 2.40 + 0.14 = 2.59\%$$

The hydrogen deficit in the mixture = 6.40 - 2.59 = 3.81%

A.3.2 The final composition of the mixture

Now the mixture has a hydrogen and oxygen deficit of 3.81% and 19.22%, respectively, whereas calcium, phosphorus, carbon, nitrogen, magnesium and sulphur exist in the same ratio by weight as in bone. The total weight of the different materials forming

the mixture, as calculated in section A.3.1, is given as follows:

$$Ca_3(PO_4)_2 + Ca(OH)_2 + \text{araldite} + \text{melamine} + MgO + S$$

$$W_{mix} = 35.550 + 1.700 + 34.935 + 4.221 + 0.365 + 0.200$$
$$= 76.971 \text{ gms}$$

Now the percentages by weight of these materials in such a mixture (after neglecting the oxygen and hydrogen deficit, which total to 23.03%), are given in table A.3. These values are used in the preparation of the required mixture for making the artificial bone-like material, as will be explained later in section A.3.4

Table A.3 The percentages by weight of the different materials in the mixture

Material	$Ca_3(PO_4)_2$	$Ca(OH)_2$	Araldite resin AT1	Melamine	MgO	S
% by weight	46.186	2.209	45.387	5.484	0.474	0.260

A.3.3 Compensation for the oxygen and hydrogen deficit in the mixture

As water (H_2O) consists of oxygen and hydrogen in the ratio by weight 8 : 1 respectively, therefore theoxygen deficit (19.22%) and some of the hydrogen deficit (i.e. about 2.4%) in the mixture may be regarded as if they are equivalent to 21·62% water

difficiency. As hydrogen has nearly no effect on the x-ray absorption in the diagnostic energy range, where photoelectric absorption is important, therefore, the remainder hydrogen deficit, i.e. 3.81 - 2.41 = 1.40%, can be entirely neglected.

The compensation for the water-equivalent difficiency (21.62%) can be achieved by using a volume of water proportional to the mass of the artificial material.

Since it is intended to use the reference step wedge, constructed from this material, in a water bath, this compensation can be obtained by making a water-filled step cavity under the step wedge in the base of the tank. The depth of each step must be calculated so that, the volume of water filling that depth corrects for the water difficiency in the amount of material present in the corresponding step of the wedge. The depths of the steps can be calculated as follows:

Suppose that the volume of a unit mass of actual bone is V_B. This mass corresponds to a mass of artificial material, $M_A = \rho_A V_A$, and an amount of water, $M_W = V_W \times 1$, i.e:

$$\rho_B V_B = \rho_A V_A + V_W \times 1$$

where,

ρ_B and ρ_A are the densities of actual bone and artificial material respectively. V_A and V_W are the volumes of artificial material and water respectively.

Since $M_W = V_W \times 1 = 0.216\ \rho_B\ V_B$; i.e. $\rho_B\ V_B = \frac{V_W}{0.216}$, therefore

$$\frac{V_W}{0.216} = \rho_A\ V_A + V_W$$

Suppose that $V_W = \alpha V_A$, then substituting in the above equation, we have:

$$\frac{\alpha V_A}{0.216} = \rho_A\ V_A + \alpha V_A, \text{ from which}$$

$$\alpha = 0.276\ \rho_A$$

Therefore,

the volume of water required for compensation $V_W = 0.276\ \rho_A\ V_A$. If the area of the groove step is made equal to that of the wedge step, then the depth of groove step "d_w" is given by:

$$d_w = 0.276\ \rho_A\ t_A$$

where t_A is the thickness of the step of the reference wedge.

A.3.4 Experimental procedures and results

The materials forming the mixture, i.e. calcium orthophosphate, calcium hydroxide, araldite AT1 expoxy resin, melamine polymer, magnesium oxide and sulphur, have been obtained as very fine powders. The proper weights of these materials, in the

proportions given in table A.3, are homogeneously mixed together, dehydrated and treated in the same way as in the case of the shellac mixture (as described in section A.2). The heating temperature of this mixture was carried out at about 130°C for 1-3 hours, to produce polymerisation of the resin.

The resulting material was found to be rigid, easy to cut, machinable and insoluble in water. When the specimen was left in water for 48 hours, its tendency to absorb water has found to be very small and negligible (about 0.06%). Its density is about 1.5 - 1.6 gms/cm^3. However, almost all the resulting specimens were found to have some cracks which arise during the heating process of the compressed mixture.

Some experiments have been carried out in order to overcome this difficulty by keeping the compressed mixture in the cylinder under a static pressure during the heating process.

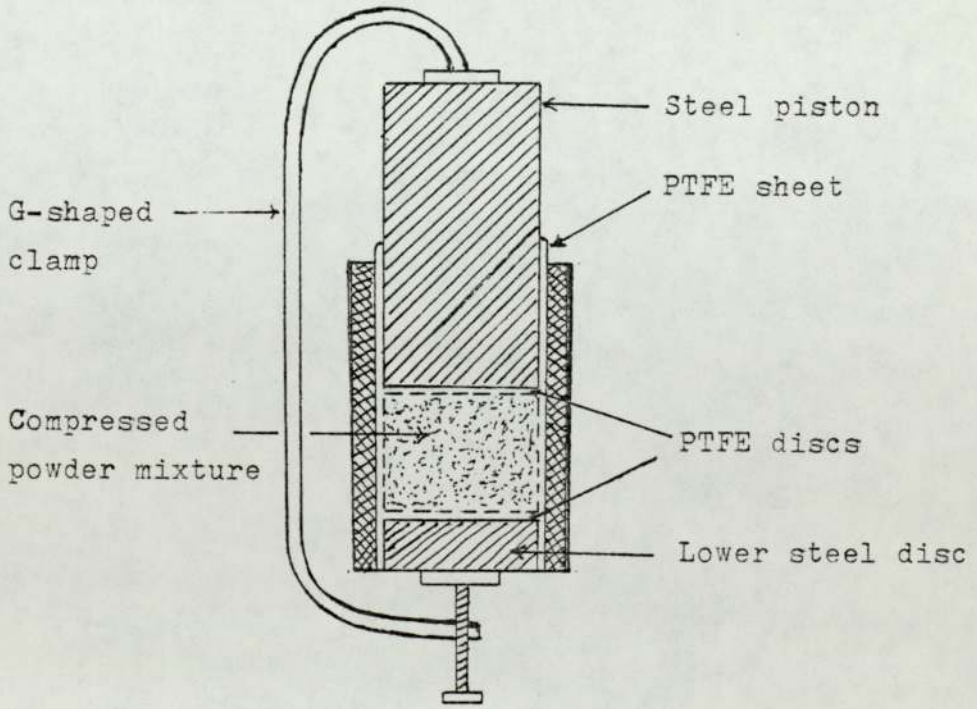

Fig. A.2. Clamping the compressed powder mixture during the heating process.

The powder mixture was placed in a strong steel cylinder (5mm thick) lined with polytetraflouro ethylene (PTFE) sheet (0.266 mm thick). The PTFE liner is used to prevent adhesion to the inside of the cylinder, the the piston and the lower steel disc, see Fig A.2. The powder mixture was compressed under 10 tons pressure and then clamped tightly using a G-shaped clamp. The cylinder with the clamped mixture were heated for 3 hours at 130^{o}C.

The resultant material was found to be rigid without any cracks. It has the same specifications as described above. Its density has found to be improved, i.e, 1.65 gm/cm^{3}. The specimen was cut into slices (about 5 mm thick) at different directions. These slices were photographed by x-ray beam, to determine the homogenity of the resulting specimen. Unfortunately it has been found that the dense materials were concentrated at one side of the specimen, corresponding to its bottom, and the light materials were concentrated at its top.

In order to covercome this difficulty, it has been suggested to rotate the cylinder in which the compressed mixture is clamped during the heating process. This experiment was carried out in this Department by Mr. M.I. Al-Jarallah. He has been able to fulfill the requirement of homogeneous distribution of the substances in the resulting material, by using a low speed of rotation (about 1.7 r.p.m.). Also, he has beenable to improve the density of the resulting material by using three strong springs for clamping the compressed mixture in the cylinder during heating. The density of the material was found to be about 1.75 gm/cm^{3}.

APPENDIX (B)

COMPUTER PROGRAMS USED IN CHAPTER (II)

PROGRAM (I)

(EQUATION 2.5)

```
'BEGIN'  'INTEGER'I;    'REAL' K,Z,S,Z1,S1,L,M,R,ANGLE;
'ARRAY'  XX[1:365],          YY[1:365];
  K:=15.707963267945;                I:=0;
'FOR' Z:=0.0 'STEP' 0.005 'UNTIL' 1.496,1.5'STEP' 0.05 'UNTIL'2.951,
3.0 'STEP' 0.2 'UNTIL' 9.81      'DO'
'BEGIN'   S:=SQRT(1+Z*Z);     Z1:=K*Z;          S1:=K*S;
L:=COS(Z1)-0.5*COS(S1)*(1+Z/S);     M:=-SIN(Z1)+0.5*SIN(S1)*(1+Z/S);
  R:=SQRT(L*L+M*M);
   NEWLINE(1);
PRINT(Z,2,3);          SPACE(5);     PRINT(L,2,6);     SPACE(5);
  PRINT(M,2,6);        SPACE(5);        PRINT(R,2,6);
I:=I+1;              XX[I]:=Z;          YY[I]:=R;
  'END';
GHREGION(0.0,11.0,0.0,2.5);
GHLIMITS(1.5,18.0,1.0,11.0);
GHCURPTO(XX,YY,1,365,10);
GHAXESSI(0.2,0.1);
GHLIMITS(0.0,18.0,0.0,11.0);
GHREGION(-1.0,11.0,-0.25,2.5);
GHCRSET(1);
  GHCRSIZE(0.1);
GHPLOTAS(2.0,-0.15,'('Z-AXIS')');
   ANGLE:=3.14159/2;
GHROTATE(-0.4,0.5,ANGLE);
GHPLOTAS(-0.4,0.5,'('R-AXIS')');



  GHUNROT;
GHGREND;
'END';
****
```

PROGRAM (2)

(EQUATION 2.14)

```
'BEGIN' 'INTEGER'NC,IFAIL,NPTS,I;
  'REAL'Z,D,PI,FIP,ACC,C1,C2,FIP1,FIP2,R,ANGLE;
   'ARRAY'P[1:301],     XX[1:140],      YY[1:140];
  'PROCEDURE' D01ACA(A,B,F,RELACC,ABSACC,NC,P,ANS,ACC,NPTS,IFAIL);
  'VALUE' A,B,RELACC,ABSACC,NC;    'REAL'A,B,RELACC,ABSACC,ANS,ACC;
  'INTEGER'NC,NPTS,IFAIL; 'REAL''ARRAY'P; 'REAL''PROCEDURE'F; 'LABEL';
'REAL''PROCEDURE'F1(X);                'VALUE'X;                'REAL'X;
'BEGIN'  'REAL' S,T,U;  T:=COS(X);  U:=D*D+1-2*D*T;  S:=SQRT(U+Z*Z);
     F1:=COS(10*PI*S)*(1+Z/S)*(D*T-1)/(U*2*PI);
  'END';
   'REAL''PROCEDURE'F2(X);          'VALUE'X;          'REAL'X;
'BEGIN' 'REAL'S,T,U;  T:=COS(X);  U:=D*D+1-2*D*T;  S:=SQRT(U+Z*Z);
     F2:=-SIN(10*PI*S)*(1+Z/S)*(D*T-1)/(U*2*PI);
   'END';
     PI:=3.14159265389;      IFAIL:=0;     NC:=0;      I:=0;
'FOR' D:=1.04   'DO'
'BEGIN'   NEWLINE(1);  PRINT(D,1,2);
'FOR' Z:=0.0 'STEP'0.02 'UNTIL' 1.481,1.5 'STEP' 0.05 'UNTIL'2.951,
3.0 'STEP'0.2 'UNTIL' 9.81  'DO'
   'BEGIN'  NEWLINE(1);  SPACE(9);      PRINT(Z,2,3);
   D01ACA(0.0,PI,F1,0.0005,0.0,NC,P,FIP1,ACC,NPTS,IFAIL);
   D01ACA(0.0,PI,F2,0.0005,0.0,NC,P,FIP2,ACC,NPTS,IFAIL);
    R:=SQRT(FIP1*FIP1+FIP2*FIP2);
  PRINT(FIP1,1,6);     SPACE(4);     PRINT(FIP2,1,6);     SPACE(4);
   PRINT(R,1,6);   SPACE(4);  PRINT(ACC,0,8);   NEWLINE(1);
I:=I+1;          XX[I]:=Z;          YY[I]:=R;



   'END';
   'END';
GREGION(0.0,11.0,0.0,2.5);
GRLIMITS(1.5,18.0,1.0,11.0);
GCURPTO(XX,YY,1,140,10);
GAXESSI(0.2,0.1);
GLIMITS(1.0,18.0,0.0,11.0);
GREGION(-1.0,11.0,-0.25,2.5);
GCRSLT(1);
GCRSIZE(0.1);
GPLOTAS(2.0,-0.15,'('Z-AXIS')');
ANGLE:=3.14159/2;
GROTATE(-0.4,0.5,ANGLE);
GPLOTAS(-0.4,0.5,'('R-AXIS')');
GOUTPUT;
GREND;
END';
***
```

PROGRAM (3)

(EQUATION 2.18)

```
'BEGIN''INTEGER'NC,IFAIL,NPTS,I;
  'REAL'Z,D,PI,FIP,ACC,C1,C2,FIP1,FIP2,R,ANGLE;
   'ARRAY'P[1:381],    XX[1:365],     YY[1:365];
  'PROCEDURE' D01ACA(A,B,F,RELACC,ABSACC,NC,P,ANS,ACC,NPTS,IFAIL);
  'VALUE' A,B,RELACC,ABSACC,NC;   'REAL'A,B,RELACC,ABSACC,ANS,ACC;
  'INTEGER'NC,NPTS,IFAIL;  'REAL''ARRAY'P; 'REAL''PROCEDURE'F; 'ALGOL';
'REAL''PROCEDURE'F1(X);              'VALUE'X;              'REAL'X;
  'BEGIN'   'REAL'S,T,U;  T:=COS(X);  U:=D*D+1-2*D*T;  S:=SQRT(U+Z*Z);
     F1:=COS(10*PI*S)*(1+Z/S)*(D*T-1)/(U*2*PI);
   'END';
    'REAL''PROCEDURE'F2(X);          'VALUE'X;          'REAL'X;
  'BEGIN'  'REAL'S,T,U;   T:=COS(X);  U:=D*D+1-2*D*T;   S:=SQRT(U+Z*Z);
     F2:=-SIN(10*PI*S)*(1+Z/S)*(D*T-1)/(U*2*PI);
   'END';
      PI:=3.141592653589;      IFAIL:=0;    NC:=0;      I:=0;
'FOR' D:=0.60      'DO'
'BEGIN'   NEWLINE(1);  PRINT(D,1,2);
'FOR' Z:=0.0 'STEP'0.005'UNTIL' 1.496,1.5 'STEP' 0.05 'UNTIL' 2.951,
3.0 'STEP'0.2 'UNTIL' 9.31   'DO'
   'BEGIN'  NEWLINE(1);  SPACE(9);      PRINT(Z,2,3);
    C1:=COS(10*PI*Z);        C2:=-SIN(10*PI*Z);
  D01ACA(0.0,PI,F1,0.0005,0.0,NC,P,FIP1,ACC,NPTS,IFAIL);
  D01ACA(0.0,PI,F2,0.0005,0.0,NC,P,FIP2,ACC,NPTS,IFAIL);
   R:=SQRT((C1*FIP1)↑2+(C2*FIP2)↑2);
PRINT(C1*FIP1,1,6);  SPACE(4);  PRINT(C2*FIP2,1,6);  SPACE(4);



  PRINT(R,1,6);     SPACE(4);     PRINT(ACC,0,8);    NEWLINE(1);
I:=I+1;     XX[I]:=Z;      YY[I]:=R;
   'END';
'END';
GHREGION(0.0,11.0,0.0,2.5);
GHLIMITS(1.5,18.0,1.0,11.0);
GHCURPTO(XX,YY,1,365,10);
GHAXESSI(0.2,0.1);
GHLIMITS(0.0,16.0,0.0,11.0);
GHREGION(-1.0,11.0,-0.25,2.5);
GHCRSET(1);
  GHCRSIZE(0.1);
GHPLOTAS(2.0,-0.15,'('Z-AXIS')');
ANGLE:=3.14159/2;
GHROTATE(-0.4,0.5,ANGLE);
GHPLOTAS(-0.4,0.5,'('R-AXIS')');
GHUNROT;
GHGREND;
'END';
****
```

PROGRAM (4)

Equations 2.14 and 2.18 (A combination of programs 2 and 3)

```
'BEGIN' 'INTEGER'NC,IFAIL,NPTS,I;
  'REAL'Z,D,PI,FIP,ACC,C1,C2,FIP1,FIP2,R,ANGLE;
'ARRAY' P[1:381], XX[1:227], YY[1:227];

  'PROCEDURE' D01ACA(A,B,F,RELACC,ABSACC,NC,P,ANS,ACC,NPTS,IFAIL);
  'VALUE' A,B,RELACC,ABSACC,NC;   'REAL'A,B,RELACC,ABSACC,ANS,ACC;
  'INTEGER'NC,NPTS,IFAIL;  'REAL''ARRAY'P; 'REAL''PROCEDURE'F; 'ALGOL';
'REAL''PROCEDURE'F1(X);                  'VALUE'X;              'REAL'X;
'BEGIN'  'REAL' S,T,U;  T:=COS(X);  U:=D*D+1-2*D*T;  S:=SQRT(U+Z*Z);
       F1:=COS(2*PI*S)*(1+Z/S)*(D*T-1)/(U*2*PI);
  'END';
   'REAL''PROCEDURE'F2(X);          'VALUE'X;              'REAL'X;
'BEGIN' 'REAL'S,T,U;  T:=COS(X);  U:=D*D+1-2*D*T;  S:=SQRT(U+Z*Z);

      F2:=-SIN(2*PI*S)*(1+Z/S)*(D*T-1)/(U*2*PI);
   'END';
      PI:=3.14159265358979;      IFAIL:=0;    NC:=0;      I:=0;
 'FOR' Z:=0.0          'DO'
'BEGIN'   NEWLINE(1);  PRINT(Z,1,2);
    C1:=COS(2*PI*Z);          C2:=-SIN(2*PI*Z);
 'FOR' D:=0.0 'STEP' 0.01 'UNTIL' 0.901,  0.901 'STEP' 0.001
'UNTIL' 0.9991    'DO'
   'BEGIN'  NEWLINE(1);  SPACE(9);      PRINT(D,1,4);
   D01ACA(0.0,PI,F1,0.0005,0.0,NC,P,FIP1,ACC,NPTS,IFAIL);
   D01ACA(0.0,PI,F2,0.0005,0.0,NC,P,FIP2,ACC,NPTS,IFAIL);
   R:= SQRT((C1*FIP1)↑2+(C2*FIP2)↑2);
  PRINT(C1*FIP1,1,6);   SPACE(4);     PRINT(C2*FIP2,1,6);  SPACE(4);
  PRINT(R,1,6);     SPACE(4);     PRINT(ACC,0,8);   NEWLINE(1);
 I:=I+1;          XX[I]:=D;          YY[I]:=R;
   'END';
'FOR' D:=1.001 'STEP' 0.001 'UNTIL' 1.0091, 1.01 'STEP' 0.01 'UNTIL'
1.091,  1.10  'STEP' 0.05  'UNTIL' 2.01          'DO'
   'BEGIN'    NEWLINE(1);     SPACE(9);     PRINT(D,1,4);
   D01ACA(0.0,PI,F1,0.0005,0.0,NC,P,FIP1,ACC,NPTS,IFAIL);
  D01ACA(0.0,PI,F2,0.0005,0.0,NC,P,FIP2,ACC,NPTS,IFAIL);
  R:=SQRT(FIP1*FIP1+FIP2*FIP2);
  PRINT(FIP1,1,6);     SPACE(4);     PRINT(FIP2,1,6);     SPACE(4);
   PRINT(R,1,6);   SPACE(4);   PRINT(ACC,0,8);    NEWLINE(1);
I:=I+1;          XX[I]:=D;          YY[I]:=R;
   'END';
   'END';
GHREGION(0.0,2.2,0.0,2.0);
GHLIMITS(1.0,12.0,1.0,11.0);
GHCURPTO(XX,YY,1,227,10);
GHAXESSI(0.1,0.1);
GHLIMITS(0.0,12.0,0.0,11.0);
GHREGION(-0.2,2.2,-0.2,2.0);
GHCRSET(1);
GHCRSIZE(0.1);
GHPLOTAS(0.3,-0.12,'('D-AXIS')');
GHPLOTAS(1.0,-0.12,'('KIRCHHOFF'S INT.: A/W.L=1')');


ANGLE:=3.14159/2;
GHROTATE(-0.12,0.5,ANGLE);
GHPLOTAS(-0.12,0.5,'('R-AXIS')');
GHUNDOT;
GHGREND;
'END';
****
```

PPOGRAM (5)

(EQUATION 2.20)

```
'BEGIN' 'INTEGER'NC,IFAIL,NPTS,I;
  'REAL'Z,D,PI,FIP,ACC,C1,C2,FIP1,FIP2,R,ANGLE;
   'ARRAY' P[1:381],   XX[1:365],  YY[1:365];

  'PROCEDURE' D01ACA(A,B,F,RELACC,ABSACC,NC,P,ANS,ACC,NPTS,IFAIL);
  'VALUE' A,B,RELACC,ABSACC,NC;   'REAL'A,B,RELACC,ABSACC,ANS,ACC;
  'INTEGER'NC,NPTS,IFAIL;  'REAL''ARRAY'P; 'REAL''PROCEDURE'F; 'ALGOL';
'REAL''PROCEDURE'F1(X);              'VALUE'X;          'REAL'X;
  'BEGIN'   'REAL'S,T,U;  T:=COS(X);  U:=D*D+1-2*D*T;  S:=SQRT(U*Z*Z);
        F1:=COS(10*PI*S)*(D*T-1)/(U*PI);
'END';
   'REAL''PROCEDURE'F2(X);          'VALUE'X;          'REAL'X;
  'BEGIN'  'REAL'S,T,U;   T:=COS(X);  U:=D*D+1-2*D*T;   S:=SQRT(U+Z*Z);

        F2:=-SIN(10*PI*S)*(D*T-1)/(U*PI);
   'END';
      PI:=3.14159265358 9;      IFAIL:=0;    NC:=0;      I:=0;
 'FOR' D:=0.0      'DO'
'BEGIN'   NEWLINE(1);  PRINT(D,1,2);
'FOR' Z:=0.0 'STEP'0.005'UNTIL' 1.496,1.5 'STEP' 0.05 'UNTIL' 2.951,
3.0 'STEP'0.2 'UNTIL' 9.81   'DO'
   'BEGIN'  NEWLINE(1);  SPACE(9);     PRINT(Z,2,3);
    C1:=COS(10*PI*Z);          C2:=-SIN(10*PI*Z);
  D01ACA(0.0,PI,F1,0.0005,0.0,NC,P,FIP1,ACC,NPTS,IFAIL);
  D01ACA(0.0,PI,F2,0.0005,0.0,NC,P,FIP2,ACC,NPTS,IFAIL);
   R:= SQRT((C1*FIP1)↑2+(C2*FIP2)↑2);
  PRINT(C1*FIP1,1,6);   SPACE(4);     PRINT(C2*FIP2,1,6);  SPACE(4);
  PRINT(R,1,6);     SPACE(4);     PRINT(ACC,0,8);   NEWLINE(1);
I:=I+1;     XX[I]:=Z;      YY[I]:=R;
   'END';
'END';
GHREGION(0.0,11.0,0.0,2.5);
GHLIMITS(1.5,18.0,1.0,11.0);
GHCURPTO(XX,YY,1,365,10);
GHAXESSI(0.2,0.1);
GHLIMITS(0.0,18.0,0.0,11.0);
GHREGION(-1.0,11.0,-0.25,2.5);
GHCRSET(1);
GHCRSIZE(0.1);
GHPLOTAS(2.0,-0.15,'('Z-AXIS')');
ANGLE:=3.14159/2;
GHROTATE(-0.4,0.5,ANGLE);
GHPLOTAS(-0.4,0.5,'('R-AXIS')');
GHUNROT;
GHGREND;
'END';
****
```

PROGRAM (6)

Equations 2.19 and 2.20

```
'BEGIN' 'INTEGER'NC,IFAIL,NPTS,I;
  'REAL'Z,D,PI,FIP,ACC,C1,C2,FIP1,FIP2,R,ANGLE;
'ARRAY' P[1:381],  XX[1:227],  YY[1:227];

  'PROCEDURE' D01ACA(A,B,F,RELACC,ABSACC,NC,P,ANS,ACC,NPTS,IFAIL);
  'VALUE' A,B,RELACC,ABSACC,NC;   'REAL'A,B,RELACC,ABSACC,ANS,ACC;
  'INTEGER'NC,NPTS,IFAIL;  'REAL''ARRAY'P; 'REAL''PROCEDURE'F; 'ALGOL';
'REAL''PROCEDURE'F1(X);                  'VALUE'X;              'REAL'X;
'BEGIN'  'REAL' S,T,U;  T:=COS(X);  U:=D*D+1-2*D*T;  S:=SQRT(U+Z*Z);
   F1:=COS(2*PI*S)*(D*T-1)/(U*PI);
  'END';
   'REAL''PROCEDURE'F2(X);          'VALUE'X;           'REAL'X;
'BEGIN' 'REAL'S,T,U;  T:=COS(X);  U:=D*D+1-2*D*T;  S:=SQRT(U+Z*Z);

  F2:=-SIN(2*PI*S)*(D*T-1)/(U*PI);
   'END';
      PI:=3.141592653589;      IFAIL:=0;    NC:=0;      I:=0;
 'FOR' Z:=0.0          'DO'
'BEGIN'   NEWLINE(1);  PRINT(Z,1,2);
    C1:=COS(2*PI*Z);          C2:=-SIN(2*PI*Z);
 'FOR' D:=0.0 'STEP' 0.01 'UNTIL' 0.901,  0.901 'STEP' 0.001
'UNTIL' 0.9991     'DO'
   'BEGIN'  NEWLINE(1);  SPACE(9);     PRINT(D,1,4);
   D01ACA(0.0,PI,F1,0.0005,0.0,NC,P,FIP1,ACC,NPTS,IFAIL);
   D01ACA(0.0,PI,F2,0.0005,0.0,NC,P,FIP2,ACC,NPTS,IFAIL);
   R:=SQRT((C1*FIP1)↑2+(C2*FIP2)↑2);
PRINT(C1*FIP1,1,6);  SPACE(4);  PRINT(C2*FIP2,1,6);  SPACE(4);
   PRINT(R,1,6);   SPACE(4);  PRINT(ACC,0,8);   NEWLINE(1);
 I:=I+1;          XX[I]:=D;          YY[I]:=R;
   'END';
'FOR' D:=1.001 'STEP' 0.001 'UNTIL' 1.0091, 1.01 'STEP' 0.01 'UNTIL'
1.091,  1.10  'STEP' 0.05  'UNTIL' 2.01          'DO'
   'BEGIN'    NEWLINE(1);    SPACE(9);    PRINT(D,1,4);
  D01ACA(0.0,PI,F1,0.0005,0.0,NC,P,FIP1,ACC,NPTS,IFAIL);
   D01ACA(0.0,PI,F2,0.0005,0.0,NC,P,FIP2,ACC,NPTS,IFAIL);
    R:=SQRT(FIP1*FIP1+FIP2*FIP2);
  PRINT(FIP1,1,6);    SPACE(4);    PRINT(FIP2,1,6);    SPACE(4);
   PRINT(R,1,6);   SPACE(4);  PRINT(ACC,0,8);   NEWLINE(1);
I:=I+1;          XX[I]:=D;          YY[I]:=R;
   'END';
   'END';
GHREGION(0.0,2.2,0.0,2.0);
GHLIMITS(1.0,12.0,1.0,11.0);
GHCURPTO(XX,YY,1,227,10);
GHAXESSI(0.1,0.1);
GHLIMITS(0.0,12.0,0.0,11.0);
GHREGION(-0.2,2.2,-0.2,2.0);
GHCRSET(1);
GHCRSIZE(0.1);
GHPLOTAS(0.3,-0.12,'('D-AXIS')');
GHPLOTAS(1.0,-0.12,'('HUYGENS A/W,L=1')');

ANGLE:=3.14159/2;
GHROTATE(-0.12,0.5,ANGLE);
GHPLOTAS(-0.12,0.5,'('R-AXIS')');
GHUNROT;
GHGREND;
   'END';
****
```

PROGRAM (7)

(EQUATION 2.26)

```
'BEGIN''INTEGER'NC,NPTS,IFAIL;
      'REAL'A2,Z21,Z12,D,A,B,K,Z1,ACC,FIP1,FIP2,R,RO;
      'ARRAY' P[1:381];
'REAL' 'PROCEDURE' S09ABA(X,IFAIL);

      'VALUE' X; 'REAL'X;          'INTEGER' IFAIL;    'ALGOL';
'PROCEDURE' D01ACA(A,B,F,RELACC,ABSACC,NC,P,ANS,ACC,NPTS,IFAIL);
      'VALUE' A,B,RELACC,ABSACC,NC; 'REAL'A,B,RELACC,ABSACC,ANS,ACC;
'INTEGER'NC,NPTS,IFAIL;'REAL''ARRAY'P;'REAL''PROCEDURE'F;'ALGOL';
      'REAL''PROCEDURE' F1(X);'VALUE' X; 'REAL'X;
'BEGIN' 'REAL'Y,Q; Q:=S09ABA(1/SQRT(A2-X*X),IFAIL);
      Y:=SQRT(A2-X*Z21*Z12);          F1:=COS(K*Y)*Q/Y;
'END';
      'REAL''PROCEDURE' F2(X);'VALUE' X; 'REAL'X;
'BEGIN' 'REAL'Y,Q; Q:=S09ABA(1/SQRT(A2-X*X),IFAIL);
      Y:=SQRT(A2-X*Z21*Z12);          F2:=-SIN(K*Y)*Q/Y;
'END';
K:=31.41592653589;          A:=100;          B:=25;
A2:=A*A;   D:=SQRT(A2-B*B);      NC:=0;      IFAIL:=0;
'FOR'Z1:=0.0 'STEP'0.02 'UNTIL'1.0 'DO'
'BEGIN'      NEWLINE(1);   PRINT(Z1,1,3);   Z21:=2*Z1;  Z12:=Z1*Z1;
D01ACA(-B,B,F1,0.0005,0,NC,P,FIP1,ACC,NPTS,IFAIL);
D01ACA(-B,B,F2,0.0005,0,NC,P,FIP2,ACC,NPTS,IFAIL);
   R:=SQRT(FIP1*FIP1+FIP2*FIP2);
'IF' Z1=0.0  'THEN'  'BEGIN'    RO:=R;   PRINT(FIP1,2,6);  SPACE(5);
PRINT(FIP2,2,6);  SPACE(5);  PRINT(R,2,6);  SPACE(5); PRINT(R/RO,1,4);
SPACE(5);      PRINT(ACC,0,8);          NEWLINE(1);       'END'
'ELSE'   'BEGIN'   PRINT(FIP1,2,6);   SPACE(5);    PRINT(FIP2,2,6);
SPACE(5);   PRINT(R,2,6);     SPACE(5);     PRINT(R/RO,1,4);
SPACE(5);          PRINT(ACC,0,8);          NEWLINE(1);       'END';
   'END';
   'END';
****
```

PROGRAM (8)

(EQUATIONS 2.32 AND 2.35)

```
'BEGIN''INTEGER'NC,NPTS,IFAIL; 'REAL'Z1,K,FIP,FIP0,ACC; 'ARRAY'P[1:381]
'PROCEDURE'D01ACA(A,B,F,RELACC,ABSACC,NC,P,ANS,ACC,NPTS,IFAIL);
'VALUE' A,B,RELACC,ABSACC,NC;   'REAL' A,B,RELACC,ABSACC,ANS,ACC;
'INTEGER'NC,NPTS,IFAIL; 'REAL''ARRAY'P; 'REAL''PROCEDURE'F;  'ALGOL';
'REAL''PROCEDURE' SINC(A);          'REAL'A;
'IF' A=0.0  'THEN' SINC:=1.0  'ELSE' SINC:=SIN(A)/A;
'REAL''PROCEDURE' F(X);   'VALUE'X;   'REAL'X;
'BEGIN'   'REAL'U;          U:=SINC(K*X*Z1);          F:=U;
    'END';
K:=1.047197551196?;          IFAIL:=0;          NC:=0;
'FOR'Z1:=0.0  'STEP'0.025'UNTIL'1.001, 1.1'STEP'0.1'UNTIL'4.01  'DO'
  'BEGIN'    NEWLINE(1);          PRINT(Z1,1,3);
D01ACA(1.0,10.0,F,0.0005,0.0,NC,P,FIP,ACC,NPTS,IFAIL);
'IF' Z1=0.0 'THEN'  'BEGIN' FIP0:=FIP;  PRINT(FIP,2,6);  SPACE(5);
 PRINT(FIP/FIP0,1,6);   SPACE(5);   PRINT(ACC,0,8);  NEWLINE(1);  'END'
'ELSE'   'BEGIN'   PRINT(FIP,2,6);   SPACE(5);     PRINT(FIP/FIP0,1,6);
  SPACE(5);    PRINT(ACC,0,8);          NEWLINE(1);          'END';
'END';
'END';
****
```

PPOGRAM (9)

(EQUATION 2.38)

```
'BEGIN''INTEGER'NC,NPTS,IFAIL; 'REAL'Z1,K,FIP,FIP0,ACC; 'ARRAY'P[1:381];
'REAL''PROCEDURE'  S17ABA(X);    'VALUE' X;        'REAL'  X;   'ALGOL';
'PROCEDURE'D01ACA(A,B,F,RELACC,ABSACC,NC,P,ANS,ACC,NPTS,IFAIL);
'VALUE' A,B,RELACC,ABSACC,NC;   'REAL' A,B,RELACC,ABSACC,ANS,ACC;
'INTEGER'NC,NPTS,IFAIL; 'REAL''ARRAY'P; 'REAL''PROCEDURE'F;  'ALGOL';
'REAL''PROCEDURE' SINC(A);          'REAL'A;
'IF' A=0.0  'THEN' SINC:=1.0  'ELSE' SINC:=2*S17ABA(A)/A;
'REAL''PROCEDURE' F(X);   'VALUE'X;   'REAL'X;
'BEGIN'   'REAL'U;          U:=SINC(K*X*Z1);          F:=U;
    'END';
K:=2.094395102392?;          IFAIL:=0;          NC:=0;
'FOR'Z1:=0.0  'STEP'0.025'UNTIL'1.001, 1.1'STEP'0.1'UNTIL'4.01  'DO'
  'BEGIN'    NEWLINE(1);          PRINT(Z1,1,3);
D01ACA(2.5,10.0,F,0.0005,0.0,NC,P,FIP,ACC,NPTS,IFAIL);
'IF' Z1=0.0 'THEN'  'BEGIN' FIP0:=FIP;  PRINT(FIP,2,6);  SPACE(5);
 PRINT(FIP/FIP0,1,6);   SPACE(5);   PRINT(ACC,0,3);  NEWLINE(1);  'END'
'ELSE'   'BEGIN'   PRINT(FIP,2,6);   SPACE(5);     PRINT(FIP/FIP0,1,6);
  SPACE(5);    PRINT(ACC,0,8);          NEWLINE(1);          'END';
'END';
'END';
****
```

PPOGRAM (10)

(EQUATION 2.39)

```
'BEGIN''INTEGER'NC,NPTS,IFAIL; 'REAL'Z1,K,FIP,FIPO,ACC; 'ARRAY'P[1:381];
'REAL''PROCEDURE' S17ABA(X);    'VALUE' X;        'REAL' X; 'ALGOL';
'PROCEDURE'D01ACA(A,B,F,RELACC,ABSACC,NC,P,ANS,ACC,NPTS,IFAIL);
'VALUE' A,B,RELACC,ABSACC,NC;   'REAL' A,B,RELACC,ABSACC,ANS,ACC;
'INTEGER'NC,NPTS,IFAIL; 'REAL''ARRAY'P; 'REAL''PROCEDURE'F;  'ALGOL';
'REAL''PROCEDURE' SINC(A);          'REAL'A;
'IF' A=0.0  'THEN' SINC:=1.0  'ELSE' SINC:=2*S17ABA(A)/A;
'REAL''PROCEDURE' F(X);   'VALUE'X;   'REAL'X;
'BEGIN'   'REAL'U;   U:=SINC(K*X*Z1);     F:=U*EXP(-X*X/400);
   'END';
K:=1.0471975511963;          IFAIL:=0;          NC:=0;
'FOR'Z1:=0.0  'STEP'0.025'UNTIL'1.001, 1.1'STEP'0.1'UNTIL'4.01  'DO'
  'BEGIN'    NEWLINE(1);        PRINT(Z1,1,3);
D01ACA(0.5,60.0,F,0.0005,0.0,NC,P,FIP,ACC,NPTS,IFAIL);
'IF' Z1=0.0 'THEN'  'BEGIN' FIPO:=FIP;  PRINT(FIP,2,6);  SPACE(5);
 PRINT(FIP/FIPO,1,4);   SPACE(5);   PRINT(ACC,0,8); NEWLINE(1);  'END'
'ELSE'   'BEGIN'   PRINT(FIP,2,6);   SPACE(5);      PRINT(FIP/FIPO,1,4);
  SPACE(5);    PRINT(ACC,0,8);          NEWLINE(1);          'END';
'END';
'END';
****
```

PROGRAM (11)

(EQUATION 2.41)

```
'BEGIN''INTEGER' NC,NPTS,IFAIL;   'REAL' Z1,K,S,T,FIP,FIPO,ACC;
  'ARRAY' P[1:381];
'REAL''PROCEDURE' S17ABA(X);    'VALUE' X;     'REAL' X;     'ALGOL';
'PROCEDURE' D01ACA(A,B,F,RELACC,ABSACC,NC,P,ANS,ACC,NPTS,IFAIL);
'VALUE' A,B,RELACC,ABSACC,NC;    'REAL' A,B,RELACC,ABSACC,ANS,ACC;
'INTEGER' NC,NPTS,IFAIL;  'REAL''ARRAY' P;  'REAL''PROCEDURE' F;   'ALGOL';
'REAL''PROCEDURE' SINC(A);          'REAL' A;
'IF' A=0.0  'THEN' SINC:=1.0  'ELSE' SINC:=2*S17ABA(A)/A;
'REAL''PROCEDURE'  F(X);      'VALUE' X;         'REAL'X;
'BEGIN'       'REAL' S,T,U;              S:=0.212*X;
     T:=S/SQRT((1-0.02*(X)↑2)↑2+(S)↑2*(1-0.01*(X)↑2)↑2);
      U:=SINC(K*X*Z1);                  F:=T*U*EXP(-X X/400);
'END'
   K:=1.0471975511963;            IFAIL:=0;          NC:=0;
'FOR' Z1:=0.0 'STEP' 0.025 'UNTIL' 1.001, 1.1 'STEP' 0.1 'UNTIL' 4.01    'DO'
'BEGIN'         NEWLINE(1);        PRINT(Z1,1,3);
   D01ACA(0.02,40.0,F,0.0005,0.0,NC,P,FIP,ACC,NPTS,IFAIL);
'IF' Z1=0.0  'THEN'  'BEGIN'   FIPO:=FIP;      PRINT(FIP,2,6);    SPACE(5);
    PRINT(FIP/FIPO,1,4);    SPACE(5);     PRINT(ACC,0,8);   NEWLINE(1);   'END'
'ELSE'      'BEGIN'      PRINT(FIP,2,6);    SPACE(5);    PRINT(FIP/FIPO,1,4);
     SPACE(5);       PRINT(ACC,0,8);        NEWLINE(1);          'END';
'END';
'END';
****
```

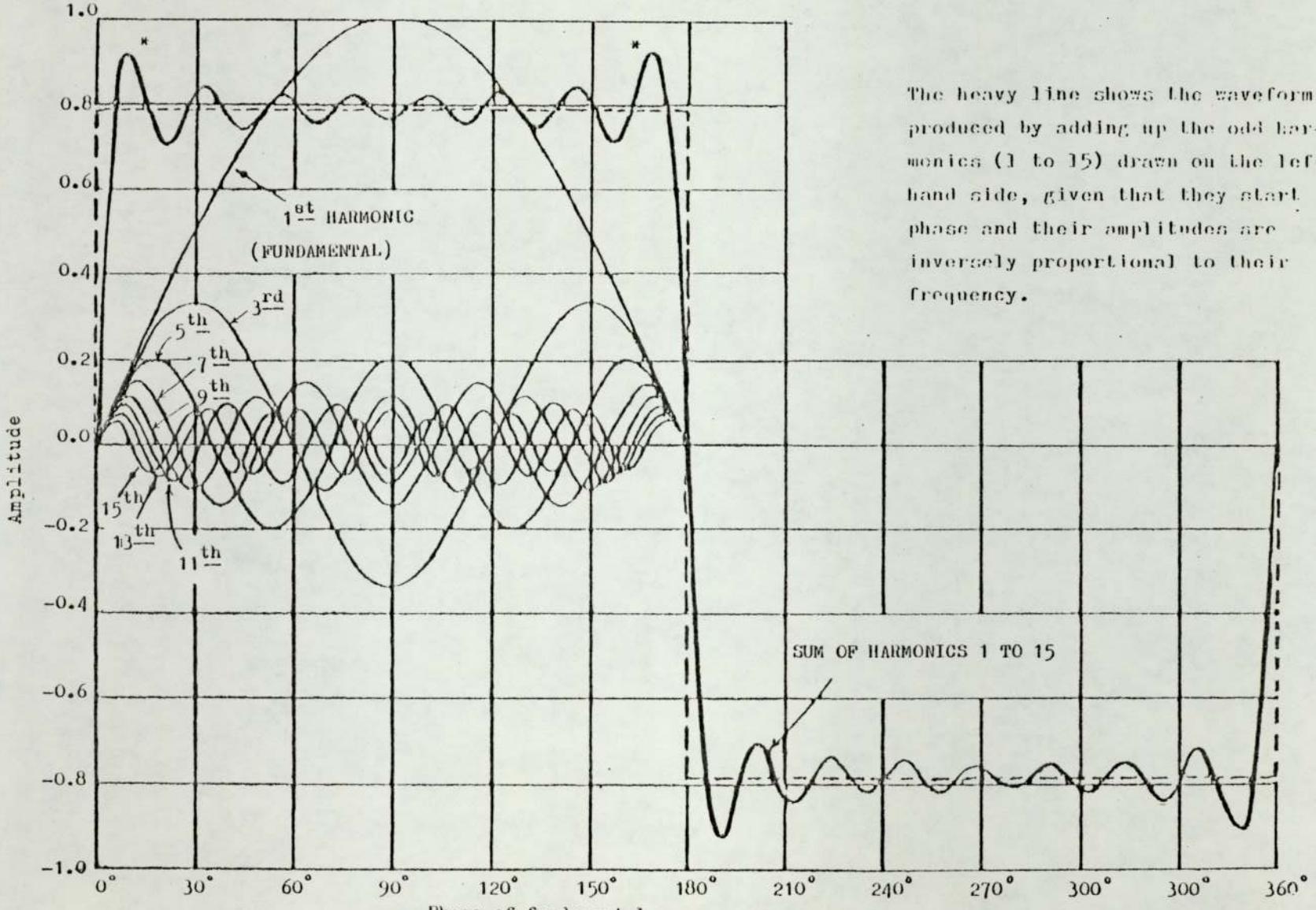

The heavy line shows the waveform produced by adding up the odd harmonics (1 to 15) drawn on the left-hand side, given that they start in phase and their amplitudes are inversely proportional to their frequency.

Fig. B.1 Fourier analysis of square wave showing Gibbs phenomenon

APPENDIX (C)

MATHEMATICAL ANALYSIS FOR MATCHING LAYERS

The matching layers may be considered as a series of transmission lines. The necessary conditions for constructing these layers, can be determined by one of the following methods:

1. by finding the values of acoustic pressure (P_x) and particle velocity (v_x) at the boundary conditions of the system;
   or
2. by determining the input impedance (Z_x) of the transmission lines (Goldman, 1962).

The second method is more feasible, since it gives the general formula which can be applied to any number of matching layers, or to any acoustic impedance transformer. However, the first method of analysis will be also considered here, for only one layer, for the purpose of comparison between the two methods.

C.1 One Matching (Transition) Layer Analysis

Consider a system in which there is a transducer at one end of a transition layer of thickness ℓ, and a loading medium at the other end, as shown in Fig.(C.1).

The acoustic pressure P_x at any point x in a system, in which both forward and backward travelling waves are present, is given by:

$$p_x = A\, e^{j(\omega t - kx)} + B\, e^{j(\omega t + kx)} \qquad \ldots\ldots (1)$$

where A and B are the pressure amplitudes in the positive x direction, and in the opposite direction, respectively.

At x=0 ,then $p_2 = p_3$,i.e.,

$$A_2 + B_2 = A_3 + B_3 \qquad \ldots\ldots\ldots(2)$$

Also, $v_2 = v_3$;where, v_2 and v_3 are the particle velocities in the transition layer(2) and the loading medium (3),respectively. Thus,

$$\frac{A_2}{\rho_2 c_2} - \frac{B_2}{\rho_2 c_2} = \frac{A_3}{\rho_3 c_3} - \frac{B_3}{\rho_3 c_3}$$

or, $$\frac{A_2}{Z_2} - \frac{B_2}{Z_2} = \frac{A_3}{Z_3} - \frac{B_3}{Z_3} \qquad \ldots\ldots\ldots (3)$$

If $B_3 = 0$, i.e. there is only a forward travelling wave in the loading medium, then, from equations (2) and (3) we have

$$A_2 = \frac{1}{2} A_3 \left(1+\frac{Z_2}{Z_3}\right) \qquad \ldots\ldots\ldots (4)$$

and

$$B_2 = \frac{1}{2} A_3 \left(1-\frac{Z_2}{Z_3}\right) \qquad \ldots\ldots\ldots (5)$$

at $x = -\ell$, we have

$$p_1 = p_2 \qquad \text{and} \qquad v_1 = v_2$$

i.e.,

$$p = A_1 e^{jk_1\ell} + B_1 e^{-jk_1\ell} = A_2 e^{jk_2\ell} + B_2 e^{-jk_2\ell} \qquad \ldots.(6)$$

and

$$v = \frac{A_1}{Z_1} e^{jk_1\ell} - \frac{B_1}{Z_1} e^{-jk_1\ell} = \frac{A_2}{Z_2} e^{jk_2\ell} - \frac{B_2}{Z_2} e^{-jk_2\ell} \qquad \ldots\ldots(7)$$

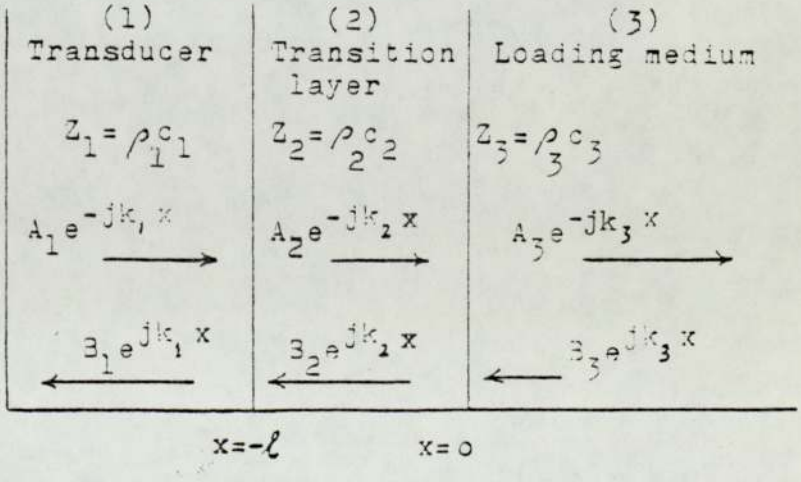

Fig. C.1 A system of one transition layer.

From equations (6) and (7) we have

$$A_1 = \frac{1}{2} e^{-jk_1\ell}\left[e^{jk_2\ell}(1+\frac{Z_1}{Z_2})A_2 + e^{-jk_2\ell}(1-\frac{Z_1}{Z_2})B_2\right] \quad .....(8)$$

and,

$$B_1 = \frac{1}{2} e^{jk_1\ell}\left[e^{jk_2\ell}(1-\frac{Z_1}{Z_2})A_2 + e^{-jk_2\ell}(1+\frac{Z_1}{Z_2})B_2\right] \quad .....(9)$$

Substituting the values of A_2 and B_2 from equations (4) and (5) into equations (8) and (9) , then

$$A_1 = \frac{1}{4} e^{-jk_1\ell} A_3\left[e^{jk_2\ell}(1+\frac{Z_1}{Z_2})(1+\frac{Z_2}{Z_3})+e^{-jk_2\ell}(1-\frac{Z_1}{Z_2})(1-\frac{Z_2}{Z_3})\right] \quad ...(10)$$

and

$$B_1 = \frac{1}{4} e^{jk_1\ell} A_3\left[e^{jk_2\ell}(1-\frac{Z_1}{Z_2})(1+\frac{Z_2}{Z_3})+e^{-jk_2\ell}(1+\frac{Z_1}{Z_2})(1-\frac{Z_2}{Z_3})\right] \quad ....(11)$$

If we write

$$(1-\frac{Z_1}{Z_2})(1+\frac{Z_2}{Z_3}) = R$$

and

$$(1+\frac{Z_1}{Z_2})(1-\frac{Z_2}{Z_3}) = Q$$

Therefore equation (3.11) may be written as:

$$B_1 = \frac{1}{4} e^{jk_1\ell} A_3\left[e^{jk_2\ell}R + e^{-jk_2\ell}Q\right] \quad .....(12)$$

If $B_1 = 0$, i.e. there is no backward-travelling wave in the transducer, then we have

$$e^{2jk_2\ell}R + Q = 0$$

or

$$(\text{Cos } 2k_2\ell)R + j(\text{Sin}2k_2\ell)R + Q = 0$$

Since R and Q are pure real, then we have

(a) $\text{Sin}2k_2\ell = 0$

i.e. $2k_2\ell = n\pi$

or $\frac{4\pi\ell}{\lambda_2} = n\pi$

therefore,

$$\ell = n\frac{\lambda_2}{4} \qquad \text{where } n \text{ is an integer}$$

(b) $\cos 2k_2\ell = +1$ or $= -1$

i.e. $R + Q = 0$; or, $-R + Q = 0$

<u>For $R + Q = 0$</u> :-

$$(1-\frac{Z_1}{Z_2})(1+\frac{Z_2}{Z_3}) + (1+\frac{Z_1}{Z_2})(1-\frac{Z_2}{Z_3}) = 0$$

or

$$1-\frac{Z_1}{Z_2}+\frac{Z_2}{Z_3}-\frac{Z_1}{Z_3} + 1 + \frac{Z_1}{Z_2} - \frac{Z_2}{Z_3} - \frac{Z_1}{Z_3} = 0$$

i.e.

$$2 - 2\frac{Z_1}{Z_3} = 0$$

or

$$Z_1 = Z_3 \qquad \text{or} \quad \rho_1 c_1 = \rho_3 c_3$$

Therefore, for complete transmission of ultrasonic waves into the loading medium the latter must have an impedance equal to that of the transducer, which is not applicable in practice.

<u>For $-R+Q = 0$</u> :-

$$-1+\frac{Z_1}{Z_2} - \frac{Z_2}{Z_3} + \frac{Z_1}{Z_3} + 1 + \frac{Z_1}{Z_2} - \frac{Z_2}{Z_3} - \frac{Z_1}{Z_3} = 0$$

$$2\frac{Z_1}{Z_2} - 2\frac{Z_2}{Z_3} = 0$$

i.e.

$$Z_2^2 = Z_1 Z_3$$

or

$$\rho_2 c_2 = \sqrt{(\rho_1 c_1)(\rho_3 c_3)} \qquad \ldots\ldots (13)$$

Therefore $\cos 2k_2\ell = -1$, is the answer

i.e. $2k_2\ell = (2n+1)\pi$; $\frac{4\pi}{\lambda_2}\ell = (2n+1)\pi$;

$\ell = (2n+1)\frac{\lambda_2}{4}$ where n is 0,1,2,3, etc.

or

$2k_2\ell = m\pi$

Therefore

$\ell = m\frac{\lambda_2}{4}$, where m is an odd number, 1,3,5, etc.

Therefore, a matching layer which offers a 100% transmission of ultrasonic waves through it, must have the following characteristics:-

(1) Its acoustic impedance Z_m must be equal to the geometric mean of the two impedances of the transducer Z_t and that of the loading medium Z_w

i.e. $Z_m = \sqrt{Z_t Z_w}$ ..... (13)

and

(b) it must have a thickness $\ell = \frac{\lambda}{4}, \frac{3\lambda}{4}, \frac{5\lambda}{4}$, etc, or $\ell = m\frac{\lambda}{4}$ where m is an odd number. In practice it is preferable to use layers of a quarter-wave length thickness rather than its multiple, since the latter, $3\lambda/4$, $5\lambda/4$ etc., contributes more attenuation as its thickness increases.

C.2 Acoustic Transmission Line Theory

Consider a system in which a transducer generates ultrasonic wave beam at one end of an acoustic transmission line which is terminated a distance "ℓ" away from the transducer by a loading medium of specific acoustic impedance Z_w, as shown in Fig.(C.2).

Since the backward travelling wave comes about by reflection, the layer forming the line, Fig.(C.2) may be considered as it has both forward and backward travelling waves. Therefore, the impedance at any point × within the line is given by:

$$Z_x = Z_m \left[\frac{P_1 e^{-jkx} + P_2 e^{jkx}}{P_1 e^{-jkx} - P_2 e^{jkx}} \right] \qquad \ldots\ldots (14)$$

where, Z_m is the specific acoustic impedance ($\rho_m c_m$) of the medium forming the line. p_1 and p_2, are the pressure amplitudes in the positive × direction and in the opposite direction, respectively. $k = \frac{2\pi}{\lambda}$; λ denotes the wavelength in the material of the line.

For the loading medium, where there is only a forward travelling wave in the positive × direction, the impedance at any point will be constant and equal to the specific acoustic impedance of the medium Z_w.

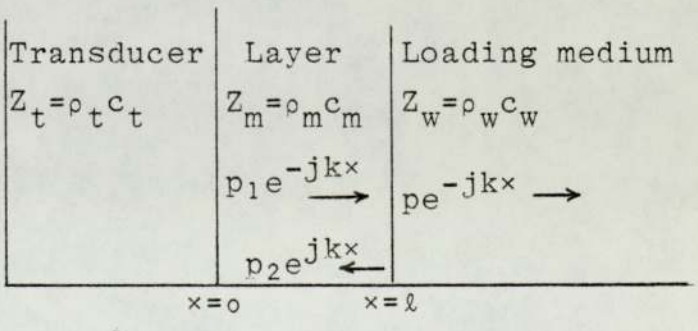

Fig. C.2 A system of one transition layer.

i.e.,

$$Z_x = Z_{sp.} = Z_w = \rho_w c_w$$

Therefore, at the termination, for which $x = \ell$, we have $Z_x = Z_w$, and whence Eq. (3.14) may be written as follows:

$$Z_w = Z_m \left[\frac{P_1 e^{-jk\ell} + P_2 e^{jk\ell}}{P_1 e^{-jk\ell} - P_2 e^{jk\ell}}\right]$$

from which we have :

$$P_2 = P_1 e^{-j2k\ell}\left[\frac{Z_w - Z_m}{Z_w + Z_m}\right] \qquad \text{.....(15)}$$

Substituting equation (15) into equation (14), we have :

$$Z_x = Z_m \frac{Z_w + jZ_m \tan k(\ell - x)}{Z_m + jZ_w \tan k(\ell - x)}$$

From this equation the acoustic impedance at x=0, i.e. at the interface between the transducer and the line, is the input impedance of the line Z_{in} and is given by

$$Z_{in} = Z_m \frac{Z_w + jZ_m \tan k\ell}{Z_m + jZ_w \tan k\ell} \qquad \text{.....(16)}$$

or

$$Z_{in} = Z_m \frac{Z_w \cos k\ell + jZ_m \sin k\ell}{Z_m \cos k\ell + jZ_w \sin k\ell} \qquad \text{.....(17)}$$

Equation (16) or equation (17) is the transmission line equation for impedance matching. There are two special cases of equation (17) which are important in impedance transformers.

(1) If the line is a half-wavelength long i.e. $\ell=\frac{\lambda}{2}$, then $k\ell=\pi$, $\sin\pi=0$, and $\cos\pi=1$. Substituting these values of sines and cosines into equation (17), we obtain:

$$Z_{in} = Z_w \qquad \ldots\ldots\ldots (18)$$

This means that if the length of the line is $\frac{\lambda}{2}$, the input impedance at one end ot the line will be equal to the specific acoustic impedance of the medium at the other end, Z_w

(2) If the line is a quarter-wavelength long i.e. $\ell=\frac{\lambda}{4}$, then $k\ell=\frac{\pi}{2}$, $\cos\pi/_2=o$, and $\sin\frac{\pi}{2}=1$. Substituting these values of the sines and cosines into equation (17), gives the following

$$Z_{in} = \frac{Z_m^{\,2}}{Z_w} \qquad \ldots\ldots\ldots (19)$$

Therefore, if the length of the line is $\frac{\lambda}{4}$, the input impedance at one end of the line may be different from the specific acoustic impedance of the medium at the other end, Z_w. If the input impedance Z_{in} of the line can be made equal to the specific acoustic impedance of the transducer Z_t, by suitable choice of the material forming the line, we will therefore have the following relation

$$Z_t = Z_{in} = \frac{Z_m^{\,2}}{Z_w}$$

i.e.

$$Z_m = \sqrt{Z_t Z_w} \qquad \ldots\ldots\ldots (20)$$

In other words, if we make a quarter-wavelength thick transition layer whose material has a specific acoustic impedance (Z_m) equal to the geometric mean ot the specific acoustic impedances of the loading medium (Z_w) and the

transducer (Z_t) i.e. $Z_m = \sqrt{Z_w Z_t}$, then by substituting the value of Z_m into equation (19), we will find that the impedance of the loading medium has been transformed to match that of the transducer. This transition layer is therefore called a matching layer.

At the boundary between two media, the ultrasonic waves transmitted from medium (1) into medium (2), for normal incidence, is given by the following expression

$$T = \frac{I_2}{I_1} = \frac{4r}{(r+1)^2} \qquad \text{.....(21)}$$

where

I_1 is the intensity of the incident waves; I_2 is the intensity of transmitted waves; T, is the transmission coefficient; and $r = Z_2/Z_1$

If we differentiate this equation with respect to r and set the result equal to zero
we obtain

$$4(r+1)^2 - 4r(r+1) \times 2 = 0$$

i.e. $r = 1$ or $Z_2/Z_1 = 1$

Therefore, the maximum power transfer occurs when $Z_1 = Z_2$. This condition exists when using a quarter-wavelength transition layer whose specific acoustic impedance $Z_m = \sqrt{Z_t Z_w}$, where the transducer sees a perfect match i.e. $Z_t = Z_{in}$, and thus we get the maximum power transfer from the transducer to the loading medium.

It can be seen that equation (20) derived above from the transmission line theory; is similar to equation (13) derived by one matching layer analysis, in the previous section.

We may now be able to derive the general equations for a number of transition layers which can be situated on the front face of the transducer in order to give an input impedance which matches that of the transducer.

Consider a series of layers, shown in Fig. (C.3), each layer is a quarter-wavelength thick, interposed between a transducer and a loading medium whose specific acoustic impedance is Z_w.

First, let us consider the layer (1), by itself, and looking into the direction of the loading medium. Its input impedance Z_{i1}, at the interface, ab, can be given by equation (19) , i.e.

$$Z_{i1} = \frac{Z_1^2}{Z_w}$$

where,

Z_1 is the specific acoustic impedance of layer (1).

Now this input impedance Z_{i1} (due to the first layer) at the interface ab, will be seen by the second layer (2), whose specific acoustic impedance is Z_2, so that its input impedance Z_{i2} at the interface cd, will be given by:

$$Z_{i2} = \frac{Z_2^2}{Z_{i1}} = \frac{Z_2^2}{Z_1^2/Z_w} = Z_w(\frac{Z_2}{Z_1})^2$$

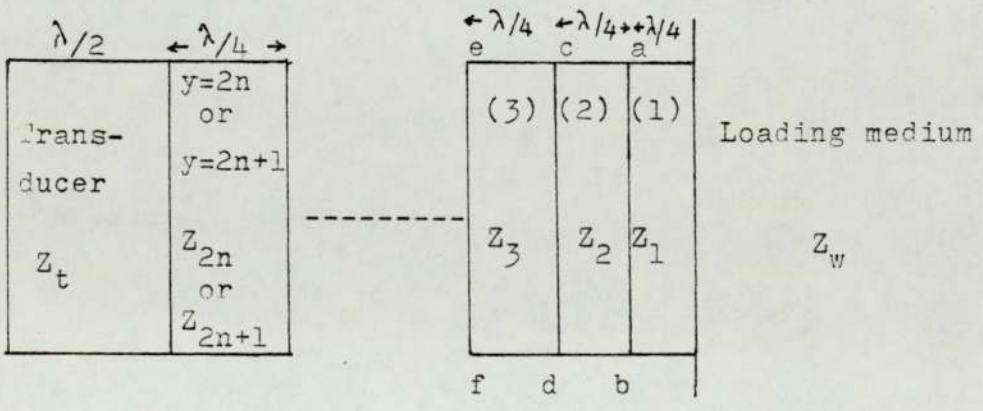

Fig. C . 3 Multiple transition layers, each is $\lambda/4$ thick.

If we considered three layers (1), (2) and (3); then the input impedance Z_{i2} (due to the first two layers (1) and (2)) appearing at the interface cd, will be seen by the third layer (3), so that its input impedance at the interface ef, is given by

$$Z_{i3} = \frac{Z_3^2}{Z_{i2}} = \frac{1}{Z_w} \left(\frac{Z_3 \times Z_1}{Z_2}\right)^2$$

Similarly, the input impedance due to four layers, will be given by

$$Z_{i4} = \frac{Z_4^2}{Z_{i3}} = Z_w \left(\frac{Z_4 . Z_2}{Z_1 . Z_3}\right)^2$$

Thus, in general, the input impedance (Z_{iy}) for a number of layers, y, may be written as:

(1) If y is an even number, i.e. y = 2n, where n is an integer 1,2,3, etc.

$$Z_{iy} = Z_w \left(\frac{Z_2 . Z_4 ..... Z_{2n}}{Z_1 . Z_3 ..... Z_{2n-1}}\right)^2 \qquad ..... (22)$$

(2) If y is an odd number, i.e. y = 2n+1; where n is an integer 1,2,3, etc.

$$Z_{iy} = \frac{1}{Z_w} \left(\frac{Z_1 . Z_3 \ ... \ Z_{2n+1}}{Z_2 . Z_4 \ ... \ Z_{2n}}\right)^2 \qquad ..... (23)$$

These equations are important for the construction of any desired number of $\frac{\lambda}{4}$ matching layers, in cases where it is not possible to construct a single matching layer having the necessary characteristics. In such cases, of using multiple matching layers, the impedance of the loading medium can be transformed so that the transducer sees a perfect match, if we make the input impedance of these series of layers Z_{iy} equal to the specific acoustic impedance of transducer Z_t, by suitable choice of the acoustic impedances of the materials forming the layers. Therefore, for optimum matching, equations

(22) and (23) may be written as follows:-

(1) For even numbers of matching layers (y=2n):

$$Z_t = Z_w \left\{ \frac{Z_2 \; Z_4 \; \ldots\ldots \; Z_{2n}}{Z_1 \; Z_3 \; \cdots\cdots \; Z_{2n-1}} \right\}^2 \qquad \ldots\ldots(24)$$

(2) For odd numbers of matching layers (y=2n+1):

$$Z_t = \frac{1}{Z_w} \left\{ \frac{Z_1 \; Z_3 \; \cdots\cdots \; Z_{2n+1}}{Z_2 Z_4 \; \cdots\cdots \; Z_{2n}} \right\}^2 \qquad \ldots\ldots(25)$$

APPENDIX (D)

ANALYSIS OF THE LATERAL RESOLUTION FOR THE CONCAVE BOWL TRANSDUCER IN THE SYSTEM

In this appendix, an analysis is carried out in order to determine, approximately, the lateral resolution of the apparatus.

The energy contribution due to any diffraction function A(r) within a radius r_1, is given by the integral:

$$\int_0^{r_1} 2\pi r A^2 \, dr$$

The effect of shock excitation applied to a bowl transducer, for which $b/a=\frac{1}{4}$, is shown by curve (1) in Fig.(D.1). This figure is reproduced from Fig.(2.23) p.86, with two straight lines drawn on it, as an approximate representation of A. From this figure, the amplitude A corresponding to any value of r, where r is the distance (in mm) from the central axis, is approximately given as follows:

(1) When, $o<r<0.42$, then

$$A \simeq 1.08 - 2.45r \qquad \ldots\ldots (1)$$

(2) When, $0.42<r<2.6$, then

$$A \simeq 0.05 - 0.0229\,(r-0.42)$$

$$\simeq 0.0596 - 0.0229r \qquad \ldots\ldots (2)$$

The total energy contribution in the circular area, whose radius r=2.6, is given by:

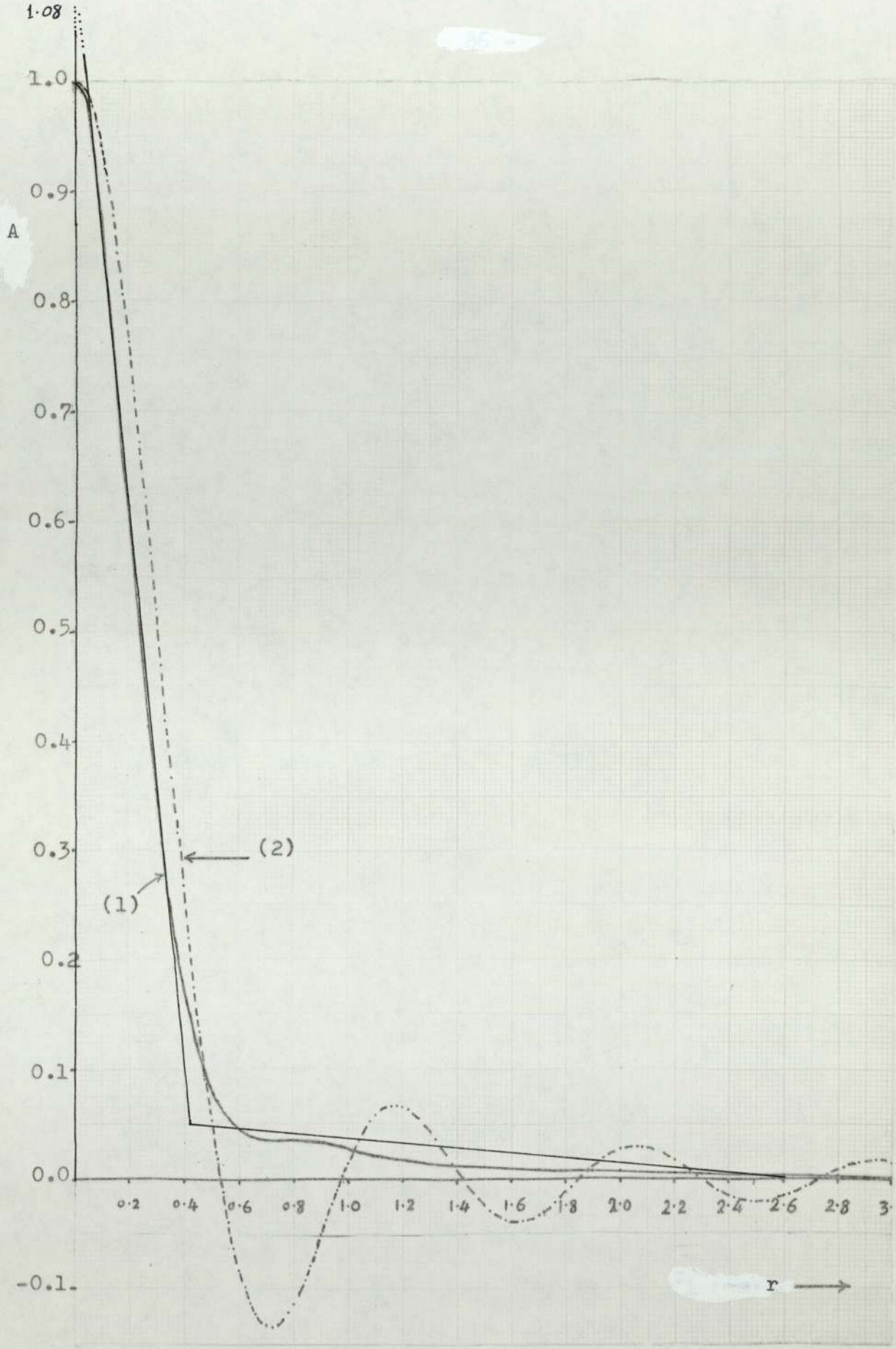

Fig. D.1 Diffraction pattern for a bowl transducer (b/a = 1/4)

(1) Due to shock excitation, with attenuation in water and a bell-shape bandwidth.

(2) Due to steady state condition at 6.85 MHz.

$$E_T = \int_{r=o}^{r=0.42} 2\pi r(A)^2 \, dr + \int_{r=0.42}^{r=2.6} 2\pi r(A)^2 \, dr$$

Substituting the values of A from Eqs.(1) and (2), then

$$E_T = 2\pi \left[\int_{o}^{0.42} r\,(1.08-2.45r)^2 dr + \int_{0.42}^{2.6} r(0.0596-0.0229r)^2 dr \right] \quad \ldots (3)$$

$$E_T \simeq 2\pi(0.0206)$$

The energy contribution at any central circular area, in the region between r=o and r=0.42, is given by:

$$E_r = \int_{0}^{r_1} 2\pi r(A)^2 \, dr$$

Substituting from Eq.(1), then

$$E_r = 2\pi \int_{o}^{r_1} r\,(1.08-2.45r)^2 \, dr \quad \ldots . (4)$$

The fractional energy distribution at a given central area of radius r_1, can be determined by dividing the value obtained by Eq.(4) by that obtained by Eq.(3).

The values of Eq.(4) have been calculated for r_1=0.3 and r_1=0.4mm, from which, we have

$$\frac{E_{0.3}}{E_T} \simeq 0.825, \text{ i.e. } 82.5\%$$

Also, $$\frac{E_{0.4}}{E_T} \simeq 0.913, \text{ i.e. } 91.3\%$$

From the previous analysis, it may be seen that the lateral resolution is about 0.3 to 0.4 mm.

REFERENCES

1. Abendschein, W.; and Hyatt, G.W. (1970). Clinical Orthopaedics of Related Res., 69, 249.

2. Amos, S.W. (1969). Principles of Transistor Circuits. Iliffe Books Ltd., London.

3. Archer-Hall, J.A.; Carpenter, P.B.; Edwards, J.P.N ; and Francois, P.E. (1973). Brit. J. Radiol,, 46,375.

4. Ardan, G.M.; and Crooks, H.E. (1971). Brit. J. Radiol., 44,625.

5. Beaver, W.L. (1974). J. Acoust. Soc, Am., 56, 1043.

6. Beyer, R.T. (1950). Am .J. Phys., 18,25.

7. Blair, H.J. (1961). Brit.J. Radiol., 34,550.

8. Blitz, J (1967). Fundamentals of Ultrasonics. Butterworths, London.

9. Borgnis, P.E. (1953). Rev. Mod. Phys., 25, 653.

10. Brown, B.; and Gordon, D. (1967). Ultrasonic Techniques in Biology and Medicine. Iliffe Books Ltd., London.

11. Cady, W.G. (1946). Piezoelectricity. McGraw-Hill, New York.

12. Christie, D.G. (1962). Appl. Mater. Res., 1, 86.

13. Coulson, C.A. (1955). Waves. Oliver and Boyd, Edinburgh and London.

14. Daniele Sette (1949). J.Acoust. Soc. Am., 21, 375.

15. Dehn, J.T. (1960). J. Acoust. Soc. Am., 32, 1692.

16. Donald, D.I.; and Brown, T.G. (1961). Brit. J. Radiol., 34, 539.

17. Ernst, P.J. (1945). J. Sci. Inst., 22, 238.

18. Ernst, P.J. (1947). J. Acoust. Soc. Am., 19, 474.

19. Faran, J. (1951). J. Acoust. Soc. Am., 23, 405.

20. Farn, C.L.S.; and Huang, H. (1968). J. Acoust. Soc. Am., 43, 252.

21. Farr, R.F.; and Scott, A.C.H. (1964). Transverse Axial Tomography.

22. Fein, L. (1949). J. Acoust. Soc. Am., 21, 511.

23. Filipczyński, L. (1956). Proc. 2nd. Conf. Ultrason., Warsaw, 29-34.

24.Filipczyński, L..; and Etienne, J. (1973). Acustica, 28, 121.

25.Finar, I.L. (1967), Organic Chemistry, 5th edition, Longman, London.

26.Freedman, A. (1970). J. Acoust. Soc. Am. 48, 221.

27.Fry, W.J.; and Dunn, F. (1962). Ultrasound: analysis and experimental methods in Biological research. Vol. IV, ed. W.L. Nastuk, pp 261. Academic Press, New York.

28.Fry, W.J.; Leichner, G.H.; Okuyama, D.; Fry, F.J.; and Fry, E.K. (1968). J. Acoust. Soc. Am., 44, 1324.

29.Goldman, R. (1962). Ultrasonic Technology. Reinhold Publishing Corporation, New York.

30.Golis, M.J. (1968). I.E.E.E. Trans. Sonics Ultrason., SU-15, 105.

31.Gooberman, G.L. (1968). Ultrasonics, Theory and Application. English Universities Press, London.

32.Gordon, D. (1959). Brit. Medical J., June 13, 1500.

33.Gordon, D. (1964). Ultrasound as a diagnostic and Surgical Tool. Livingstone Ltd., Edinburgh and London.

34.Hartley, J.B. (1961). Brit. J. Radiol, 34, 550.

35.Holm, H.H.; and Northeved, A. (1968). Acta Chirurgica Scand., 134, 177.

36.Holmes, J.H. and Lowry, D.H. (1958). Trans, America Clin. Climat. Assoc., 70, 225.

37.Hopwood, F.L. (1946). J. Sci. Inst., 23, 63.

38.Howry, D.H. (1957). Ultrasound in Biology and Medicine, Washington Publication No.3, p.49.

39.Hueter, T.F.; and Bolt, R.H. (1955). Sonics, Wiley, New York.

40.Jahnke; Emde; Lösch, F. (1960). Tables of Higher Functions (Six Edition). McGraw-Hill.

41.Johns, H.E. (1961). The Physics of Radiology (second Edition). Charles Thomas Publisher, U.S.A.

42.Jaffe, B.; Roth, R.S.; and Marzullo, S. (1955). J. Res. Natn. Bur. Stand., 55, 239.

43.Kasparyants, A.A. (1960). Soviet Phys. Acoust., 6, 47.

44.Kawai, H. (1969). Jap. J. appl. Phys., 8, 975.

45.Kaye, G.W.C.; and Laby, T.H. (1968). Tables of Physical and Chemical Constants. Longmans, London.

46.Kennedy, E.B. (1951). Radiography, 17, 190.

47.Kinsler, L.E; and Frey, P. (1962). Fundamentals of Acoustics. Wiley, New York.

48.Kossoff, G. (1963). J. Acoust. Soc. Am., 35, 905.

49.Kossoff, G.; Robinson, D.E. Liu, C.N.; and Garrett, W.J. (1964). Ultrasonics, 2, 29.

50.Kossoff, G., Robinson, D.E.; and Garrett, W.J. (1965). I I.E.E.E. Trans. Sonics Ultrason., SU-12 (No.2), 31.

51.Kossoff, G.; Robinson, D.E.; and Garrett, W.J. (1966). Proc. Int. Conf. Diagnostic Ultrasound 1st.333.

52.Kossoff, G. (1966). I.E.E.E. Trans. Sonics Ultrason, SU-13, (No.1), 20.

53.Kossoff, G.; Robinson, D.E.; and Garrett, W.J. (1968). J.Acoust. Soc. Am., 44, 1310.

54.Kossoff, G. (1971). Ultrasonics, 9, 196.

55.Lale, P.G. (1969). Proc. 8th. Int. Conf. Med. Biol. Engng., 10.

56.Lele, P.P. (1962). J. Physiol., 160, 594.

57.Lel, P.P. (1963). Expl. Neural, 8, 47.

58.Lockwood, J.C.; and Willette, J.G. (1973a). J. Acoust. Soc. Am., 53, 735.

59.Lockwood, J.C.; and Willette, J.G. (1973b). J. Acoust. Soc. Am., 54, 1762.

60.Lutsch, A. (1962). J. Acoust. Soc. Am., 34, 131.

61.McCready, V.R.; and Hill. C.R. (1971). Brit. J. Radiol., 44, 747.

62.McInnes, J. (1954). Radiography, 20,159.

63.McInnes, J. (1956). Radiography, 22, 43.

64.Makow, D.M.; and McRae, D.L. (1968). J. Acoust. Soc. Am., 44, 1346.

65.Marklein, W.R. The General Electric Company, Schenectady, New York, U.S.A.

66.Martin, D.F. and Breazeale, M.A. (1971). J. Acoust. Soc. Am., 49, 1668.

67.Mason, W.P. (1958). Physical Acoustics and the Properties of Solids, Van Nostrand, New York.

68.Mattsson, O. (1955). Acta Radiol., Supp. 120.

69.Mole, L.A.; Hunter, J.L.; and Davenport, J.M. (1972). J. Acoust. Soc. Am., 52, 837.

70.National Bureau of Standards (1969), 29, (U.S.A.).

71.Newell, J.A. (1961). Brit. J. Radiol.; 34, 546.

72.Oberhettinger, F. (1961). J. Res. Natn. Bur. Stand., 65B,1.

73.Olofsson, F. (1963). Acustica, 13, 361.

74.O'Neil, H.T. (1949). J. Acoust. Soc. Am., 21, 516.

75.Papadakis, E.P.; and Fowler, K.A. (1971). J.Acoust. Soc. Am., 50, 729.

76.Reekie, D.; and Davison, M (1971) Brit. J. Radiol. 44, 535.

77.Reid, J.M. (1968). J. Acoust. Soc. Am., 44, 1319.

78.Robinson, D.E.; Lees, S.; and Bess, L. (1974). I.E.E.E. Trans. Acoust. Speech Sig. Proc., ASSP-22, 395.

79.Robinson, D.E.; Kossoff, G.; and Garrett, W.J. (1966). Ultrasonics, 4, 186.

80.Rooney, J.A.; and Nyborg, W.L. (1972). Am. J. Phys., 40, 1825.

81.Rooney, J.A. (1973). J. Acoust. Soc. Am., 54, 429.

82.Sigelmann, R.E.; and Reid. J.M. (1973). J. Acoust. Soc. Am., 53, 1351.

83.Stevenson, J.J. (1950). Brit. J. Radiol, 23, 319.

84.Tarnóczy, T. (1965). Ultrasonics, 3, 115.

85.Thorpe's Dictionary of Applied Chemistry, Vol.I, 142d; Vol.VII, 156a; and Vol.X, 727d.

86.Twersky, V. (1964). J. Acoust. Soc. Am., 36, 1314.

87.Watson, W. (1951). Radiography, 17, 67 and 221.

88.Wells, P.N.T. (1969). Physical Principles of Ultrasonic Diagnosis. Academic Press, London.

89.Wells, P.N.T. (1972). Ultrasonics in Clinical Diagnosis. Churchill Livingstone, Edinburgh and London.

90.Wells, P.N.T.; Bullen, M.A.; Follett, D.H.; Freundlich, H.F.; and James, J.A. (1963). Ultrasonics, 1, 106.

91. Wells, P.N.T.; McCarthy, C.F.; Ross, F.G.M.; and Read, A.E.A. (1969). Brit. J. Radiol., 42, 818.

92. Westwater, F.L.; and Waddell, W.A. (1961). An Introduction to Servomechanisms. English Universities Press, London.

93. White, D.N.; Clark, J.M.; Chesebrough, J.N.; White, M.N.; and Champbell, J.K. (1968). J Acoust. Soc. Am., 44, 1339.

94. Wild, J.J. (1950). Surgery, 27, 183.

95. Wild, J.J.; and Reid, J.M. (1956). Brit. J. Phys. Med., 19, 248.

96. Willard, G.W. (1947). Bell Lab. Record, 25, 194.

97. Willard, G.W. (1949). J. Acoust. Soc. Am., 21, 360.

98. Zemanek, J. (1971). J. Acoust. Soc. Am., 49, 181.